

DYNAMIC ANALYSIS OF TENSION-LEG
PLATFORMS

A Dissertation

by

DIA AREF MALAEB

Submitted to the Graduate College of
Texas A&M University
in partial fulfillment of the requirements for the degree of
DOCTOR OF PHILOSOPHY

December 1982

Major Subject: Civil Engineering

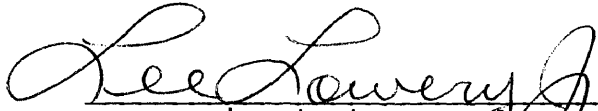
DYNAMIC ANALYSIS OF
TENSION-LEG PLATFORMS

A Dissertation

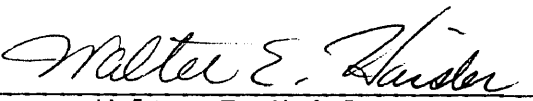
by

DIA AREF MALAEB

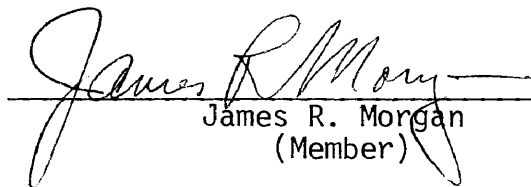
Approved as to style and content by:



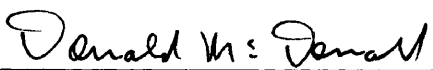
Lee L. Lowery, Jr.
(Chairman of Committee)



Walter E. Haisler
(Member)



James R. Morgan
(Member)



Donald McDonald
(Head of Department)



Giulio Venezian
(Member)

ABSTRACT

Dynamic Analysis of Tension-Leg Platforms. (December 1982)

Dia Aref Malaeb, B.S., Texas Tech University;

M.S., Texas Tech University

Chairman of Advisory Committee: Dr. Lee L. Lowery Jr.

The dynamic response of tension-leg platforms subjected to wave loading and ground motion was investigated using a deterministic dynamic analysis. The model employed in this study is based on derived coupled nonlinear stiffness coefficients and closed form inertia and drag forcing functions derived using Morison's equation. The forcing functions include relative motion between the fluid particles and the structure, and are integrated manually, thereby avoiding the need for expensive numerical integration. The set of coupled nonlinear differential equations was integrated sequentially in the time domain using the Newmark Beta method. A computer program was developed to simulate the time history response of the platform motion. With this program, a parametric study to identify parameters affecting the dynamic response of the platform was performed. Some of the parameters studied were wave period, wave height, water depth, initial tension, and cable stiffness. Horizontal and vertical ground motion components were used to study the effect of earthquakes on tension-leg platforms.

Coupling between the six degrees of freedom (surge, sway, heave, pitch, roll and yaw) was found to have a significant effect on the structural response. The strongest coupling was that between heave and surge or heave and sway. Nonlinear drag forces also were found to be

significant in that they represent the fluid damping and therefore result in response reductions with time. Stiffness nonlinearities were found to be important for large surge or sway. The displacement response to combined wave and earthquake loading was found to be dominated by waves; however, platform accelerations were significantly affected by the earthquake.

ACKNOWLEDGEMENTS

The author wishes to express his deep appreciation to Dr. James R. Morgan for his guidance and valuable assistance throughout this research effort. Dr. Lee L. Lowery is gratefully acknowledged for his patience in serving as the author's committee chairman. Drs. Guilio Venezian and Ahsan Kareem are gratefully acknowledged and particularly thanked for their constructive criticisms and helpful recommendations. The author also expresses his appreciation to Dr. Walter E. Haisler for his assistance as a member of the Graduate Committee and to Dr. Edward S. Fry for his assistance as the representative of the Graduate College.

The support provided for the conduct of this research by the National Science Foundation (PFR-8006467), the Texas A&M Research Foundation, and by the Department of Civil Engineering at Texas A&M University is also acknowledged. Thanks are also expressed to Mrs. Kay Struzick for her efficiency and patience in typing this dissertation and to Mr. Gary Struzick for valuable assistance in preparing the figures contained herein.

DEDICATION

To my parents

TABLE OF CONTENTS

Chapter		Page
I.	INTRODUCTION.	1
	Objective.	1
	Research Plan.	2
	Review of Previous Research.	3
II.	FORMULATION OF STIFFNESS.	6
	General.	6
	Derivation of Nonlinear Stiffness.	6
	Degrees of Freedom.	6
	Derivation of Stiffness Coefficients.	8
III.	ENVIRONMENTAL LOADS	22
	General.	22
	Regular Waves.	22
	Selection of Wave Theory.	23
	Justification for Using Morison's Equation.	26
	Random Waves	30
	Wave Drift Forces.	35
	Procedure for Wave Force Calculation	37
	Summary of Wave Forces	41
	Earthquake Forces.	43
	Horizontal Ground Motion.	43
	Vertical Ground Motion.	46
IV.	MATHEMATICAL MODEL.	53
	Equations of Motion.	53

TABLE OF CONTENTS (Continued)

Chapter	Page
Solution Procedure	54
Computer Code.	56
Summary of Dynamic Analysis Model.	59
V. RESPONSE OF THE MODEL	60
General.	60
Response to Regular Waves.	60
Time Histories.	61
Response Spectra.	61
Parametric Study.	76
Wave Height.	76
Water Depth.	76
Cable Stiffness.	80
Initial Tension.	80
Direction of Wave Propagation.	83
Illustration of Nonlinearity and Coupling.	88
Summary of Response to Regular Waves	91
Response to Random Waves	93
Time Histories.	93
Effect of Drift Forces.	100
Response to Earthquake Forces.	101
Horizontal Component.	104
Time Histories	104
Initial Conditions	108
Water Depth.	110

TABLE OF CONTENTS (Continued)

Chapter	Page
	Comparison with Response to Waves. 112
	Vertical Component. 115
	Summary of Response to Earthquakes. 120
VI.	SUMMARY, CONCLUSIONS AND RECOMMENDATIONS. 122
	Summary. 122
	Conclusions. 123
	Recommendations. 125
	REFERENCES. 127
	APPENDIX A: DERIVATION OF WAVE FORCES. 131
	Horizontal Forces. 131
	Inertia Force on Columns. 131
	Drag Force on Columns 133
	Inertia Forces on Hulls and Cross Bracings. . . 135
	Drag Forces on Hulls and Cross Bracings 137
	Heave Forces 140
	Vertical Inertia Force on Hulls 140
	Vertical Drag Force on Hulls. 142
	Dynamic Pressure on Corner Column Bases 144
	Forces Producing Pitch and Roll. 145
	Moments Due to Inertia Force on Columns 145
	Moments Due to Drag Force on Columns. 145
	Pitch Moment from Horizontal Inertia and Drag Forces on Hulls 148
	Roll Moment from Horizontal Inertia and Drag Forces on Hulls 148

TABLE OF CONTENTS (Continued)

Chapter	Page
Pitch Moment from Vertical Inertia and Drag Forces on Hulls	148
Roll Moment from Vertical Inertia and Drag Forces on Hulls	153
Pitching Moment from Dynamic Pressure on Corner Column Bases	154
Rolling Moment from Dynamic Pressure on Corner Column Bases	154
Yaw Moments	154
Limits for $\alpha = 0^\circ$ and $\alpha = 90^\circ$	155
Limits of Hull Forces for $\alpha = 0^\circ$	155
Limits of Hull Forces for $\alpha = 90^\circ$	157
APPENDIX B: DERIVATION OF EARTHQUAKE FORCES	159
Fluid Inertia and Drag Forces Due to Interaction	159
Inertia Forces on Columns	159
Drag Forces on Columns	160
Inertia Forces on Hulls	163
Moments Due to Inertia Forces on Hulls	163
Drag Forces on Hulls	164
Moments Due to Drag Forces on Hulls	164
Yaw Moments	165
APPENDIX C: PLATFORM DATA	166
Data Used for Evaluation of Platform Motion	166
VITA	168

LIST OF TABLES

Table		Page
1	Variation "of Frequency Parameter" with Respect to Wave Period and Cylinder Diameter	28
2	Amplification Factors of a Sinusoidal Forcing Function $F = 1000 \sin (40 \pi t)$ Input at the Base of the Cable. . .	48
3	Amplification Factors of a Sinusoidal Forcing Function $F = 1000 \sin (20 \pi t)$ Input at the Base of the Cable. . .	49
4	Periods of Vibration and Response Amplitudes.	62
5	Maximum Values of Velocities and Accelerations.	62
6	Platform Response Amplitudes for Random Sea Loading . . .	100
7	Response to Vertical Ground Motion.	120

LIST OF FIGURES

Figure		Page
1	Typical Tension-Leg Platform.	7
2	Coordinate System and Structural Degrees of Freedom . . .	9
3	Buoy with a Unit Displacement in the Surge Direction. . .	9
4	Static Equilibrium Forces	11
5	Forces Resulting from a Surge Displacement.	11
6	Restoring Forces: a) at Equilibrium Position b) after Heave Displacement.	13
7	Restoring Forces Corresponding to a Pitch Rotation. . . .	15
8	Horizontal Restoring Forces Corresponding to a Yaw Rotation.	18
9	Leg Forces Resulting from a Yaw Rotation.	18
10	Schematic Diagram of Elementary, Sinusoidal Progressive Waves	25
11	Formation of Irregular Sea Waves.	30
12	Pierson-Moskowitz Sea Spectrum.	33
13	JONSWAP Sea Spectrum.	33
14	Velocity of Element dz Along ith Column Arising from Pitch or Roll	39
15	Modeling of TLP for Horizontal Ground Motion.	44
16	Forces on the Platform Caused by Horizontal Ground Motion.	44
17	Amplitudes of Propagated Wave in the Cable for Different Damping Ratios; $F = 1000 \sin(40 \pi t)$	50
18	Amplitudes of Propagated Waves in the Cable for Different Damping Ratios; $F = 100 \sin(20 \pi t)$	51
19	Flow Chart of Computer Program.	57
20	Time History Plot of Surge Displacement (including Inertia and Drag Forces).	63

LIST OF FIGURES (Continued)

Figure		Page
21	Time History Plot of Sway Displacement (including Inertia and Drag Forces).	63
22	Time History Plot of Heave Displacement (including Inertia and Drag Forces).	64
23	Time History Plot of Pitch Displacement (including Inertia and Drag Forces).	64
24	Time History Plot of Roll Displacement (including Inertia and Drag Forces).	65
25	Time History Plot of Yaw Displacement (including Inertia and Drag Forces).	65
26	Time History Plot of Surge Displacement (including only Inertia Forces).	66
27	Time History Plot of Sway Displacement (including only Inertia Forces).	66
28	Time History Plot of Heave Displacement (including only Inertia Forces).	67
29	Time History Plot of Pitch Displacement (including only Inertia Forces).	67
30	Time History Plot of Roll Displacement (including only Inertia Forces).	68
31	Time History Plot of Yaw Displacement (including only Inertia Forces).	68
32	Response Spectrum for Surge Displacement.	70
33	Response Spectrum for Sway Displacement	70
34	Response Spectrum for Heave Displacement for $\alpha = 0^\circ$	72
35	Response Spectrum for Heave Displacement for $\alpha = 90^\circ$	72
36	Time History of Coupled Heave Response.	73
37	Time History of Uncoupled Heave Response.	73
38	Response Spectrum of Pitch Rotation	74

LIST OF FIGURES (Continued)

Figure		Page
39	Response Spectrum of Roll Rotation.	74
40	Response Spectrum of Yaw Rotation	75
41	Variation of Surge Response Amplitude with Wave Height. .	75
42	Variation of Heave Response Amplitude with Wave Height. .	77
43	Variation of Pitch Response Amplitude with Wave Height. .	77
44	Variation of Sway Response Amplitude with Water Depth . .	78
45	Variation of Heave Response Amplitude with Water Depth. .	78
46	Variation of Roll Response Amplitude with Water Depth . .	79
47	Variation of Surge Response Amplitude with Cable Stiffness	79
48	Variation of Heave Response Amplitude with Cable Stiffness	81
49	Variation of Pitch Response Amplitude with Cable Stiffness	82
50	Variation of Sway Response Amplitude with Initial Tension	84
51	Variation of Heave Response Amplitude with Initial Tension	85
52	Variation of Roll Response Amplitude with Initial Tension	86
53	Variation of Surge or Sway with the Direction of Wave Propagation.	87
54	Variation of Heave with the Direction of Wave Propagation	89
55	Variation of Pitch and Roll with the Direction of Wave Propagation.	89
56	Variation of Yaw with the Direction of Wave Propagation	90

LIST OF FIGURES (Continued)

Figure		Page
57	Plot of Cable Restoring Force for Surge Displacement. . .	90
58	Plot of Cable Restoring Force for Pitch Displacement. . .	92
59	Plot of Cable Restoring Force for Heave Displacement. . .	92
60	Wave Profile Corresponding to Pierson-Moskowitz Spectrum.	94
61	Wave Profile Corresponding to JONSWAP Spectrum.	94
62	Time History Plot of Surge Response to Pierson- Moskowitz Spectrum (U = 20 m/sec)	95
63	Time History Plot of Heave Response to Pierson- Moskowitz Spectrum (U = 20 m/sec)	95
64	Time History Plot of Pitch Response to Pierson- Moskowitz Spectrum (U = 20 m/sec)	96
65	Time History Plot of Surge Response to Pierson- Moskowitz Spectrum (U = 30 m/sec)	96
66	Time History Plot of Heave Response to Pierson- Moskowitz Spectrum (U = 30 m/sec)	97
67	Time History Plot of Pitch Response to Pierson- Moskowitz Spectrum (U = 30 m/sec)	97
68	Time History Plot of Surge Response to JONSWAP Spectrum .	98
69	Time History Plot of Heave Response to JONSWAP Spectrum .	98
70	Time History Plot of Pitch Response to JONSWAP Spectrum .	99
71	Time History Plot of Surge Drift Force Using JONSWAP Sea Spectrum.	99
72	Time History Plot of Surge Response to Combined Drift Forces and Random Waves Using JONSWAP Spectrum.	102
73	Time History Plot of Heave Response to Combined Drift Forces and Random Waves Using JONSWAP Spectrum.	102
74	Time History Plot of Pitch Response to Combined Drift Forces and Random Waves Using JONSWAP Spectrum.	103

LIST OF FIGURES (Continued)

Figure		Page
75	Acceleration Time History for the East-West Component of El Centro, 1940.	105
76	Time History of Surge Response for El Centro Earthquake .	106
77	Time History of Heave Response for El Centro Earthquake .	106
78	Time History of Pitch Response for El Centro Earthquake .	107
79	Time History of Surge Response to the S16E Component of Pacoima Dam Record of San Fernando Earthquake, 1971 . . .	107
80	Time History of Surge Response to Combined El Centro Earthquake and 17 Second Wave	109
81	Time History of Surge Response to Combined 17 Second Wave and El Centro Earthquake Loading with Earthquake Introduced at Different Times	109
82	Time History of Surge Response to El Centro in 1000 m Water Depth	111
83	Variation of Surge Response with Water Depth for 17 Second Wave, El Centro Earthquake, and Combined Loading	111
84	Variation of Heave Response with Water Depth for 17 Second Wave, El Centro Earthquake, and Combined Loading	113
85	Comparison of Surge Response to 17 Second Wave with that from Combined Loading in 1000 m Water Depth.	113
86	Time History of Surge Response to 17 Second Wave and Combined Loadings with El Centro Earthquake Introduced at $t = 200$ Seconds.	114
87	Time History of Heave Response to El Centro (Vertical) Earthquake.	114
88	Time History of Heave Velocity Response to El Centro (Vertical) Earthquake	116
89	Time History of Heave Acceleration Response to El Centro (Vertical) Earthquake.	116

LIST OF FIGURES (Continued)

Figure		Page
90	Time History of Heave Response to Pacoima Dam (Vertical) Earthquake	117
91	Time History of Heave Velocity Response to Pacoima Dam (Vertical) Earthquake	117
92	Time History of Heave Acceleration Response to Pacoima Dam (Vertical) Earthquake	118
93	Time History of Heave Response to Taft Lincoln School (Vertical) Earthquake	118
94	Time History of Heave Velocity Response to Taft Lincoln School (Vertical) Earthquake.	119
95	Time History of Heave Acceleration Response to Taft Lincoln School (Vertical) Earthquake.	119

CHAPTER I

INTRODUCTION

Objective

Offshore production platforms have been manufactured predominantly as fixed steel template jackets or concrete gravity structures for operations in water depths up to 300 meters. Manufacturing, installation, and maintenance costs of fixed platforms rise rapidly as water depths increase. Recently, however, attention has been focused on the design of tension-leg platforms. Relatively small increases in manufacturing and installation costs with added water depth make the tension-leg platform an attractive alternative for deep water production.

The design of tension-leg production platforms requires an understanding of the dynamic behavior of the structure during storm waves, wind, ground motion conditions, etc. In order to design a reliable structure, it is necessary for the engineer to take into account the effect of platform motion on personnel, equipment, and operations. It is also necessary to take into account the anchoring system and the forces in the mooring legs produced by wave actions and platform motions.

The primary objective of this research is to develop a complete and accurate deterministic approach for the dynamic analysis of tension-leg platforms (TLP's) subjected to wave forces and ground motion. A mathematical model is developed based on a set of coupled nonlinear

The format of this dissertation follows the style of the Journal of the Structural Division, ASCE.

differential equations for sway, surge, heave, pitch, roll, and yaw motions. The nonlinearity of the coupled differential equations of motion makes a power spectral analysis in the frequency domain infeasible. Thus, a time domain analysis was selected for investigating the dynamic characteristics of the anchored structure. The advantage of this approach is that nonlinear functional relationships, which require approximations in the spectral models, can be handled exactly in the time domain.

The time domain dynamic analysis model developed herein is capable of obtaining the following:

- 1) Time histories of displacement response in the direction of all degrees of freedom (surge, sway, heave, pitch, roll, and yaw) when the platform is subjected to wave loading and/or ground motion.
- 2) Response spectra (i.e., variation of response amplitudes with respect to wave period) for all degrees of freedom.
- 3) Effects of variations in several different parameters.
- 4) Effects of coupling and nonlinearities.

Research Plan

In order to accomplish the objectives set forth in this project, the following research plan was developed and undertaken:

- 1) Literature search and choice of the most appropriate dynamic analysis of TLP's.
- 2) The development of a deterministic dynamic analysis model.
- 3) Verification of mathematical model.

4) Parametric studies to identify design criteria.

Many attempts have been made to simulate, or calculate, the dynamic response of tension-leg platforms. A review of previous work was undertaken with the objective of sorting out the important parameters influencing the structure's behavior. Previous attempts to model the response of tension-leg platforms have neglected either coupling or nonlinearities or both, and none have addressed the possible effects of ground motion.

The development of a complete deterministic dynamic analysis model involves the formulation of a nonlinear stiffness matrix, selection of a suitable wave theory, derivation of complete forcing functions, selection of an efficient numerical method capable of carrying out the solution of nonlinear coupled differential equations in the time domain, and development of an appropriate computer code to perform the dynamic response calculations. Wave forces and ground motion are two of the environmental loadings which could be applied to the offshore structure. Time histories of the complete response of the model to these environmental forces are generated. A parametric study is carried out in an effort to determine the significant design parameters that need to be considered in the design and analysis of tension-leg platforms.

Review of Previous Research

Various methods of dynamic analysis for offshore structures subjected to wave loading have been presented in recent technical literature (2, 5, 6, 12, 14, 22-24, 31, 35, 38). Linear or piecewise linear mathematical models to analyse response in the frequency domain have

been employed by many researchers (2, 5, 14, 24, 31, 38); whereas nonlinear time domain analyses were performed by others (6, 12, 23, 35).

Frequency domain or spectral analysis models are based on a linear formulation of the dynamic problem. Nonlinear terms inherent in the forcing function, and the relative displacement, velocity, and acceleration between the structure and the fluid particles are neglected. Wave forces are integrated up to the mean water level and at the original position of the platform. It is also assumed in frequency domain analysis that coupling between degrees of freedom can be neglected or taken into account by linear superposition. Moreover, spectral models are capable only of finding maximum response amplitudes, and not time histories of the response as is the case in time domain analyses.

Nonlinear and coupling effects are important and can have significant effects on the structure's dynamic behavior. Time domain (or deterministic) models are capable of handling all kinds of nonlinearities. In time domain analysis force integration is carried out up to the instantaneous wetted surface and at the displaced and rotated position of the platform. The benefits of time domain analysis include the ability to incorporate any type of nonlinearity in force which can be adequately described, and the availability of response time histories to aid in assessment of the effects of coupling between degrees of freedom. Such nonlinear and coupling effects cannot be easily included in a frequency domain even with approximations such as equivalent linearization or linear superposition.

Previous nonlinear deterministic models did not account for all types of nonlinearity and coupling. Typically they included a numerical

integration of wave force equations along each segment of the platform at each iteration for every time step. Some also included a nonlinear finite element formulation to describe the nonlinear stiffness of the anchor lines. These analyses are generally very expensive. The current model attempts to eliminate or minimize the effects of the following assumptions which are common to most published analyses:

- 1) Equivalent linearization of nonlinear terms in the anchoring stiffness and fluid drag forces.
- 2) Neglecting coupling effects between degrees of freedom.
- 3) Numerical integration of wave forces at every time step.
- 4) Omission of ground motion in the forcing functions.

Frequency domain analysis is inexpensive and may be adequate for a preliminary look at the dynamics of the problem but it is not sufficient for a complete and accurate prediction of a coupled nonlinear response of the structure. Hence, a deterministic approach is needed to account for the nonlinear and coupled behavior involved in the problem. The complete deterministic model presented in this research attempts to satisfy the requirements listed above and to include the effects of ground motion as well as water waves.

CHAPTER II

FORMULATION OF STIFFNESS

General

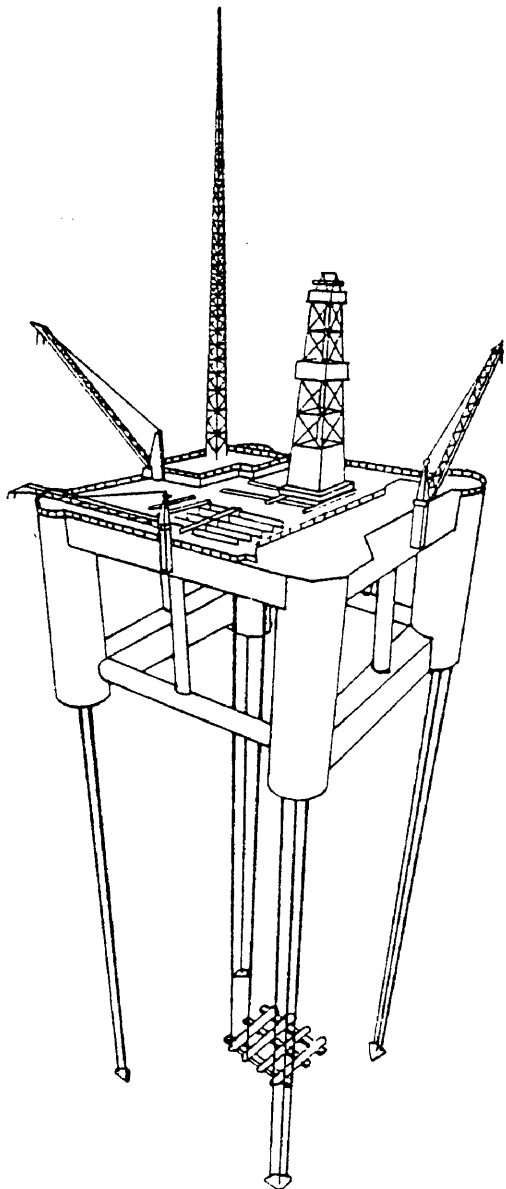
A review of previous work related to dynamic analysis of TLP's indicates a need for a complete nonlinear deterministic dynamic analysis model. The development of such a model involves the formulation of a nonlinear stiffness matrix which describes the behavior of the anchoring cables and buoyant forces. The model developed in this research utilizes nonlinear stiffness coefficients based on derived stiffness-displacement relationships which are functions of the instantaneous position of the structure. These stiffness functions are coupled as well as nonlinear.

The tension-leg platform considered in this model consists of four corner columns which are linked to vertical tethers, four middle columns, two main hulls, and two cross bracings (see Figure 1). Specifications of the structure dimensions, masses, mass moments of inertia, added masses, center of gravity, depth of submergence (draft), cable stiffness and initial cable tension are required to complete the description of the TLP. This chapter presents details of the development of a complete nonlinear stiffness formulation.

Derivation of Nonlinear Stiffness

Degrees of Freedom

Since the structure is considered as a rigid body, the motion will consist of six degrees of freedom: three translational and three



- Corner Column - 16 m
- Middle Column - 3.5 m
- Hulls - 13 x 9.5 m
- Cross Braces - 16 m

Figure 1. Typical Tension-Leg Platform

rotational. The coordinate axes and the degrees of freedom used in the analysis are presented in Fig. 2. Surge, sway, and heave are defined as the horizontal motion along the x-axis, the horizontal motion along the y-axis, and the vertical motion along the z-axis, respectively. Pitch, roll, and yaw are defined as the rotational motion about the y-axis, the rotational motion about the x-axis, and the rotational motion about the z-axis, respectively. For the purpose of this report, the surge, sway, heave, pitch, roll, and yaw are numbered 1 through 6, respectively.

Derivation of Stiffness Coefficients

A nonlinear stiffness matrix $[K]$ including all six degrees of freedom is formulated, where k_{ij} is the force in degree of freedom "i" due to an arbitrary displacement in the direction of degree of freedom "j", with all other degrees of freedom restrained. To derive the nonlinear stiffness coefficients, each degree of freedom is given an arbitrary displacement and the forces developed constitute the coefficients in the corresponding column of the stiffness matrix. The coefficients of the first column of the stiffness matrix are found by giving the structure an arbitrary displacement x in the surge direction as shown in Figure 3. The static equilibrium forces exerted on the structure at its original position are shown in Figure 4. The static equilibrium forces are the weight of the structure, W , the buoyancy force, B , and the initial tension (or pretensioning force), $4T_0$. Through summation of forces in the vertical direction one obtains:

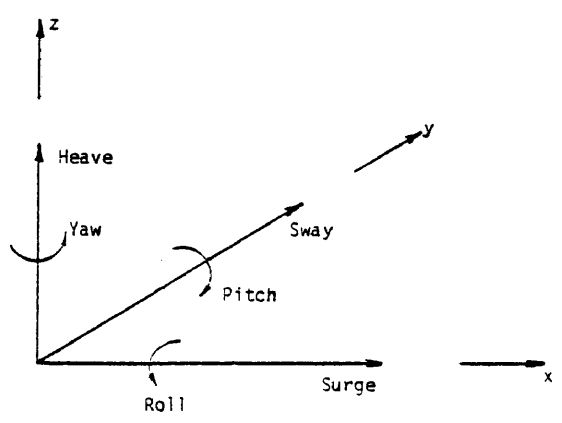


Fig. 2 - Coordinate System and Structural Degrees of Freedom

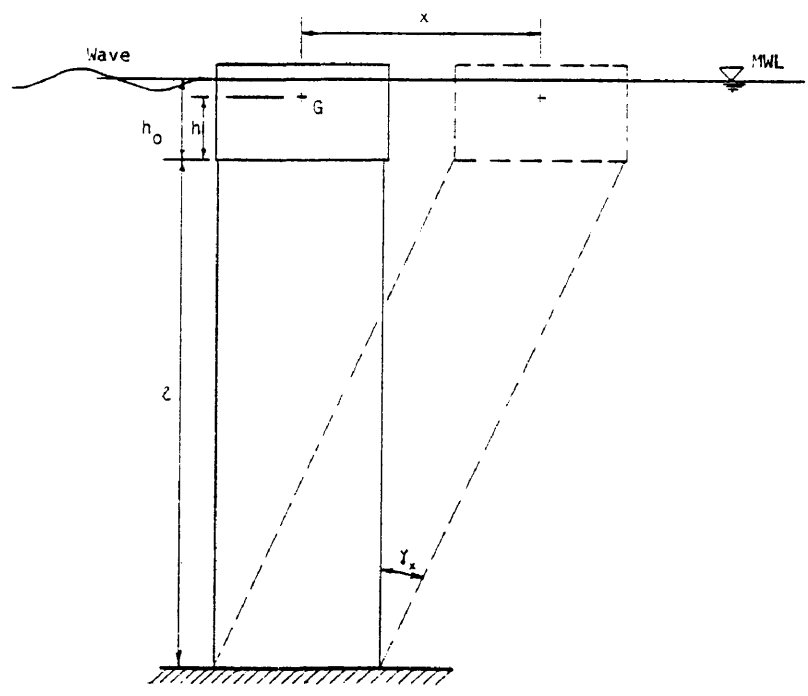


Fig. 3 - Buoy with a Unit Displacement in the Surge Direction

$$\begin{aligned}
 +\uparrow \Sigma F_z &= 0 \\
 \Rightarrow F_B - 4T_0 - W &= 0 .
 \end{aligned} \tag{1}$$

The forces acting on the structure with a displacement, x , in the direction of surge are shown in Figure 5. A sum of forces in the x -direction yields:

$$\begin{aligned}
 \pm \Sigma F_x &= 0, \\
 k_{11} - 2[2(T_0 + \Delta T_1)_x] &= 0, \text{ and} \\
 k_{11} &= 4(T_0 + \Delta T_1) \sin \gamma_x,
 \end{aligned} \tag{2}$$

where T_0 is the value of the initial tension in each leg, ΔT_1 , is the increase in tension in each leg from the x -displacement, and γ_x is the angle of inclination of the legs with respect to the vertical, and it is given by:

$$\sin \gamma_x = \frac{x}{l'} = \frac{x}{\sqrt{l^2 + x^2}} .$$

The elongation in the chain length is

$$\Delta l_1 = l' - l = \sqrt{l^2 + x^2} - l,$$

hence

$$\Delta T_1 = k_c \Delta l_1,$$

where k_c is the stiffness of the chain for each leg.

Now, summing the forces in the vertical direction gives:

$$\begin{aligned}
 +\uparrow \Sigma F_z &= 0, \\
 k_{31} + F_B - W - 2[2(T_0 + \Delta T_1)_z] &= 0, \text{ and} \\
 k_{31} + (F_B - W) - 4(T_0 + \Delta T_1) \cos \gamma_x &= 0,
 \end{aligned}$$

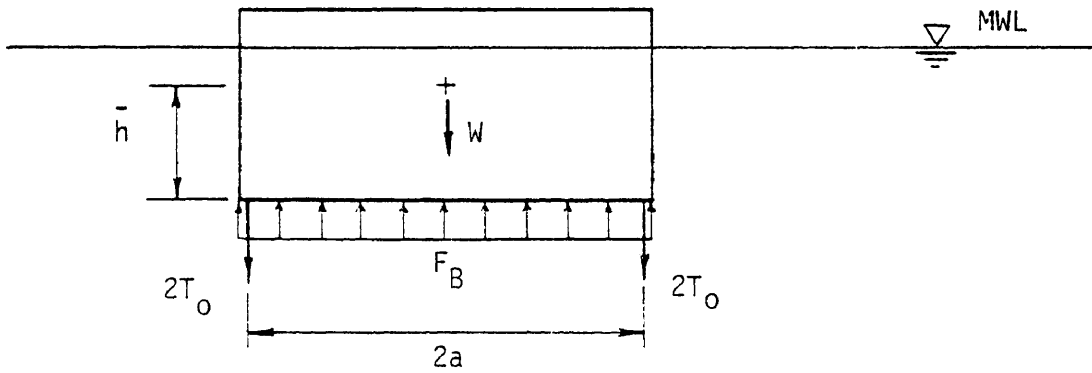


Fig. 4 - Static Equilibrium Forces

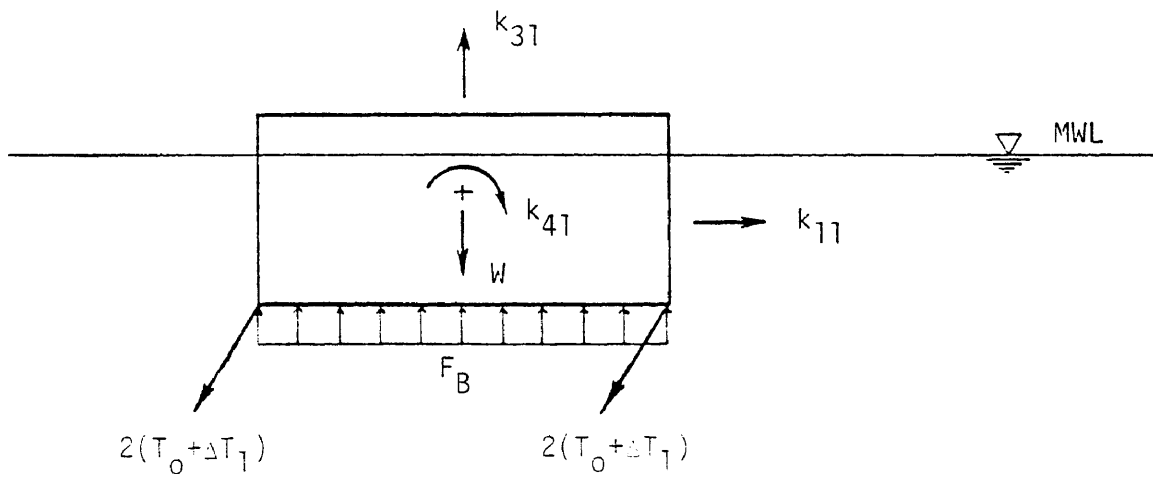


Fig. 5 - Forces Resulting from a Surge Displacement

where

$$\cos \gamma_x = \frac{\ell}{\ell'} = \frac{\ell}{\sqrt{\ell^2 + x^2}} .$$

Recalling Equation (1), $F_B - W = 4T_0$,

$$k_{31} = 4T_0(\cos \gamma_x - 1) + 4 \Delta T_1 \cos \gamma_x . \quad (3)$$

In summing the moments about the y-axis vertical forces produce no moment; therefore only horizontal components of the tension in the chain are considered:

$$\begin{aligned} \curvearrowright + M_G &= 0, \\ k_{41} + 4(T_0 + \Delta T_1)_x (\bar{h}) &= 0, \\ \Rightarrow k_{41} &= -4(T_0 + \Delta T_1) \sin \gamma_x (\bar{h}) . \end{aligned}$$

Combining this with Equation (2) yields:

$$k_{41} = -\bar{h}k_{11} . \quad (4)$$

The coefficients of the second column of the stiffness matrix are found by giving the structure an arbitrary displacement in the sway direction with all other degrees of freedom (d.o.f.'s) restrained. The coefficients are identical to those of the first column with change in notations as follows:

$$k_{22} = 4(T_0 + \Delta T_2) \sin \gamma_y , \quad (5)$$

$$k_{32} = 4T_0(\cos \gamma_y - 1) + \Delta T_2 \cos \gamma_y , \text{ and} \quad (5)$$

$$k_{52} = + \bar{h} k_{22} ; \quad (7)$$

where

$$\sin \gamma_y = \frac{y}{\sqrt{l^2 + y^2}} ,$$

$$\cos \gamma_y = \frac{l}{\sqrt{l^2 + y^2}} ,$$

and

$$\Delta_T = k_c (\sqrt{l^2 + y^2} - l) .$$

The coefficients of the third column of the stiffness matrix are found by giving the structure an arbitrary displacement in the heave direction, keeping all other d.o.f.'s restrained. The corresponding forces acting on the structure are shown in Figure 6. A sum of forces in the z-direction yields:

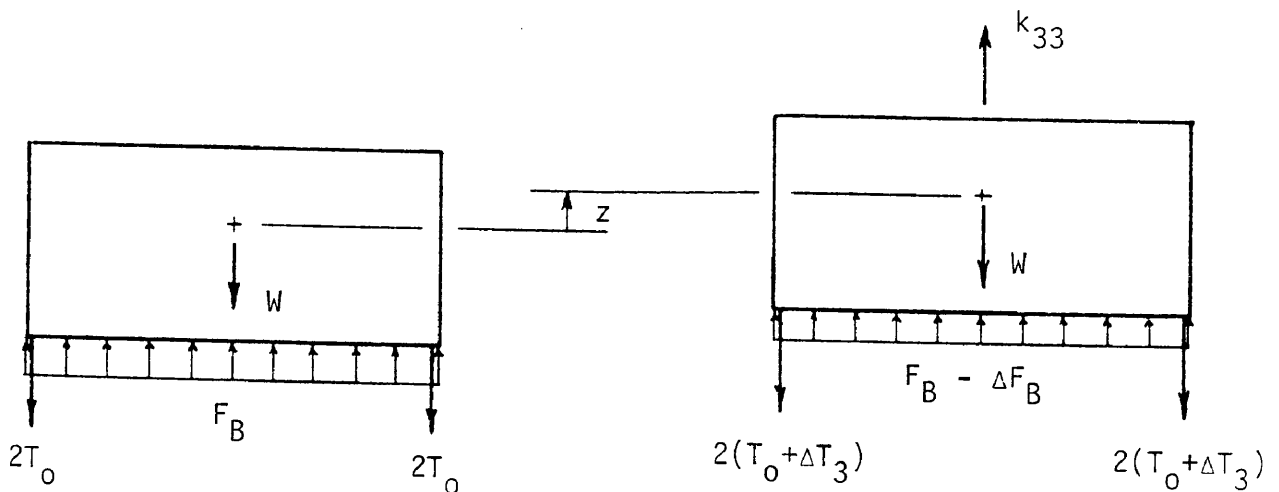


Fig. 6 - Restoring Forces: a) at Equilibrium Position
b) after Heave Displacement

$$+\uparrow \Sigma F_z = 0 ,$$

$$k_{33} - W - 4(T_0 + \Delta T_3) + (F_B - \Delta F_B) = 0 , \text{ and}$$

$$k_{33} + (F_B - W - T_0) - \Delta F_B - 4\Delta T_3 = 0 .$$

However, $(F_B - W - 4T_0) = 0$ from Equation (1); therefore,

$$k_{33} = \Delta F_B + 4\Delta T_3 , \quad (8)$$

where $\Delta F_B = \rho g \Delta V$, ρ is the mass density of water, g is the acceleration of gravity, ΔV is the change in submerged volume, and ΔT_3 is the change in tension in each leg arising from heave.

The coefficients of the fourth column of the stiffness matrix are found by giving the structure an arbitrary rotation about the y-axis with all other d.o.f.'s restrained. Figure 7 shows the corresponding forces acting on the structure. Summing the moments about the y-axis gives:

$$\curvearrowright +\Sigma M_G = 0$$

$$k_{44} - F_B e_4 - 2(T_0 + \Delta T_4) r + 2(T_0 - \Delta T_4) s = 0$$

which can be written as:

$$k_{44} = F_B e_4 + 2 \Delta T_4 r + 2 \Delta T_4' + 2 T (r-s), \quad (9)$$

where e_4 is the eccentricity of the buoyancy force calculated according to the formula $e_4 = \frac{I_y}{V}$, where I_y is the moment of inertia of the cross section of the structure intersecting the water surface, about the y-axis, and V is the volume of the submerged portion of the structure.

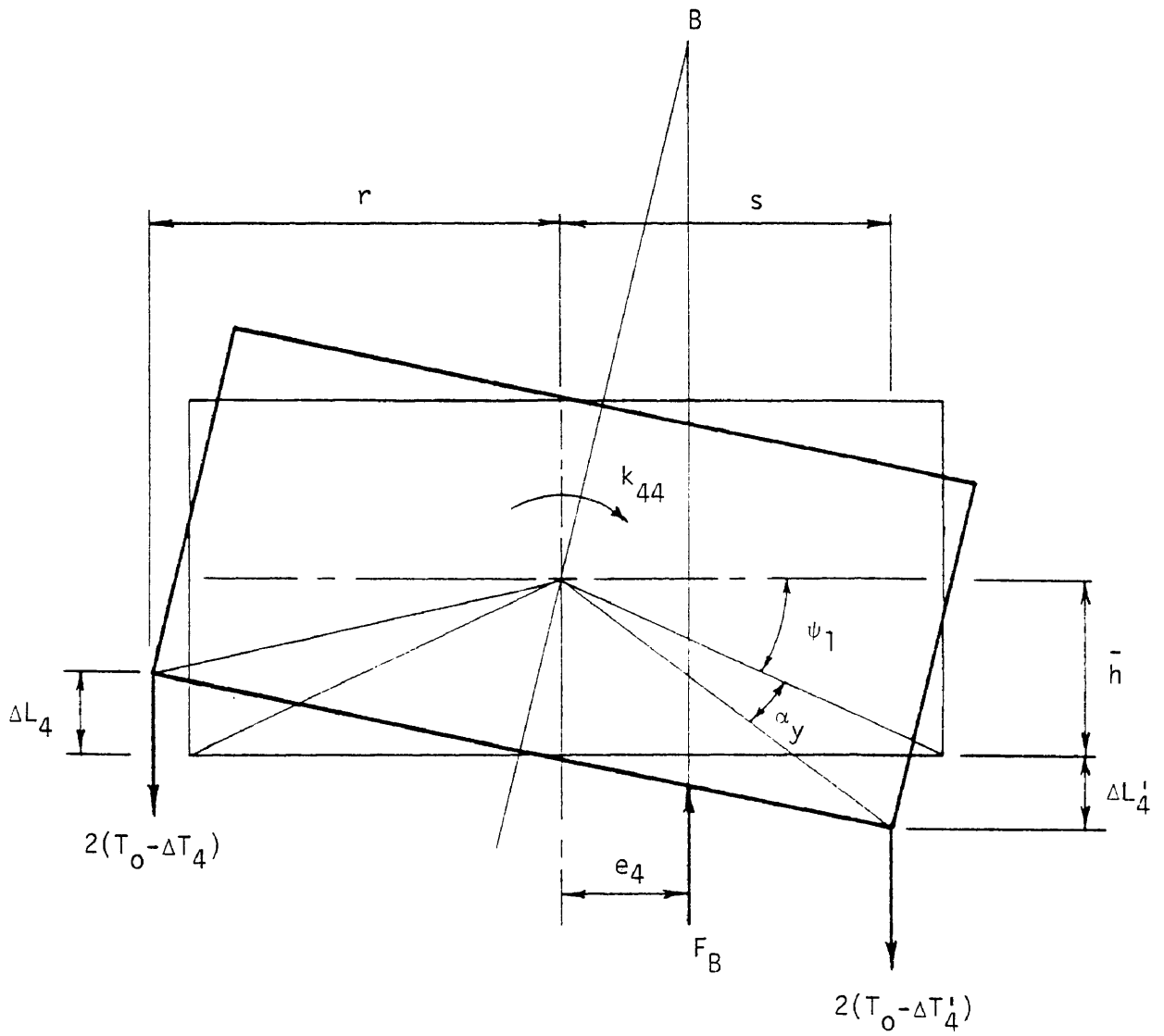


Fig. 7 - Restoring Forces Corresponding to a Pitch Rotation

From geometry (see Figure 7) d , r , s , ψ_1 , ΔL_4 , and $\Delta L_4'$ are calculated as follows:

$$d_1 = \sqrt{\bar{h}^2 + a^2} \quad ,$$

$$r = d_1 \cos (\psi_1 - \alpha_y) \quad ,$$

$$s = d_1 \cos (\psi_1 + \alpha_y) \quad ,$$

$$\psi_1 = \tan^{-1} (\bar{h}/a) \quad ,$$

$$\Delta L_4 = \bar{h} - d_1 \sin (\psi_1 - \alpha_y) \quad , \text{ and}$$

$$\Delta L_4' = d_1 \sin (\psi_1 + \alpha_y) - \bar{h} \quad .$$

Summing the forces in the vertical direction gives:

$$+\uparrow \Sigma F_z = 0 \quad ,$$

$$k_{34} + F_B - 2(T + \Delta T_4) - 2(T - \Delta T_4') - W = 0 \quad ,$$

$$k_{34} + (F_B - 4T - W) - 2\Delta T_4 + 2\Delta T_4' = 0 \quad ,$$

$$k_{34} = 2 \Delta T_4 - 2 \Delta T_4' \quad , \tag{10}$$

where $\Delta T_4 = k_c \Delta L_4$ and $\Delta T_4' = k_c \Delta L_4'$

The coefficients of the fifth column of the stiffness matrix are found by imposing an arbitrary rotation about the x-axis, keeping all other d.o.f.'s restrained. The resulting coefficients are identical to those of the fourth column with a change in notation as follows:

$$k_{55} = F_B e_5 + 2 \Delta T_5 u + 2 \Delta T_5' v + 2T(u - v), \text{ and} \quad (11)$$

$$k_{35} = 2 \Delta T_5 - 2 \Delta T_5' , \quad (12)$$

where

$$d_2 = \sqrt{\bar{h}^2 + b^2} ,$$

$$u = d_2 \cos (\psi_2 + \alpha_x) ,$$

$$v = d_2 \cos (\psi_2 - \alpha_x) ,$$

$$\psi_2 = \tan^{-1} (\bar{h}/b) ,$$

$$\Delta L_5 = \bar{h} - d_2 \sin (\psi_2 - \alpha_x) ,$$

$$\Delta L_5' = d_2 \sin (\psi_2 + \alpha_x) - \bar{h} ,$$

$$\Delta T_5 = k_c \Delta L_5 ,$$

and $\Delta T_5' = k_c \Delta L_5' .$

The coefficients of the sixth column of the stiffness matrix are found by giving the structure an arbitrary rotation about the z-axis with all other d.o.f.'s restrained. The forces acting on the structure arising from yaw rotation are depicted in Figure 8.

A sum of the moments about the z-axis gives:

$$\left(\overset{\curvearrowright}{+\Sigma M_z} = 0 \right) ,$$

$$k_{66} - 4(T + \Delta T_6) \phi \sqrt{a^2 + b^2} = 0 , \text{ and}$$

$$k_{66} = 4(T + \Delta T_6) \frac{\phi(a^2 + b^2)}{\sqrt{\ell^2 + \phi^2(a^2 + b^2)}} , \quad (13)$$

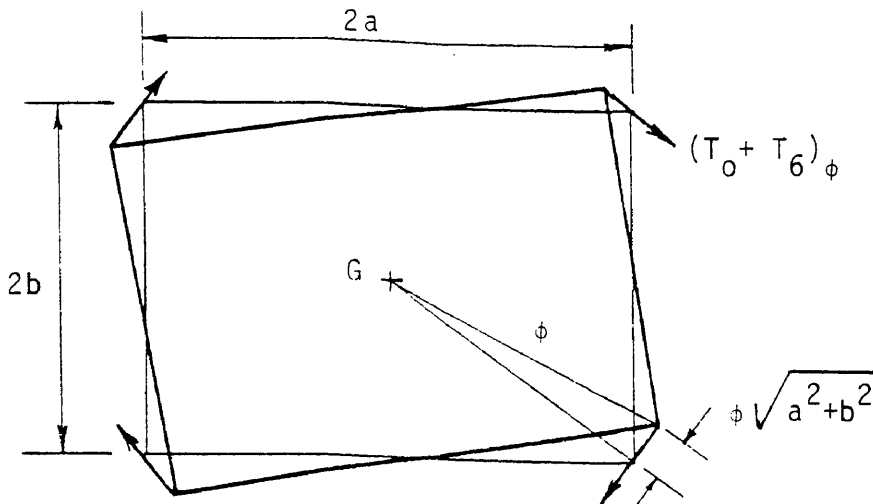


Fig. 8 - Horizontal Restoring Forces Corresponding to a Yaw Rotation

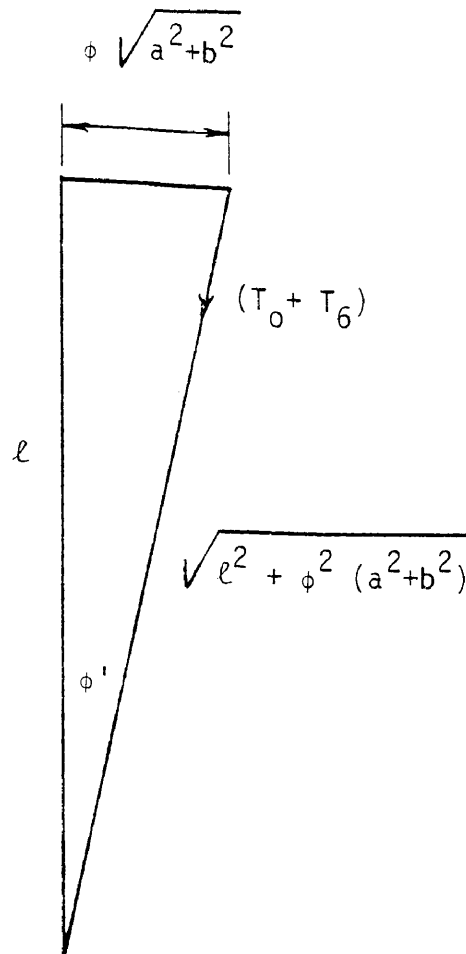


Fig. 9 - Leg Forces Resulting from a Yaw Rotation

where

$$\frac{\phi \sqrt{a^2 + b^2}}{\sqrt{\ell^2 + \phi^2(a^2 + b^2)}} = \sin \phi' , \text{ and}$$

$$\Delta T_6 = k_c (\ell^2 + \phi^2 (a^2 + b^2) - \ell) .$$

A summation of forces in the vertical direction gives:

$$\uparrow + \Sigma F_z = 0 , \text{ and}$$

$$k_{36} + F_B - W - 4(T + \Delta T_6) \cos \phi' = 0 ;$$

but $F_B - W = 4T_0$; therefore,

$$k_{36} = 4T (\cos \phi' - 1) + 4 \Delta T_6 \cos \phi' , \quad (14)$$

where

$$\cos \phi' = \frac{\ell}{\sqrt{\ell^2 + \phi^2(a^2 + b^2)}} \quad (\text{see Figure 9}) .$$

Two significant aspects can be noted concerning the derived stiffness coefficients: coupling and nonlinearity. Coupling terms are the nondiagonal coefficients of the stiffness matrix. Heave is coupled to surge, sway, pitch, roll, and yaw, respectively (Equations (3), (6), (10), (12), and (14)). Further, pitch is coupled to surge, (Equation (4)), and roll is coupled to sway (Equation (7)).

The stiffness matrix, including all of the coupling terms detailed above, is:

$$\begin{array}{l}
 \text{Surge} \\
 \text{Sway} \\
 \text{Heave} \\
 \text{Pitch} \\
 \text{Roll} \\
 \text{Yaw}
 \end{array}
 \begin{bmatrix}
 k_{11} & 0 & 0 & 0 & 0 & 0 \\
 0 & k_{22} & 0 & 0 & 0 & 0 \\
 k_{31} & k_{32} & k_{33} & k_{34} & k_{35} & k_{36} \\
 k_{41} & 0 & 0 & k_{44} & 0 & 0 \\
 0 & k_{52} & 0 & 0 & k_{55} & 0 \\
 0 & 0 & 0 & 0 & 0 & k_{66}
 \end{bmatrix}$$

As will be shown later in this report, coupling has a significant effect on the calculated response of the structure. Coupled equations of motion are intractable in frequency domain models, and nonlinear time domain analysis published in the literature generally neglected coupling effects.

As shown above, the stiffness matrix is asymmetric. This implies that some degrees of freedom are coupled to other degrees of freedom, but not vice versa. For example, this is apparent in the heave degree of freedom (third row and third column of the stiffness matrix). The heave row contains only nonzero terms; i.e., heave is coupled to surge, sway, pitch, roll, and yaw. However, the heave column contains only one nonzero term (k_{33}); i.e., as the structure moves in the vertical direction (heaves), there is no resulting motion in the other directions. By the same argument, pitch is coupled to surge, and roll is coupled to sway, but not vice versa. Moreover, other types of coupling occur between degrees of freedom as can be seen later in the derivation of the forcing functions.

Another significant aspect of the stiffness matrix is the non-linearity of its coefficients. For example, sine and cosine terms and

square and square root terms contribute to the nonlinearities of the stiffness coefficients (see Equations (1) through (14)). Since each coefficient k_{ij} is equal to the stiffness force at degree of freedom "i" due to an arbitrary (and not a unit) displacement in the direction of degree of freedom "j", the sum of coefficients in each row of the stiffness matrix will give the total stiffness force " K_i " of that particular degree of freedom. Hence,

$$K_i = \sum_{j=1}^6 k_{ij} \quad (15)$$

Here, $\{K\}$ represents a force vector equivalent to the product of the stiffness matrix and the displacement vector in a linear system.

CHAPTER III

ENVIRONMENTAL FORCES

General

Tension-leg platforms can be subjected to various environmental loads including waves, currents, earthquakes, wind, ice, etc. In this model, only wave and earthquake forces are considered. The effect of current on the dynamic effect of the TLP is small (Kirk & Etok, 1979), and hence it is not considered in this analysis. Dynamic effects of wind forces, however, are of significant importance in the analysis of TLP's (Kareem, 1980) but are out of the scope of this research.

The forces acting on the platform are classified as hydrostatic (arising from buoyancy), restoring stiffness (arising from the pre-tensioned cables), hydrodynamic, and inertial (arising from ground motion). The hydrodynamic forces consist of inertia and drag caused by wave particle acceleration and velocity, and of slowly varying drift (in irregular waves) caused by cross-modulation effects between wave frequency components in the sea spectrum. Earthquake excitations consist of horizontal and vertical base accelerations arising from earthquake ground motions.

Regular Waves

The formulation of wave forces involves the selection of a wave theory that yields a reasonable representation of the water waves in terms of particle kinematics. It also involves the selection of a force calculation method which utilizes the fluid particle velocities

and accelerations obtained from the wave theory to yield wave forces that agree well with experimental results and best represent the actual forces produced by the waves.

Selection of Wave Theory

Theoretical simulation of water waves, and of sea motion in general, involves rigorous mathematical analysis. The basic hydrodynamic equations that govern the wave kinematics are the equation of continuity (Laplace's equation) and the equation of momentum (Bernoulli's equation) (47). The form and solution of these equations vary, depending on the intended application of wave kinematics. However, in general, all solutions assume incompressible, inviscid, and irrotational fluid particles. The simplest solution of the hydrodynamic equations involves a further assumption, that the waves are of small amplitude ($H/2$) compared to the water depth (d) and the wavelength (L). This solution was introduced by Airy (Reference 1), and became known as the linear wave theory.

Higher order wave theories are not based on the assumption of small amplitude to solve the hydrodynamic equations. Instead, they include higher order terms (terms higher than first order) in the solution. Stokes (Ref. 49) developed equations for waves of finite amplitude by accounting for higher order terms. The Stokes wave theories have been developed for terms up to fifth order. The successively higher order theories give wave surface profiles that are steeper in the crests and flatter in the trough than those given by the linear wave theory. Dean (Ref. 11) developed the stream function wave theory.

This theory, which is a numerical one, has demonstrated good agreement with experimental wave channel test results for a wide range of H/T^2 ratios (Ref. 27). Many other analytical and numerical wave theories have been developed and can be found in the literature (see for example Refs. 9, 10, 25, 34).

The linear wave theory has been found to give wave forces close to those obtained using higher order wave theories, provided a proper method of calculating wave forces is used with a suitable choice of the fluid added mass and drag coefficients (Refs. 23, 24, 35). In addition, it has been shown to provide good solutions in deep water; i.e., for water depth to wave-length ratio greater or equal to 0.5 (Ref. 27). For the range of water depths, wave periods and wave heights used in this analysis the linear wave theory is applicable (Ref. 26). Therefore, the linear wave theory is used in this model because it is practical, easy to apply, reliable over a large segment of the whole wave regime, and sufficient to obtain the kinematics of waves to be used in the dynamic analysis of TLP's in deep water.

A schematic diagram of an elementary, sinusoidal progressive wave is presented in Fig. 10. In deep water, the velocity and acceleration of the fluid particle at depth z below the mean water level are respectively given by the linear wave theory as:

$$u = \frac{\pi H}{T} e^{-kz} \cos [k(\bar{X} - ct)] \quad (16)$$

and

$$\dot{u} = \frac{2\pi^2 H}{T^2} e^{-kz} \sin [k(\bar{X} - ct)] \quad (17)$$

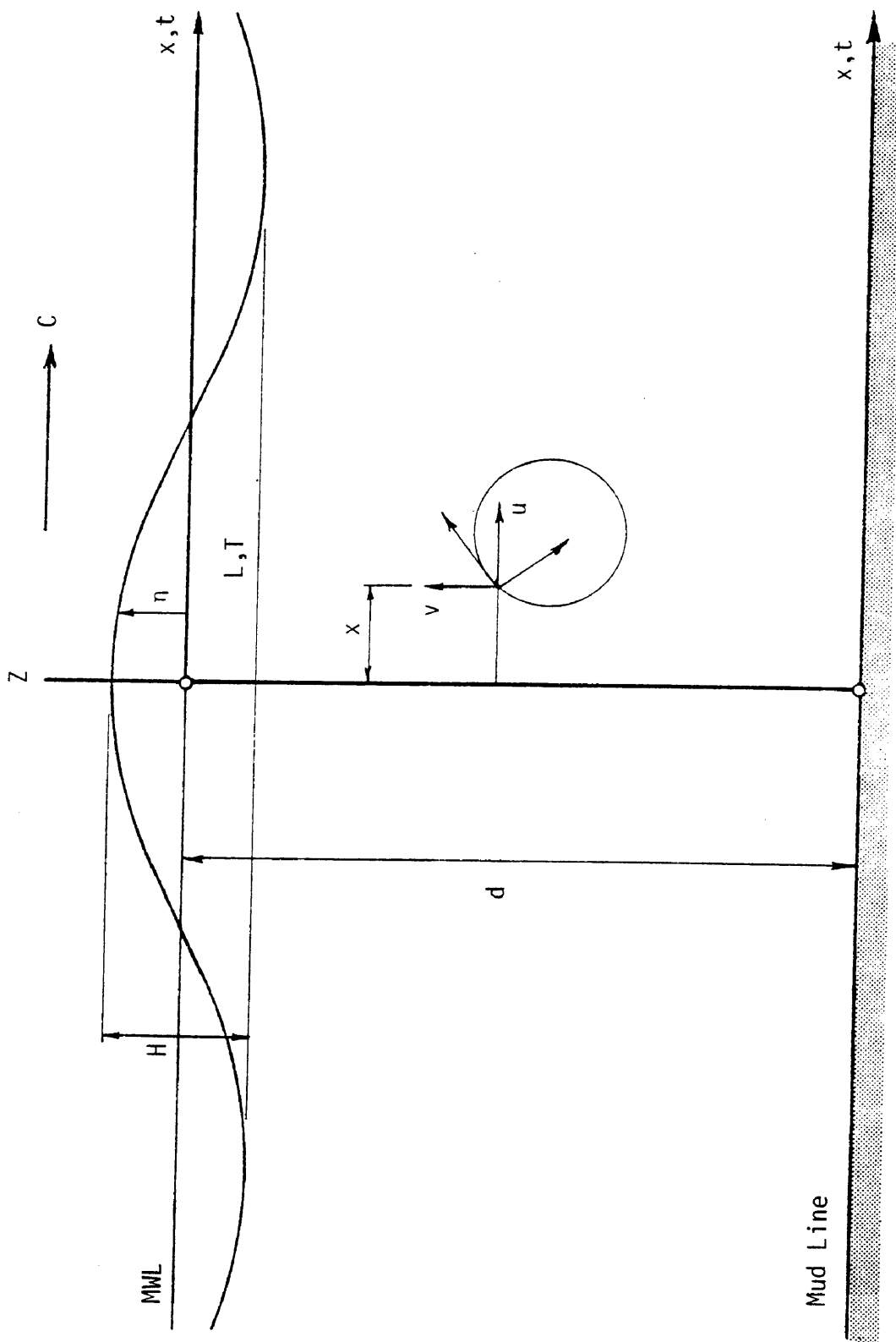


Fig. 10 - Schematic Diagram of Elementary, Sinusoidal Progressive Waves

where H , T , and c are the wave height, period, and celerity, respectively, and $k = 2\pi/\text{wavelength}$.

Justifications for Using Morison's Equation

Experimental studies by Morison, et al. (Ref. 33), led to the formulation of a wave force equation that became known as Morison's equation. This equation has been widely used in the last three decades in the calculation of wave forces on offshore structures. The equation consists of a drag term, as in the case of flow of constant velocity, and an inertia term due to the acceleration of the fluid particle.

The original form of Morison's equation is:

$$F = 0.5 \rho C_d D |U|U + C_m \rho \pi D^2/4 \frac{dU}{dt} \quad (18)$$

where F is the force per unit length experienced by a cylinder; U and dU/dt represent the undisturbed velocity and acceleration of the fluid, respectively; C_d and C_m are the drag and inertia coefficients, and ρ is the fluid mass density.

Morison's equation has been widely accepted for force computations because of good correlation with experimental results in a large number of practical cases. However, the use of Morison's equation gave rise to a great deal of discussion on what values of the two coefficients should be used (47). Experimental results by different researchers were scattered and divergent. However, the force transfer coefficients C_d and C_m , for one-dimensional flow over a circular cylinder, have been well studied by Sarpkaya (Ref. 45) and Garrison (Ref. 15), and their experimental results have produced a very promising approach for the

systematic analysis of test data. Sarpkaya and Isaacson (47) presented the results of extensive experimental studies related to the variation of C_m and C_d with Reynold's number and the so-called Keulegan-Carpenter number. They also presented the variation of C_m and C_d with respect to a "frequency parameter" β , where

$$\beta = \frac{\text{Reynold's number}}{\text{Keulegan Carpenter number}} = \frac{U_m D / \nu}{U_m T / D} = D^2 / \nu T$$

The value of β remains constant for a wave of constant period, T , and constant temperature (and hence constant kinematic viscosity, ν). They presented C_m and C_d versus Keulegan-Carpenter number, K , for different values of the frequency parameter, β , ranging from 500 to 5000. For high values of β , the variation of C_m with respect to K was found to remain constant and have a value ranging between 1.5 and 2.0.

The platform used in this study consists of members having diameters ranging between 3.5 and 16.0 meters. Table 1 shows the variation of β with respect to wave periods and cylinder diameters used in this study.

It can be seen that the minimum value of β within the range of periods and diameters used is 4083. Therefore, according to experimental data (47), the variation of C_m with respect to the frequency parameter, β , can be neglected. Since β is a function of the wave period, T , the variation of C_m with respect to T also is negligible. Hence, the use of a constant value of the added mass is reasonable. A similar argument also applies to the coefficient of drag C_d .

Morison's equation provided a hypothesis that expresses the force both as a function of time and other independent parameters, for the

TABLE 1
Variation "of Frequency Parameter" with Respect
to Wave Period and Cylinder Diameter

T	ω	$\beta = D^2/\nu T$	
(sec)	(rad/sec)	D = 3.5 m	D = 16.0 m
5	1.25	24,500	512,000
6	1.05	20,416	426,000
8	.78	15,312	320,000
10	.63	12,250	256,000
15	.42	8,166	170,000
20	.31	6,125	128,000
25	.25	4,900	102,000
30	.21	4,083	85,000

case where the wave slope and associated pressure gradient are roughly constant across the diameter of the cylinder and the wave scattering is negligible. Morison also assumed that in the region near the cylinder the kinematics of the undisturbed flow do not change in the incident wave direction. However, since the kinematics of the flow do vary with distance, the above assumptions restrict the D/L ratio to a small value. Sarpkaya (Ref. 46) and Leonard, et al. (Ref. 27), suggested that the application of Morison's equation be limited to D/L values of less than 0.2. They also suggested that in cases where D/L is larger than 0.2, wave diffraction occurs. In the diffraction dominated region the total inertial force results from the sum of two components (Ref. 46): the force from the pressure field of the undisturbed fluid (the incident wave), and that from the disturbances

caused by the presence of the body (scattered wave).

Diffraction forces arise from the scattering of incident waves by the structure. These forces become significant when the structural member dimensions reach a substantial fraction of the wave length. Models for describing the force arising from diffraction have been developed by McCamy and Fuchs (Ref. 29) and others, generally by the use of potential theory with finite elements or finite difference methods. Significant contributions to the computation of hydrodynamic forces and moments on large gravity-type platforms have been made by Hogben and Standing (Ref. 19), Garrison and Stacy (Ref. 16), Mei (Ref. 32), Isaacson (20), and others, using diffraction theory.

In conclusion, the use of Morison's equation in wave force calculations is justified if the following conditions are met:

- 1) For D/L to be less than 0.2, with the largest diameter of 16 meters used in the analysis, the wave length should be larger than $5D$, i.e., 80 meters.
- 2) For a maximum diameter of 16 meters, the wave height should be greater than 5 meters to avoid the diffraction dominated region (see Ref. 46).
- 3) The original form of the equation should be modified in order to account for the relative velocity and acceleration between the oscillating structure and the fluid particles.
- 4) Reasonable values of the force transfer coefficients C_d and C_m may be obtained from the literature (e.g., recommendations of Garrison (Ref. 15) and Sarpkaya (Ref. 46)).

Random Waves

A random sea is comprised of a group of waves, of various sizes, lengths, and directions, jumbled together as a result of wind-generated disturbances of different intensities, locations, and directions. A wind-wave surface is characterized by the presence of a great number of individual, sinusoidal waves with different frequencies, lengths, heights, and phase angles. Figure 11 shows an irregular wave pattern formed by linearly superimposing four regular waves having different characteristics.

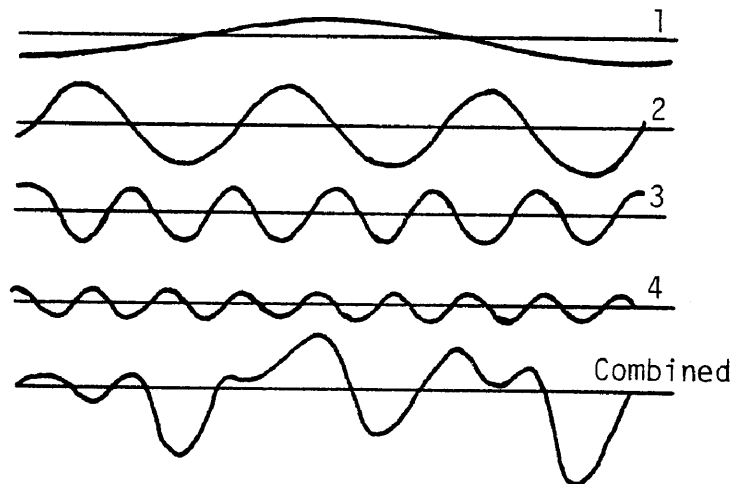


Fig. 11 - Formation of Irregular Sea Waves

One way to define an irregular, or random, sea is that its total energy must include the sum of the energies of all the individual regular waves that make up the sea. Mathematically, a wave system may be described by what is known as a wave spectrum which provides information about the energy distribution in the regular wave system as a function of frequency.

The surface elevation spectrum, $S_{\eta}(\omega)$, is an important tool for a wide range of design and analysis situations in the offshore environment. Many well known one-dimensional surface elevation spectra have been employed to describe ocean waves. The most commonly used spectra are the Pierson-Moskowitz (39), the Bretschneider (4), and, more recently, the J.O.N.S.W.A.P. spectrum (17).

The Pierson-Moskowitz spectrum may be written as

$$S_{\eta}(\omega) = \frac{\alpha g^2}{\omega^5} \exp \left\{ -\frac{\beta \omega_0^4}{\omega^4} \right\} \quad (19)$$

where

$$\alpha = 0.0081 ,$$

$$\beta = 0.74 , \text{ and}$$

$$\omega_0 = g/U ,$$

U is the characteristic windspeed at 19.5 m above still-water level, and g is the acceleration of gravity (Ref. 40). The Bretschneider spectrum is similar to that of Pierson-Moskowitz except that it is given in terms of the significant wave height, H_s , and peak frequency, ω_0 , rather than the characteristic wind speed, U .

The J.O.N.S.W.A.P. spectrum accounts for the effect of fetch-

limited conditions and is much more sharply peaked than the Pierson-Moskowitz spectrum. It may be written as

$$S_{\eta}(\omega) = \frac{\alpha g^2}{\omega^5} \exp \{-1.25 (\frac{\omega_0}{\omega})^4\} \gamma^a \quad (20)$$

where $a = \exp \{-(\omega - \omega_0)^2 / 2\sigma^2 \omega_0^2\}$,

$$\sigma = \begin{cases} \sigma_a = 0.07 & \text{for } \omega \leq \omega_0 \\ \sigma_b = 0.09 & \text{for } \omega > \omega_0 \end{cases} ,$$

$$\alpha = 0.066 (gF/U^2)^{-0.22} ,$$

$$\omega_0 = 2.84 (2\pi) (gF/U^2)^{-0.33}$$

$$\gamma = 3.3 ,$$

U = characteristic windspeed , and

F = fetch

In this study, only spectra of Pierson-Moskowitz and J.O.N.S.W.A.P. (Figures 12 and 13 are employed to study the dynamic response of tension-leg platforms of irregular waves.

The linear wave theory allows linear superposition of a finite number of waves with amplitudes derived from the spectrum $S_{\eta}(\omega)$. The surface elevation may thus be written as (Refs. 3, 50):

$$\eta(x, t) = \sum_{j=1}^N a_j \cos(k_j x - \omega_j t + \theta_j) \quad (21)$$

where $a_j = \sqrt{2 S_{\eta}(\omega_j) \Delta\omega}$,

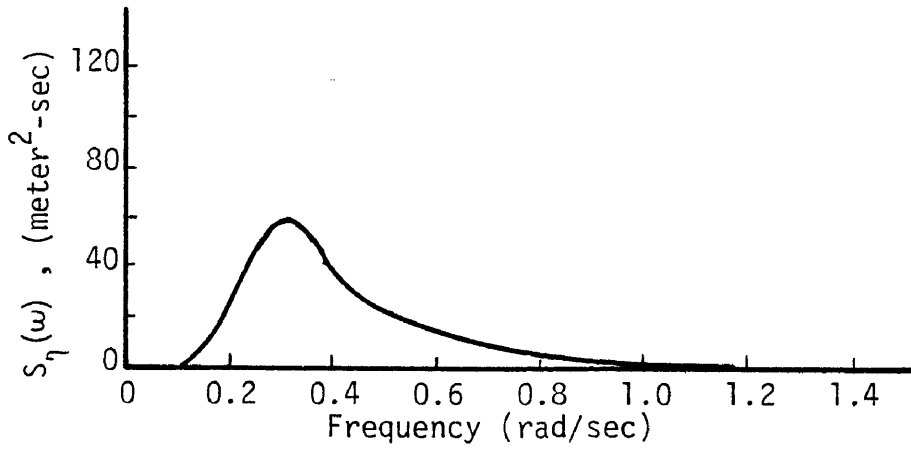


Fig. 12 - Pierson-Moskowitz Sea Spectrum

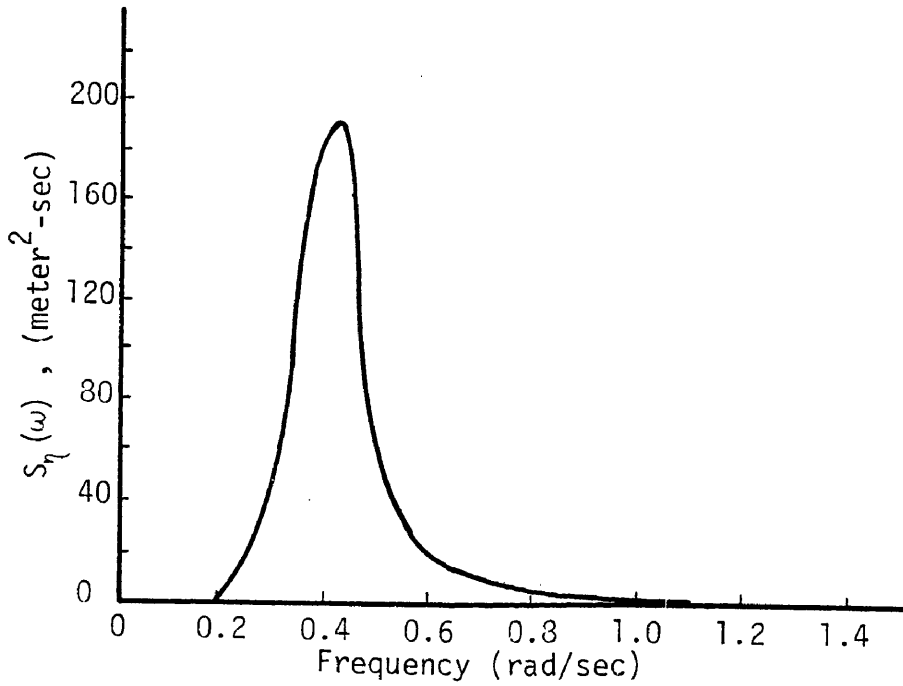


Fig. 13 - JONSWAP Sea Spectrum

$$\theta_j = \text{phase angle} ,$$

and k_j is the wave number given by the linear wave theory as

$$\omega_j^2 = g k_j \tanh k_j d ,$$

where d is the water depth.

Both Pierson-Moskowitz and JONSWAP spectra show that ω is only significant in the range of 0.1 to 1.2 radian/second. In this study, 12 frequencies are considered in the above range with $\Delta\omega$ of 0.1 radian/second.

Further application of the linear wave theory yields the kinematics of the random wave. Thus the horizontal fluid velocity u can be written as

$$u = \sum_{j=1}^N \omega_j a_j \frac{\cosh k_j (z + d)}{\sinh k_j d} \cos (k_j x - \omega_j t + \theta_j) \quad (22)$$

The horizontal fluid acceleration is the time derivative of the horizontal velocity, hence

$$\frac{du}{dt} = \sum_{j=1}^N \omega_j^2 a_j \frac{\cosh k_j (z + d)}{\sinh k_j d} \sin (k_j x - \omega_j t + \theta_j) \quad (23)$$

Similarly, the vertical component of the fluid velocity and acceleration can be written, respectively, as

$$v = \sum_{j=1}^N \omega_j a_j \frac{\cosh k_j (z + d)}{\sinh k_j d} \sin (k_j x - \omega_j t + \theta_j) \quad (24)$$

and

$$\frac{dv}{dt} = \sum_{j=1}^N -\omega_j^2 a_j \frac{\cosh k_j (z + d)}{\sinh (k_j d)} \cos (k_j x - \omega_j t + \theta_j) \quad (25)$$

Wave forces and moments are then calculated in the same method as for regular waves using Morison's equation.

Wave Drift Forces

Wave drift forces on surface piercing cylinders are second order quantities. They arise as a result of second order terms in Bernoulli's equation. These forces are small in magnitude but can be important in the horizontal oscillations of moored objects such as tension-leg platforms.

Wave drift forces consist of two components: a steady component and an oscillating component. The steady component arises from the incident, diffracted and radiated waves and is present in regular or in random seas (7). The oscillating component is present only in irregular waves or random seas. It is a slowly-varying force with a period much higher than those of the wave; i.e., on the order of 100 seconds. The period of the oscillating component is caused by cross-modulation effects between wave components in the wave spectrum and is dependent on the frequency difference in the wave components. When this period approaches that of the moored structure, the response of the structure can be significantly amplified; however, wave damping can considerably reduce the effect of slowly-varying drift forces (52).

Experimental as well as theoretical studies have been conducted to determine drift forces and their effect on ships (7, 8, 13, 18, 30, 36, 40-44, 52). A well documented review of the various approaches is presented by Chakrabarti (Ref. 8). The theoretical studies are based on either conservation of momentum and energy principles or on the

pressure field on the surface of the object.

Havelock (18), Maruo (30) and Newman (36) have shown that the drift force is proportional to the square of the wave height. The mean drift force (steady component) on a surface piercing cylinder of radius r in regular wave groups of height H is given by

$$F_d = \rho g \frac{r}{8} H^2 R^2(\omega) \quad (26)$$

where $R^2(\omega)$ is a reflection coefficient that can be calculated experimentally as:

$$R(\omega) = \sqrt{\frac{F_d}{\rho g \frac{r}{8} H^2}} \quad (27)$$

The reflection coefficient is given by Kirk & Etok (24) as a function of wave frequency as:

$$R(\omega) = \begin{cases} 1.3 rw^2/g & ; \text{ for } rw^2/g \leq 1 \\ 1.3 & ; \text{ for } rw^2/g > 1 \end{cases}$$

In random waves the mean drift force is obtained from the expression

$$\bar{F} = \rho g r \int_0^{\infty} S_{\eta}(\omega) R^2(\omega) d\omega \quad (28)$$

where $S_{\eta}(\omega)$ is the wave amplitude spectrum of the random sea (Ref. 42).

The spectrum of the slowly-varying component of the drift force in regular or irregular waves is given by Pinkster (41) and Rye (43) as

$$S_{F_d}(\omega) = 2 \rho^2 g^2 r^2 \int_0^{\infty} S_{\eta}(\omega') S_{\eta}(\omega' + \omega) R^2(\omega' + \frac{\omega}{2}) d\omega' \quad (29)$$

Maruo (Ref. 30) derived drift force equations based on the conservation of wave momentum and energy. Newman (Ref. 36) extended the momentum relations derived by Maruo to obtain drift forces on arbitrary shaped bodies in terms of the Kochin function. More recently, Salvesen (44) used the formulations based on Maruo and Newman to calculate the drift forces on tension-leg platforms using a finite element approach, but only considered regular wave conditions. In this study, Equation (29) is used, because of its simplicity and practicality, with the J.O.N.S.W.A.P. sea spectrum $S_{\eta}(\omega)$ to obtain the spectrum of the slowly varying drift force on each of the surface piercing cylinders. More complex drift formulation procedures are not utilized herein since drift forces are out of the scope of this research.

Using Fourier transforms, the drift force spectrum is transformed into a function of time, $F_d(t)$, thus,

$$F_d(t) = \int_0^{\infty} \sqrt{S_{F_d}(\omega)} \cos(\omega t + \theta) \quad (30)$$

Equation (30) is integrated numerically with the limits of integration from 0.02 to 1.2 rad./sec, thus,

$$F_d(t) = \sum_{i=1}^N \sqrt{S_{F_d}(\omega_i) \Delta\omega_i} \cos(\omega_i t + \theta_i) \quad (31)$$

Since the drift force acts only on surface piercing cylinders, therefore only the four corner columns and four middle columns are considered in evaluating the total drift force on the platform.

Procedure for Wave Force Calculation

Wave forces are calculated from a modified version of Morison's equation and include the relative velocity and acceleration between the structure and the fluid particle. Equation (18) is modified to

account for the relative motion between the structure and the fluid particle, and separated into drag and inertia terms. The drag and inertia forces on an element dz along the length of the cylinder become:

$$\delta F_d = \frac{\rho}{2} C_D D U_{rel} |U_{rel}| dz , \quad (32)$$

and

$$\delta F_I = \rho \frac{\pi D^2}{4} [C_m \dot{U} - (C_m - 1) \ddot{x}] dz \quad (33)$$

where ρ is the mass density of the fluid, D is the diameter of the cylinder, U_{rel} is the relative velocity given by

$$U_{rel} = u - [\dot{x} - (z - \bar{z})\dot{\alpha} + \frac{1}{2} x_i \dot{\alpha}^2] , \quad (34)$$

and

$$\ddot{x} = \ddot{x} - (z - \bar{z}) \ddot{\alpha} + \frac{1}{2} x_i \ddot{\alpha}^2 \quad (35)$$

Equations (34) and (35) are derived based on Figure 14 where \dot{x} , \ddot{x} , $\dot{\alpha}$, $\ddot{\alpha}$ are the velocity, acceleration, angular velocity, and angular acceleration of the center of gravity (in this case the center of rotation) of the structure, respectively.

Substituting Equations (34) and (35) into Equations (32) and (33), respectively, yields:

$$\delta F_d = \frac{\rho}{2} C_D D |u - [\dot{x} - (z - \bar{z})\dot{\alpha} + \frac{1}{2} x_i \dot{\alpha}^2]| \{u - [\dot{x} - (z - \bar{z})\dot{\alpha} + \frac{1}{2} x_i \dot{\alpha}^2]\} dz, \quad (36)$$

and

$$\delta F_I = \rho \frac{\pi D^2}{4} [C_m \dot{u} - (C_m - 1) \{\ddot{x} - (z - \bar{z}) \ddot{\alpha} + \frac{1}{2} x_i \ddot{\alpha}^2\}] dz \quad (37)$$

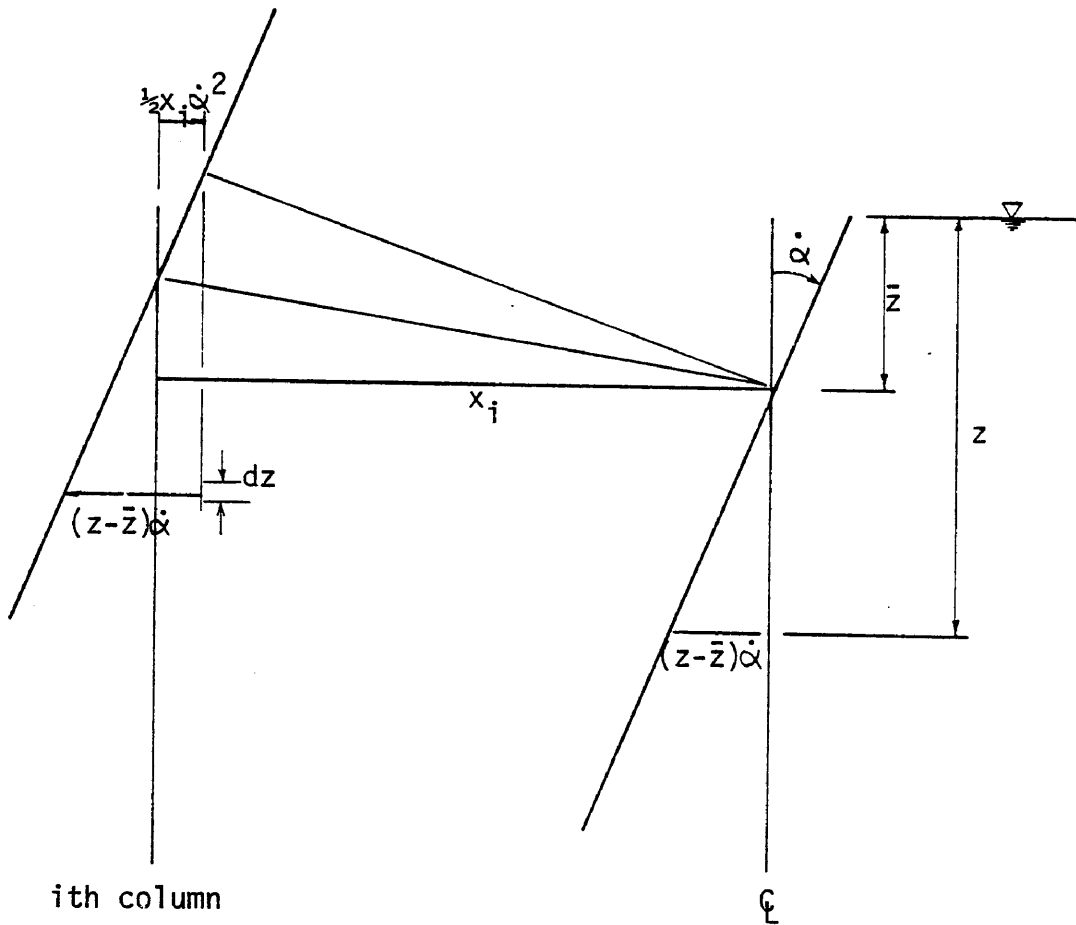


Fig. 14 - Velocity of Element dz Along i th Column
Arising from Pitch or Roll

These two equations are integrated along the length of each column and hull to obtain the total instantaneous force on the structure. The contribution of the wave forces on the cables to the total wave force on the platform is very small. Jeffreys and Patel (Ref. 21) showed that the modification of the overall platform response to waves due to the inertia and drag forces on the tethers is negligible. Therefore, in this study, the wave forces on the cables are neglected in the dynamic analysis.

The moments of these forces about the axes of rotation are found by multiplying the force equations by the appropriate moment arms and then integrating over the length of each cylinder to obtain the total moments. It should be noted that despite the nonlinearity of the drag force and moment equations and the coupling of pitch and surge or roll and sway in both the inertia and drag equations, a closed form integration can be carried out by hand, thereby avoiding the need for time consuming numerical integration. This method of force calculation is the major contributor to the efficiency of the mathematical model and computer program developed in this study.

A force calculation method similar to that of Kirk and Etok (Ref. 24) is used with the following major changes:

- 1 - Inclusion of drag forces
- 2 - Incorporation of relative motion between structure and fluid particles
- 3 - Accounting for instantaneous position of structure
- 4 - Inclusion of coupling terms in wave force derivation

Summary of Wave Forces

The following outline contains a complete description of the wave force equations which must be derived:

- 1) Horizontal forces
 - a) Inertia forces on columns
 - b) Drag forces on columns
 - c) Inertia forces on hulls and cross braces
 - d) Drag forces on hulls and cross braces
 - e) Slowly varying drift forces on surface piercing columns
- 2) Vertical forces
 - a) Vertical inertia forces on hulls
 - b) Vertical drag forces on hulls
 - c) Dynamic pressure on corner column bases
- 3) Moments of forces about x, y, and z axes
 - a) Moments due to inertia forces on columns
 - b) Moments due to drag forces on columns
 - c) Moments due to horizontal inertia forces on hulls
 - d) Moments due to horizontal drag forces on hulls
 - e) Moments due to vertical inertia forces on hulls
 - f) Moments due to vertical drag forces on hulls
 - g) Moments due to dynamic pressure on corner column bases

Details of the complete derivation of wave forces and moments are presented in Appendix A. A summary of the resulting forces is given below:

Horizontal forces

$$\text{Surge (x-axis): } F_{x_T} = \sum_{i=5}^{12} (F_{I_i} + F_{D_i}) \cos \alpha + F_x + \bar{F}_x \quad (38)$$

$$\text{Sway (y-axis): } F_{y_T} = \sum_{i=5}^{12} (F_{I_i} + F_{D_i}) \sin \alpha + F_y + \bar{F}_y \quad (39)$$

Vertical forces

$$\text{Heave (z-axis): } F_{z_T} = F_v + \bar{F}_v + F_{cv} \quad (40)$$

Moments

Pitch (about y-axis):

$$M_{y_T} = \sum_{i=5}^{12} (M_{I_i} + M_{D_i}) \cos \alpha + M_{v_y} + M_{H_y} + M_{P_y} \quad (41)$$

Roll (about x-axis):

$$M_{x_T} = \sum_{i=5}^{12} (M_{I_i} + M_{D_i}) \sin \alpha + M_{v_x} + M_{H_x} + M_{P_x} \quad (42)$$

$$\text{Yaw (about z-axis): } M_{z_T} = \sum_{i=5}^{12} (F_{I_i} + F_{D_i}) y_i \quad (43)$$

where $\sum_{i=5}^{12}$ is the summation over the corner columns (5-8) and the middle columns (9-12), α is the orientation angle or angle of wave incidence, F_x and \bar{F}_x are the x-components of the total horizontal inertia

and drag forces on the hulls, F_y and \bar{F}_y are the y-components of the total horizontal inertia and drag forces on the hulls, F_v and \bar{F}_v are the total vertical inertia and drag forces on the hulls, F_{cv} is the total vertical dynamic pressure force on the bases of the corner columns, M_I and M_D are the moments of the horizontal forces on the columns about an axis perpendicular to the wave direction, M_{V_y} and M_{H_y} are the moments of the vertical and horizontal hull forces about the y-axis, M_{P_y} is the moment of the dynamic pressure on the bases of the corner columns about the y-axis, M_{V_x} and M_{H_x} are the moments of the vertical and horizontal hull forces about the x-axis, M_{P_x} is the moment of the dynamic pressure on the bases of the corner columns about the x-axis, and y_i is the moment arm, of column i, for moments about the z-axis.

Earthquake Forces

Horizontal Ground Motion

Platform motion would result from the horizontal and/or vertical acceleration(s) of the anchors caused by earthquake ground motion. The platform and the anchoring system can be modeled as a spring-mass system (Figure 15). Neglecting structural damping in the cables, the forces acting on the platform may be represented as shown in Figure 16. The equation of dynamic equilibrium thus can be written as:

$$\tilde{F}_I + F_S = F_{fluid} \quad , \quad (44)$$

where \tilde{F}_I is the inertia force on the mass, F_S is the stiffness force

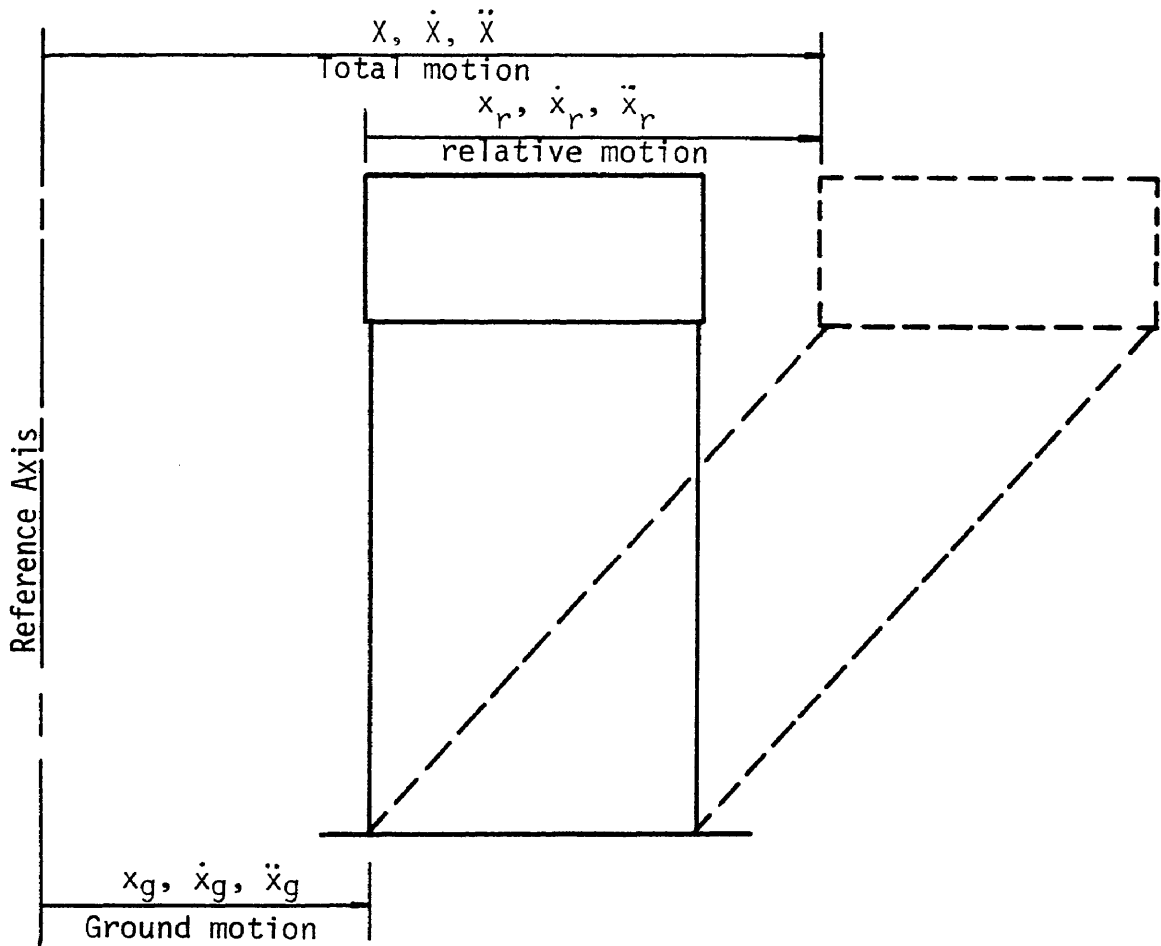


Fig. 15 - Modeling of TLP for Horizontal Ground Motion

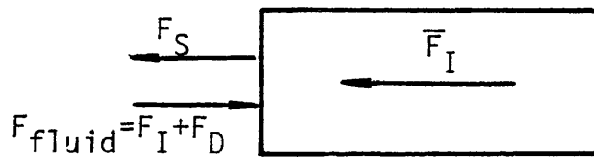


Fig. 16 - Forces on the Platform Caused by Horizontal Ground Motion

provided by the horizontal component of the cables, and F_{fluid} is the force arising from the fluid-structure interaction caused by the relative acceleration and velocity between the platform and the water.

Equation 44 can be rewritten as:

$$m \ddot{x} + k x_r = F_{\text{fluid}} , \quad (45)$$

where \ddot{x} is the total platform acceleration, x_r is the relative displacement (total displacement minus ground displacement), m is the platform mass and k is the horizontal cable stiffness. Substituting $\ddot{x} = \ddot{x}_r + \ddot{x}_g$, where \ddot{x}_g is the ground acceleration, yields:

$$m \ddot{x}_r + m \ddot{x}_g + k x_r = F_{\text{fluid}} , \quad (46)$$

which can be rewritten as:

$$m \ddot{x}_r + k x_r = -m \ddot{x}_g + F_{\text{fluid}} , \quad (47)$$

where $m \ddot{x}_g$ is an effective load resulting from ground motion.

Two different loading conditions are studied, one where both waves and the earthquake occur simultaneously, and one when the earthquake occurs in a calm sea. For the first case, the fluid inertia and drag forces derived earlier can be used for F_{fluid} in Equation 47. In a calm sea, a simpler formulation is developed for the inertia and drag forces arising from the interaction between the structure and the fluid particle (see Appendix B).

An additional effect of the horizontal ground motion is the pitch and heave arising from their coupling to surge as mentioned earlier in this report (see Chapter II). The resulting equations of motion for

pitch and heave are similar to Equation 47.

Vertical Ground Motion

In order to formulate the equation of motion of the TLP subjected to vertical ground motion, the platform and the cable are modeled as a spring-mass-dashpot system similar to that for the horizontal component of ground motion. It is assumed that the cables may be represented by a massless spring. To verify this assumption, a wave propagation analysis is performed on the system to study the effect of cable inertia on the pattern of wave propagation. A computer program developed by Lowery (28) based on a wave propagation approach suggested by Smith (48) is utilized. The program, developed for pile driving analysis, is modified to adapt for the TLP cable analysis. The TLP system is discretized as a set of elements consisting of lumped masses, massless springs and dashpots. The mass of each cable element is calculated as:

$$m_i = \rho_c L_i A \quad ,$$

where ρ_c is the mass density of the cable, L_i is the length of each element, and A is the cross-sectional area of the cable. The total structural mass of the platform is lumped in one element.

The spring stiffness of each cable element is calculated as

$$k_i = \frac{EA}{L_i} \quad ,$$

where E is the modulus of elasticity of the cable. The material damping of the cable is modeled as dashpots representing viscous damping

and producing forces proportional to the magnitude of the velocity and opposite to the direction of motion. The coefficient of viscous damping of each cable element is given by

$$c = 2 \xi \sqrt{k_i m_i} ,$$

where ξ is the damping ratio ranging between 0.1 to 1% for material damping and between 1 and 5% for structural damping.

A sinusoidal forcing function of period ranging between 0.05 second and 0.1 second is input at the base of the system. The results of the wave propagation analysis are summarized in Table 2 and Table 3 for forcing function periods of 0.05 and 0.1 seconds, respectively. The variations of the amplification factor of the amplitude of the output force in each element for the different values of damping ratios, are shown in Figures 17 and 18, for input function periods of 0.05 and 0.1 second, respectively.

The amplification of the amplitude of the input wave is caused by the effect of boundary conditions. The platform acts as a stiff and heavy element and hence it is considered to act as a boundary that is between a fixed and a free condition. Hence, for an undamped system, the amplification factor changes between 1.0 (corresponding to a free boundary) and 2.0 (corresponding to a fixed boundary). It is noted, however, that the period of the wave as it reaches the top of the platform is the same as that input at the base of the cables.

From the results of the above analysis, it is noticed that as the damping ratio increases, the amplification factor decreases and for

TABLE 2. Amplification Factors of a Sinusoidal Forcing Function
 $F = 1000 \sin(40 \pi t)$ Input at the Base of the Cable

Element No.	Damping Ratio ξ , %													
	0	0.05	0.1	0.2	0.3	0.4	0.5	0.6	0.7	0.8	0.9	1.1%	1%	
1	1.000	1.000	1.000	1.009	1.000	1.000	1.000	1.000	1.000	1.000	1.000	1.000	1.000	1.000
2	1.088	1.078	1.071	1.061	1.053	1.047	1.041	1.036	1.032	1.028	1.025	1.019	1.021	1.021
3	1.169	1.153	1.141	1.121	1.105	1.092	1.081	1.071	1.064	1.056	1.050	1.039	1.044	1.044
4	1.251	1.226	1.208	1.178	1.153	1.134	1.118	1.104	1.094	1.083	1.075	1.059	1.067	1.067
5	1.329	1.298	1.272	1.232	1.199	1.174	1.152	1.135	1.121	1.108	1.098	1.079	1.088	1.088
6	1.398	1.363	1.333	1.282	1.242	1.210	1.183	1.163	1.145	1.131	1.118	1.097	1.107	1.107
7	1.473	1.425	1.390	1.329	1.280	1.241	1.211	1.187	1.167	1.151	1.136	1.112	1.124	1.124
8	1.545	1.489	1.444	1.370	1.313	1.268	1.234	1.207	1.185	1.167	1.151	1.126	1.138	1.138
9	1.612	1.546	1.492	1.406	1.340	1.290	1.252	1.222	1.199	1.179	1.163	1.135	1.148	1.148
10	1.661	1.592	1.531	1.433	1.360	1.305	1.264	1.232	1.208	1.188	1.170	1.142	1.156	1.156
11	1.695	1.619	1.553	1.448	1.370	1.313	1.270	1.238	1.215	1.192	1.174	1.146	1.159	1.159

TABLE 3. Amplification Factors of a Sinusoidal Forcing Function

$F = 1000 \sin (20 \pi t)$ Input at the Base of the Cable

Element No.	Damping Ratio ξ , %										
	0%	0.1	0.2	0.4	0.6	0.8	1.0	2.0	3.0	5.0	7.0%
1	1.000	1.000	1.000	1.000	1.000	1.000	1.000	1.000	1.000	1.000	1.000
2	1.037	1.015	1.007	1.004	1.004	1.005	1.006	1.005	1.003	1.000	1.000
3	1.074	1.033	1.017	1.008	1.009	1.010	1.011	1.013	1.015	1.002	1.001
4	1.096	1.050	1.027	1.013	1.013	1.014	1.016	1.017	1.019	1.003	1.001
5	1.123	1.064	1.037	1.017	1.016	1.018	1.020	1.020	1.014	1.004	1.002
6	1.148	1.079	1.046	1.021	1.019	1.021	1.023	1.025	1.017	1.006	1.003
7	1.169	1.093	1.054	1.025	1.022	1.024	1.026	1.027	1.020	1.008	1.005
8	1.197	1.105	1.061	1.028	1.024	1.026	1.029	1.029	1.022	1.010	1.005
9	1.214	1.116	1.066	1.031	1.026	1.028	1.030	1.031	1.024	1.011	1.006
10	1.230	1.123	1.070	1.032	1.027	1.029	1.032	1.032	1.025	1.013	1.006
11	1.240	1.127	1.072	1.033	1.028	1.030	1.032	1.034	1.026	1.015	1.007

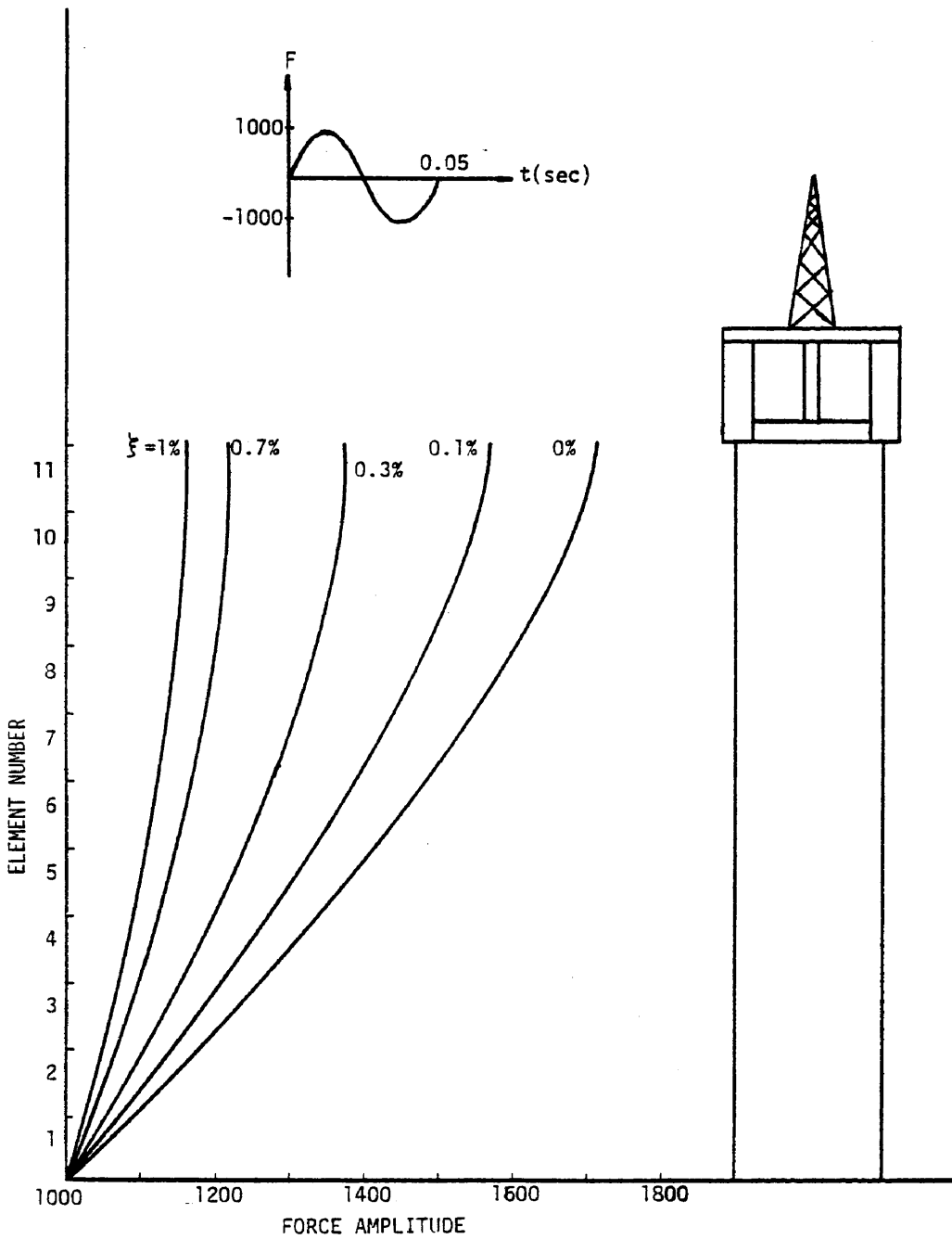


Fig. 17 - Amplitudes of Propagated Wave in the Cable for Different Damping Ratios; $F = 1000 \sin(40\pi t)$

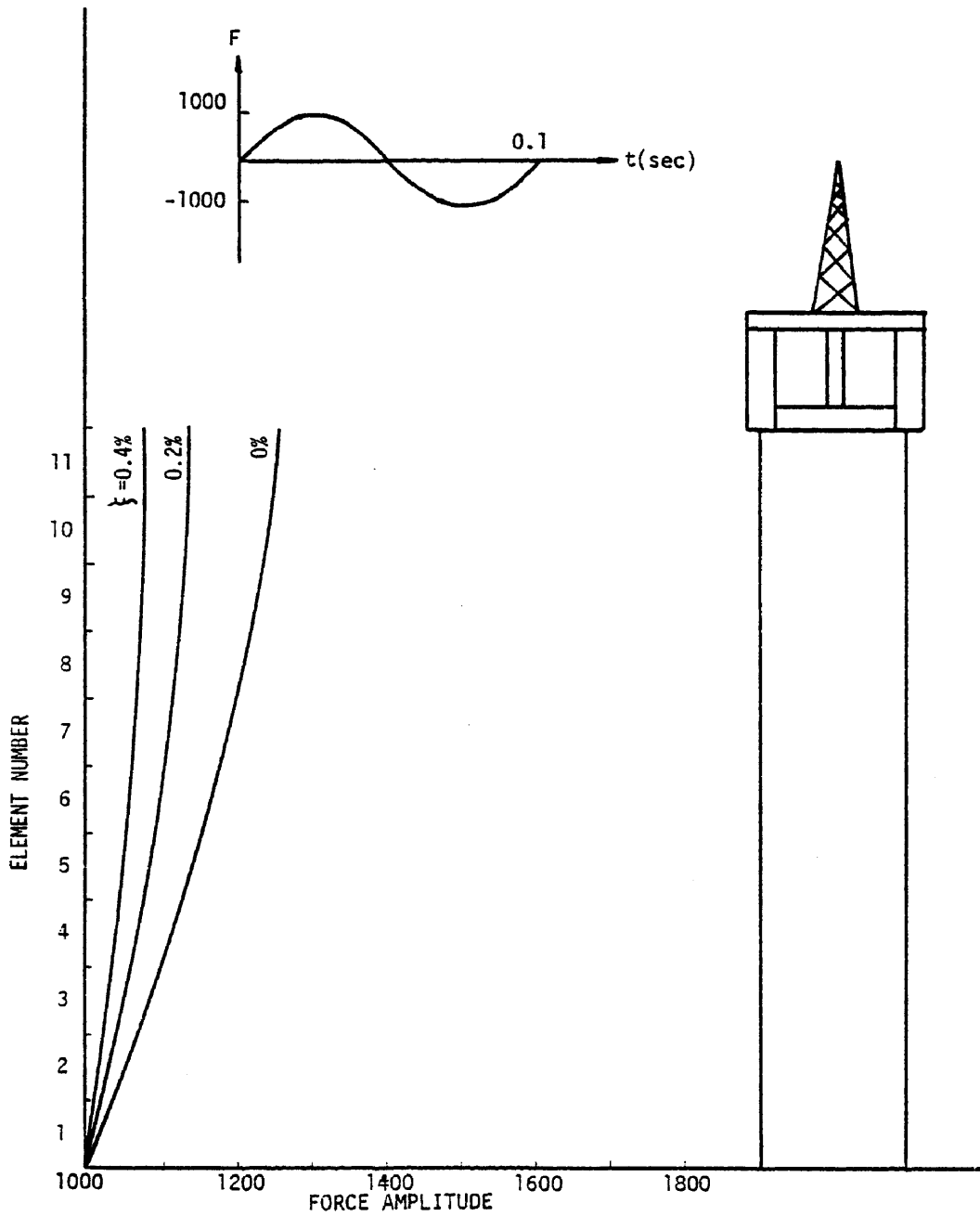


Fig. 18 - Amplitudes of Propagated Waves in the Cable for Different Damping Ratios; $F = 100 \sin(20 \pi t)$

$\xi > 1\%$ the amplification factor approaches 1.0. The author believes that the damping ratio of the cable (material and structural) is not less than 1%; therefore, it can be concluded that the effect of considering the cable mass in the analysis is negligible. Therefore, the assumption of a single massless spring, and an equation of motion similar to Equation 47 is justified.

CHAPTER IV

MATHEMATICAL MODEL

The structure used in the analysis is represented schematically in Figure 3. The center of gravity of the platform is assumed to be located a distance z from the mean water level and a coordinate system is attached at its origin to the equilibrium position of the center of gravity. The center of rotation (pitch, roll, yaw) is assumed to be located at the center of gravity. The platform is modeled as a rigid body free to translate in three directions (surge, sway, heave) and rotate about the three axes (pitch, roll, yaw), with restoring forces that represent the legs (cables or chains) and buoyant forces.

The structure is represented by a mathematical model which can be reduced to a system of coupled nonlinear differential equations that are solved by direct numerical integration on a digital computer. The equations of motion are integrated in a stepwise manner using the Newmark β -method (Ref. 37). This chapter presents the development of a mathematical model, a solution procedure, and a computer code to perform the numerical calculations of the dynamic analysis of tension-leg platforms.

Equations of Motion

Once the nonlinear stiffness equations have been derived and the wave and earthquake forces are formulated, a set of coupled nonlinear differential equations can be assembled to form the basis for a deterministic dynamic analysis of tension-leg platforms. The equations of

motion are represented by Equation 48 in matrix form as

$$[M]\{\ddot{x}\} + [K]\{x\} = \{F(x, \dot{x}, \ddot{x}, t)\} \quad (48)$$

where $[M]$ is the mass matrix for all six degrees of freedom,

$[K]$ is a 6 x 6 nonlinear stiffness matrix,

$\{F\}$ is the vector of forcing functions,

$\{x\}$ is the structural displacement vector,

$\{\dot{x}\}$ is the structural velocity vector,

$\{\ddot{x}\}$ is the structural acceleration vector, and

t is the time.

Equation 48 can be rewritten in vector form as

$$\{m_i \ddot{x}_i\} + \{K_i\} = \{F_i(x, \dot{x}, \ddot{x}, t)\} \quad (49)$$

where $\{m_i \ddot{x}_i\}$ is the inertial force vector in which m_i is the mass of degree of freedom "i", and \ddot{x}_i is the acceleration of the structure in the direction of degree of freedom "i", $\{K_i\}$ is the coupled nonlinear stiffness force vector (see Equation 15), and $\{F_i(x, \dot{x}, \ddot{x}, t)\}$ is the vector of nonlinear external forces (waves or earthquakes). The equations of motion generally describe the dynamic equilibrium between the inertia, the restoring, and the exciting forces.

Solution Procedure

The equations of motion are both coupled and nonlinear. Hence a time domain analysis method is required, as mentioned earlier in the report, to calculate the response of the structure to various types of loading. The general approach to solving nonlinear equations of

motion is through an integration of the acceleration and velocity curves in the time domain.

Two well known methods of integration have been widely used for time domain dynamic analysis of fixed, or floating, offshore structures. The first one is the Newmark-Beta method, and the second one is the Newton-Raphson technique. The latter does not work well for heave, roll, or pitch (see Ref. 35). The Newmark-Beta method is more general and has been used in time domain models for dynamic analysis of fixed offshore structures, with good results (Ref. 6).

The Newmark-Beta method is used to integrate, in a stepwise manner, the equations of motion and to obtain time histories of the structure's response in an iterative manner. The iterative method can be used to determine the accelerations, velocities, and displacements of the structure at time t_{n+1} based on corresponding values at time t_n and the accelerations at t_{n+1} . The equations have the following form:

$$\dot{x}_i(t_{n+1}) = \dot{x}_i(t_n) + (1-\gamma)\Delta t \ddot{x}_i(t_n) + \gamma\Delta t \ddot{x}_i(t_{n+1}) , \quad (50)$$

and

$$x_i(t_{n+1}) = x_i(t_n) + \Delta t \dot{x}_i(t_n) + \left(\frac{1}{2} - \beta\right)(\Delta t)^2 \ddot{x}_i(t_n) + \beta(\Delta t)^2 \ddot{x}_i(t_{n+1}) \quad (51)$$

The value of γ is usually set to 1/2 by damping considerations and the value of β is chosen in the range of 1/8 to 1/4 for reasons of convergence. Values of γ and β of 1/2 and 1/6, respectively, are used in this model. The vector of accelerations at time t_{n+1} are found by

substituting the vectors of velocities and displacements into the equations of motion as follows:

$$\{\ddot{x}_i\} = \frac{1}{m_i} [\{F(x_i(t_{n+1}), x_i(t_{n+1}), \ddot{x}_i(t_{n+1}), t_{n+1})\} - \{K_i(x_i(t_{n+1}))\}] \quad (52)$$

Equations (50), (51), and (52) are solved in an iterative manner. An assumed value of \ddot{x}_i at t_{n+1} is usually chosen equal to the value at the previous time step. New values of x_i and \dot{x}_i at t_{n+1} are then calculated from Equations (50) and (51), and a new value of \ddot{x}_i is computed from Equation (52). This process is repeated until the assumed and the calculated values of acceleration converge within a predetermined tolerance. The value of the tolerance is established through compromise between accuracy and computing cost. The β -method readily accepts both continuous forcing functions (as in case of waves) and discrete forcing functions (as in case of earthquakes), and is extended for the purpose of this study to three dimensions and six degrees of freedom.

Computer Code

A compact and inexpensive computer program has been developed to perform the numerical calculations of the motion of anchored as well as floating structures subjected to the action of waves, currents, and earthquakes. A flow chart of the computer program is depicted in Figure 19.

The structural geometry, material properties, wave properties and ground acceleration are input to the program. The displacement,

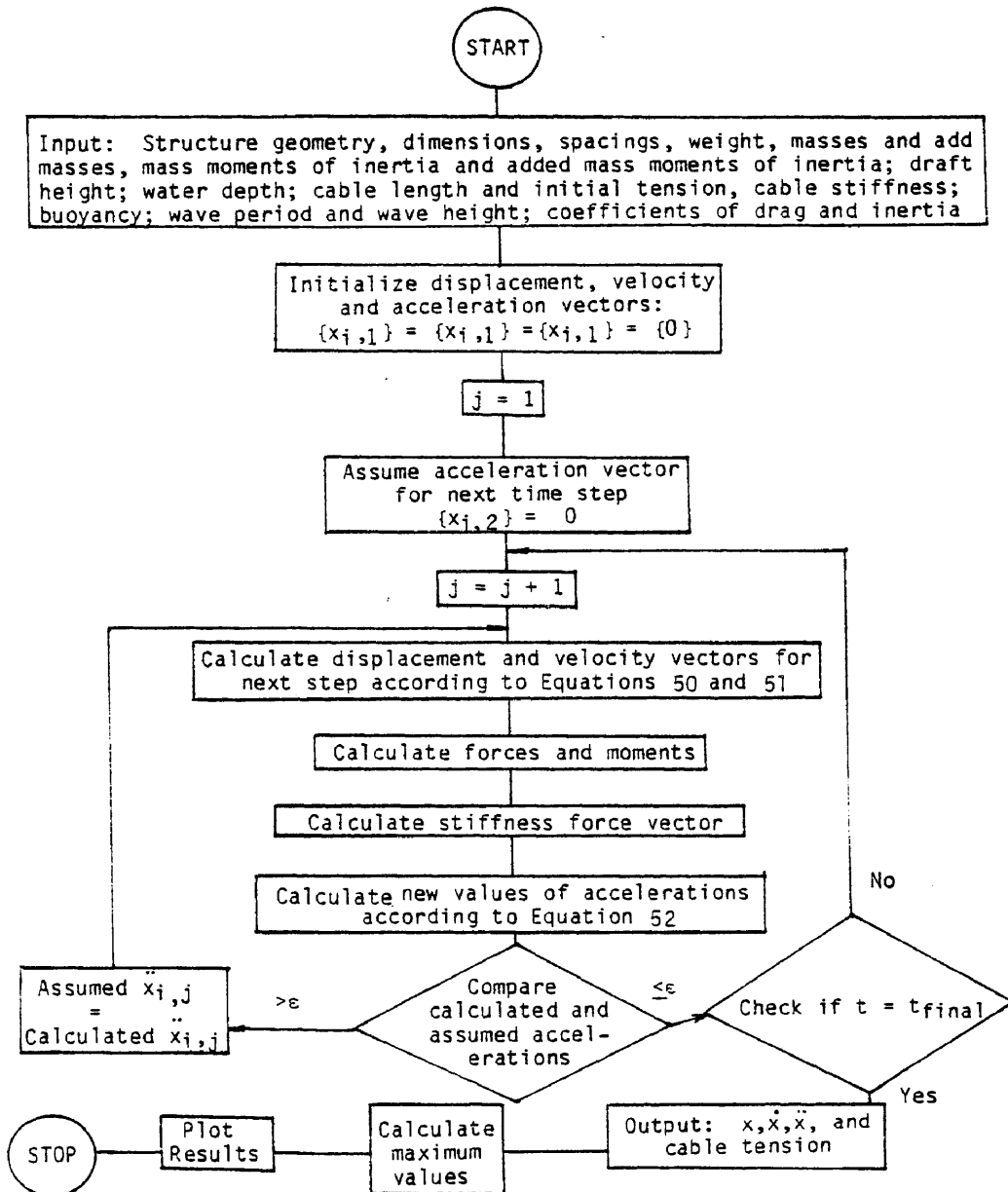


Figure 19. Flow Chart of Computer Program

velocity and acceleration vectors are initialized and an assumption for the acceleration vector is made for the next time step. New displacement and velocity vectors are then calculated based on the assumed acceleration. The forces and stiffnesses corresponding to these values of displacements, velocities, and accelerations are then calculated. Finally, using the equations of motion a new value of the acceleration is calculated and compared with the assumed value. The process is repeated until the difference between the calculated value and the assumed value of the acceleration is less than a predetermined convergence factor. Once the equations of motion are satisfied, the final acceleration value for this time step becomes the assumed value of the acceleration for the next time step, and the whole process is repeated.

At each time step the program calculates:

- The six components of motion (surge, sway, heave, pitch, roll, and yaw) together with velocities and accelerations.
- The total forces and moments due to waves or earthquake.
- The stiffness vector (restoring forces).
- The tension and tension variation of each leg.

At the end of the analysis the program calculates the maximum values of the displacements, velocities, and accelerations of the structure, and the maximum tension and tension variation of each of the four legs. If plots are desired, the variables of interest can be scaled with respect to their maximum values and plotted versus time.

Summary of Dynamic Analysis Model

A complete nonlinear deterministic dynamic analysis model has been developed in this chapter. The model is based on a set of coupled nonlinear differential equations integrated in the time domain using Newmark's Beta Method. Wave kinematics are calculated from the linear wave theory, and wave forces are calculated from a modified form of Morison's equation. Earthquake forces are calculated based on accelerations obtained from ground motion records. The coupling and nonlinearities of the equations of motion are contributed by both the stiffness and the forcing functions.

A computer program is written to perform the numerical solution and obtain time histories of the response in all degrees of freedom. The tension forces in the anchoring legs can be calculated from displacement time histories of the different degrees of freedom, and time histories of these forces can be generated. Data used in the computer program are taken from Kirk and Etok (Ref. 24) with slight changes in some cases for the sake of a complete and meaningful testing of the model (see Appendix C).

CHAPTER V

RESPONSE OF THE MODEL

General

The major objective of the dynamic analysis model presented herein is to simulate the response of tension-leg platforms to ocean-environment loading. In this chapter, the model is tested by the application of wave loading and earthquake forces. Time histories of surge, sway, heave, pitch, roll, and yaw are calculated by the model. The relative importance of design variables for tension-leg platforms is found through a parametric analysis. These parameters studied include: wave period, wave height, water depth, cable stiffness, initial tension, and direction of wave propagation. The importance of coupling and nonlinearity is demonstrated through comparison of the response of the coupled system to that of the uncoupled, and the response including nonlinear terms to that by existing linear models.

Response to Regular Waves

The platform data listed in Appendix C were used to test the mathematical model developed herein. A coefficient of inertia (C_m) of 1.5 and a coefficient of drag (C_d) of 1.0 were used in the wave force calculations of Chapter II, and assumed to be constant throughout the analysis. A wave height of 15.0 meters and a wave period of 17 seconds were chosen to describe a "significant wave" to be used in the regular wave analysis. Simulation of various regular sea states of interest was done by varying the wave height and the wave period.

Time Histories

Time histories of response in the direction of each of the six degrees of freedom were obtained. Time histories of surge, sway, heave, pitch, roll, and yaw, respectively, for the significant wave described above and for a wave propagation angle of 35 degrees from the x-axis are depicted in Figures 20-25. Responses for all six degrees of freedom, with inertia and without drag, are presented in Figures 26-31 for the same sea state. A comparison between the responses including drag forces and those that exclude drag reveals that the nonlinear drag forces (sometimes called interaction forces) contribute a significant amount of damping to the displacement response. The periods of forced vibration for all six degrees of freedom of the structure for the sea state described above are shown in Table 4. Also included in Table 4 are the response amplitudes (or maximum values) of the structure's six degrees of freedom for both cases (including drag and excluding drag). Table 5 includes the maximum values of the platform velocities and accelerations for all six degrees of freedom. The time histories of the motion (displacements, velocities, and accelerations) are important input for analysis of the tension in the anchor legs, as well as in analyzing the stresses in the various members of the structure caused by hydrodynamic and earthquake forces.

Response Spectra

Plots of maximum amplitude of vibration versus wave period (or wave frequency) will be referred to herein as response spectra. Two

TABLE 4

Periods of Vibration and Response Amplitudes

Degree of Freedom	Period (sec)	Response Amplitude	
		Undamped	Damped
Surge	70	16.45 m	14.17 m
Sway	70	14.00 m	10.41 m
Heave	5	.97 m	.70 m
Pitch	6	.22°	.21°
Roll	6	.15°	.146°
Yaw	50	.18°	.16°

TABLE 5

Maximum Values of Velocities and Accelerations

Degree of Freedom	Maximum Velocity	Maximum Acceleration
Surge	2.51 m/s	.722 m/s ²
Sway	1.95 m/s	.520 m/s ²
Heave	.173 m/s	.076 m/s ²
Pitch	.139°/s	.119°/s ²
Roll	.095°/s	.082°/s ²
Yaw	.032°/s	.011°/s ²

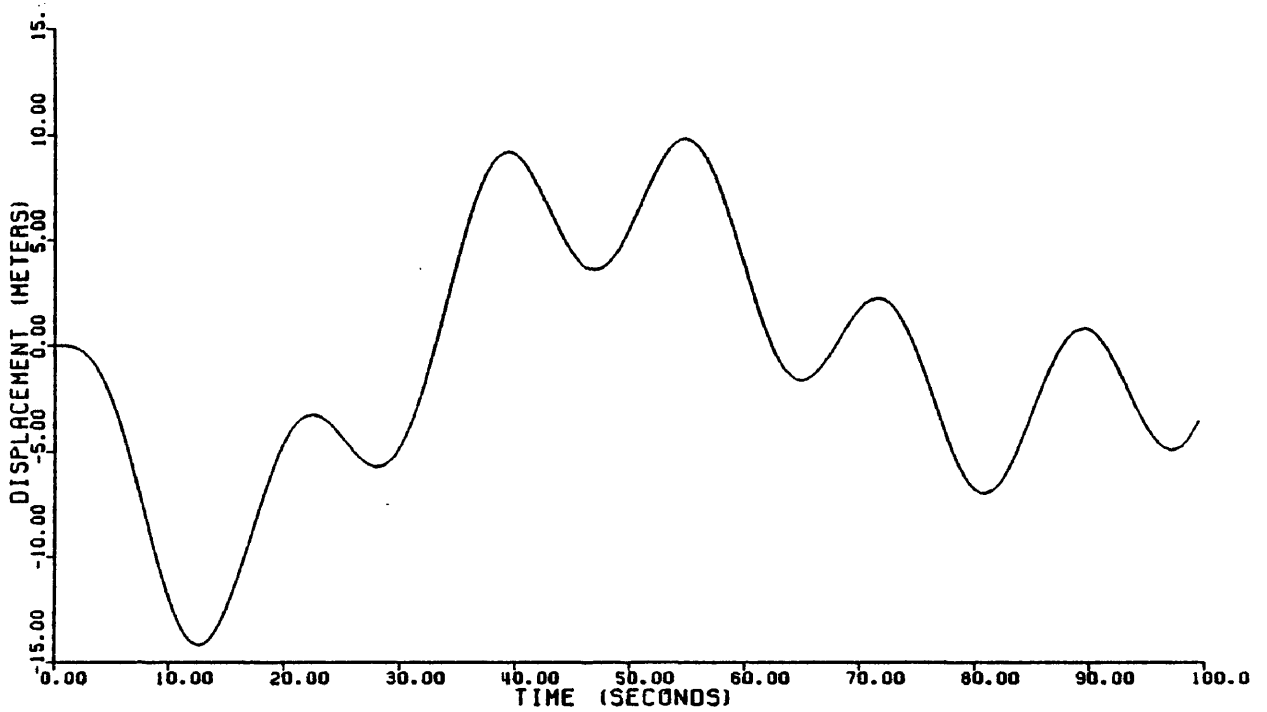


Fig. 20 - Time History Plot of Surge Displacement
(including Inertia and Drag Forces)

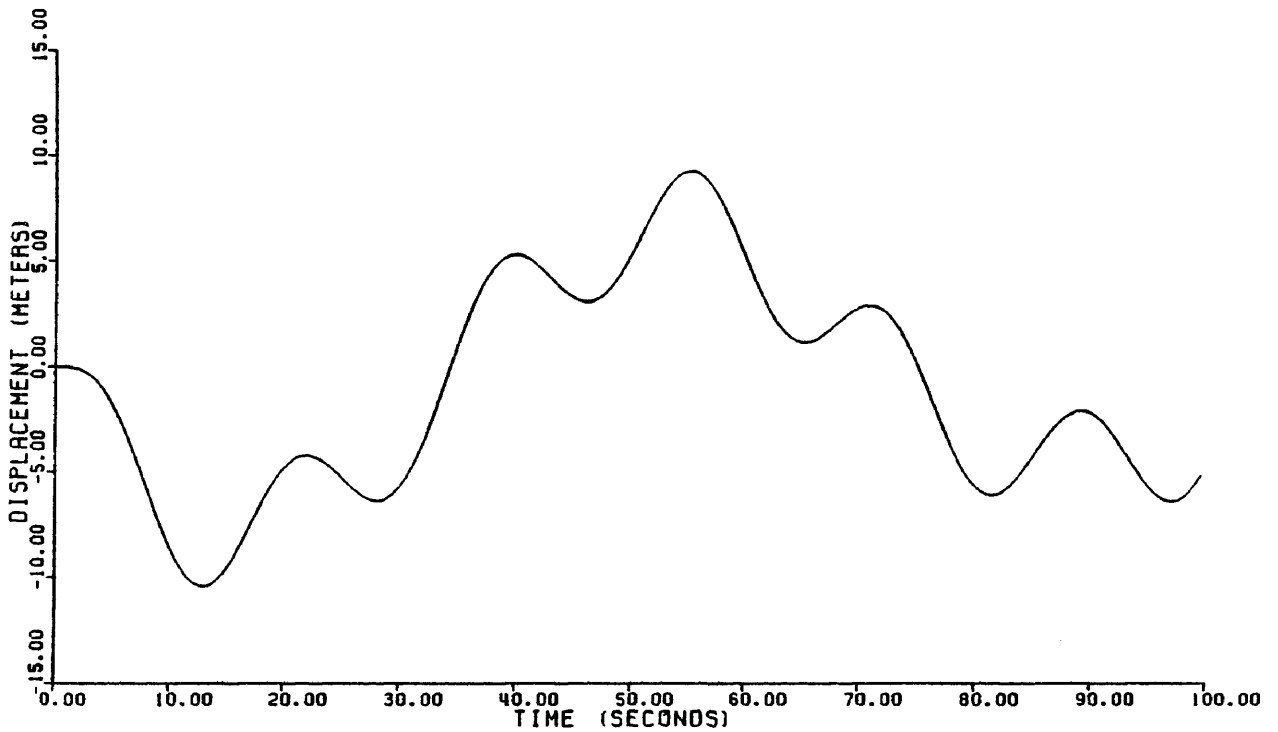


Fig. 21 - Time History Plot of Sway Displacement
(including Inertia and Drag Forces)

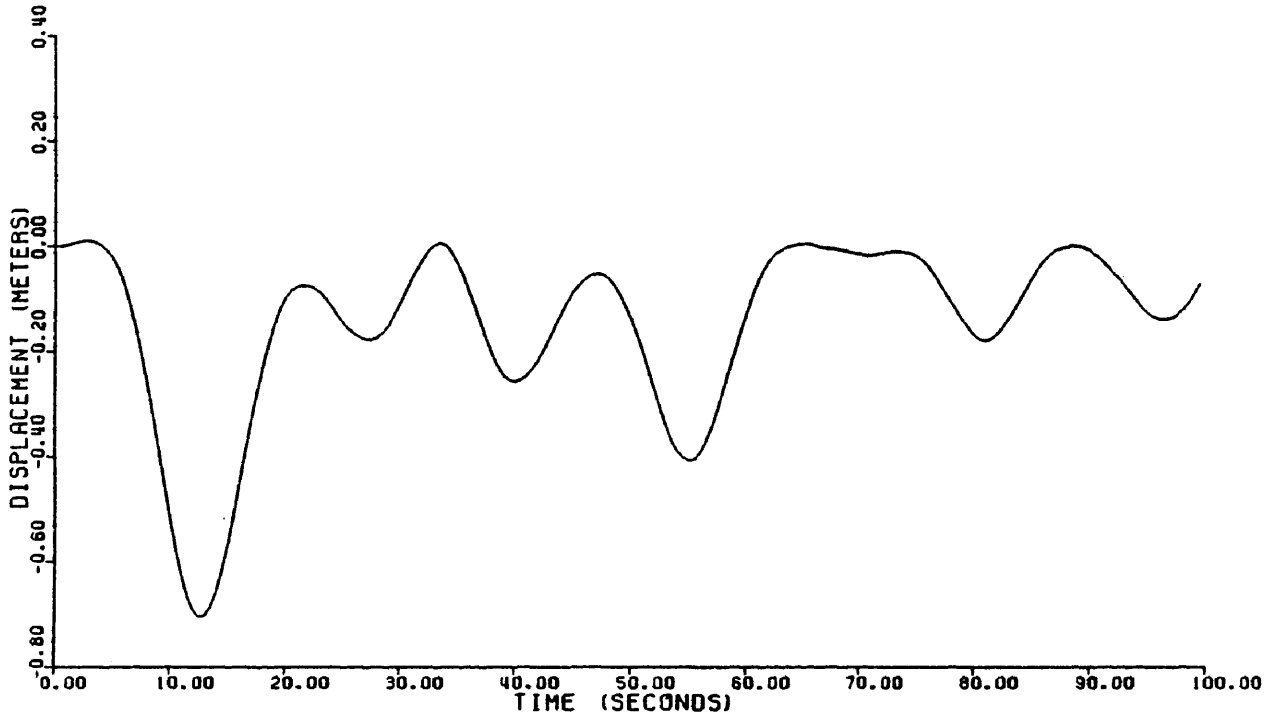


Fig. 22 - Time History Plot of Heave Displacement
(including Inertia and Drag Forces)

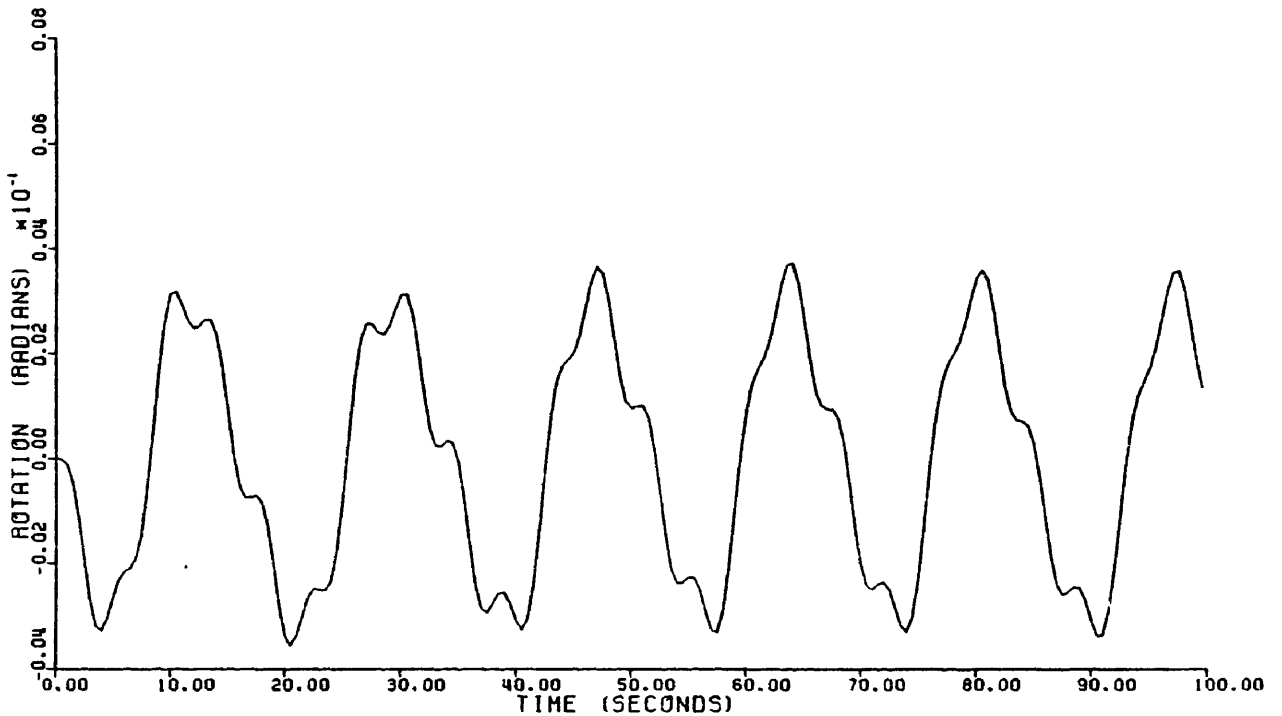


Fig. 23 - Time History Plot of Pitch Displacement
(including Inertia and Drag Forces)

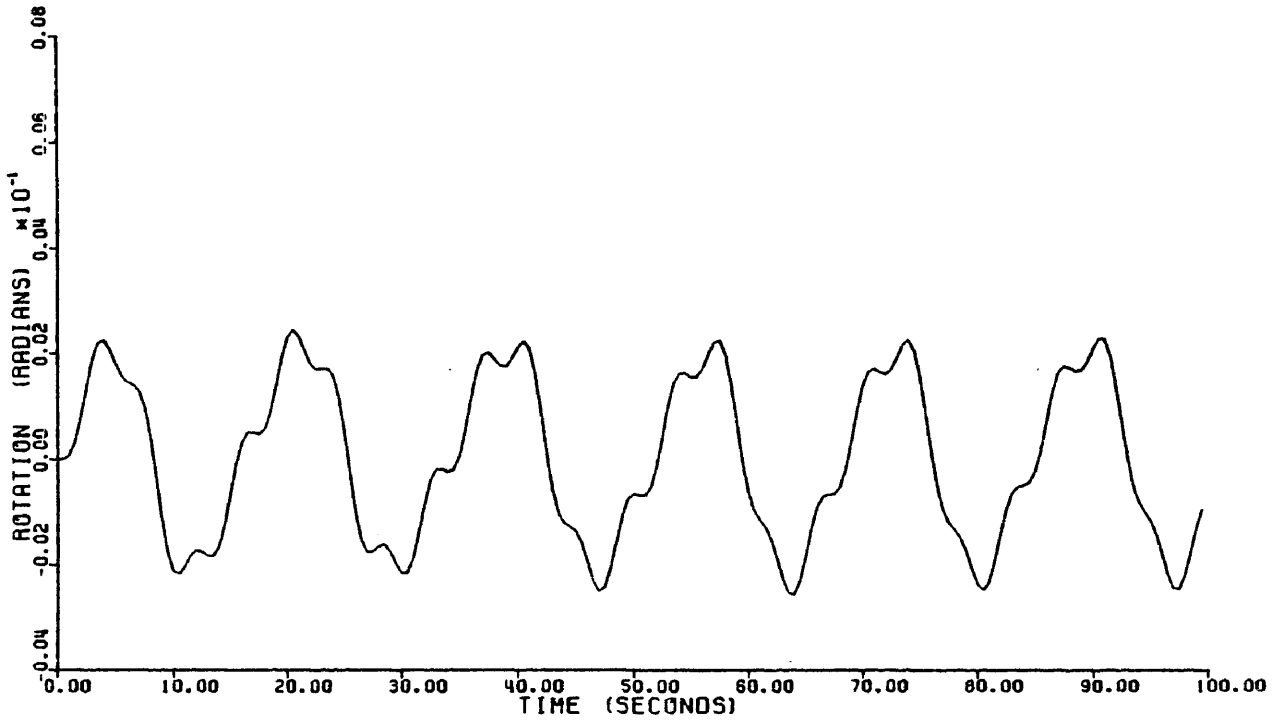


Fig. 24 - Time History Plot of Roll Displacement
(including Inertia and Drag Forces)

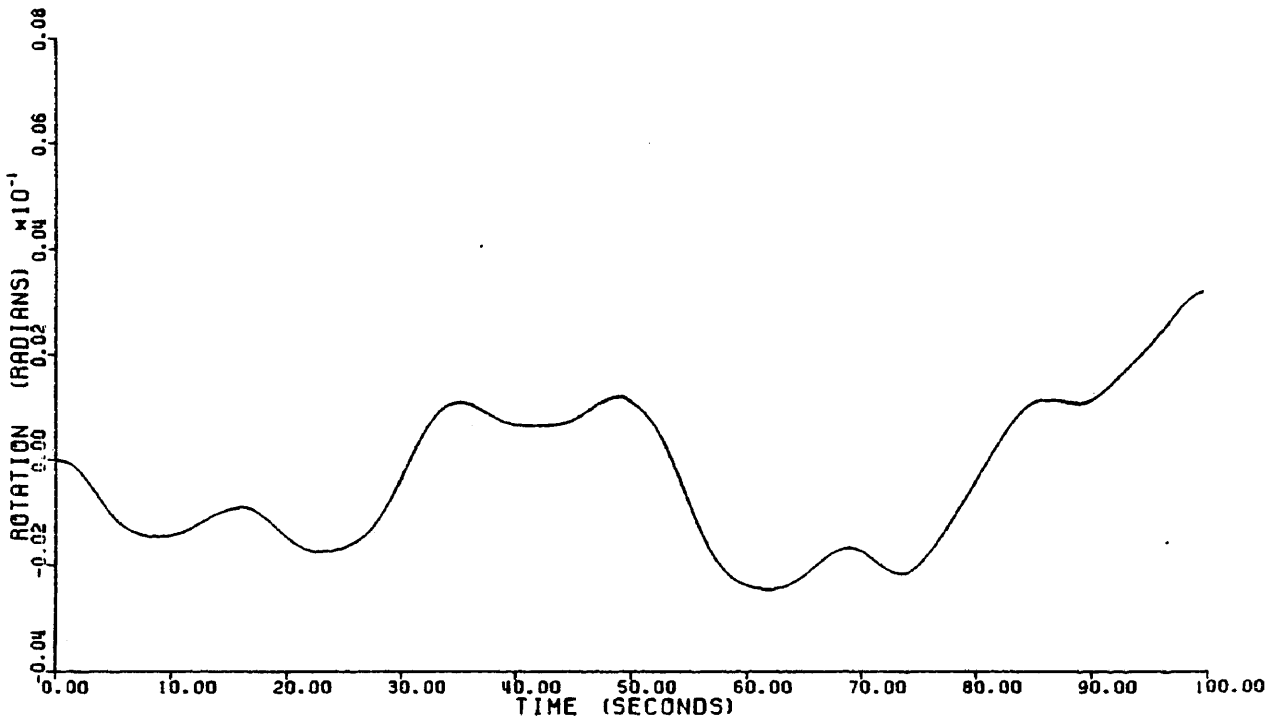


Fig. 25 - Time History Plot of Yaw Displacement
(including Inertia and Drag Forces)

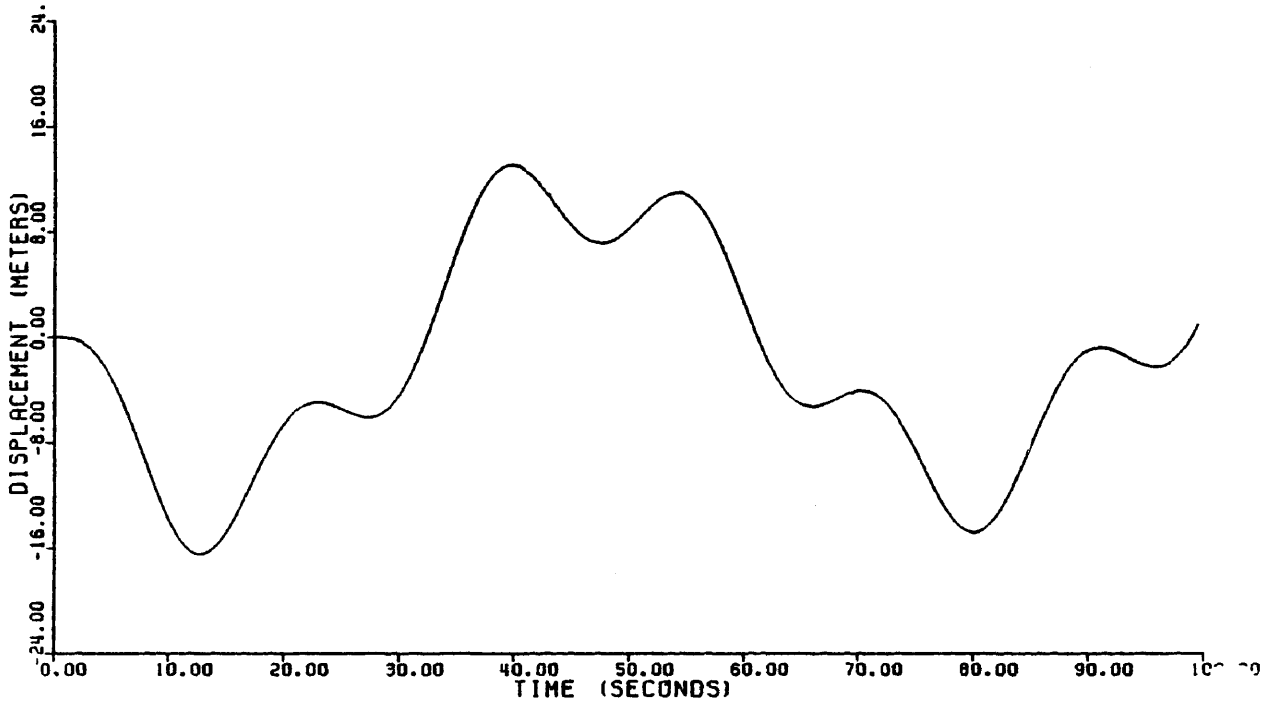


Fig. 26 - Time History Plot of Surge Displacement
(including only Inertia Forces)

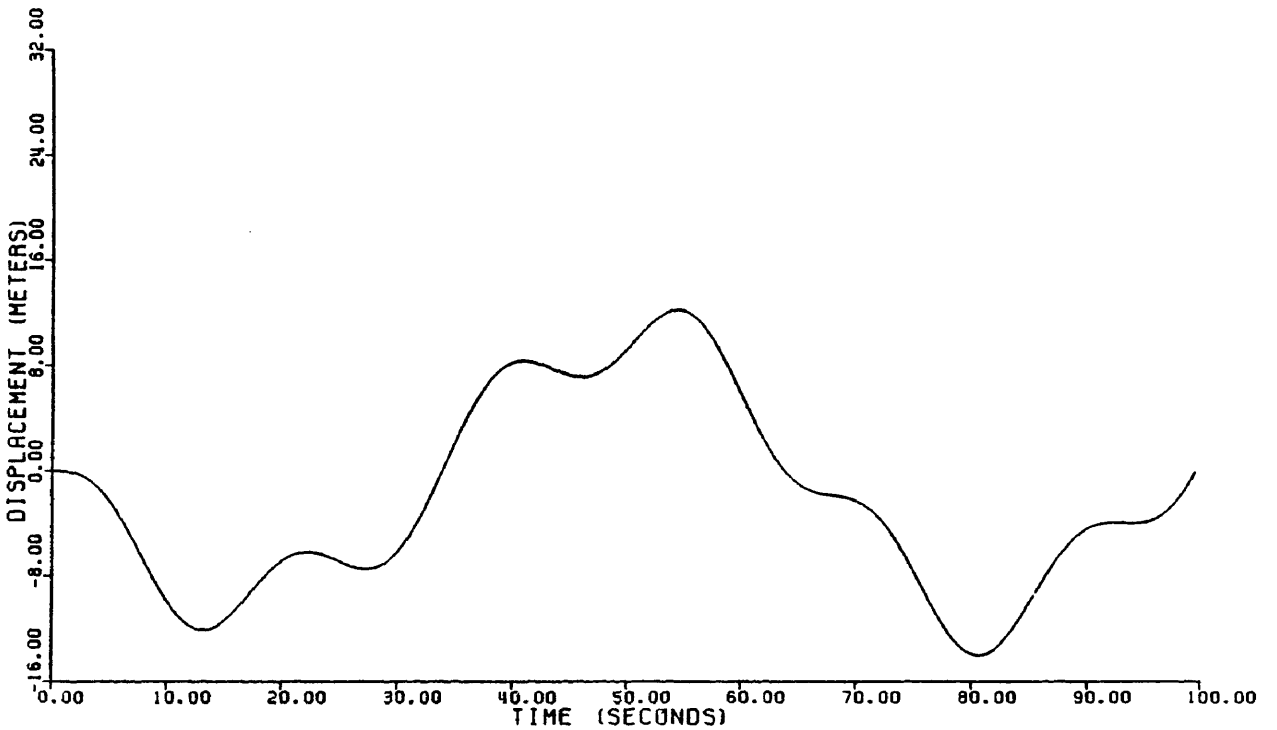


Fig. 27 - Time History Plot of Sway Displacement
(including only Inertia Forces)

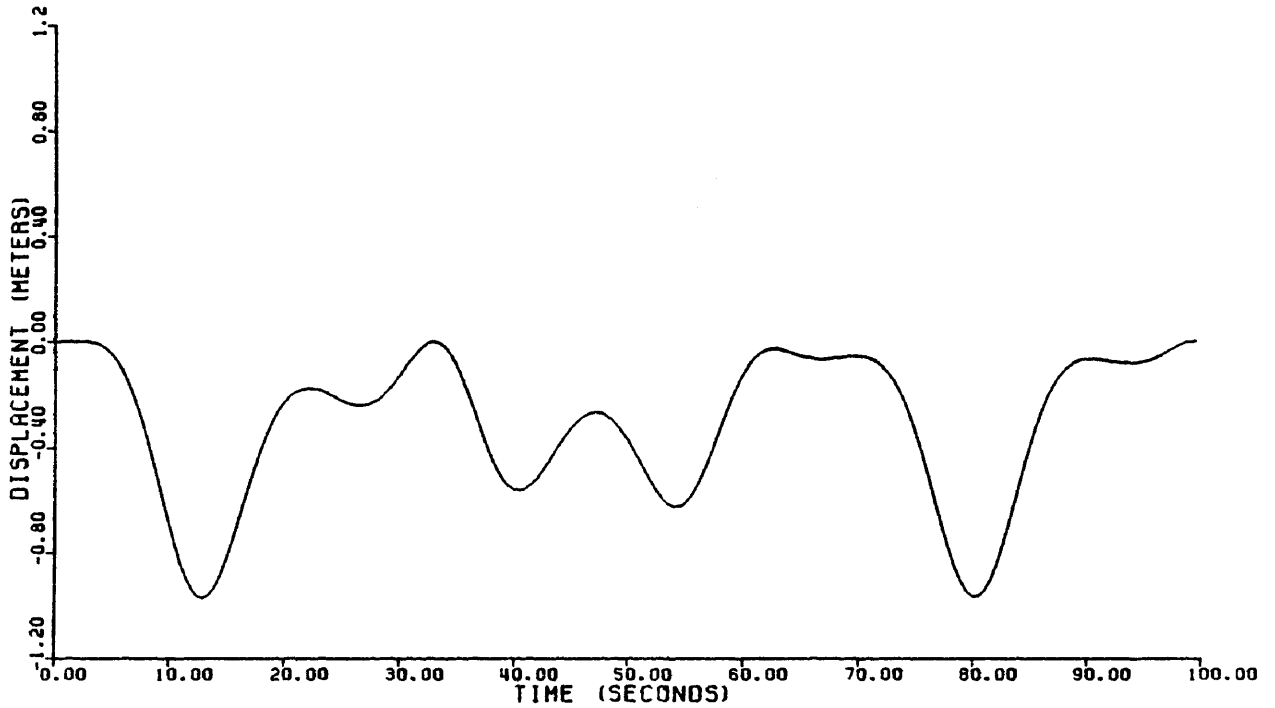


Fig. 28 - Time History Plot of Heave Displacement
(including only Inertia Forces)

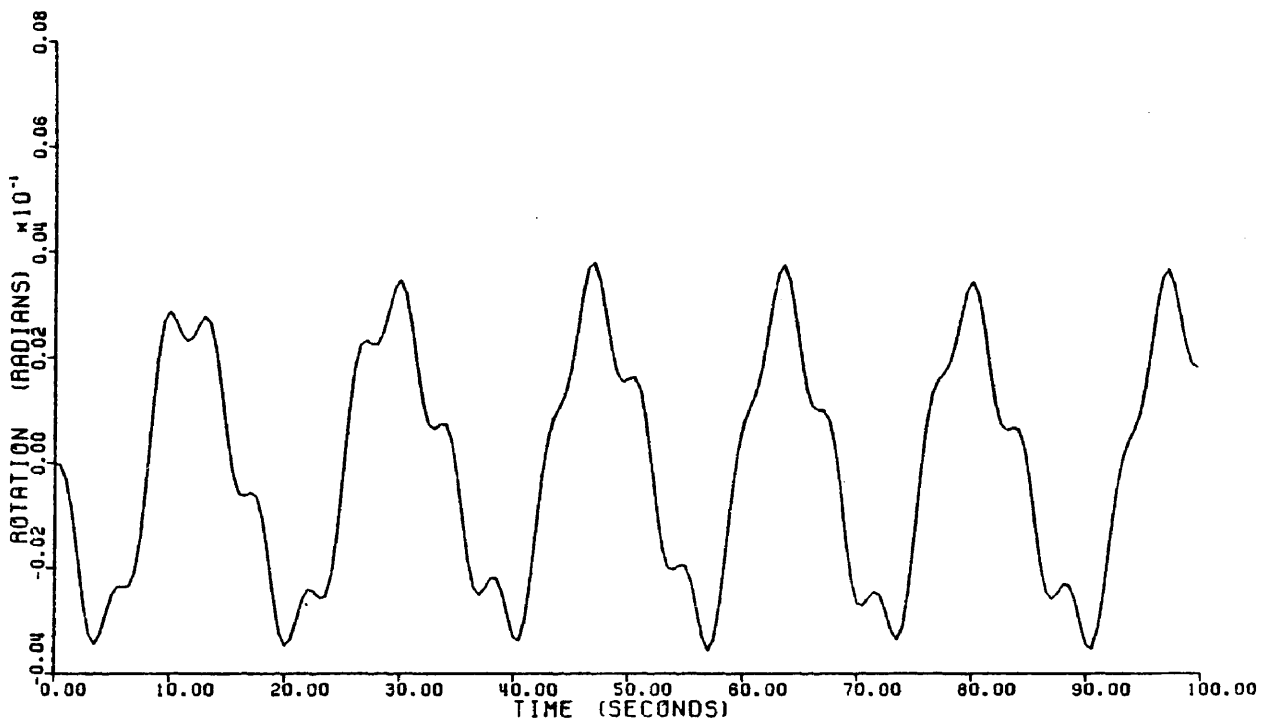


Fig. 29 - Time History Plot of Pitch Displacement
(including only Inertia Forces)

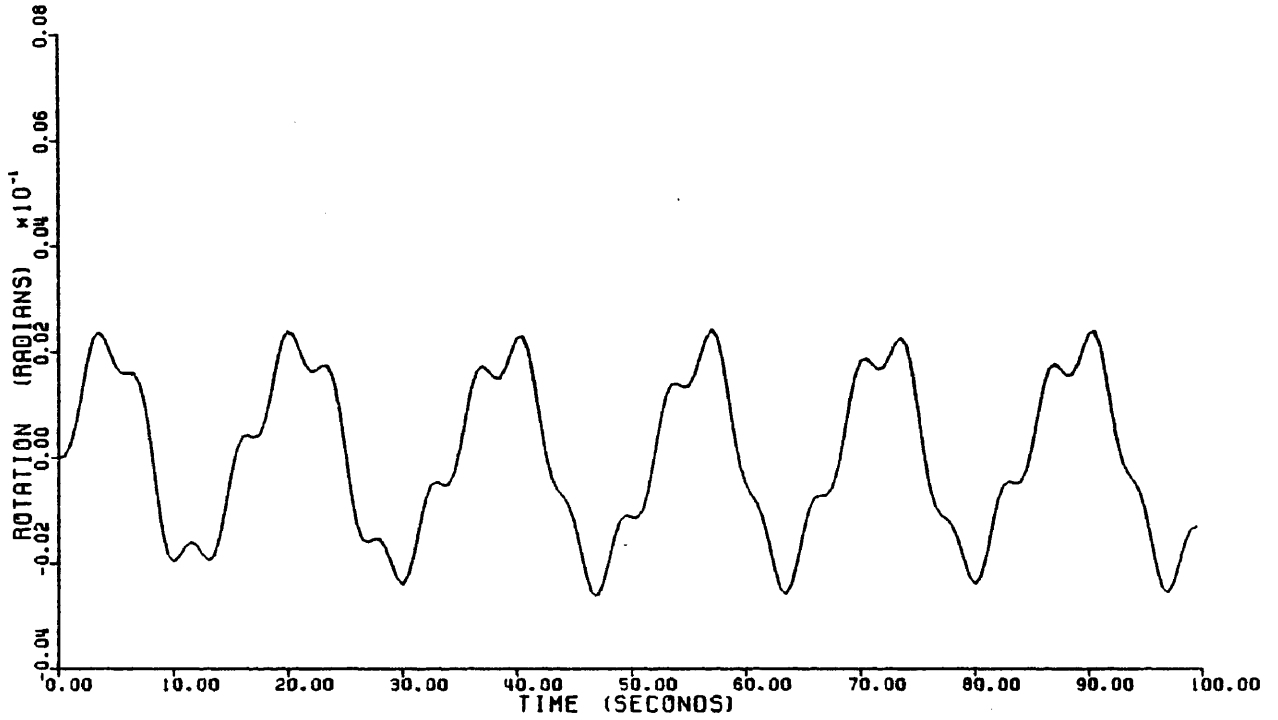


Fig. 30 - Time History Plot of Roll Displacement
(including only Inertia Forces)

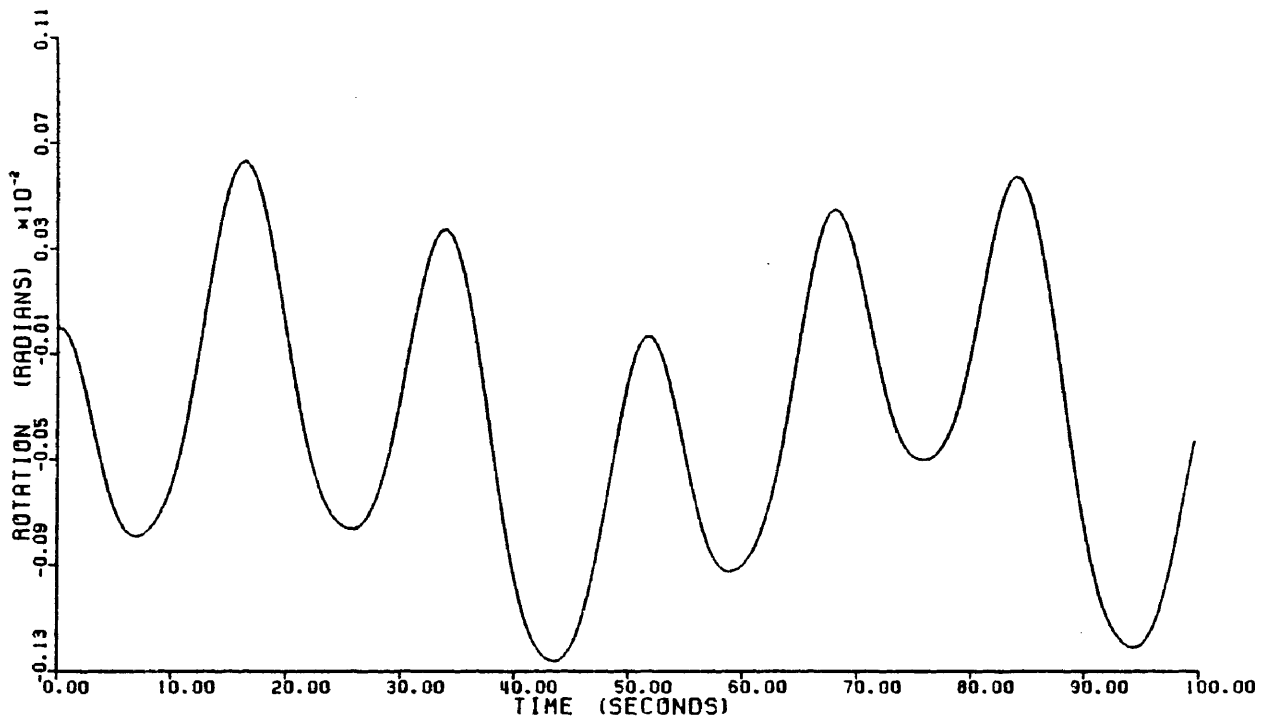


Fig. 31 - Time History Plot of Yaw Displacement
(including only Inertia Forces)

cases were studied in order to develop response spectra for the six degrees of freedom of the platform: case 1 including only fluid inertia forces (i.e., excluding drag forces), and case 2 including both inertial and drag forces.

The response spectra for surge ($\alpha = 0^\circ$) and sway ($\alpha = 90^\circ$) are shown in Figures 32 and 33, respectively. It can be seen that both surge and sway amplitudes reach a peak at a wave period of approximately 5 seconds and another peak at a period near 7 seconds. Zero response amplitudes, corresponding to zero resultant wave forces, occur at wave periods of 5.5 and 9.5 seconds at which the wave lengths are 47 and 140 meters, respectively. This arises from a "force cancellation" caused by spacing of middle and corner columns. For wave periods greater than 9.5 seconds the response amplitudes increase consistently (but not necessarily linearly) as seen in the figures. The dashed lines in Figures 32 and 33 indicate the response of surge and sway for case 1 (inertia forces only), whereas the solid lines depict the response spectra for case 2 (inertial and drag forces). It is clear that drag forces result in a decreased response amplitude throughout the range of wave periods. For example, for $T = 16$ seconds the surge response amplitude is approximately 11 meters for case 1 and 10 meters for case 2; i.e., drag accounts for a response reduction of about 10 percent. For a wave period of 8 seconds, however, the response amplitude is 8.6 meters for case 1 and 5.5 meters for case 2; i.e., drag accounts for a reduction in response of more than 35 percent. Therefore, a significant overestimation of the response amplitude can result from neglecting drag.

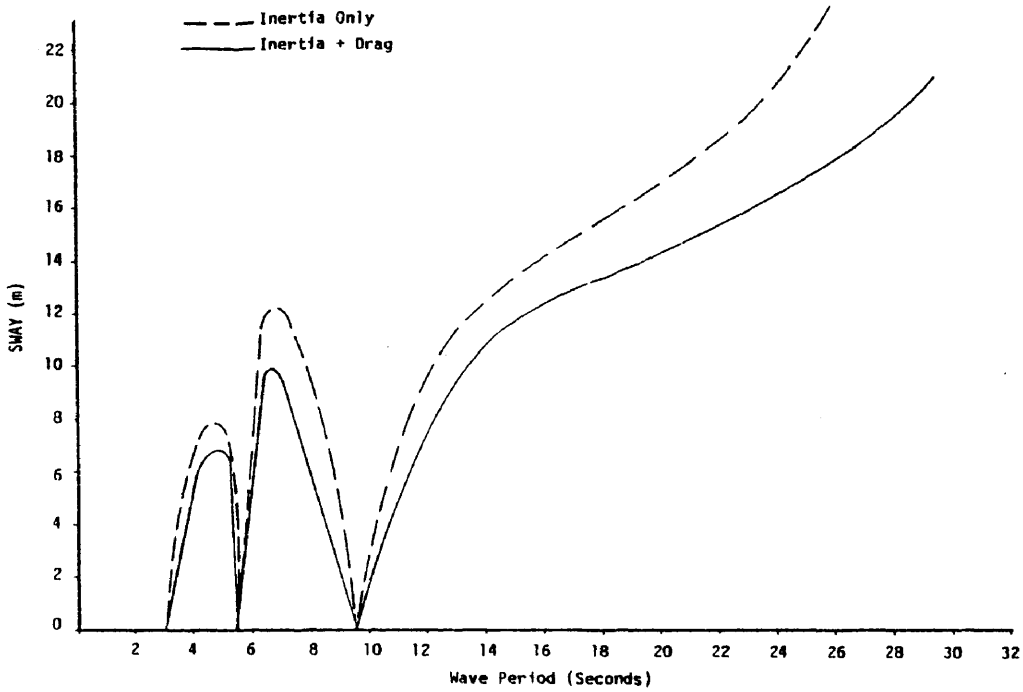


Fig. 32 - Response Spectrum for Surge Displacement

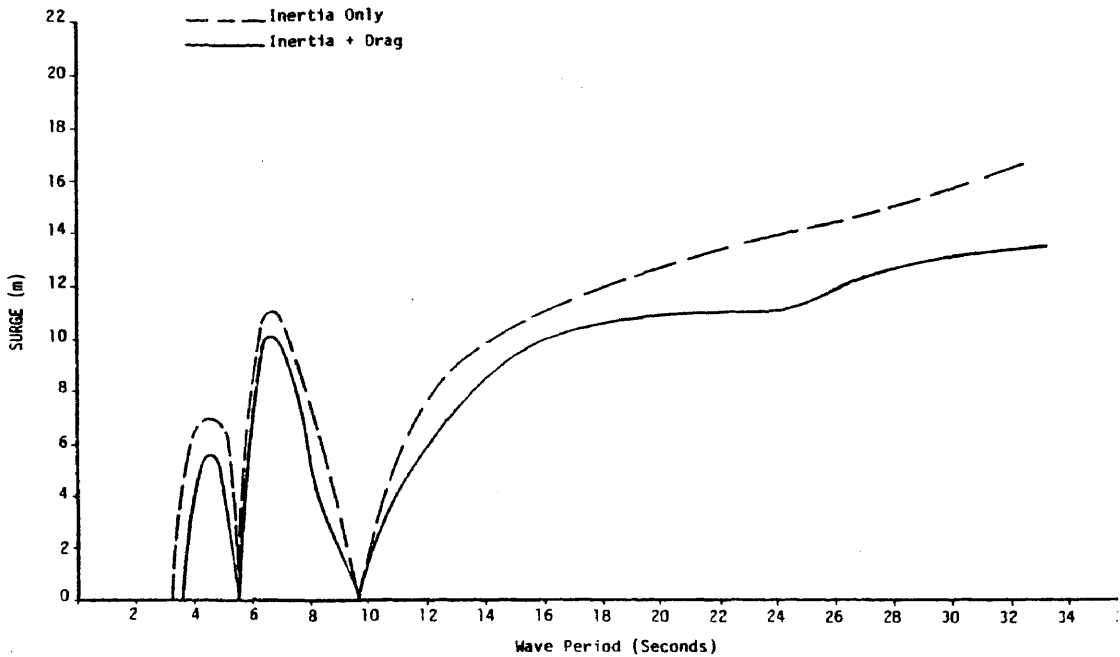


Fig. 33 - Response Spectrum for Sway Displacement

The response spectra of heave for $\alpha = 0^\circ$ and $\alpha = 90^\circ$, respectively, are illustrated in Figures 34 and 35. It can be seen that heave response spectra show similar trends to those of surge and sway. This arises from a strong coupling of heave to surge ($\alpha = 0^\circ$) and heave to sway ($\alpha = 90^\circ$) in the stiffness equations as presented in Chapter II. The calculations of the cable tensions caused by the platform displacements in six degrees of freedom can give misleading results if coupling of heave to sway and surge is ignored. The time histories for coupled and uncoupled heave response for $T = 17$ seconds and $H = 15$ meters are shown in Figures 36 and 37, respectively. Based on a comparison of these dramatically different curves, the author concludes that coupling effects should not be neglected.

The results of response amplitude calculations for pitch and roll (Figures 38 and 39) indicate that at low wave periods the response for pitch and roll reaches its maximum value. Pitch and roll also exhibit the "force cancellation" phenomenon described for sway and surge. The effect of drag on pitch and roll also can be seen in the figures, but the percentage of reduction in response amplitudes is small.

The response spectrum for yaw at $\alpha = 35^\circ$ is given in Figure 40. A sharp peak in yaw response amplitude occurs at a wave period of 6 seconds. The response amplitude decreases rapidly for periods larger than 6 seconds and is negligible for periods larger than 10 seconds. The peak yaw response may occur at different wave periods for different angles of wave propagation.

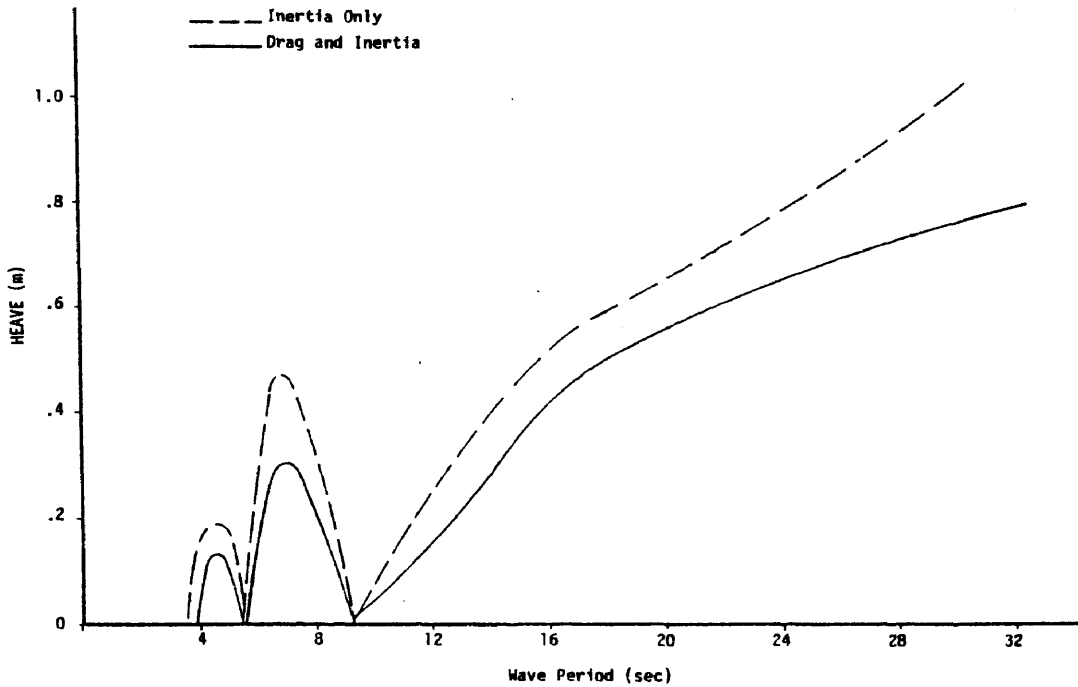


Fig. 34 - Response Spectrum for Heave Displacement for $\alpha = 0^\circ$

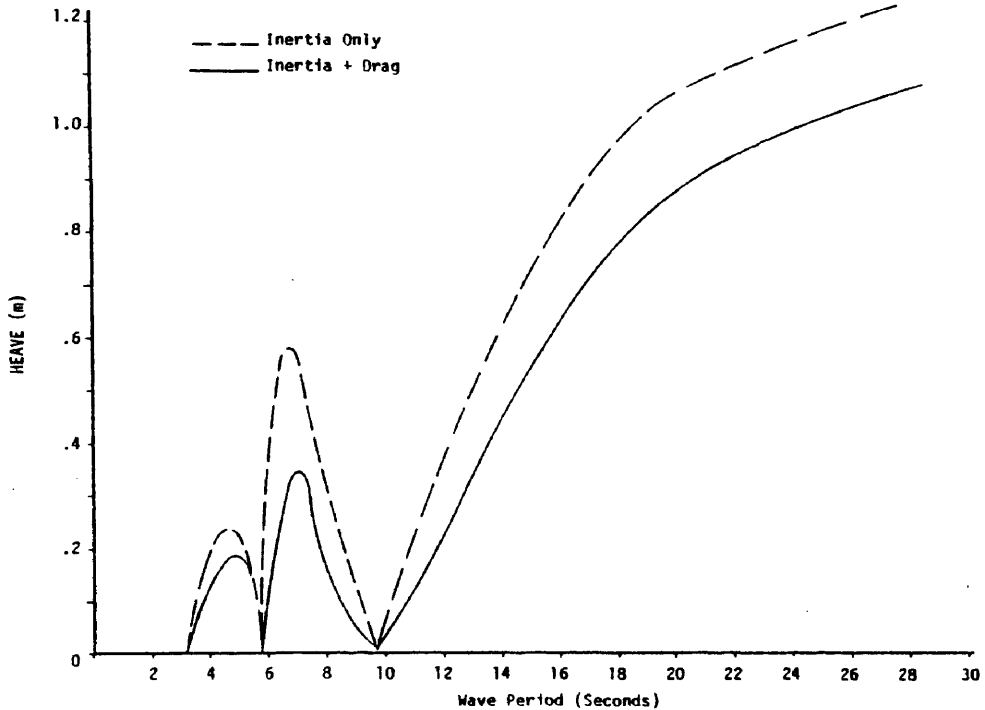


Fig. 35 - Response Spectrum for Heave Displacement for $\alpha = 90^\circ$

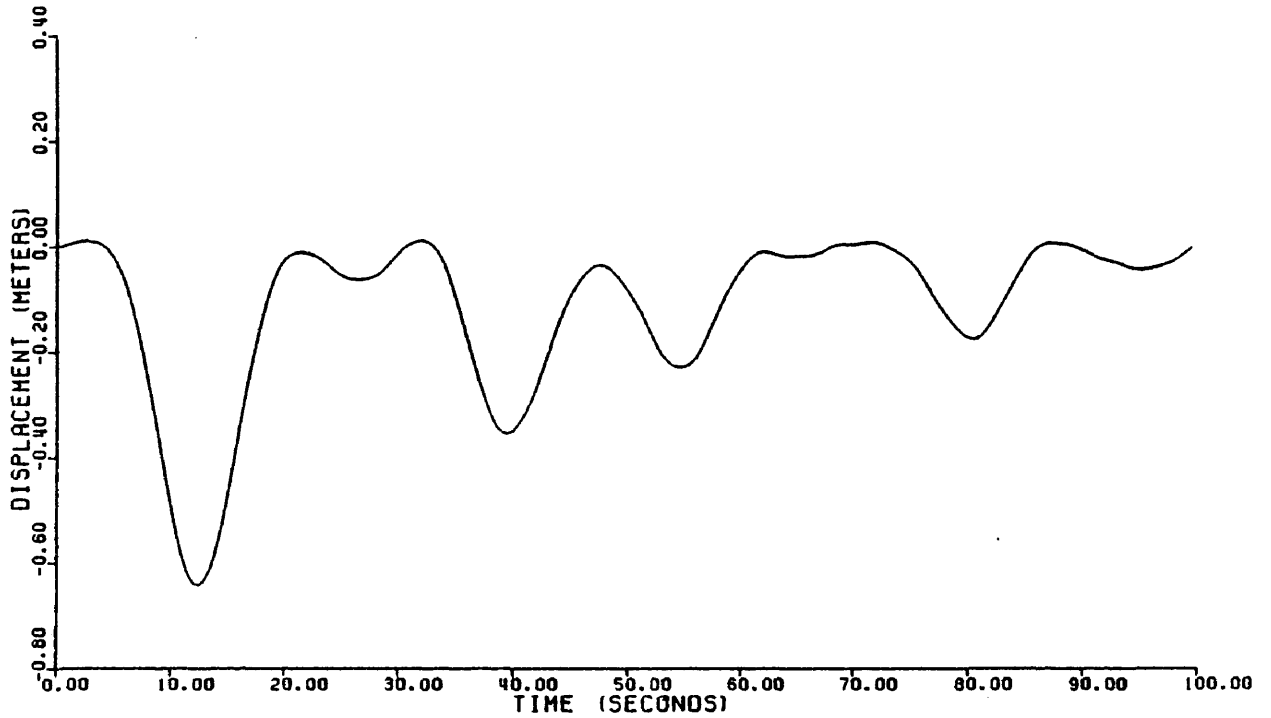


Fig. 36 - Time History of Coupled Heave Response

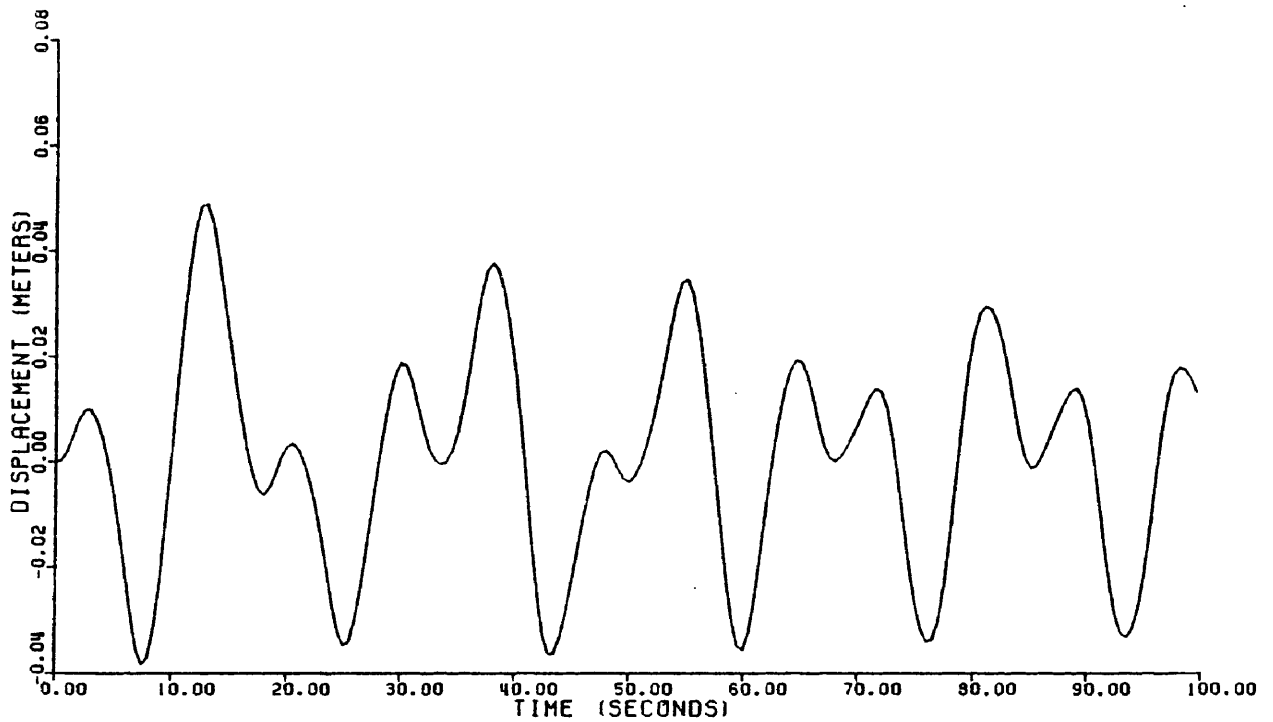


Fig. 37 - Time History of Uncoupled Heave Response

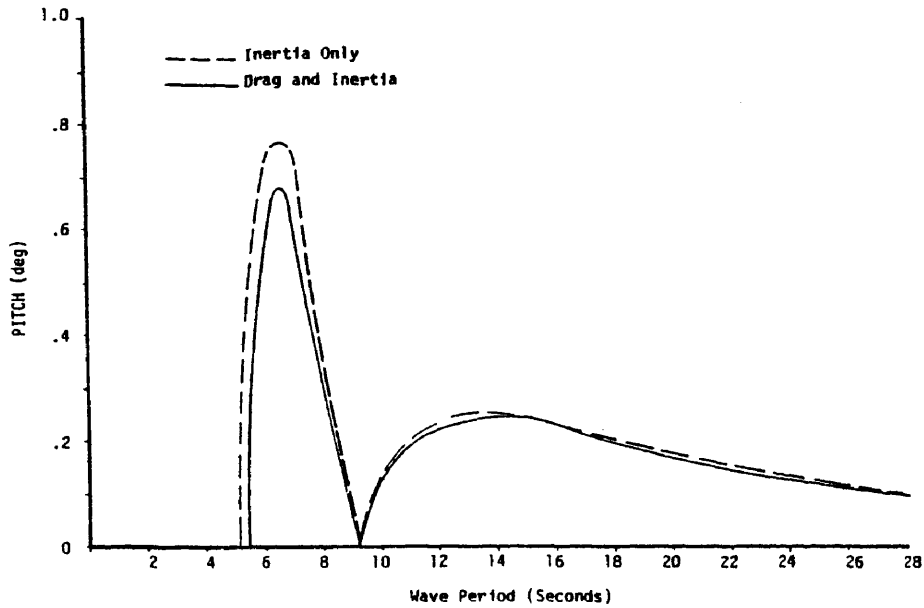


Fig. 38 - Response Spectrum of Pitch Rotation

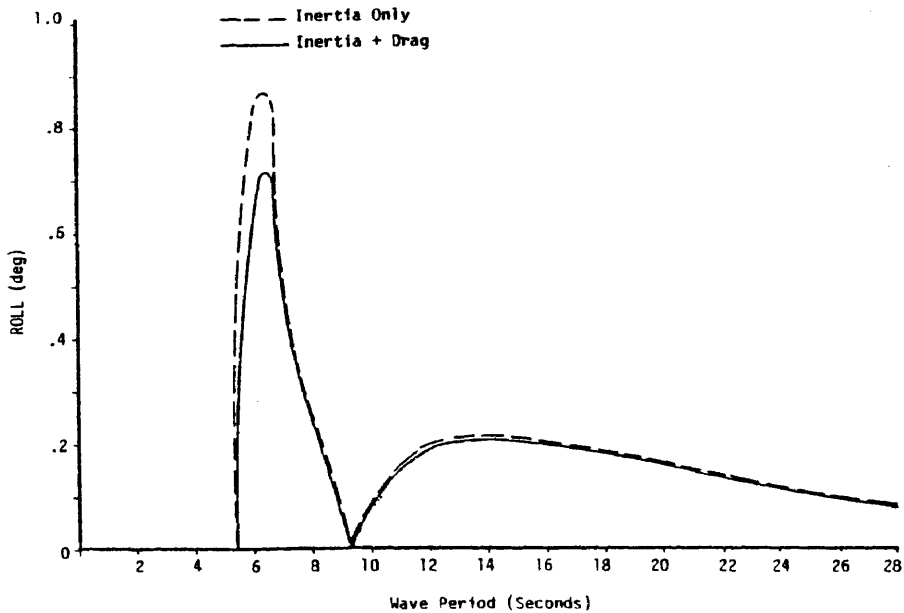


Fig. 39 - Response Spectrum of Roll Rotation

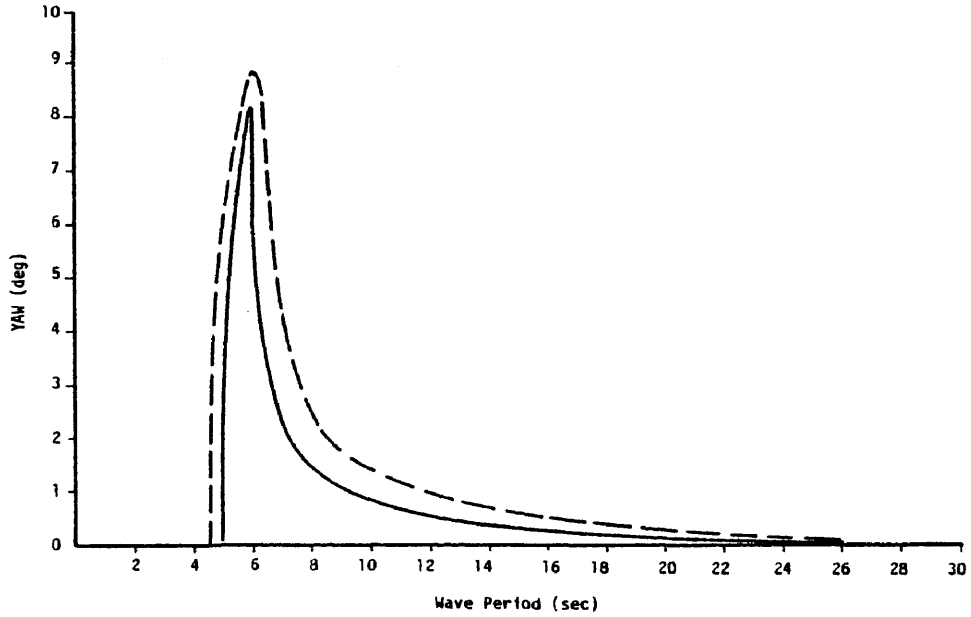


Fig. 40 - Response Spectrum of Yaw Rotation

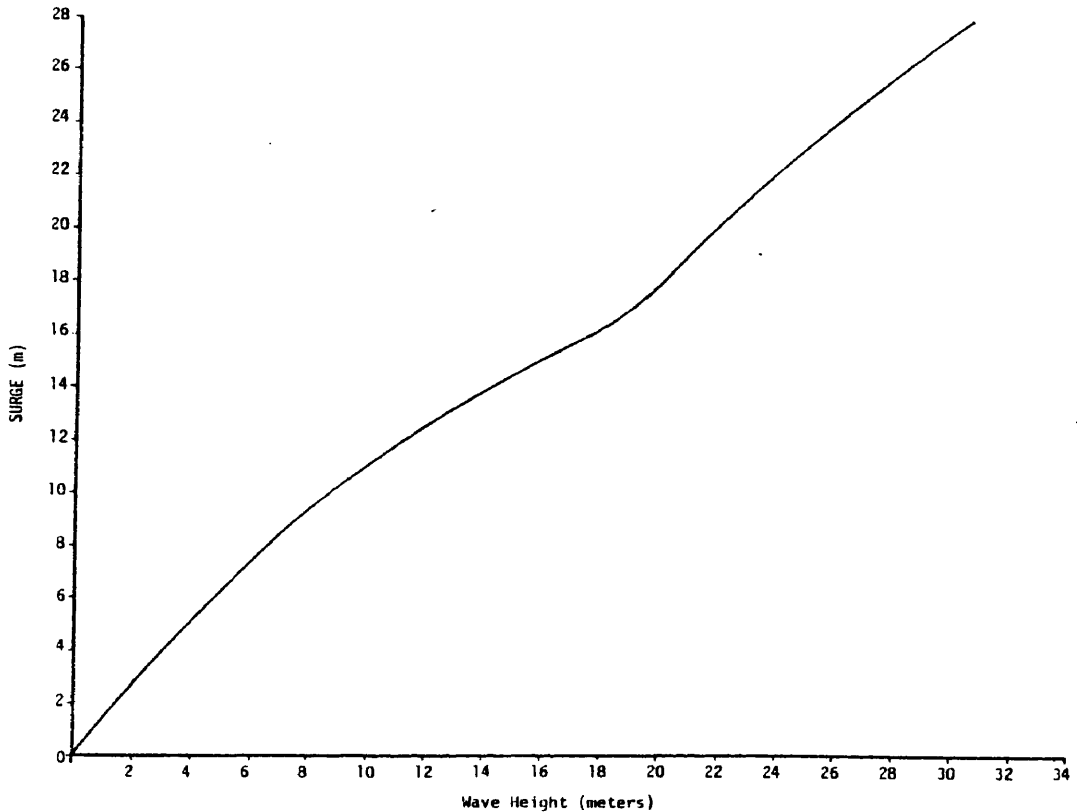


Fig. 41 - Variation of Surge Response Amplitude with Wave Height

Parametric Study

Wave Height

Wave heights were varied in the range 0-30 meters for a constant wave period of 17 seconds. Response amplitude versus wave height plots for surge, heave, and pitch are given in Figures 41-43. The plots indicate a relationship that is essentially linear for small wave heights (i.e., for wave heights smaller than about 15 meters). For large wave heights, however, this linearity does not hold true. For example, in Figure 41 there is a significant shift in slope for wave heights greater than about 19 meters. Attempts to normalize response spectra with respect to wave height, therefore, must consider only the range of wave heights where linear relationships are applicable.

Water Depth

Water depths were varied in the range 100-1000 meters for the significant sea state used in the rest of the analysis. Figures 44-46 illustrate the variation of response amplitudes of sway, heave, and roll, respectively, with water depth. As can be seen in the above plots, the roll response amplitude increases linearly with water depth. The sway response amplitude, however, does not vary linearly with water depth. While sway and roll amplitudes increase (linearly or otherwise) with water depth, that of heave decreases sharply in the range 100-400 meters and then it starts to increase slowly for depths greater than 400 meters (see Figure 45). Decrease in heave for deeper water arises from the decrease in cable stiffness ($k = AE/L$) corresponding to an

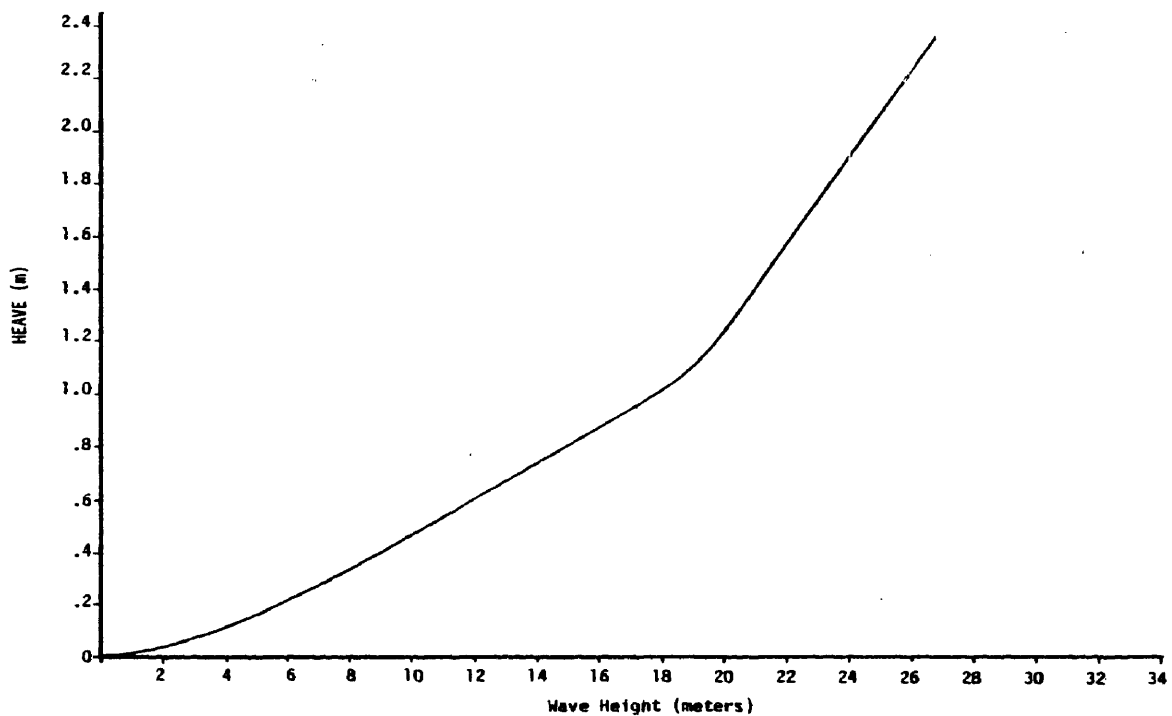


Fig. 42 - Variation of Heave Response Amplitude with Wave Height

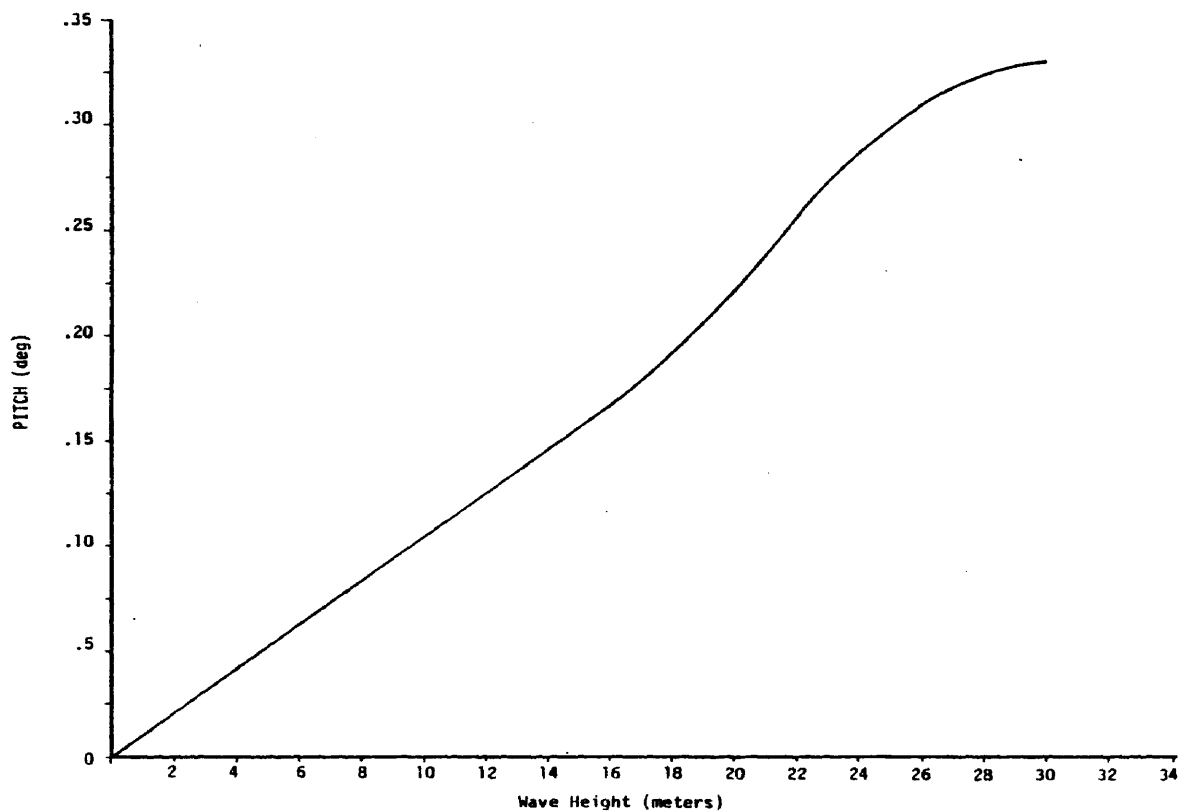


Fig. 43 - Variation of Pitch Response Amplitude with Wave Height

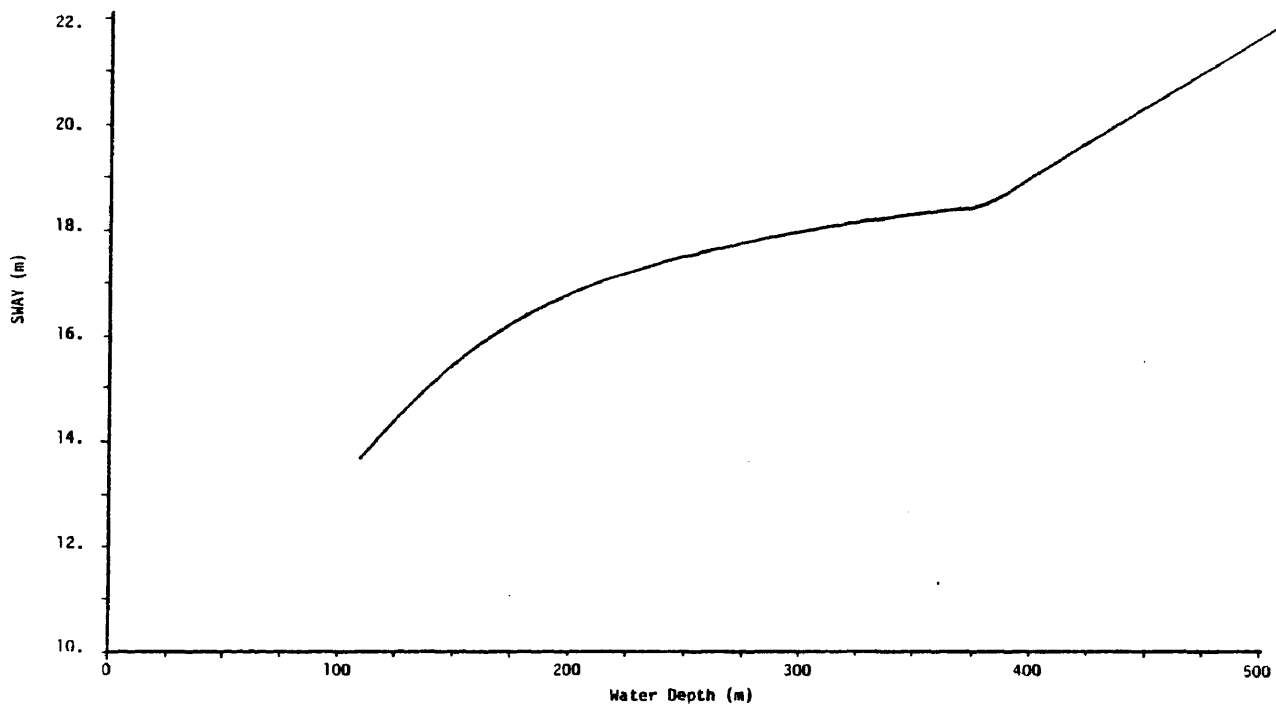


Fig. 44 - Variation of Sway Response Amplitude with Water Depth

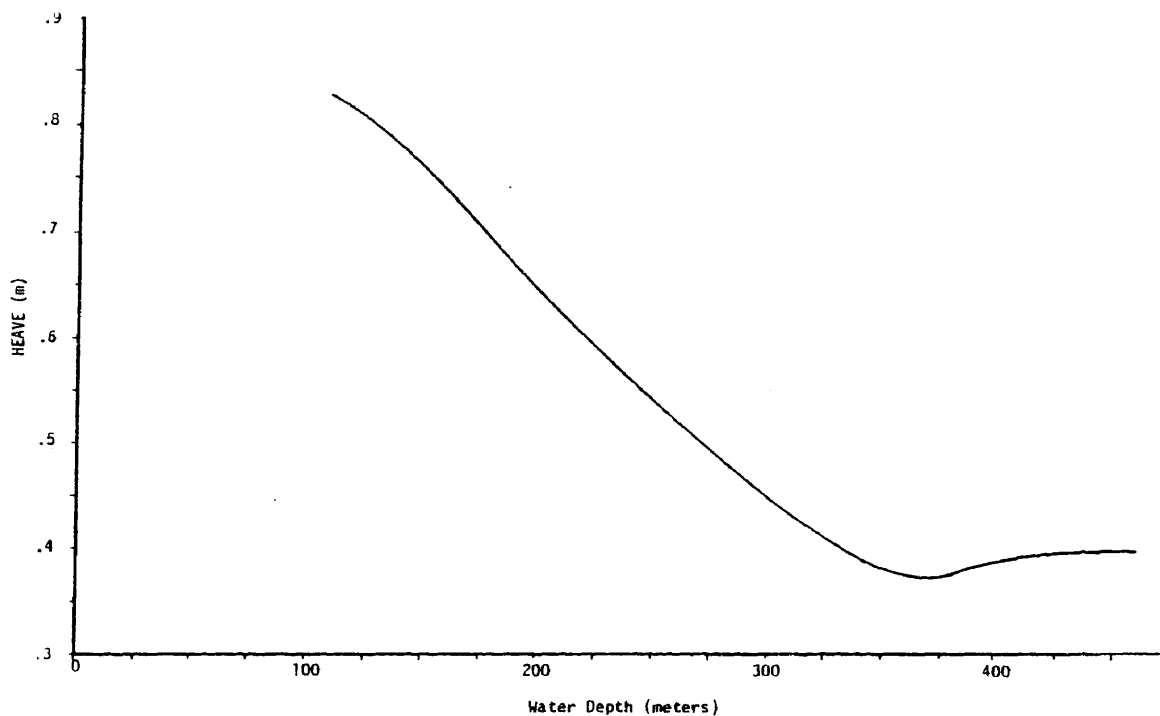


Fig. 45 - Variation of Heave Response Amplitude with Water Depth

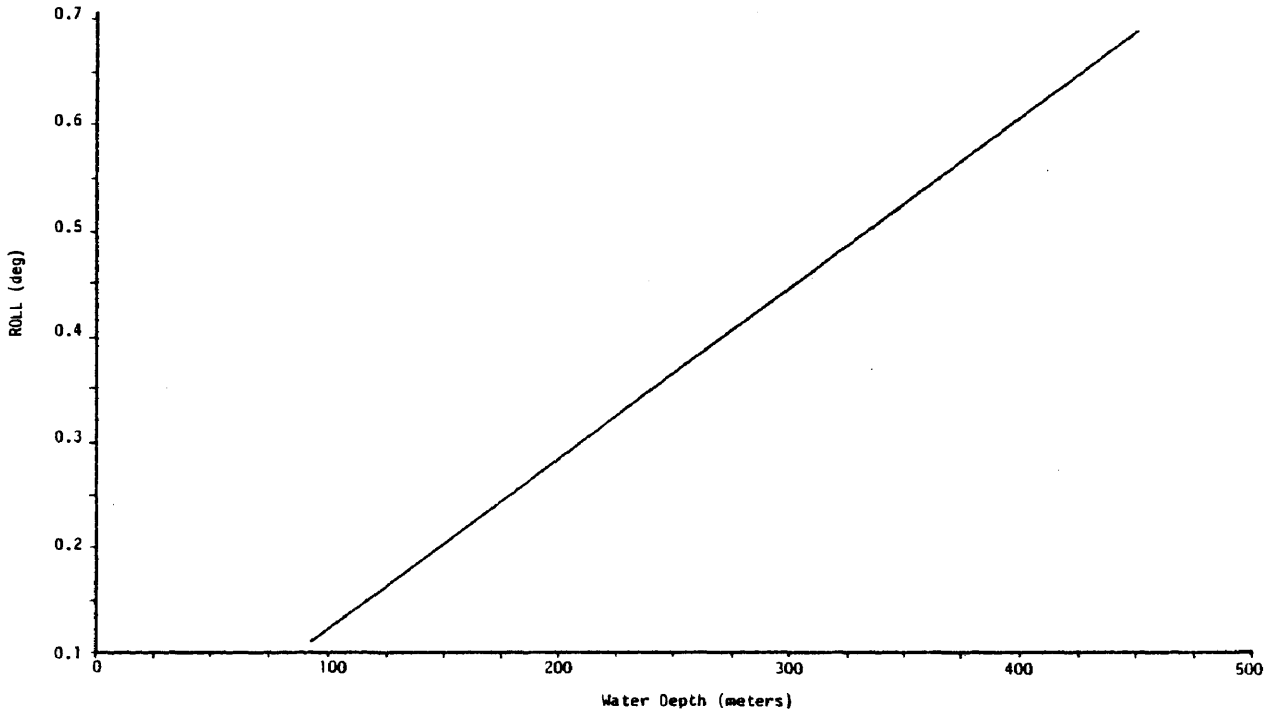


Fig. 46 - Variation of Roll Response Amplitude with Water Depth

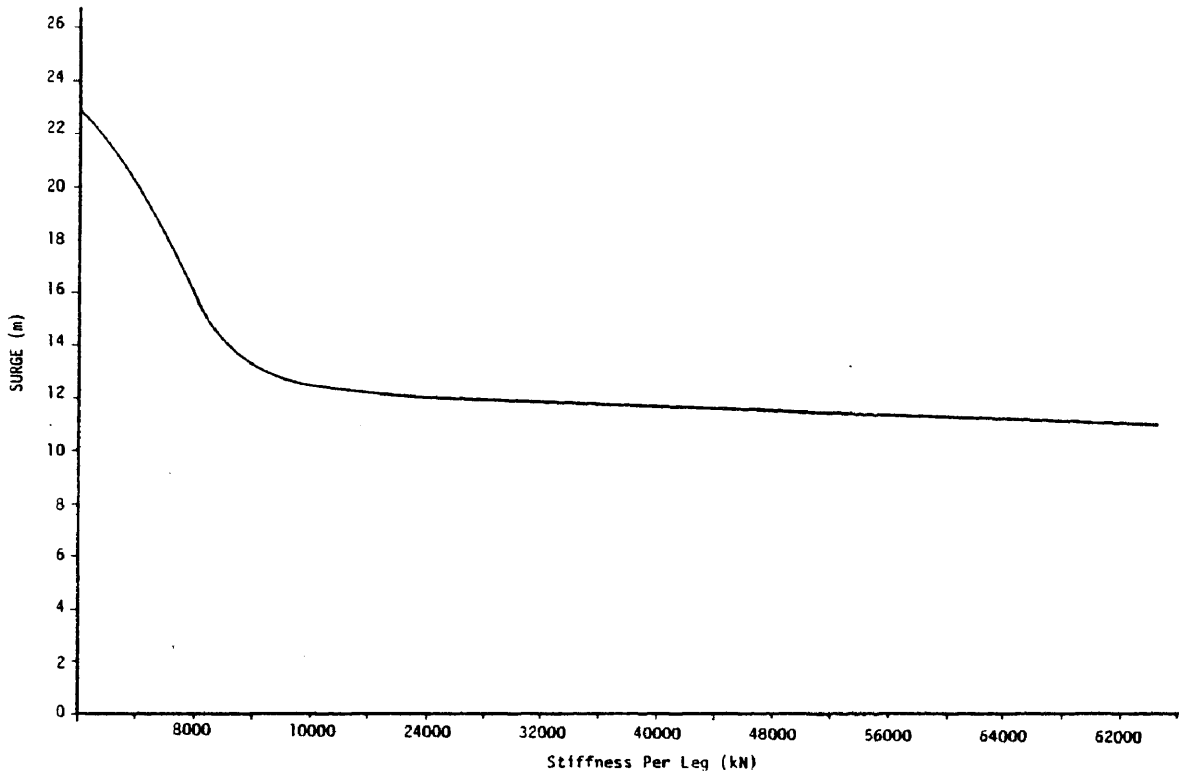


Fig. 47 - Variation of Surge Response Amplitude with Cable Stiffness

increase in cable length. The less stiff the cables, the smaller is the effect of coupling between heave and surge or between heave and sway. Therefore, as the platform surges or sways in increasing water depths, the heave is less dependent on sway or surge; hence heave response amplitudes are smaller. Surge and pitch response amplitude variations with water depth are similar to those of sway and roll, respectively. Yaw response amplitude variation with water depth was found to be small and hence can be neglected.

Cable Stiffness

The stiffness of the tension legs may be varied by increasing the number of chains per leg, the cross-sectional area, or the elastic modulus of the chains. The variation of response amplitudes of surge, heave, and pitch, respectively, with respect to cable stiffness, at a constant water depth of 125 meters are shown in Figures 47-49. The plots show that the response of the structure drops sharply with an increase in cable stiffness up to about 20,000 kN/m for pitch and 12,000 kN/m for surge and heave. The effect of additional stiffness decreases rapidly as seen in the figures.

Initial Tension

Changing the initial tension involves changes in other variables such as buoyancy, added mass, draft (depth of submerged portion of platform), and cable length. Since for a constant water depth the cable length plus the draft should be equal to the water depth, the buoyancy, added mass, and cable tension are calculated for different

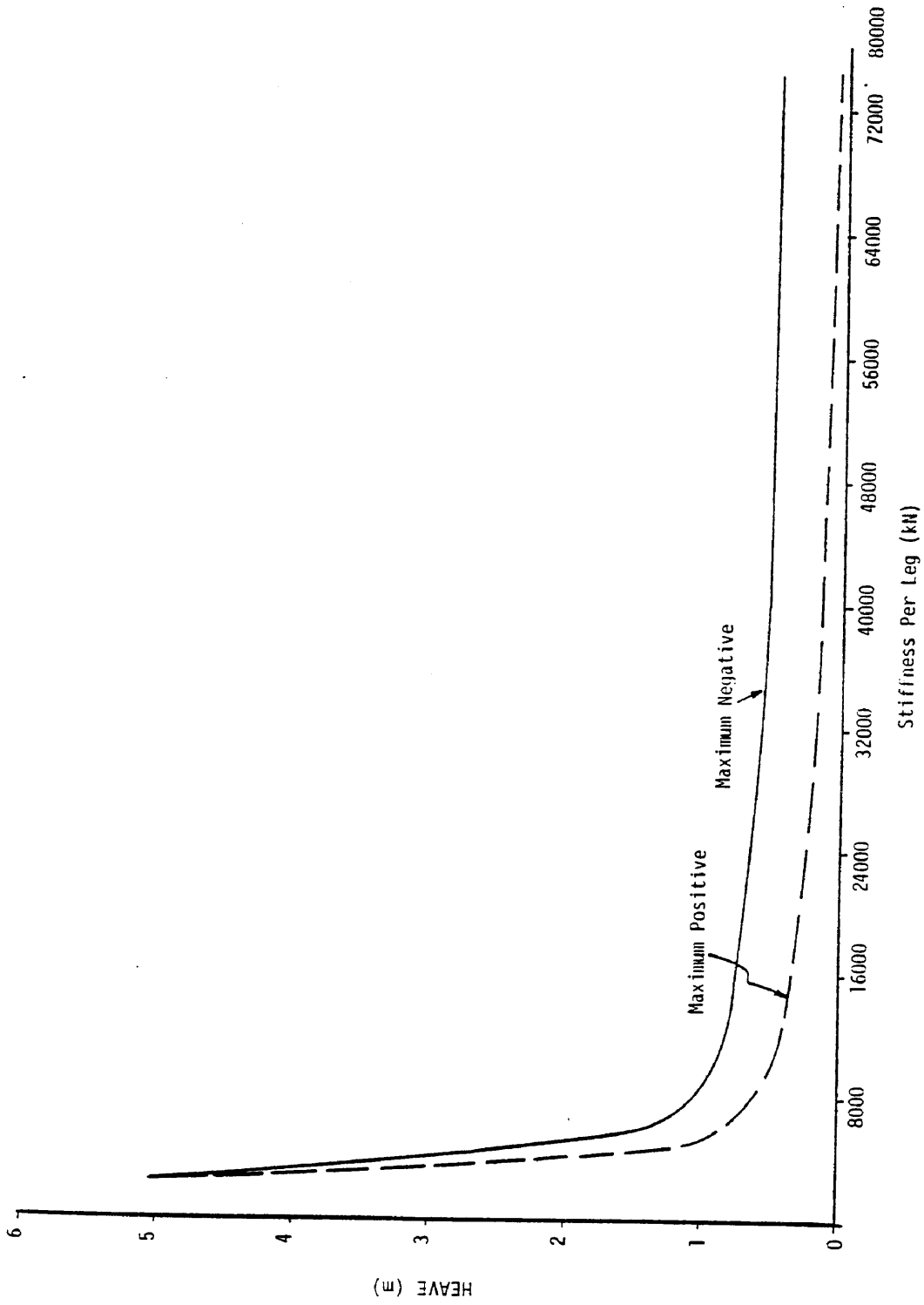


Fig. 48 - Variation of Heave Response Amplitude with Cable Stiffness

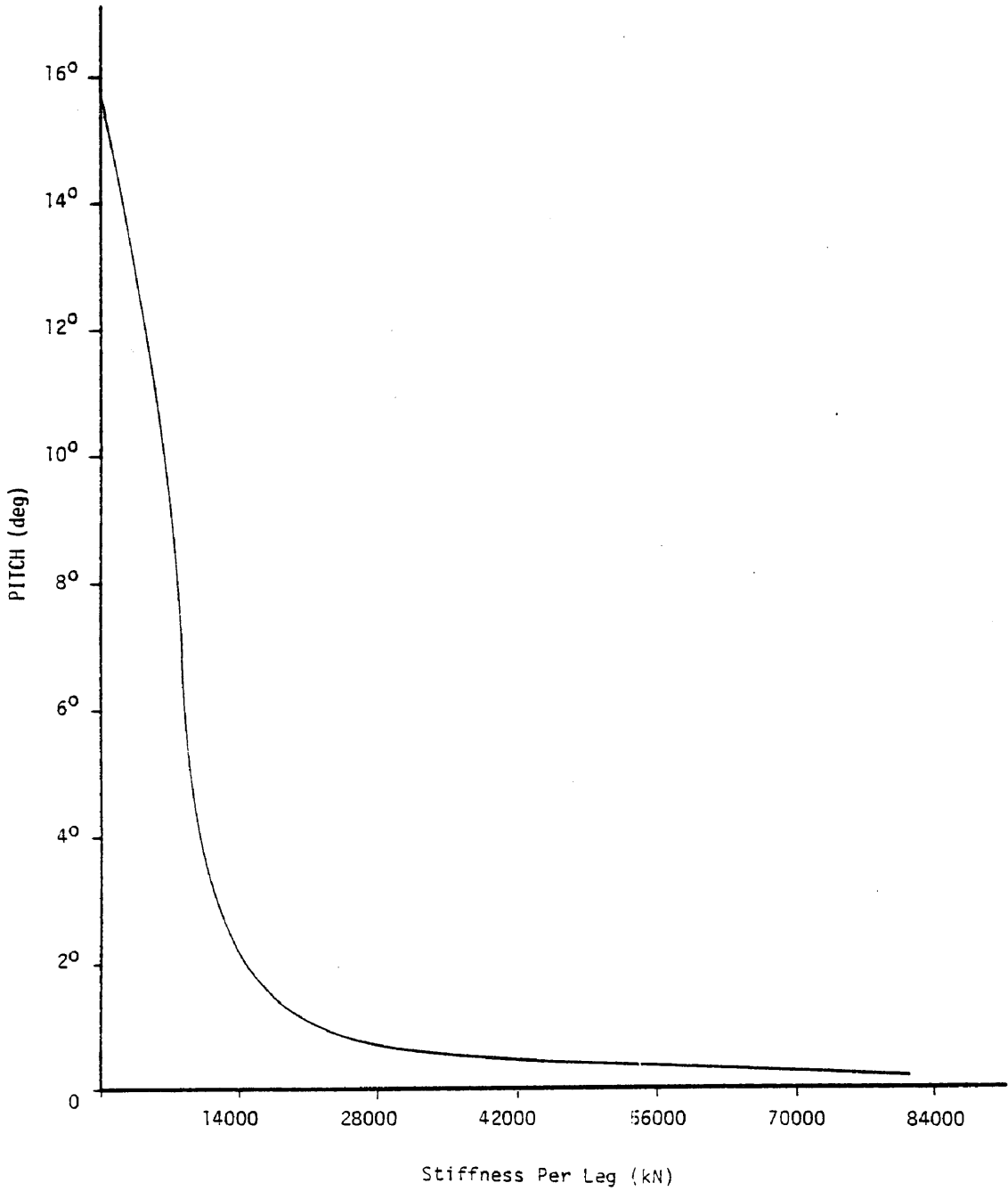


Fig. 49 - Variation of Pitch Response Amplitude with Cable Stiffness

cable length-draft combinations. The variables involved were changed in a manner such that the variation in cable tension ranged from zero to 100,000 kN per leg. Cable stiffness was kept constant at 73,888 kN/m, and water depth was 160 meters.

Response amplitudes for sway, heave, and roll, respectively, versus initial cable tension are depicted in Figures 50-52 for a 90° wave incidence angle. A significant decrease in response can be seen for initial tensions of up to 45,000 kN/leg in the case of sway and heave, and 35,000 kN/leg in the case of roll. As the initial tension is increased further, the response amplitudes start to increase until they reach a peak and then decrease again. While one would expect a continuous decrease in response from an increase in initial tension, the results obtained here show that this is not always the case. For the range of initial tensions where the response amplitudes increase, the structure's stiffness changes and the natural periods of vibration reach a range where the forcing function can cause resonance (see Figure 52).

Direction of Wave Propagation

In order to gain a better understanding of the effects of change in direction of wave propagation on the response of the structure, the platform properties and member dimensions were modified slightly such that the structure becomes symmetric. The angle of wave propagation (α) was varied in the range between zero and 90°. The response of surge and sway to direction of wave propagation is presented in Figure 53. Surge has a maximum amplitude at $\alpha = 0^\circ$ and a zero amplitude at

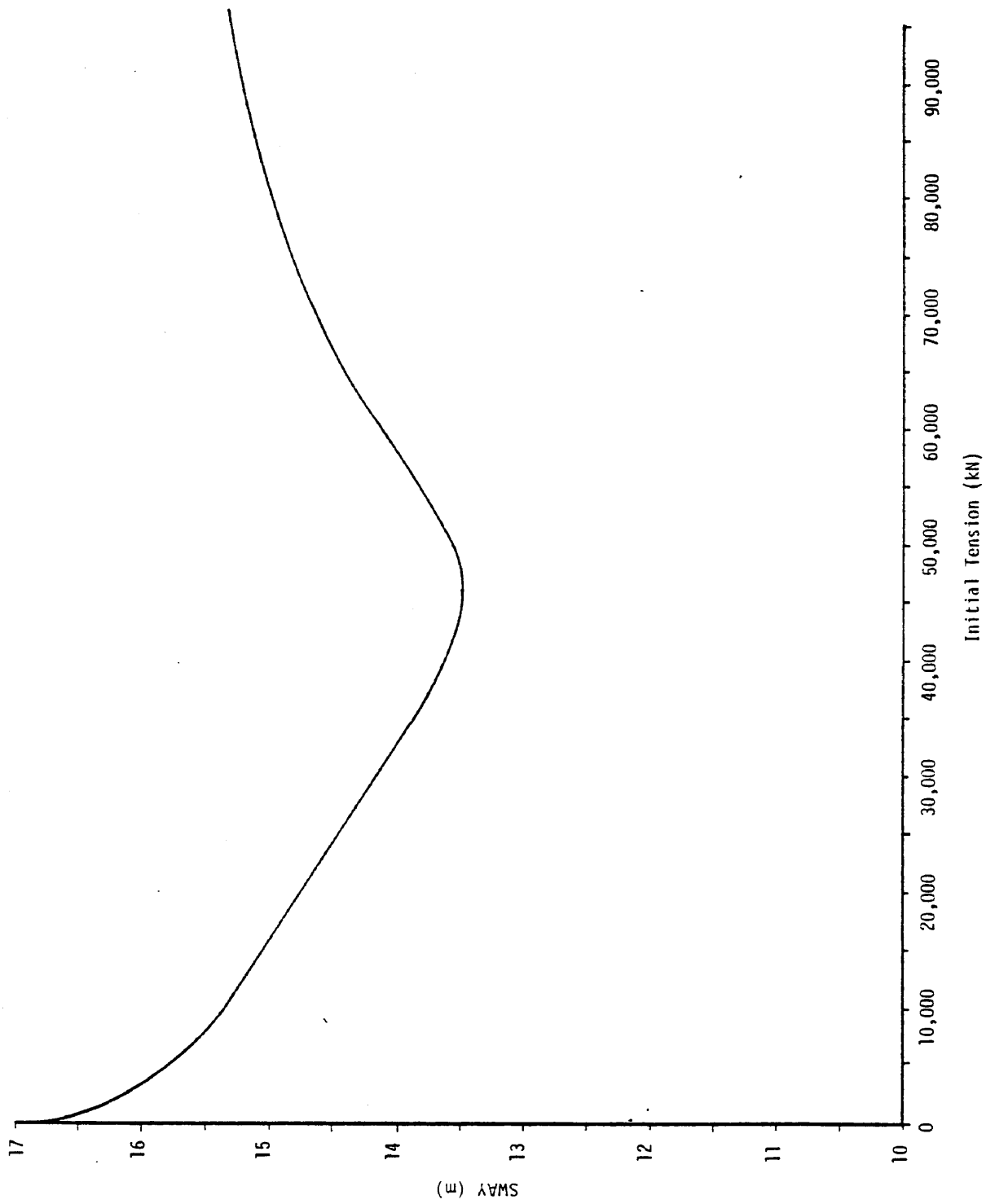


Fig. 50 - Variation of Sway Response Amplitude with Initial Tension

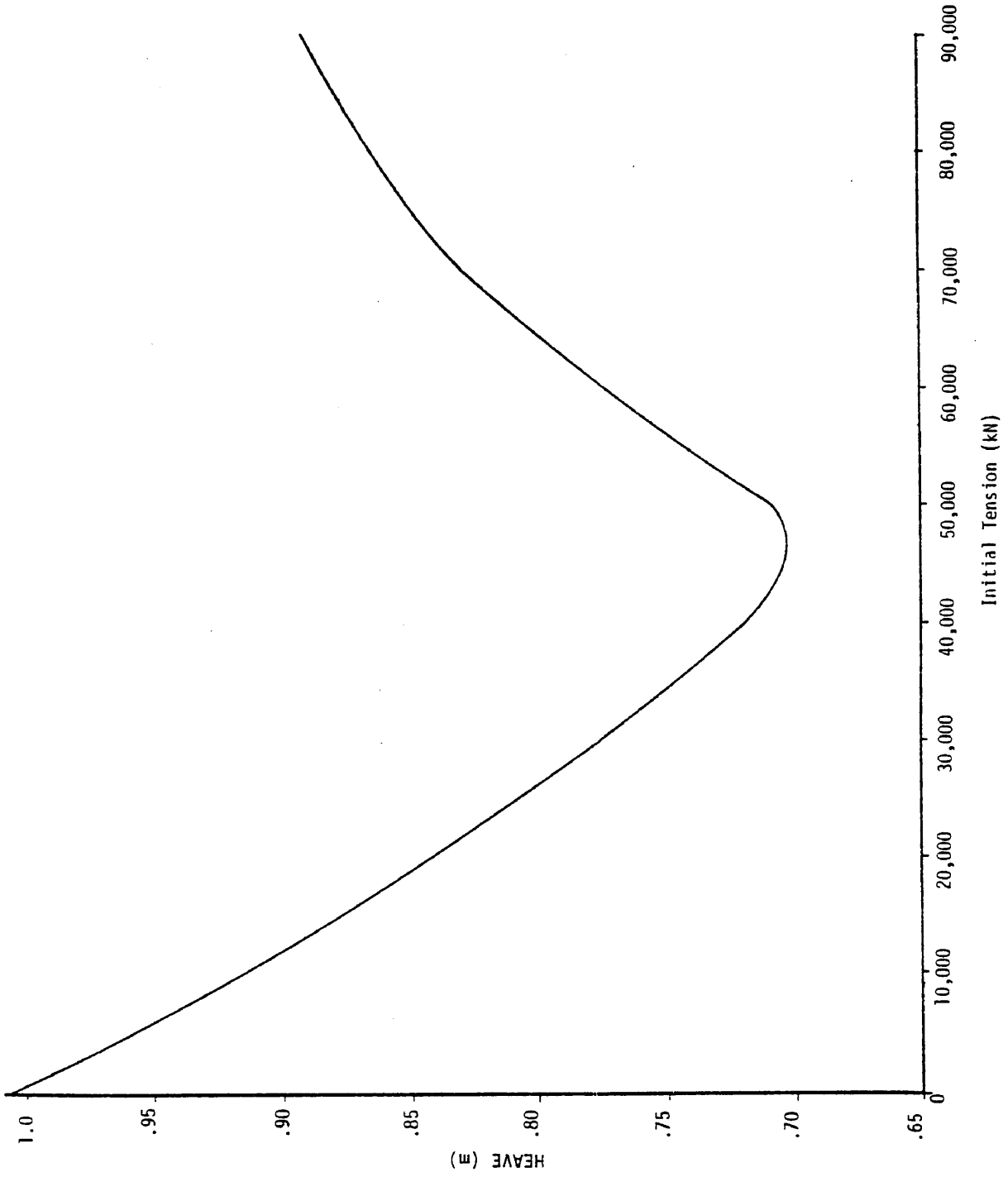


Fig. 51 - Variation of Heave Response Amplitude with Initial Tension

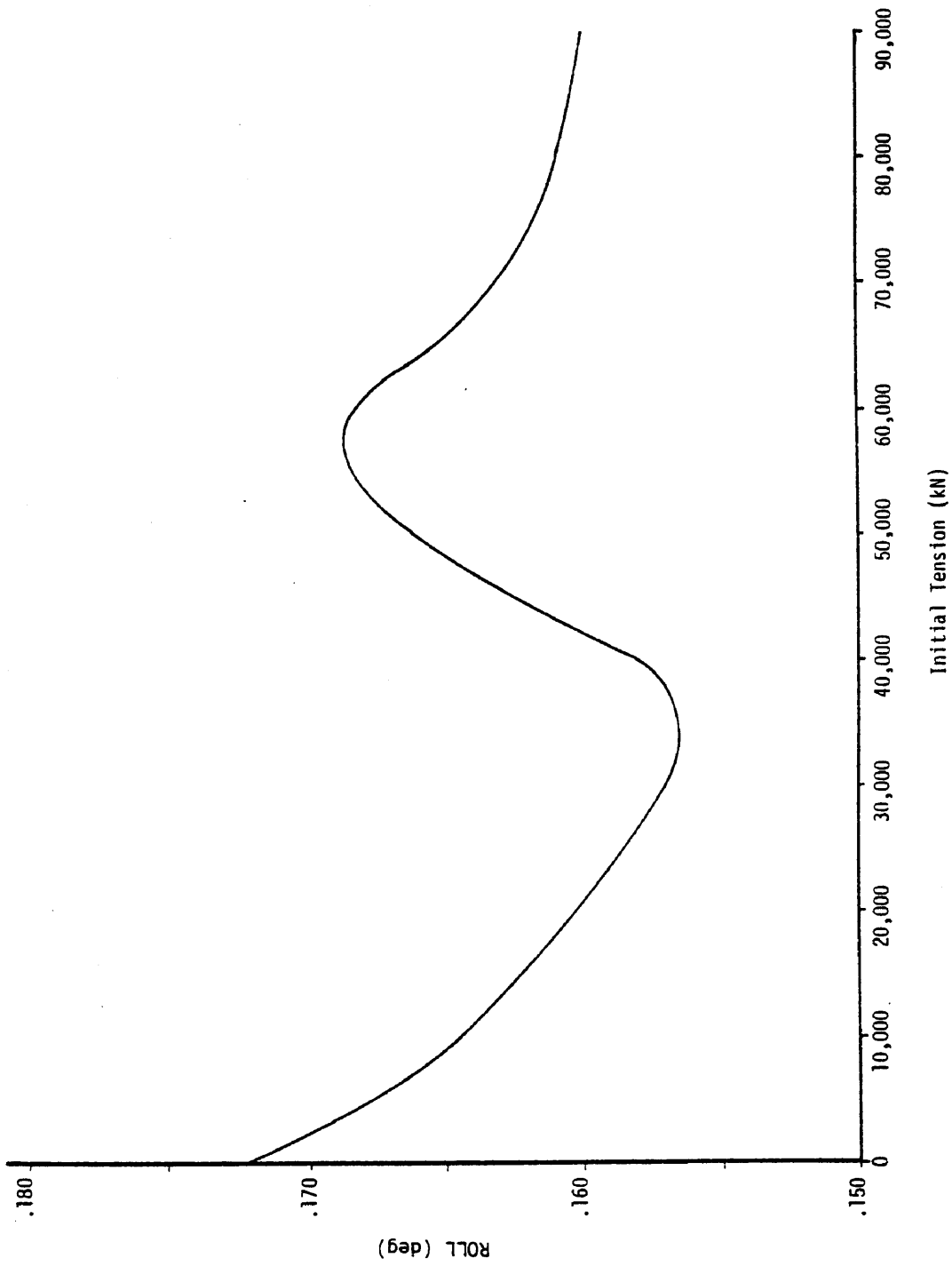


Fig. 52 - Variation of Roll Response Amplitude with Initial Tension

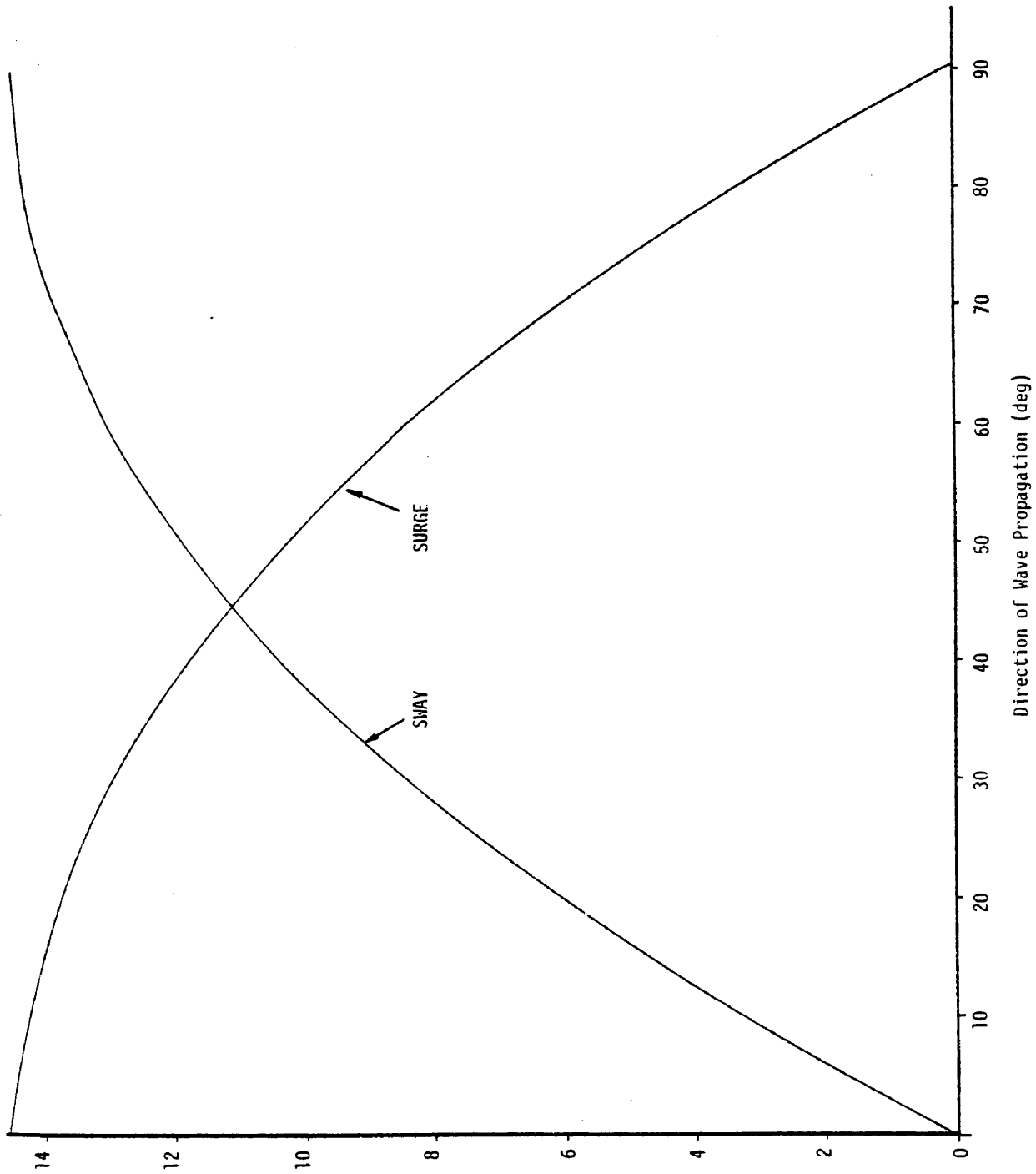


Fig. 53 - Variation of Surge or Sway with the Direction of Wave Propagation

$\alpha = 90^\circ$. On the other hand, sway has a zero amplitude at $\alpha = 0^\circ$ and a maximum amplitude at $\alpha = 90^\circ$. Surge and sway have the same value at $\alpha = 45^\circ$, and the combined response of surge and sway reaches its maximum at $\alpha = 45^\circ$.

The variation of heave response amplitude with respect to angle of wave propagation is illustrated in Figure 54. The heave response is minimum at both $\alpha = 0^\circ$ and $\alpha = 90^\circ$, maximum at $\alpha = 45^\circ$ and symmetric about $\alpha = 45^\circ$. This plot is similar to a combined surge-sway plot because of the coupling of heave to both surge and sway. The variation of pitch and roll response amplitudes is presented in Figure 55. As shown in the plots, pitch varies nearly parabolically for $\alpha < 45^\circ$ and linearly for $\alpha > 45^\circ$, and roll varies linearly for $\alpha < 45^\circ$ and parabolically for $\alpha > 45^\circ$. Pitch and roll curves also are symmetric about $\alpha = 45^\circ$.

The yaw response variation with respect to α is shown in Figure 56. Zero yaw occurs at $\alpha = 0^\circ$, $\alpha = 90^\circ$, and $\alpha = 45^\circ$ (since the structure is symmetric). Maximum yaw occurs at $\alpha = 20^\circ$ and $\alpha = 70^\circ$ and the yaw curve is symmetric about $\alpha = 45^\circ$.

Illustration of Nonlinearity and Coupling

Drag terms have been shown to reduce maximum displacement response amplitudes by as much as 35 percent. Nonlinearities in the stiffness relationships also are significant. The variation of leg stiffnesses with respect to surge displacement is shown in Figure 57. It can be seen that the force-displacement relationship may be considered linear for surge displacements of up to 5 meters without appreciable error.

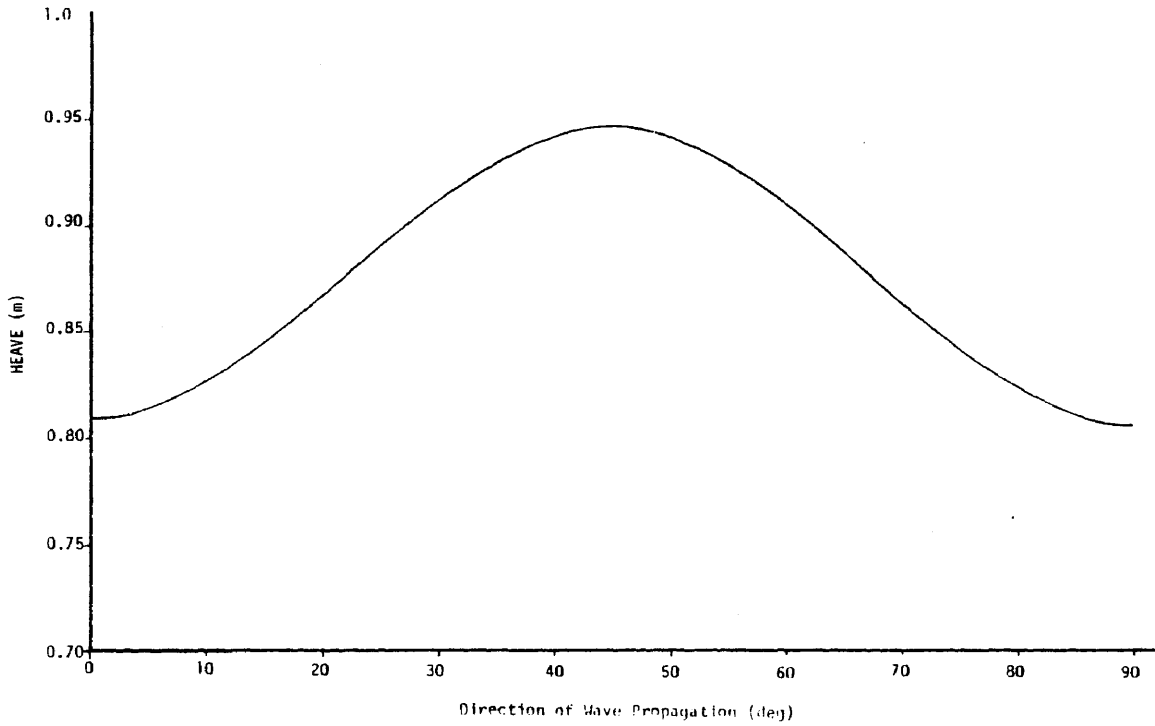


Fig. 54 - Variation of Heave with the Direction of Wave Propagation

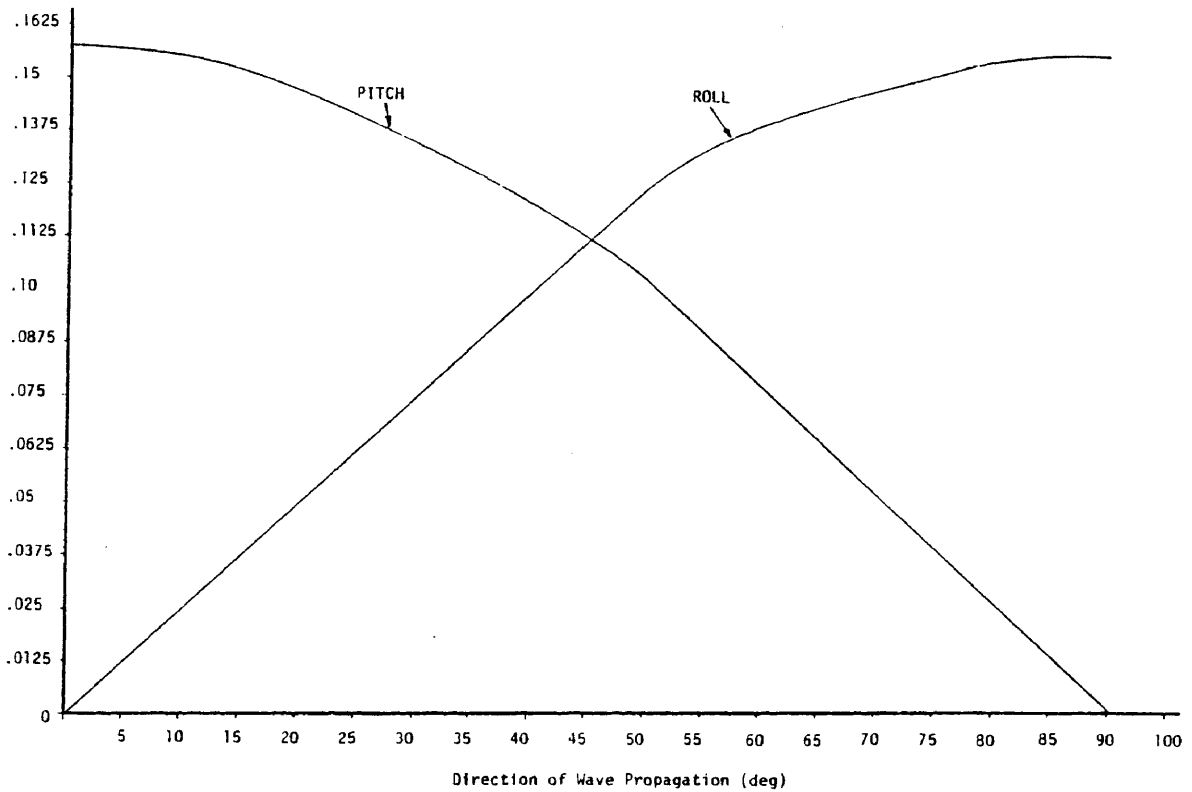


Fig. 55 - Variation of Pitch and Roll with the Direction of Wave Propagation

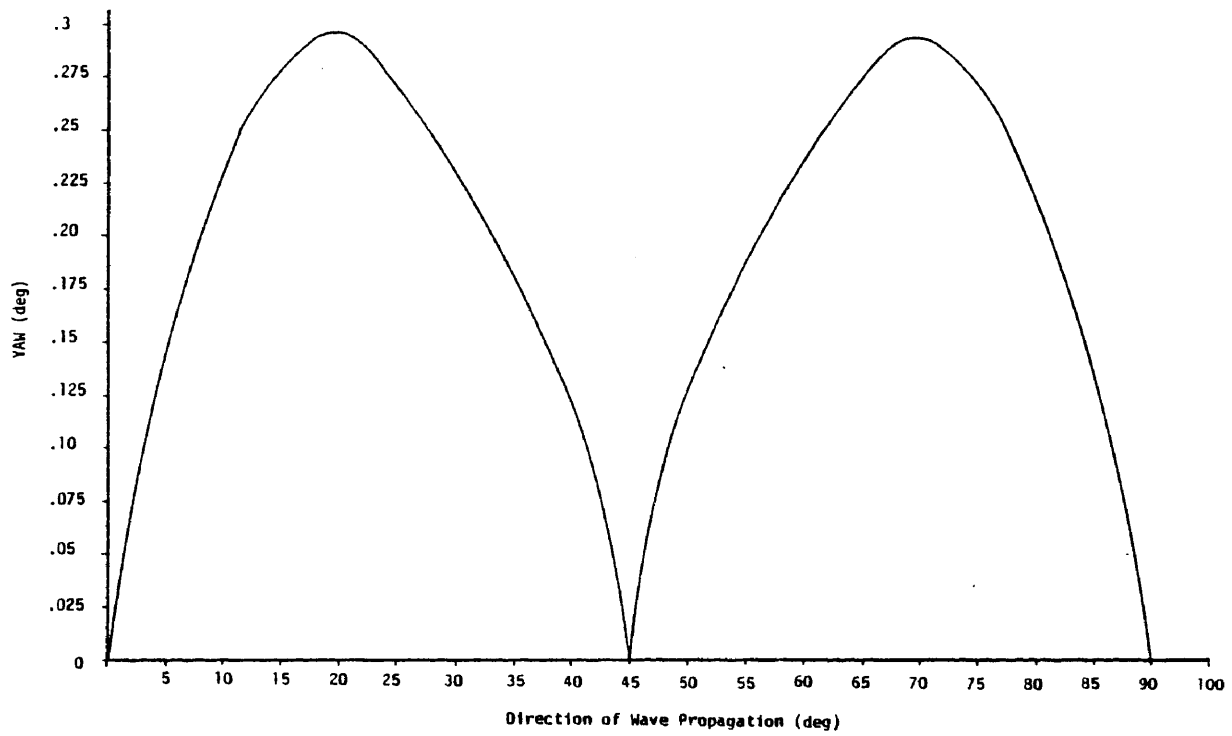


Fig. 56 - Variation of Yaw with the Direction of Wave Propagation

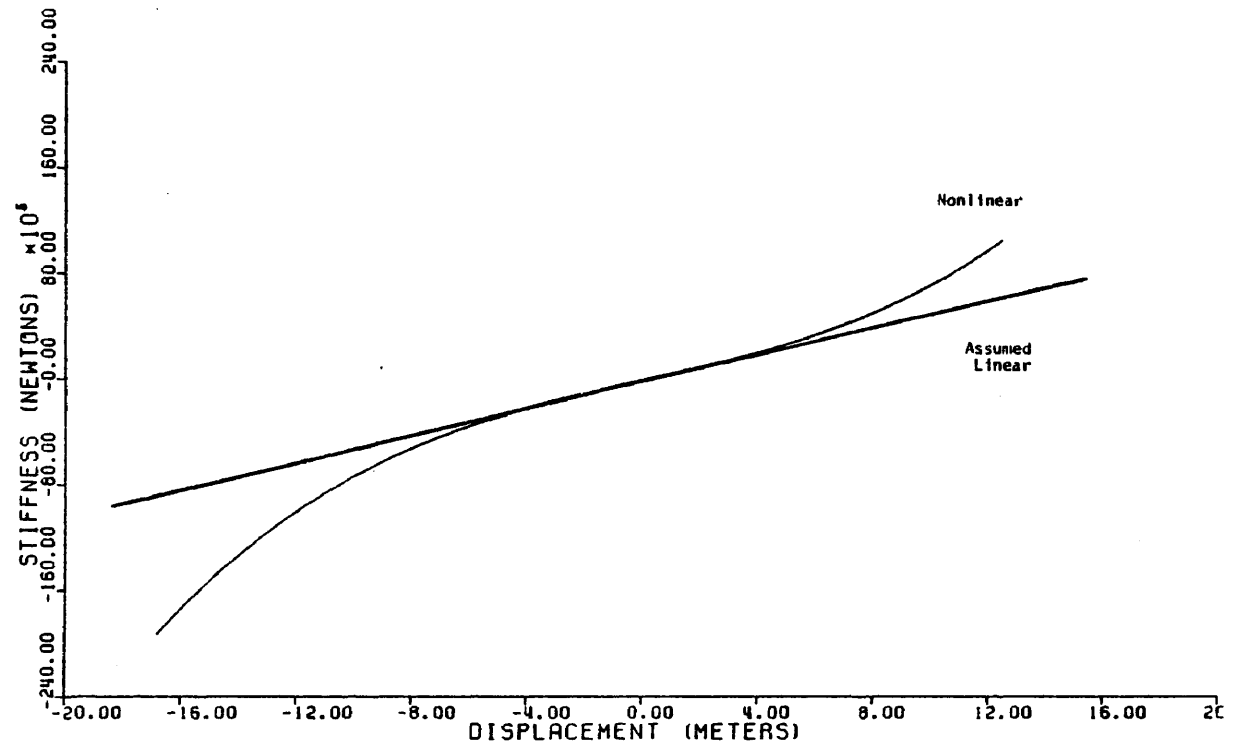


Fig. 57 - Plot of Cable Restoring Force for Surge Displacement

However, for larger displacements the computed forces differ significantly from those projected by an assumed linear stiffness.

The effect of coupling is apparent from a comparison of the responses computed assuming coupled and uncoupled degrees of freedom, respectively. A force-pitch displacement curve is presented in Figure 58. Whereas the curve obtained with coupled pitch and surge exhibits a hysteretic characteristic, the straight line represents the results if it is assumed that no coupling exists. A similar comparison for heave displacement response is presented in Figure 59. In both cases there is substantial difference between the uncoupled and coupled responses.

Summary of Response to Regular Waves

The dynamic analysis model developed as part of this research was thoroughly tested for response to regular waves. A parametric analysis study was performed in an effort to emphasize the relative importance of each individual parameter to the behavior of tension-leg platforms. The dynamic response in all of the structures six degrees of freedom were plotted versus each parameter. Important concepts can be obtained from these plots in order to facilitate the design of TLP's. The general trends of the response amplitudes are found to be in agreement with those presented in Ref. 24.

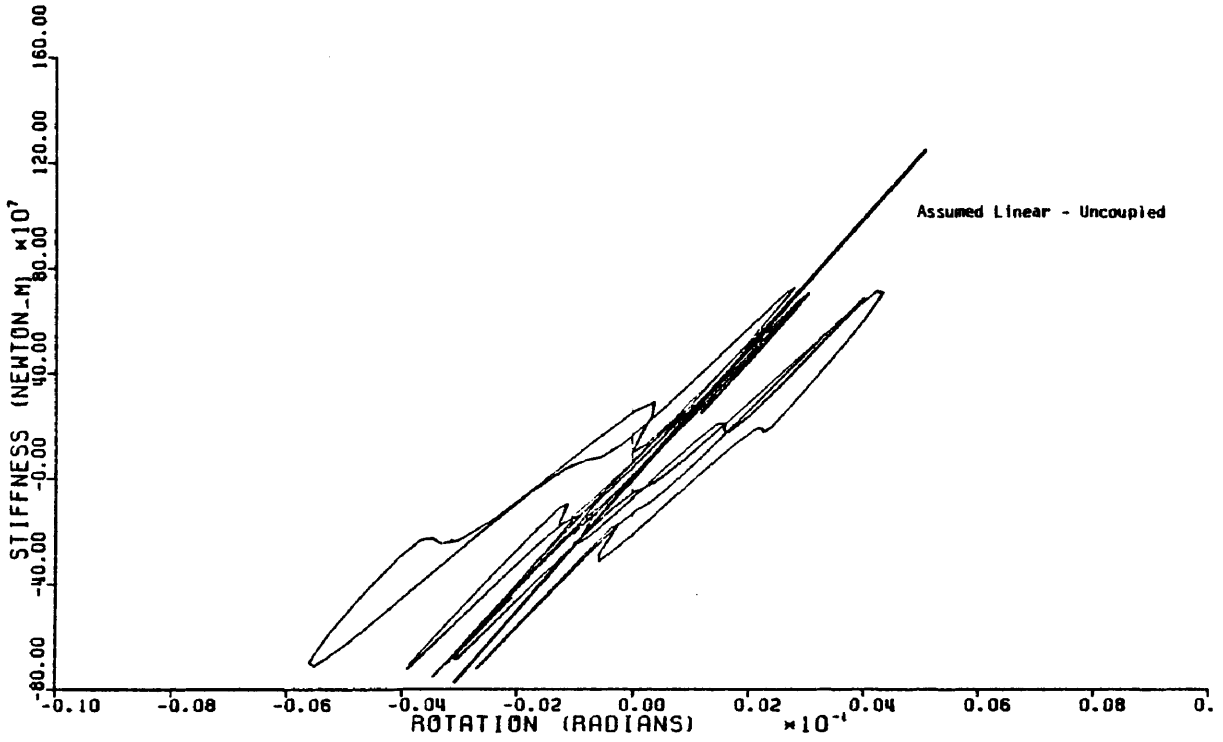


Fig. 58 - Plot of Cable Restoring Force for Pitch Displacement

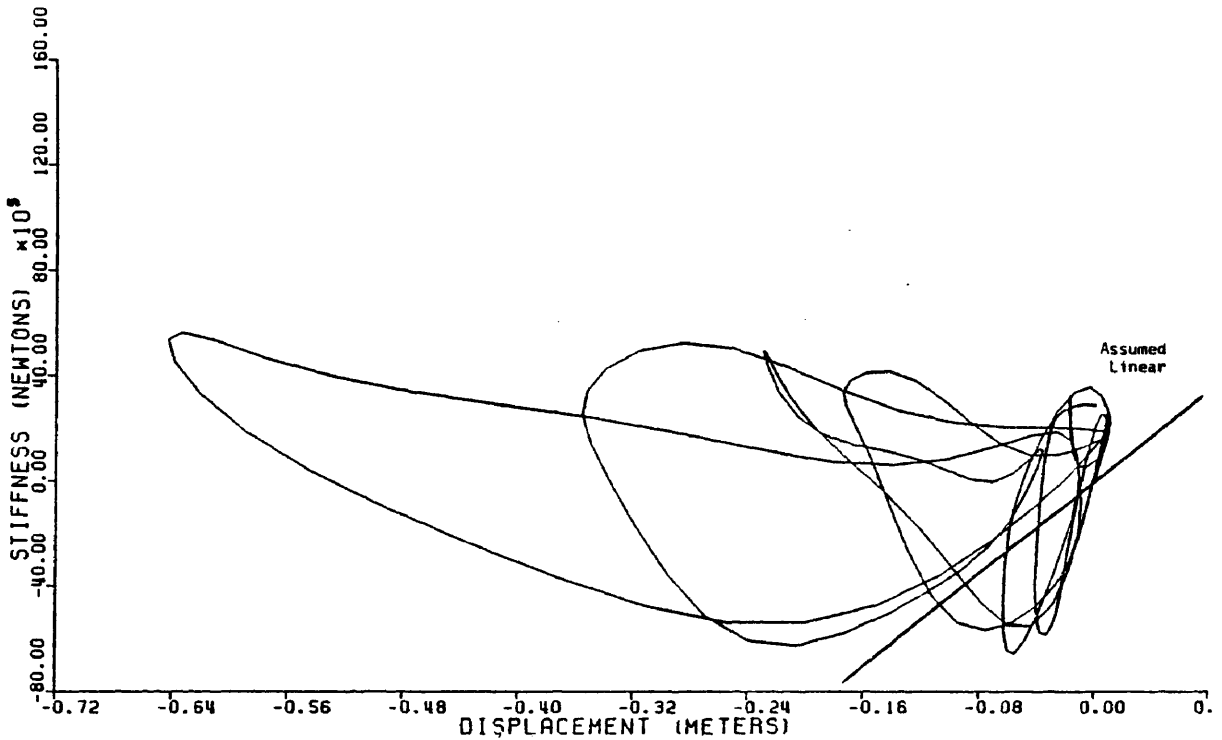


Fig. 59 - Plot of Cable Restoring Force for Heave Displacement

Response to Random Waves

Time Histories

The platform response to simulated random sea states is investigated. Time histories of platform motion are obtained for two unidirectional wave spectra: those of Pierson-Moskowitz and JONSWAP. Plots of wave profile versus time for the Pierson-Moskowitz and the JONSWAP spectra are given in Figures 60 and 61, respectively. The apparent randomness of the wave profiles depends on the phase angle of each of the wave components.

The behavior of the platform to simulated random waves is studied for a 400 second duration of the wave at a wave incidence angle of zero degrees. Surge, heave, and pitch time histories for the Pierson-Moskowitz sea spectrum are shown in Figures 62, 63, and 64, respectively for a characteristic windspeed of 20 meter/second, and in Figures 65, 66, and 67 for a 30 meter/second characteristic windspeed. The surge, heave, and pitch responses corresponding to the JONSWAP sea spectrum are also presented (Figures 68, 69, and 70). The response amplitudes of each of the three degrees of freedom for all three sea states described above are given in Table 6.

It is observed from the above results that the general behavior of the platform subjected to simulated random waves is not much different from the response of the platform to regular waves of various periods and amplitudes. It is also found that random waves do not cause resonance of platform motions. Based on these observations, and the costly numerical integrations required to formulate random wave

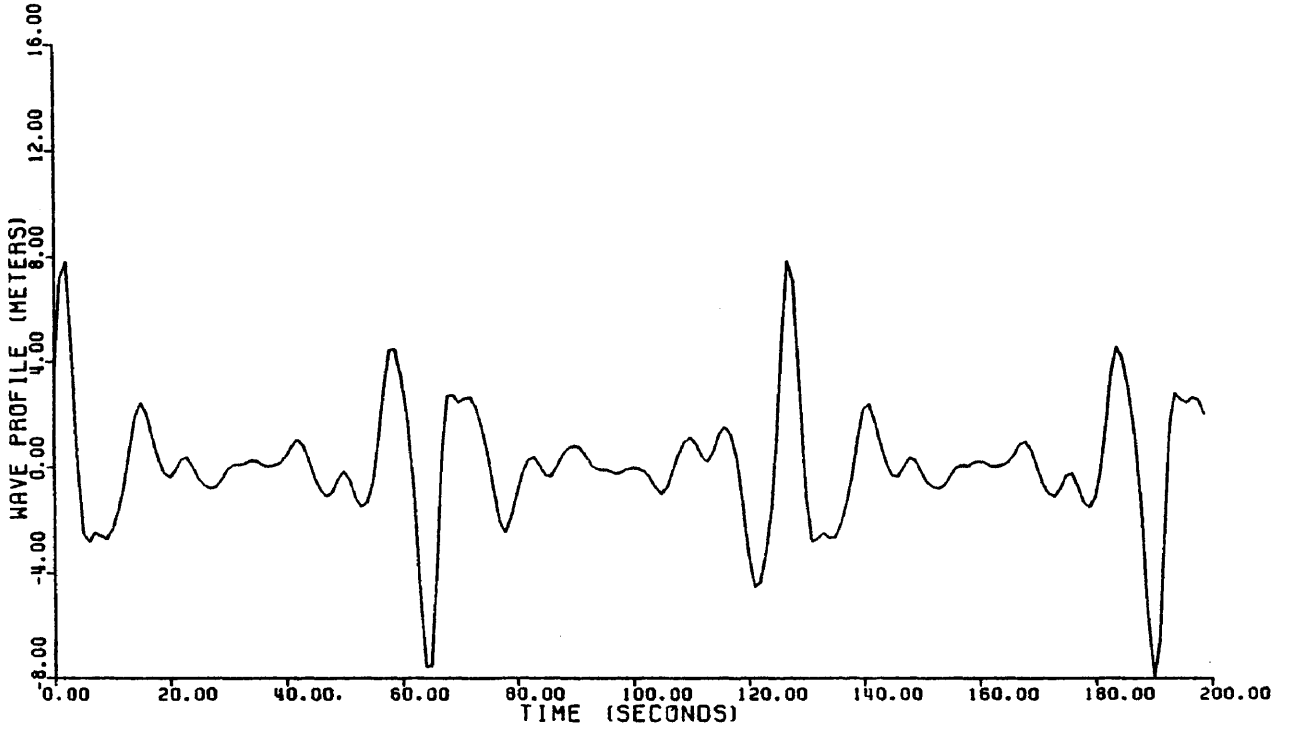


Fig. 60 - Wave Profile Corresponding to Pierson-Moskowitz Spectrum

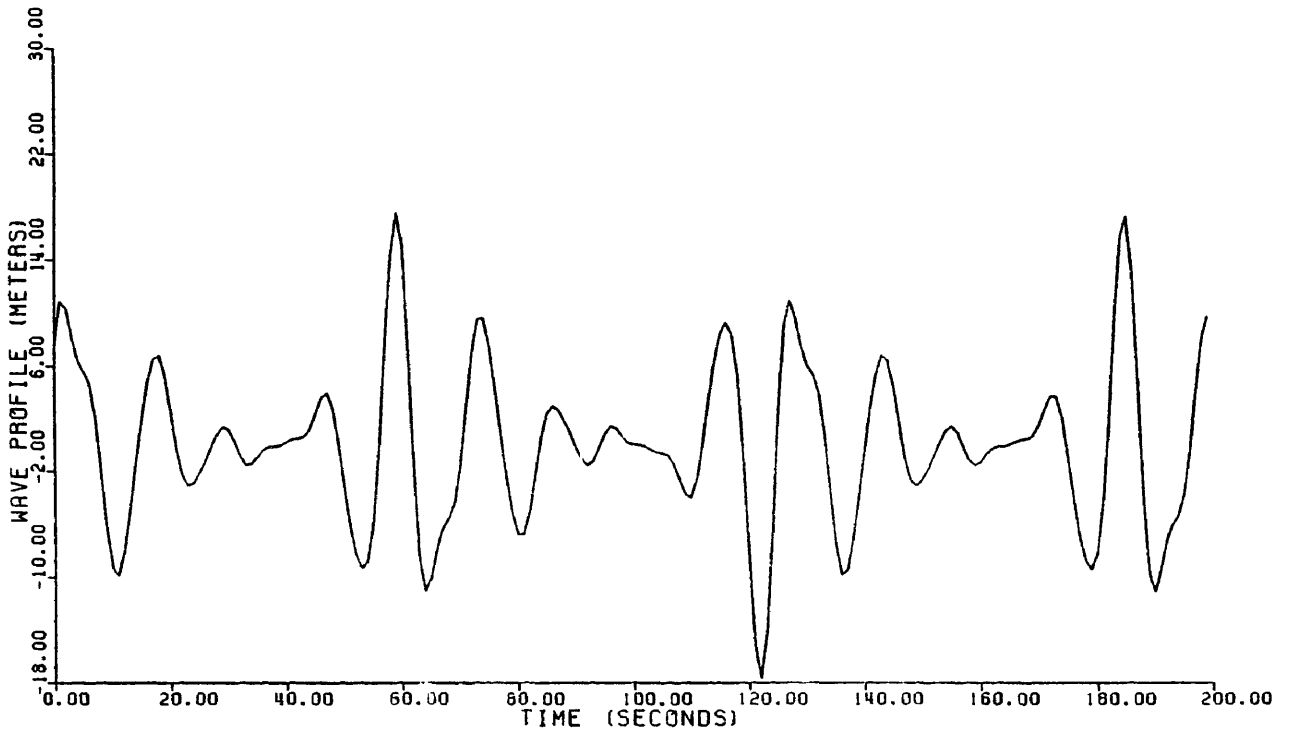


Fig. 61 - Wave Profile Corresponding to JONSWAP Spectrum

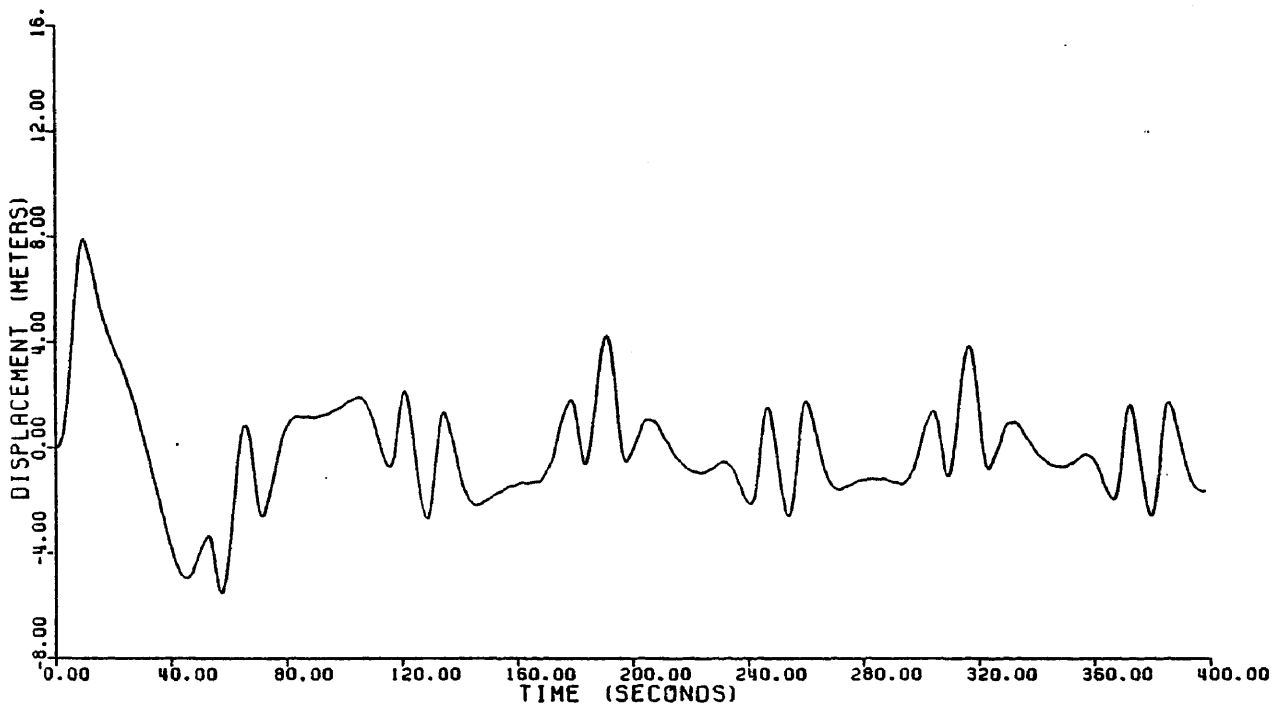


Fig. 62 - Time History Plot of Surge Response to Pierson-Moskowitz Spectrum ($U = 20$ m/sec)

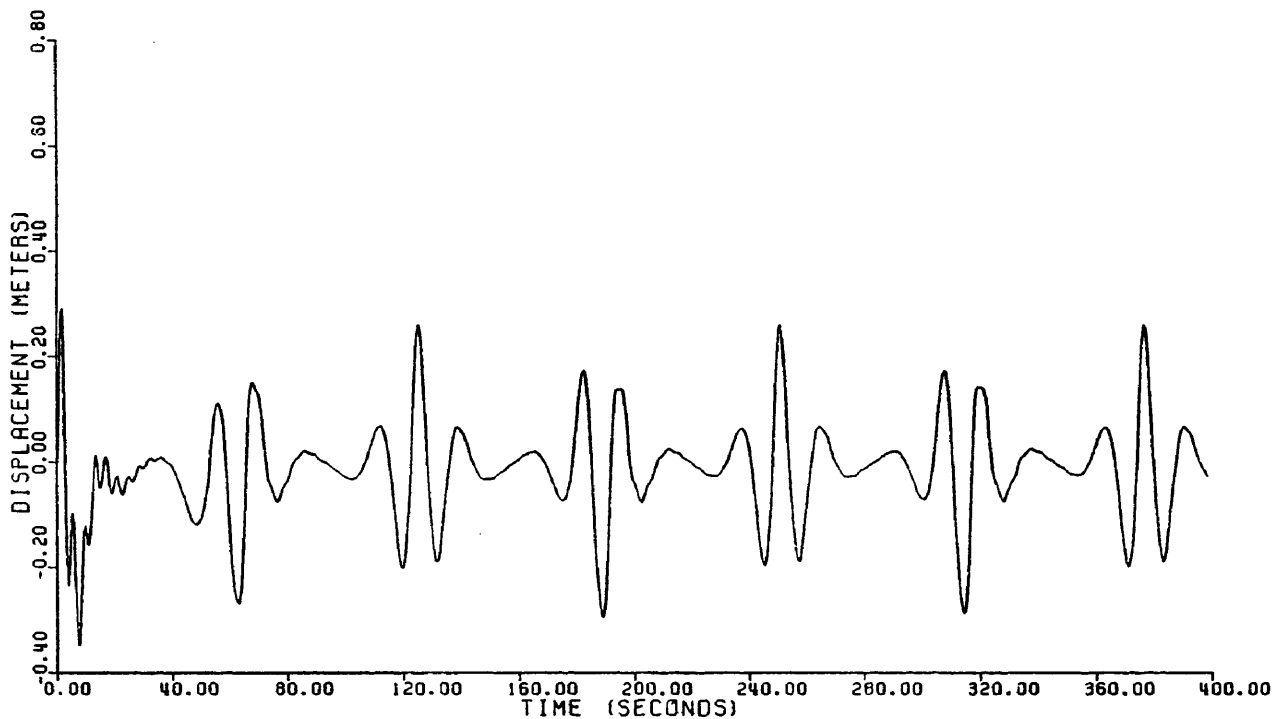


Fig. 63 - Time History Plot of Heave Response to Pierson-Moskowitz Spectrum ($U = 20$ m/sec)

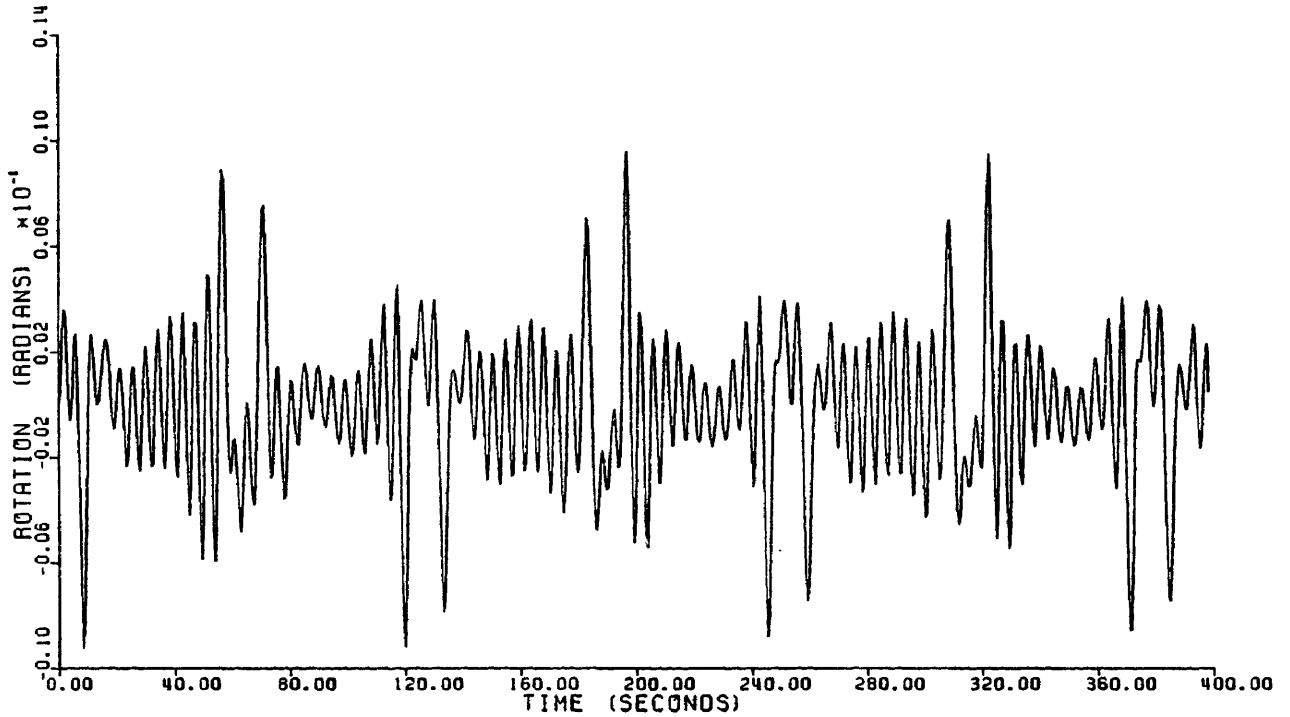


Fig. 64 - Time History Plot of Pitch Response to Pierson-Moskowitz Spectrum ($U = 20$ m/sec)

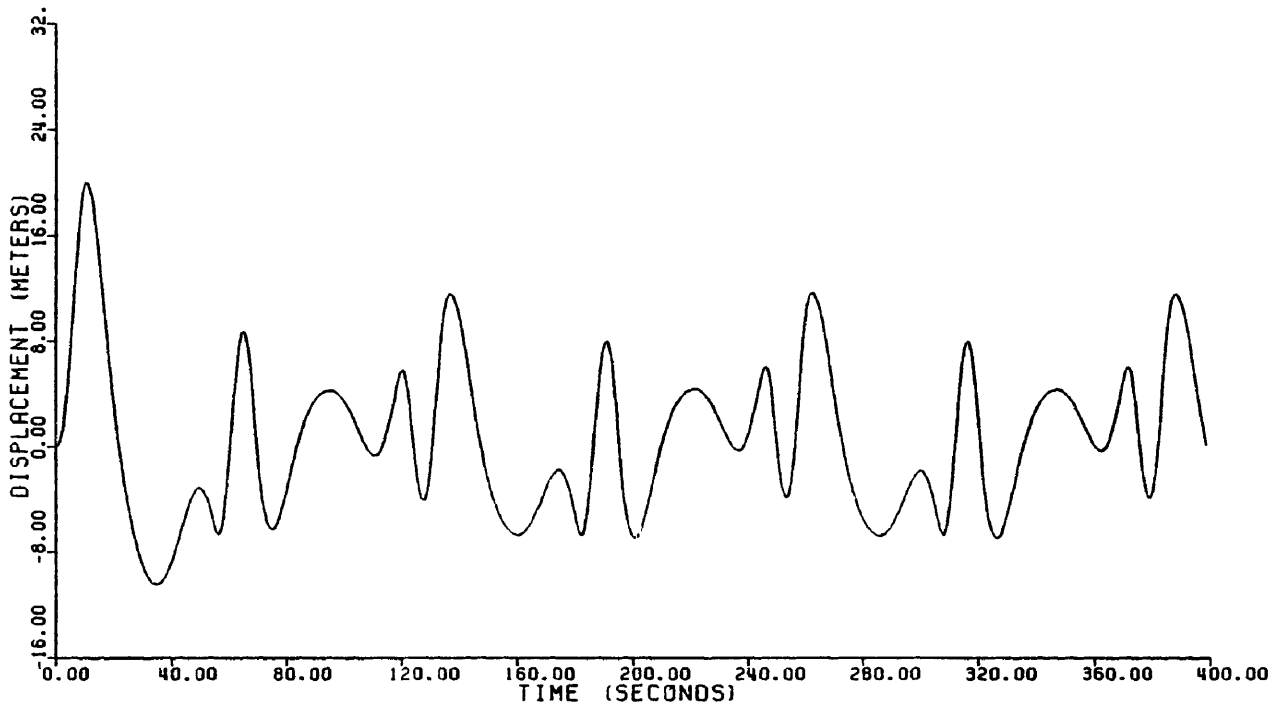


Fig. 65 - Time History Plot of Surge Response to Pierson-Moskowitz Spectrum ($U = 30$ m/sec)

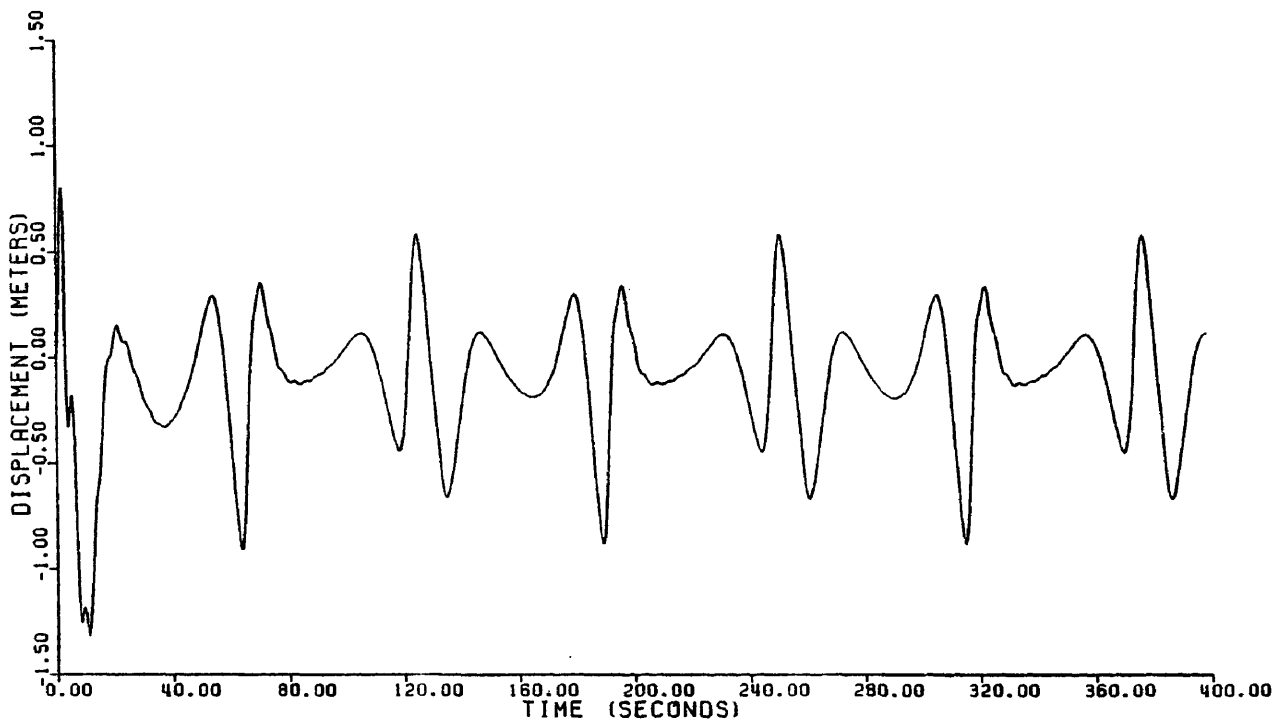


Fig. 66 - Time History Plot of Heave Response to Pierson-Moskowitz Spectrum ($U = 30$ m/sec)

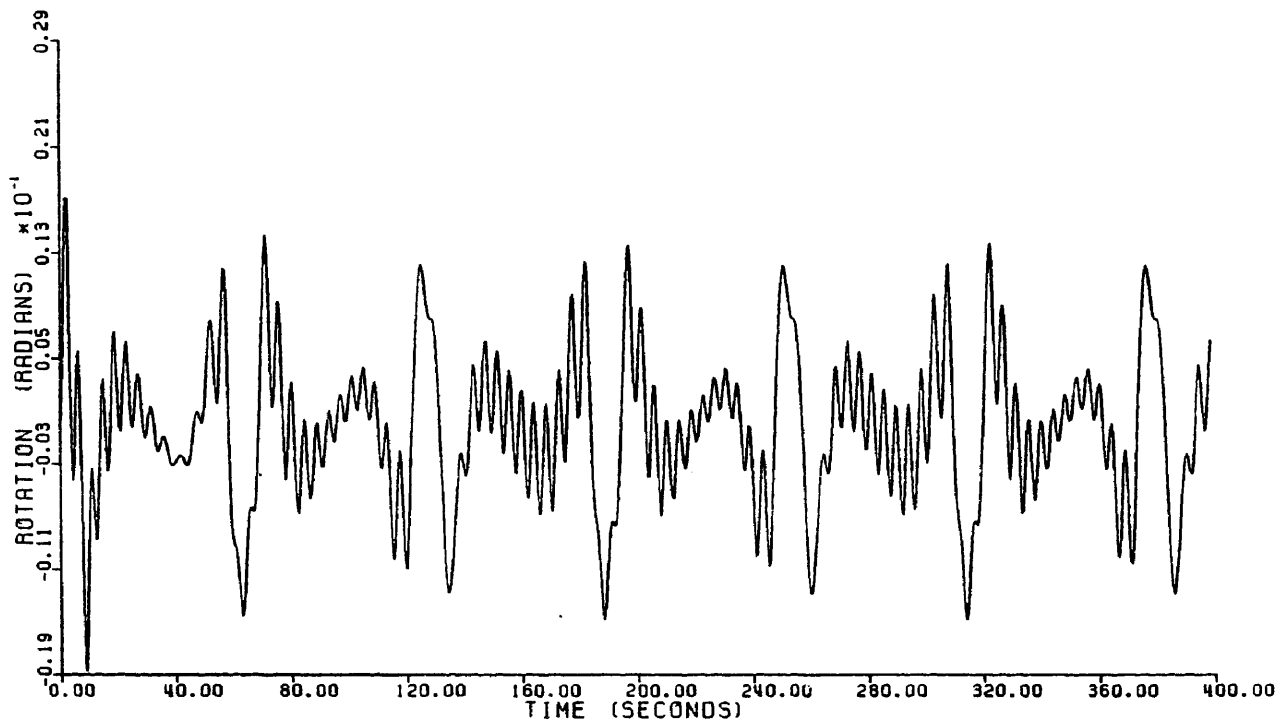


Fig. 67 - Time History Plot of Pitch Response to Pierson-Moskowitz Spectrum ($U = 30$ m/sec)

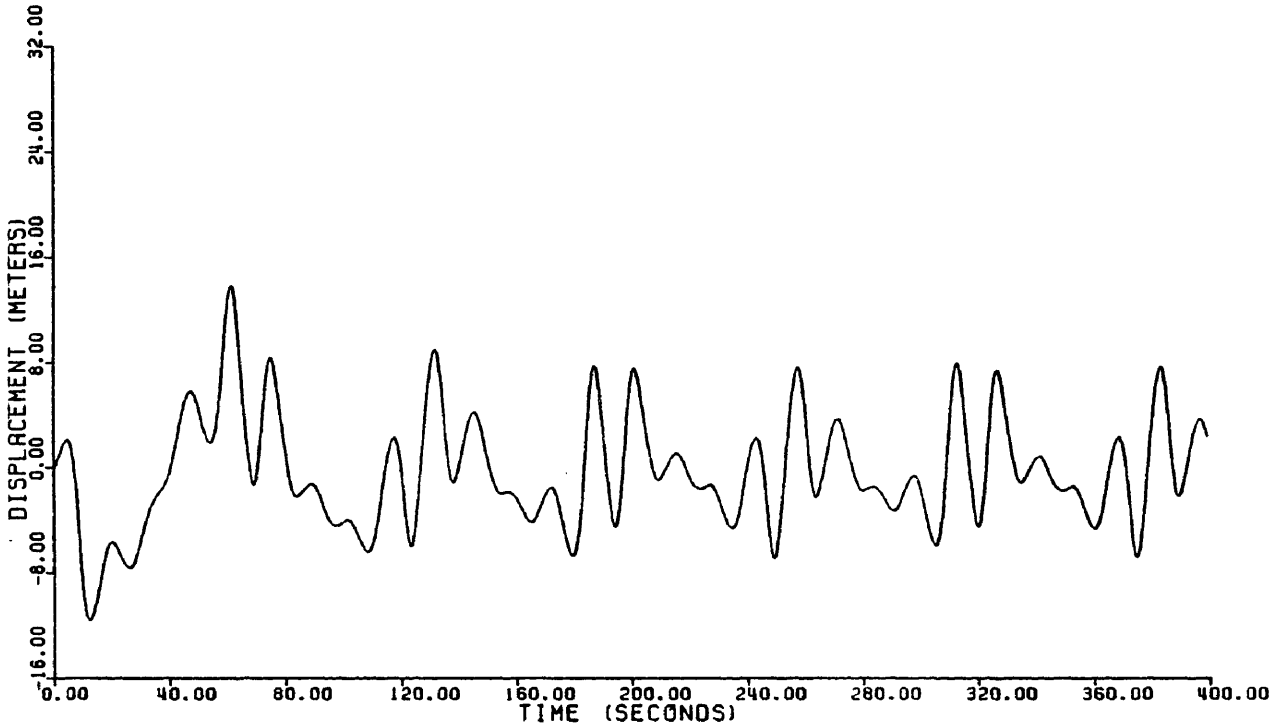


Fig. 68 - Time History Plot of Surge Response to JONSWAP Spectrum

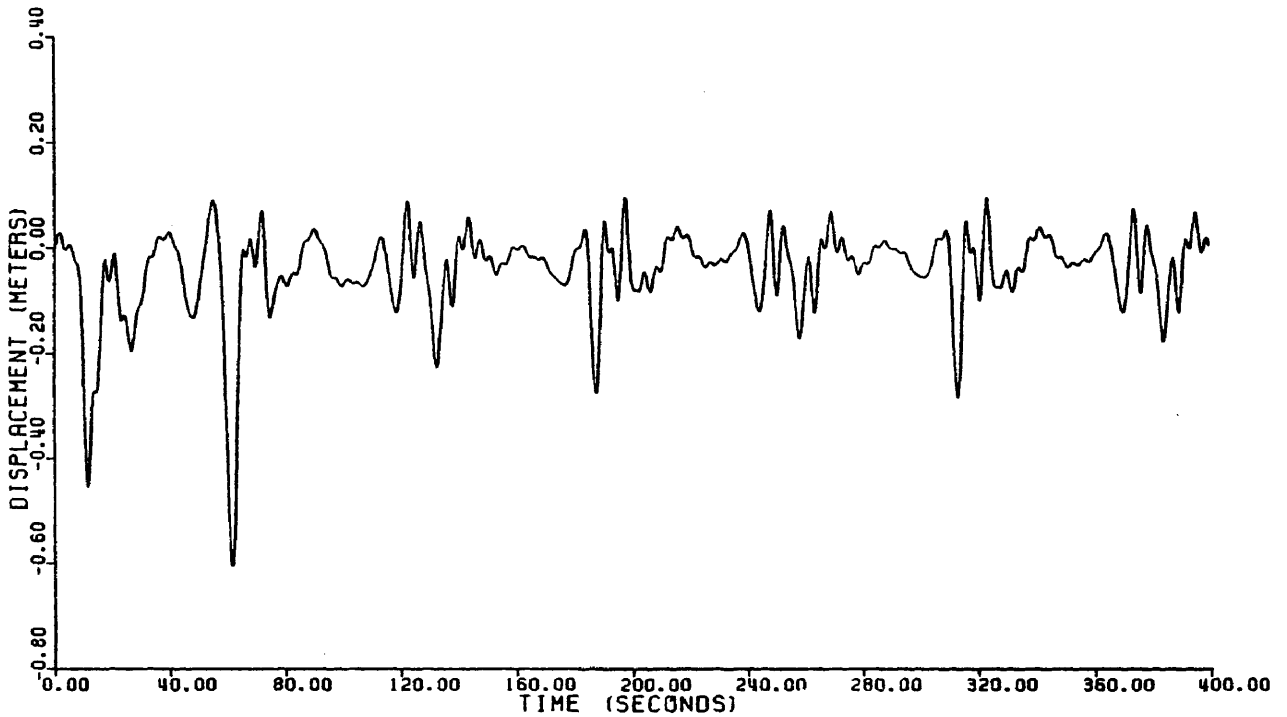


Fig. 69 - Time History Plot of Heave Response to JONSWAP Spectrum

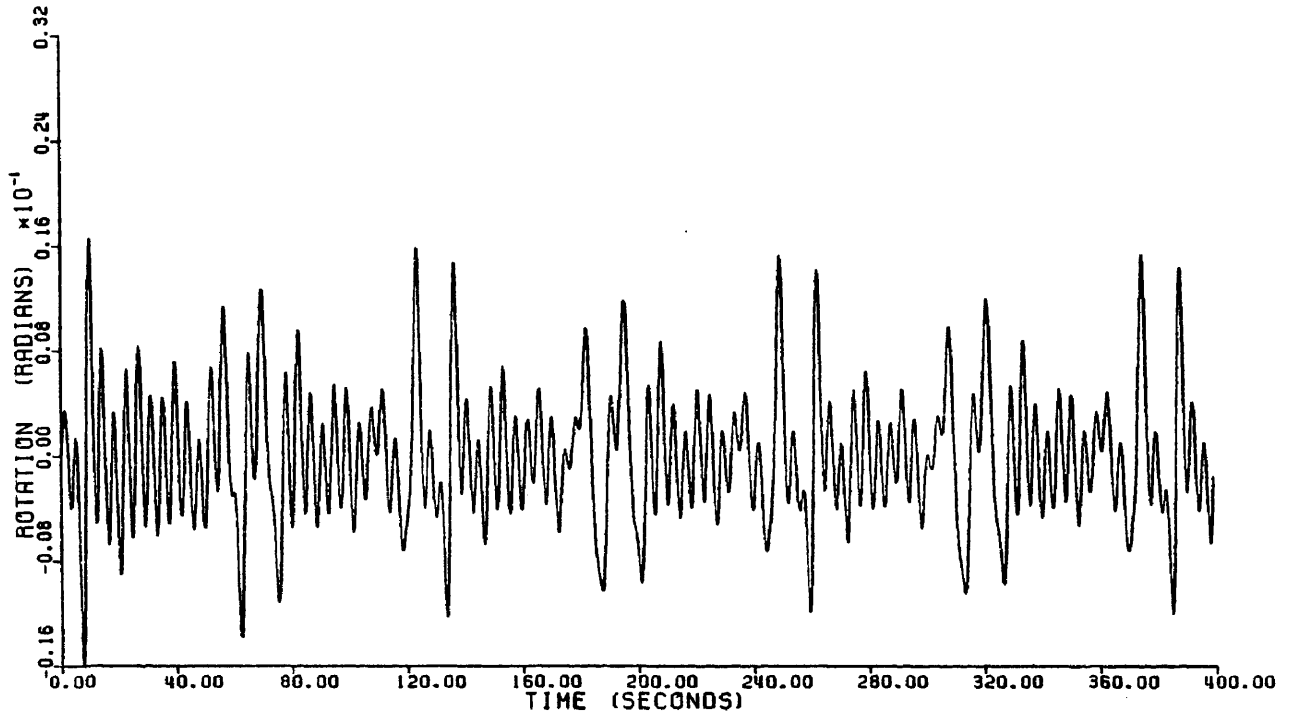


Fig. 70 - Time History Plot of Pitch Response to JONSWAP Spectrum

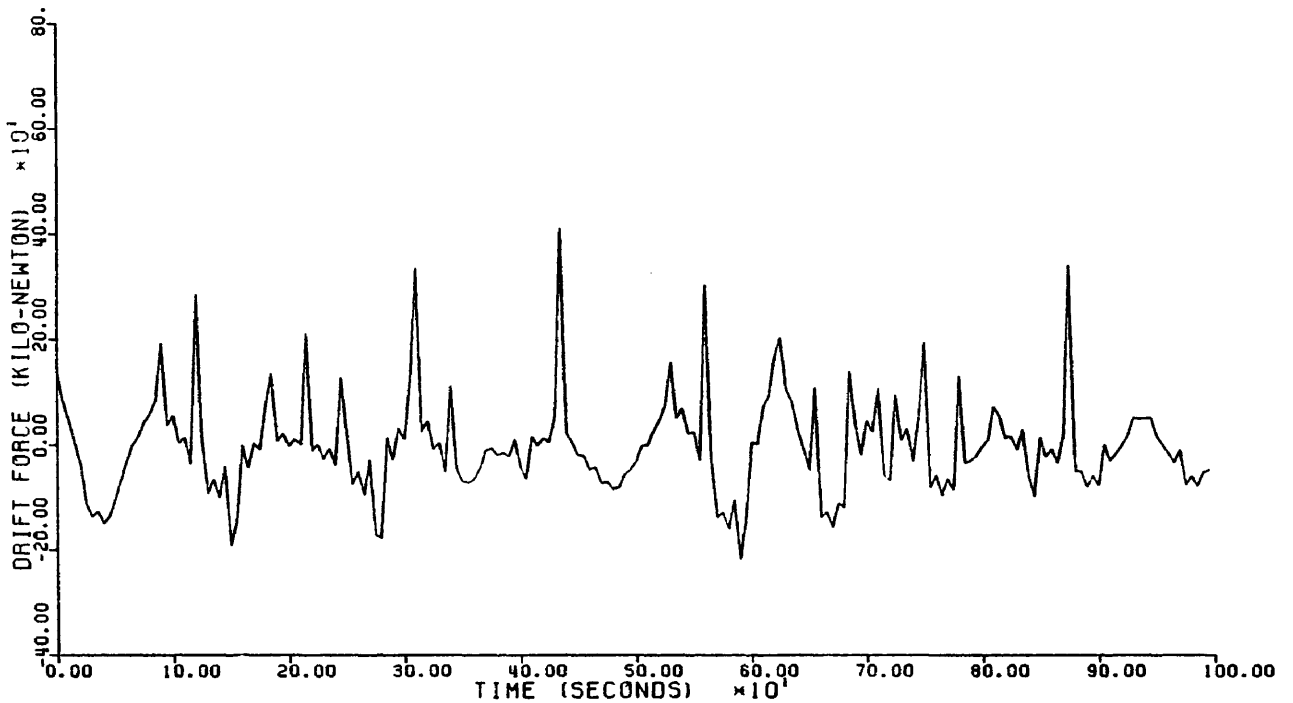


Fig. 71 - Time History Plot of Surge Drift Force Using JONSWAP Sea Spectrum

forces, it is suggested that regular wave trains be used to provide the necessary information about the behavior of tension-leg platforms.

TABLE 6
Platform Response Amplitudes for Random Sea Loading

Sea Spectrum	Surge Amplitude (m)	Heave Amplitude (m)	Pitch Amplitude (degrees)
Pierson-Moskowitz (U = 20 m/s)	8.0	0.35	0.570
Pierson-Moskowitz (U = 30 m/s)	20.0	1.30	1.089
JONSWAP	14.0	0.61	0.917

Effect of Drift Forces

Slowly-varying wave drift forces can be significant in the dynamic analysis of floating and articulated structures with high natural periods. In Chapter III, a drift force spectrum was used to obtain slowly varying wave drift forces as a function of wave frequency and energy density. A fourier transform was used to obtain a time history of the drift force. The variation of the surge drift force with respect to time using the JONSWAP sea spectrum is shown in Figure 71.

The effect of drift forces on the tension-leg platform was studied by including the surge drift force in the random force calculations. The response of the TLP to combined random waves and slowly varying drift forces was studied for a 400 second duration. Time histories of the resulting surge, heave and pitch are presented in Figures 72, 73, and 74. A comparison of the platform response for the case of random waves without drift forces to that for the case of combined random waves and slowly varying drift forces reveals no significant difference between the two cases. The reason for this may be attributed to two factors: 1) the use of a drift force spectrum instead of a more involved velocity potential approach based on the conservation of momentum and energy, and 2) the time duration of 400 seconds may not be sufficient for the full effects of drift forces to develop. Consequently, the above observations do not necessarily suggest that drift forces are insignificant. However, no attempt is made in this research to study a more detailed analysis of the effect of drift forces on the response of the platform since they are outside the main scope of the present study.

Response to Earthquake Forces

The response of the dynamic analysis model presented in this report to wave forces was tested and a parametric analysis was performed. The results obtained show that the model successfully simulates the dynamic behavior of tension-leg platforms subjected to ocean waves. In this section, the response behavior of the platform subjected to ground motion is studied using the above model. Earthquake excitation

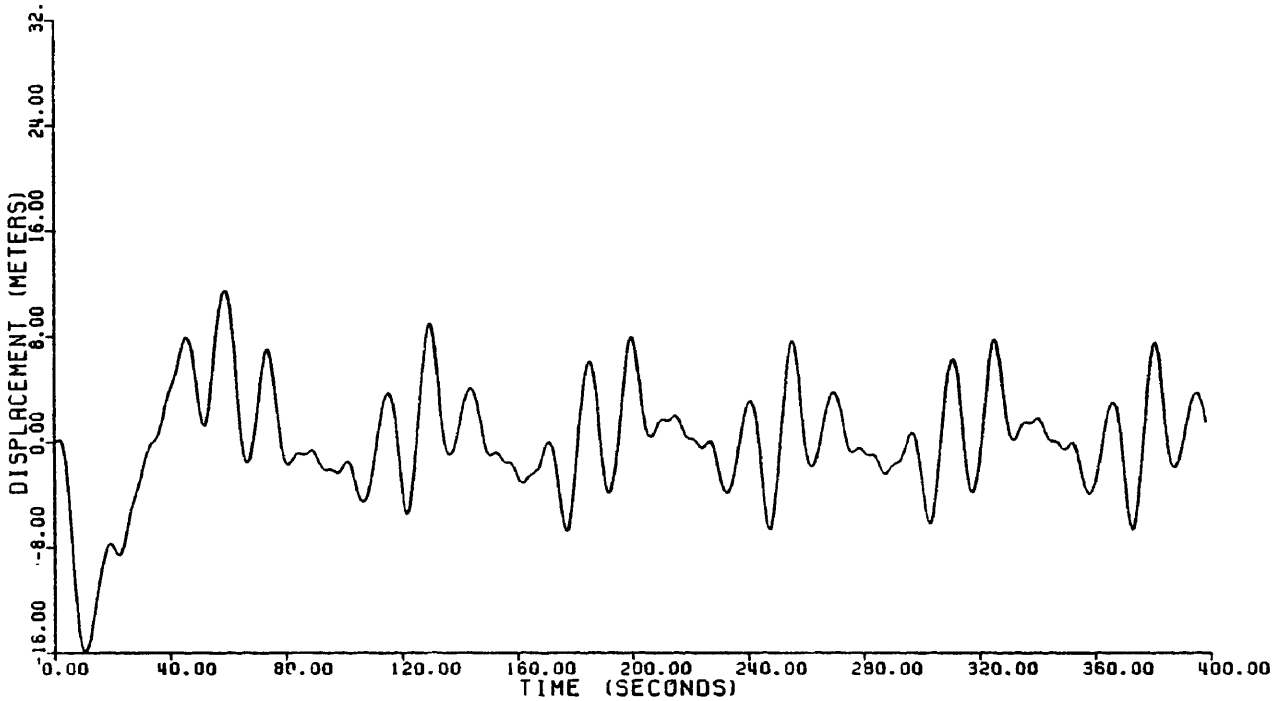


Fig. 72 - Time History Plot of Surge Response to Combined Drift Forces and Random Waves Using JONSWAP Spectrum

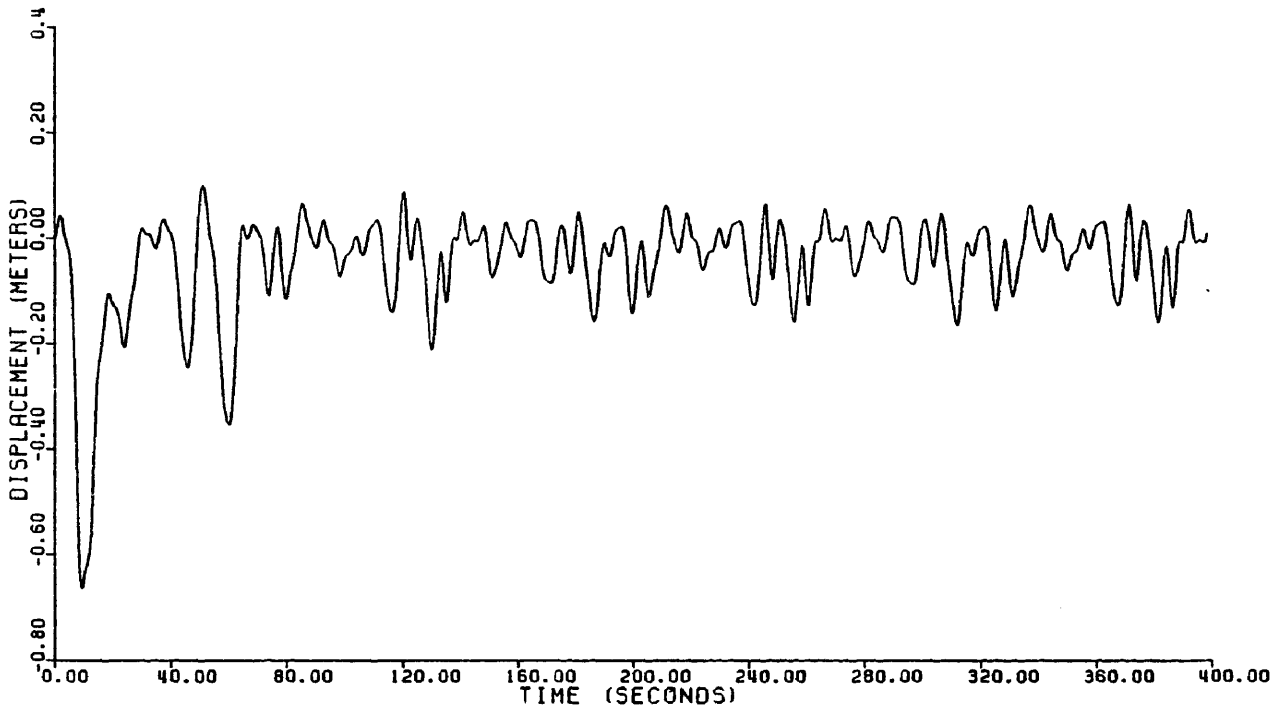


Fig. 73 - Time History Plot of Heave Response to Combined Drift Forces and Random Waves Using JONSWAP Spectrum

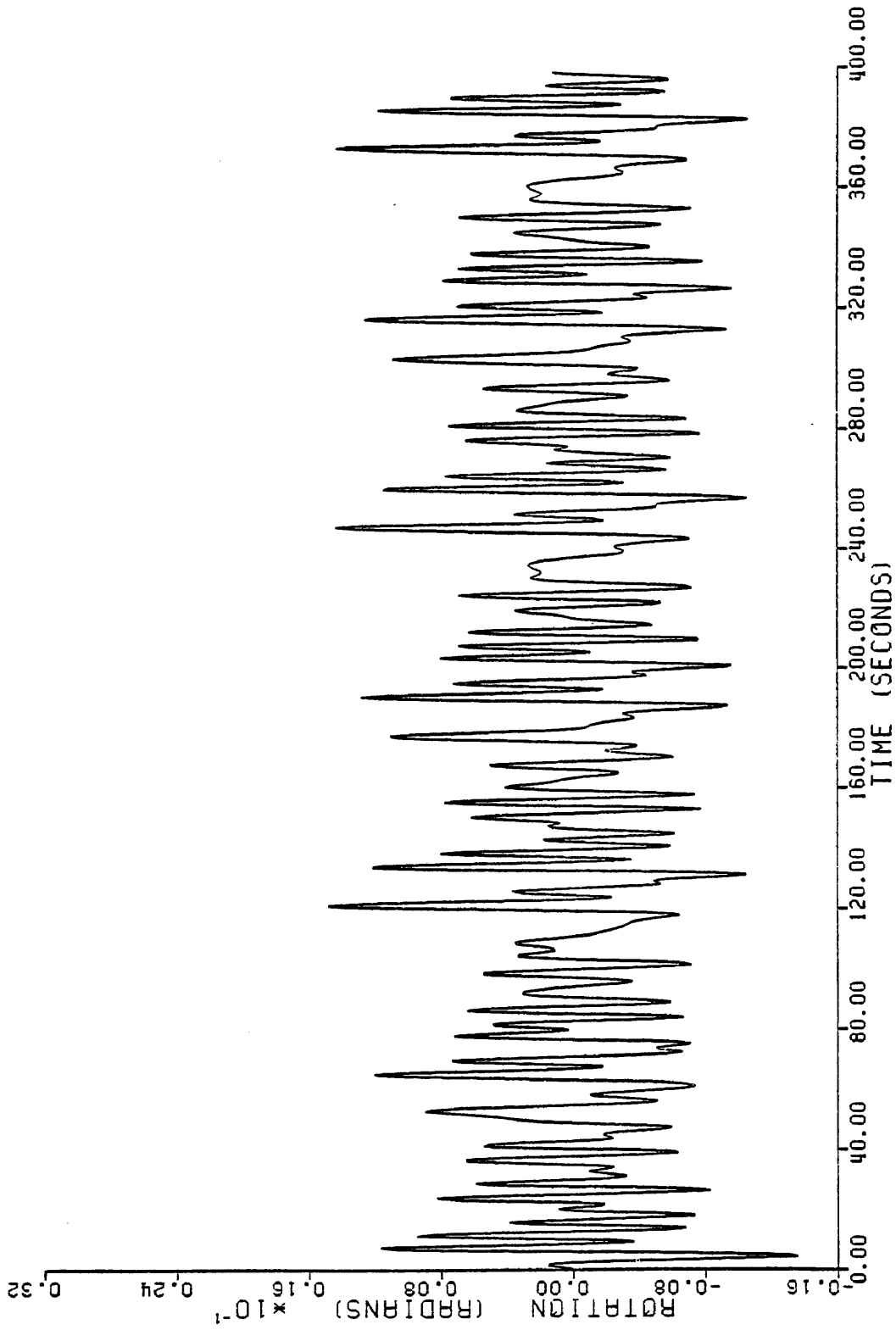


Fig. 74 - Time History Plot of Pitch Response to Combined Drift Forces and Rarcom Waves Using JONSWAP Spectrum

consists of horizontal and vertical base accelerations based on ground motion records. The primary earthquake record used in the analysis was that of El Centro (Imperial Valley Earthquake, 1940). Figure 75 shows the time history of the East-West component of the El Centro earthquake. Other ground motion records used include Pacoima Dam (San Fernando Earthquake, 1971) and Taft Lincoln School Tunnel (Kern County Earthquake, 1952).

Horizontal Component

In order to study the effect of the horizontal component of the earthquake on the response of the TLP, two cases were studied: case 1 for earthquakes occurring in a calm sea, and case 2 for earthquakes and waves occurring simultaneously. The derivation of earthquake forces and corresponding fluid drag and inertial forces arising from relative motion between structure and fluid particles for a calm sea (case 1) is given in Appendix B. The forces corresponding to case 2 are easily obtained by superimposing the inertial forces arising from ground motion with forces developed for waves only. The forces derived in case 1 were checked by comparing the response obtained from case 1 with that obtained from case 2 (setting wave height equal to zero to simulate a calm sea).

Time Histories

Response time histories of surge, heave, and pitch for El Centro earthquake occurring in a calm sea are shown in Figures 76-78. Surge response during the 30-second duration of the earthquake reaches a

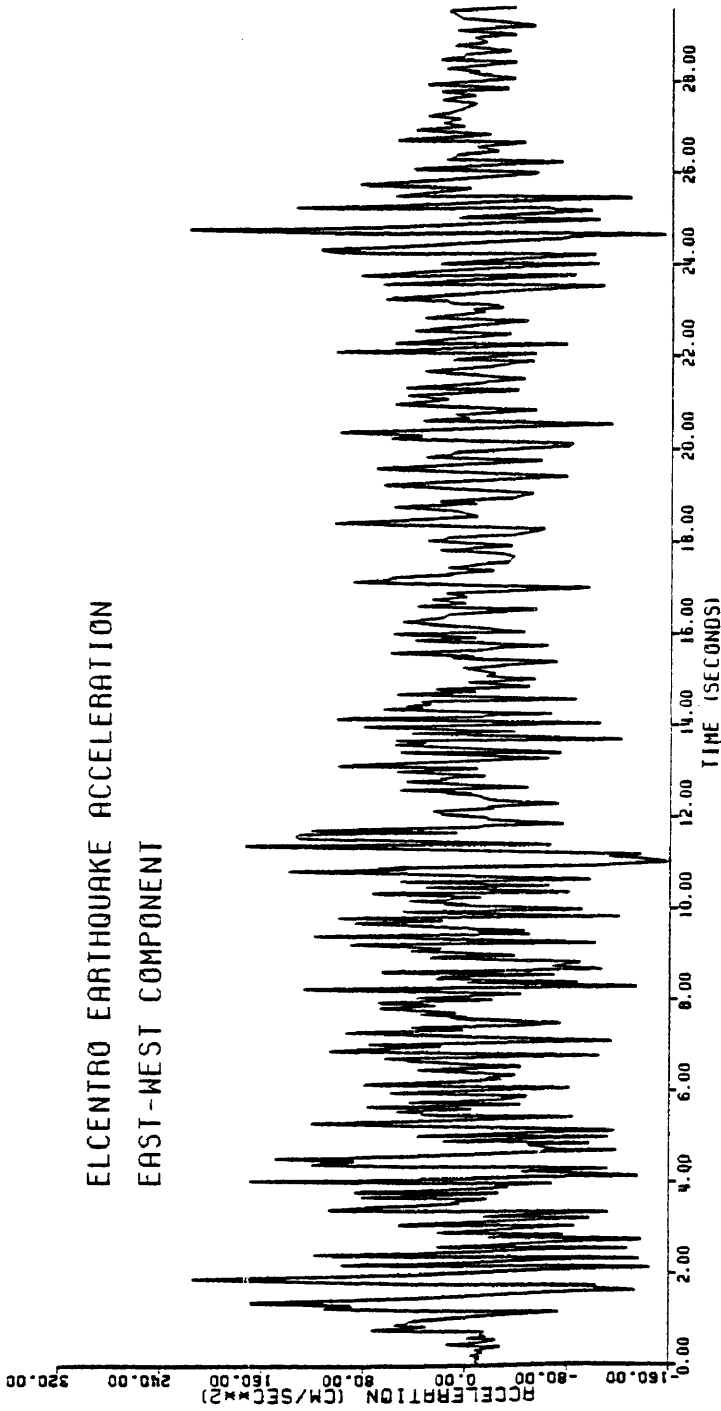


Fig. 75 - Acceleration Time History for the East-West Component of El Centro, 1940

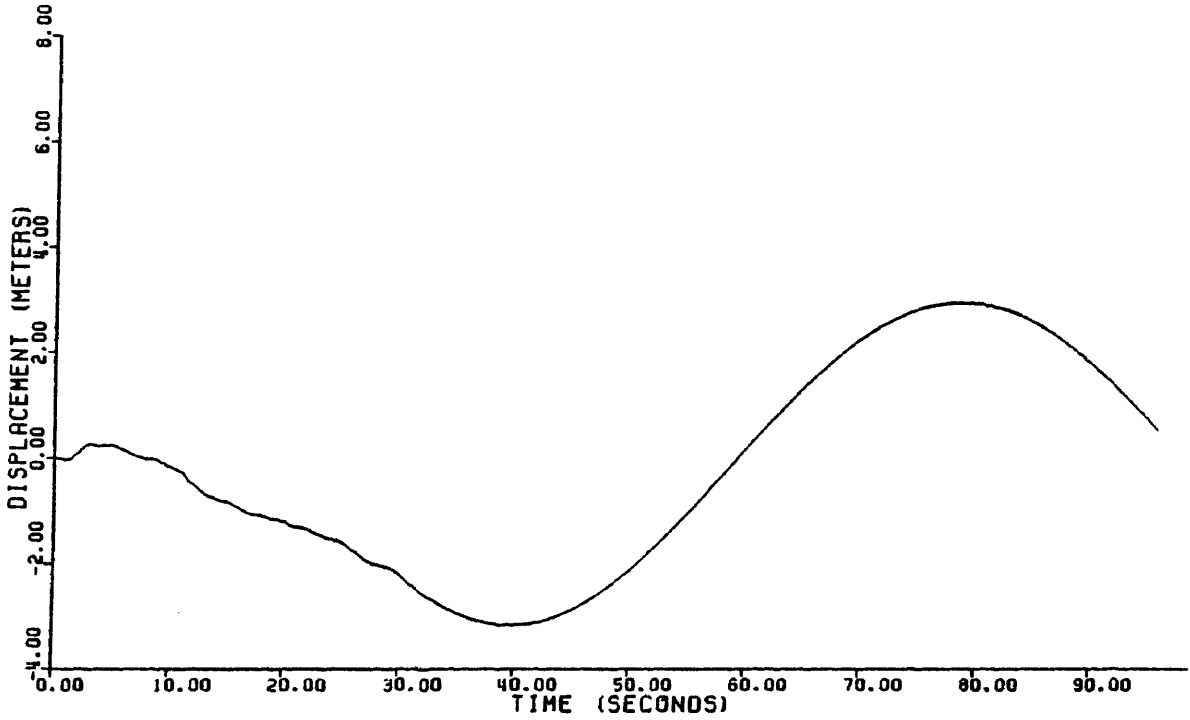


Fig. 76 - Time History of Surge Response for
El Centro Earthquake

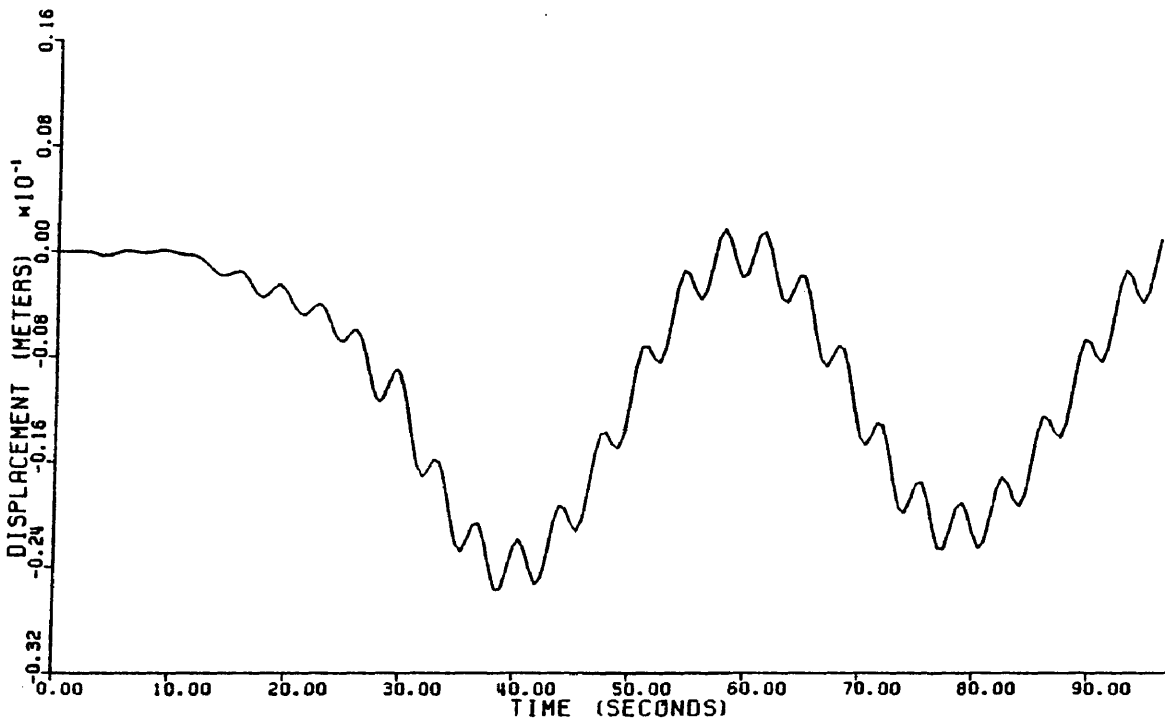


Fig. 77 - Time History of Heave Response for
El Centro Earthquake

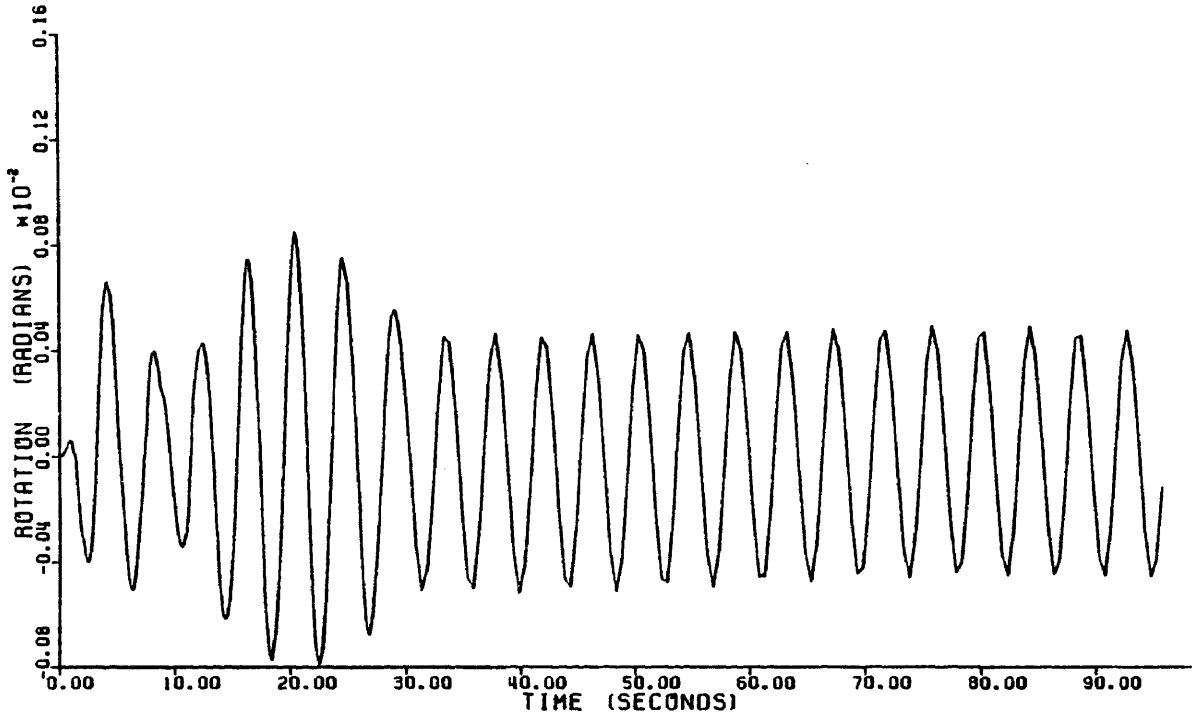


Fig. 78 - Time History of Pitch Response for El Centro Earthquake

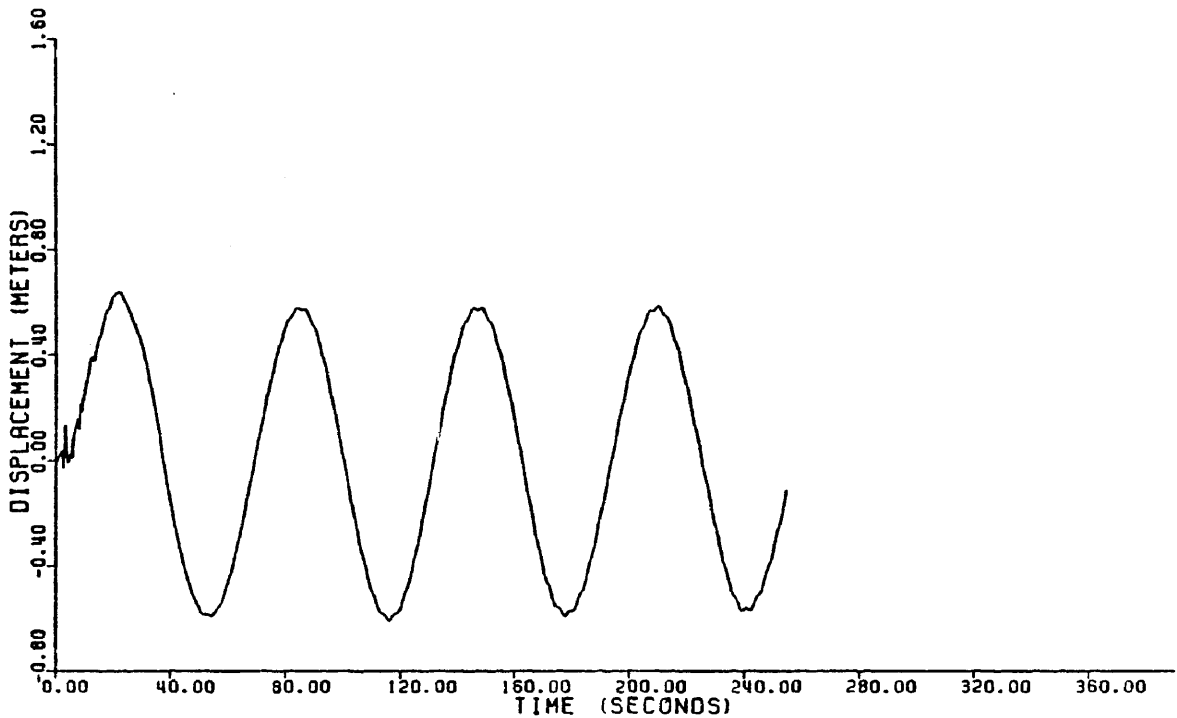


Fig. 79 - Time History of Surge Response to the S16E Component of Pacoima Dam Record of San Fernando Earthquake, 1971

maximum of 2 meters. At the end of the 30 seconds the structure attains some velocity and displacement that act as initial values for the free vibration of the platform. The surge response reaches a maximum of about 3.5 meters in the free vibration region. Heave and pitch arise from the effects of coupling with surge, but their magnitudes are found to be small. Also, a time history of surge response to Pacoima Dam earthquake is shown in Figure 79. The maximum surge in this case was about 0.6 meters.

Earthquakes may also occur simultaneously with waves. Figure 80 illustrates the time history response of surge to a combined loading of El Centro (EW) earthquake and a 17-second wave. It can be seen that the displacement response is dominated by the wave forces rather than by the earthquake. While the effect of earthquakes on the displacement response time history of surge is small for combined waves and earthquakes, there is a significant effect on the acceleration time history. The maximum acceleration caused by the wave only is 0.7 m/sec^2 and that from the earthquake and wave combined is 2.0 m/sec^2 . In this case the increase of surge acceleration caused by the earthquake is found to be as much as 300%. This high platform acceleration can have significant effect on personnel, equipment and operations.

Initial Conditions

Initial conditions for the combined earthquake and wave loading are of two types: (1) initial displacement and velocity of the earthquake time history, and (2) initial displacement, velocity, and acceleration of the structure. The initial displacement and velocity for

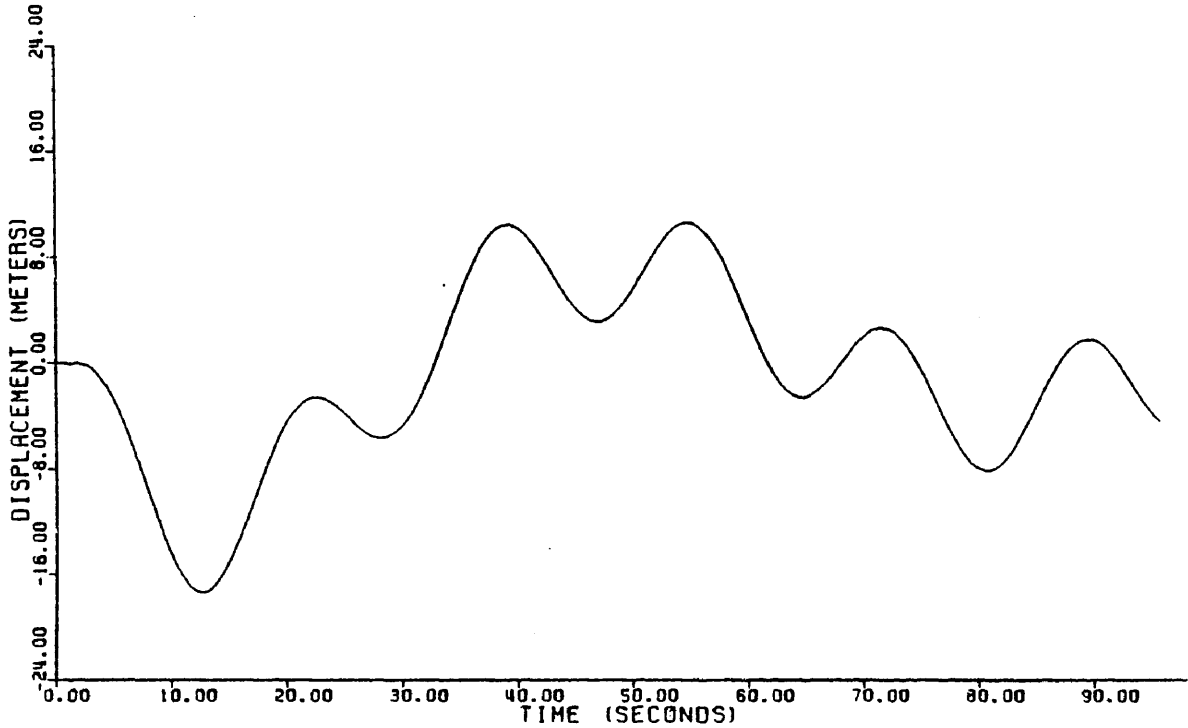


Fig. 80 - Time History of Surge Response to Combined El Centro Earthquake and 17 Second Wave

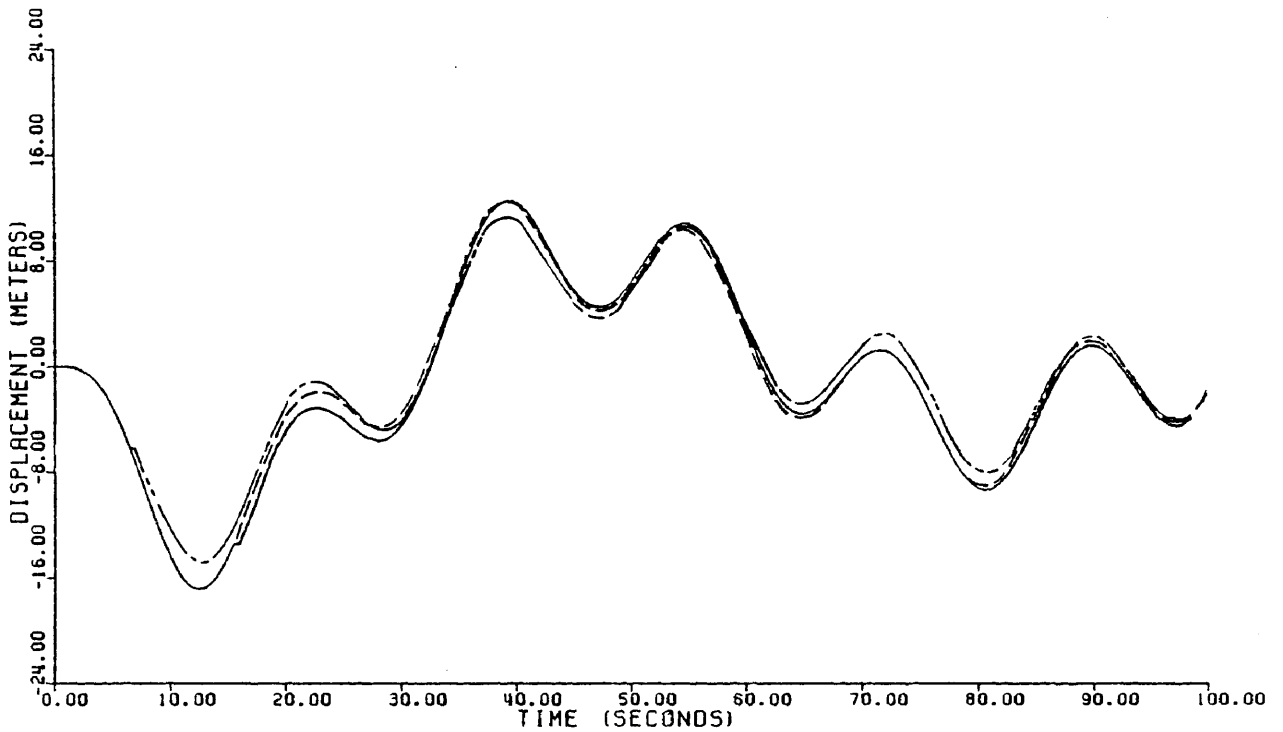


Fig. 81 - Time History of Surge Response to Combined 17 Second Wave and El Centro Earthquake Loading with Earthquake Introduced at Different Times

the ground motion record are on the order of few centimeters and centimeters per second, respectively. The structure's initial displacement and velocity arising from wave action just before the earthquake occurs, however, are on the order of meters and meters per second, respectively. Therefore any initial conditions of the ground for the earthquake time history are negligible compared to those of the structure just before the earthquake occurs. Therefore, for simplicity's sake, zero initial conditions were assumed for the ground.

To emphasize the effect of initial conditions on the time history of surge, first the wave was started and then the earthquake was introduced some time after the wave loading had started. The surge time history responses for a 17-second wave with El Centro (EW) earthquake introduced at $t = 7$ seconds and at $t = 16$ seconds, after the onset of the wave, are shown in Figure 81. It can be seen that the time histories are affected by the initial conditions of the structure at the time of the earthquake. However, because of the dominance of wave induced displacements, this does not seem to have a significant effect on the displacement time histories.

Water Depth

The effect of variations in water depth for both earthquake and combined wave and earthquake loading was studied. A time history of surge response to only earthquake motion for a water depth of 1000 meters is presented in Figure 82. The maximum surge attained is 8.5 meters at the period of 170 seconds, while that for a 200-meter water depth (see Figure 76) was 3.5 meters at a period of 75 seconds. Hence,

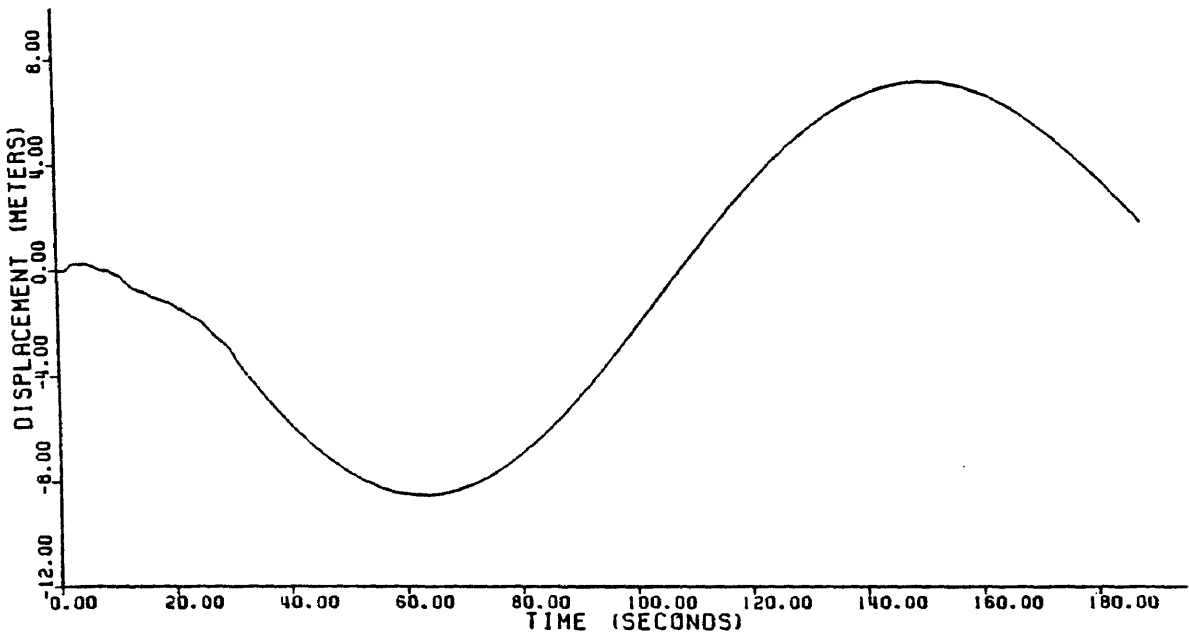


Fig. 82 - Time History of Surge Response to El Centro in 1000 m Water Depth

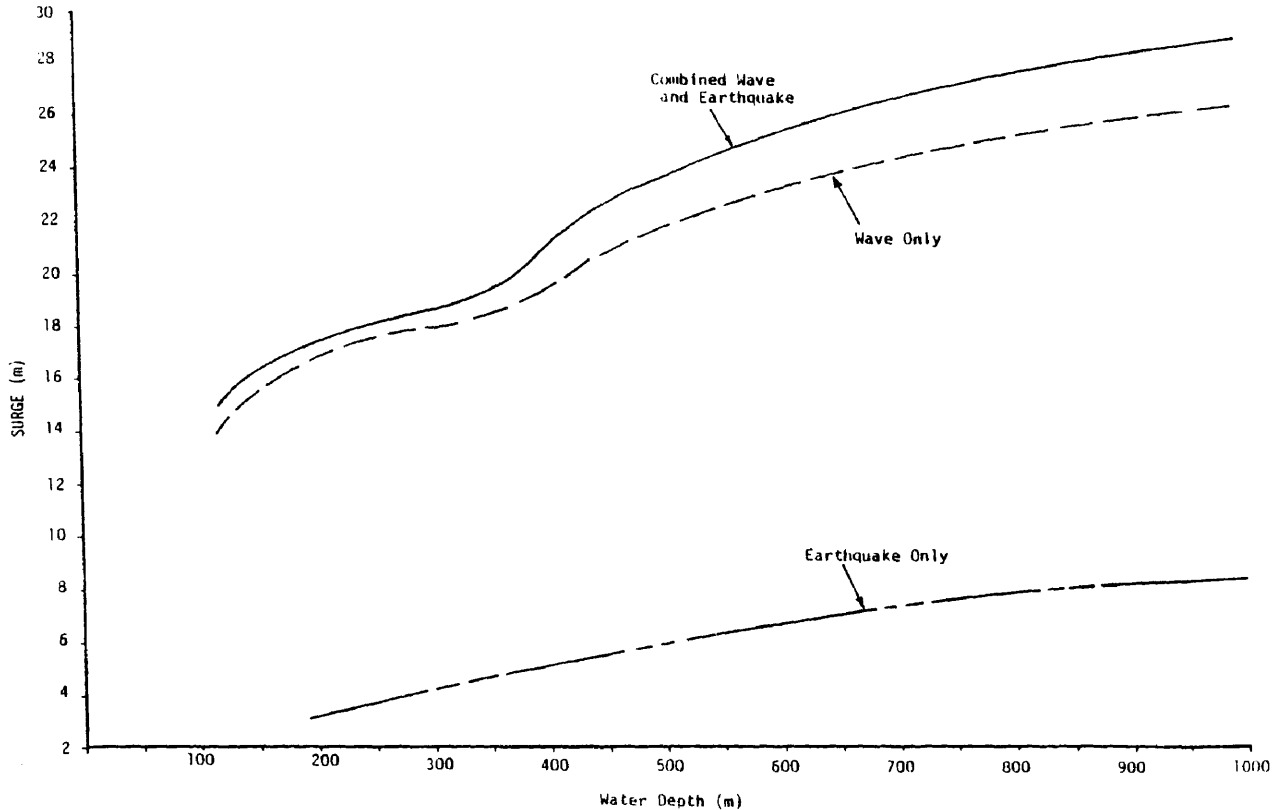


Fig. 83 - Variation of Surge Response with Water Depth for 17 Second Wave, El Centro Earthquake, and Combined Loading

both amplitude and period of surge response increase with water depth. Surge response amplitudes are plotted versus water depth for three cases (Figure 83): earthquake only, wave only, and wave and earthquake combined. It can be seen that the response amplitude varies nonlinearly with water depth for all three cases. A similar plot is presented in Figure 84 for heave response amplitude versus water depth.

Comparison with Response to Waves

A comparison of the time histories and response amplitudes for the above three cases is presented in order to evaluate the effect of earthquakes on the motion of the platform. Time histories of surge response to waves and combined wave and earthquake forces in a water depth of 1000 meters are shown in Figure 85. The increase in response amplitude caused by the inclusion of the earthquake is as much as 10 percent for this case. The same percentage of increase as above can be seen in Figure 86 for a 200-meter water depth with the earthquake introduced at $t = 200$ seconds (i.e., in the steady state region of the vibration).

Referring to Figures 83 and 84, it can be seen that to predict the response amplitude for combined wave and earthquake loading, one cannot simply superpose the maximum response amplitude arising from only earthquake forces to that arising from only wave forces. For example, at a water depth of 1000 meters the maximum surge response amplitude caused by earthquake motion alone is 8.5 meters; that from wave action alone is 26.5 meters; and that associated with the combined loading is 29.0 meters. Therefore, it would be too conservative to design for 35.0 meters ($26.5 + 8.5$) instead of for 29.0 meters. The

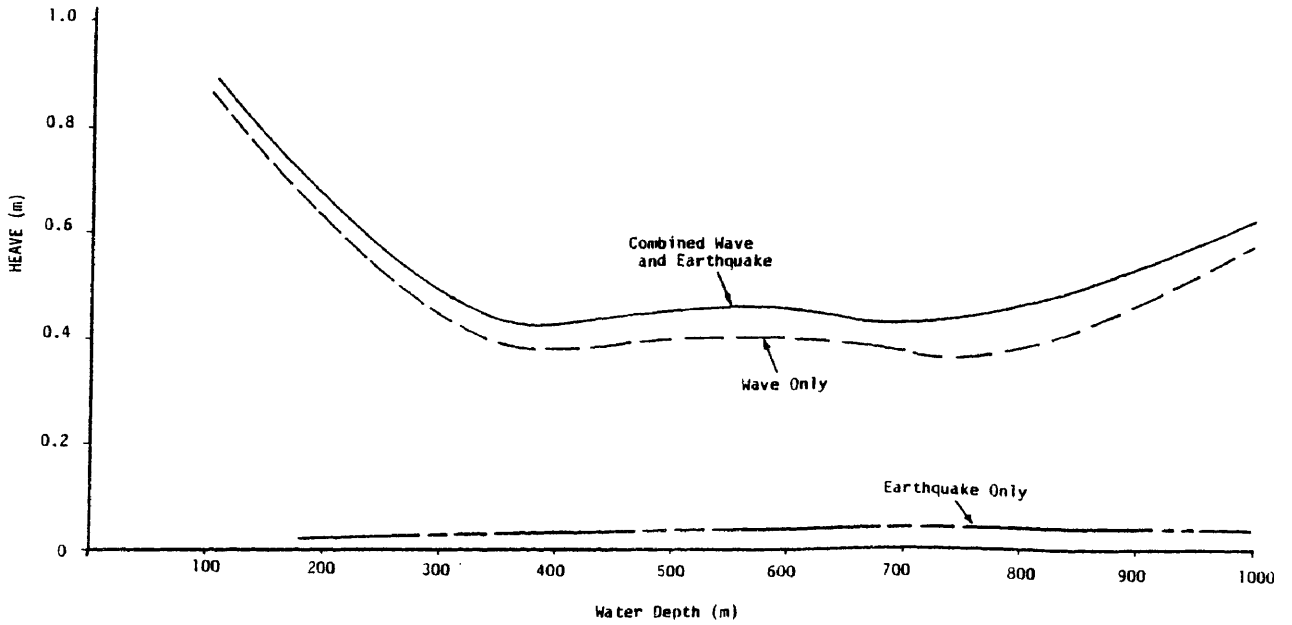


Fig. 84 - Variation of Heave Response with Water Depth for 17 Second Wave, El Centro Earthquake, and Combined Loading

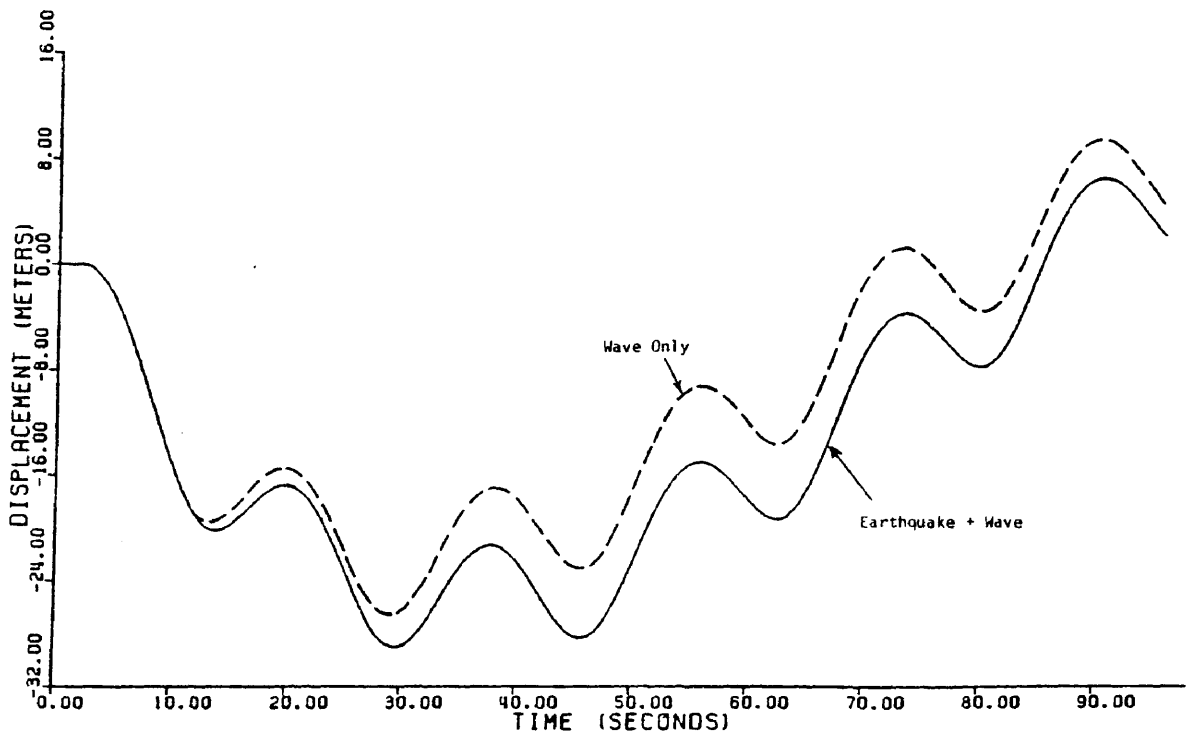


Fig. 85 - Comparison of Surge Response to 17 Second Wave with that from Combined Loading in 1000 m Water Depth

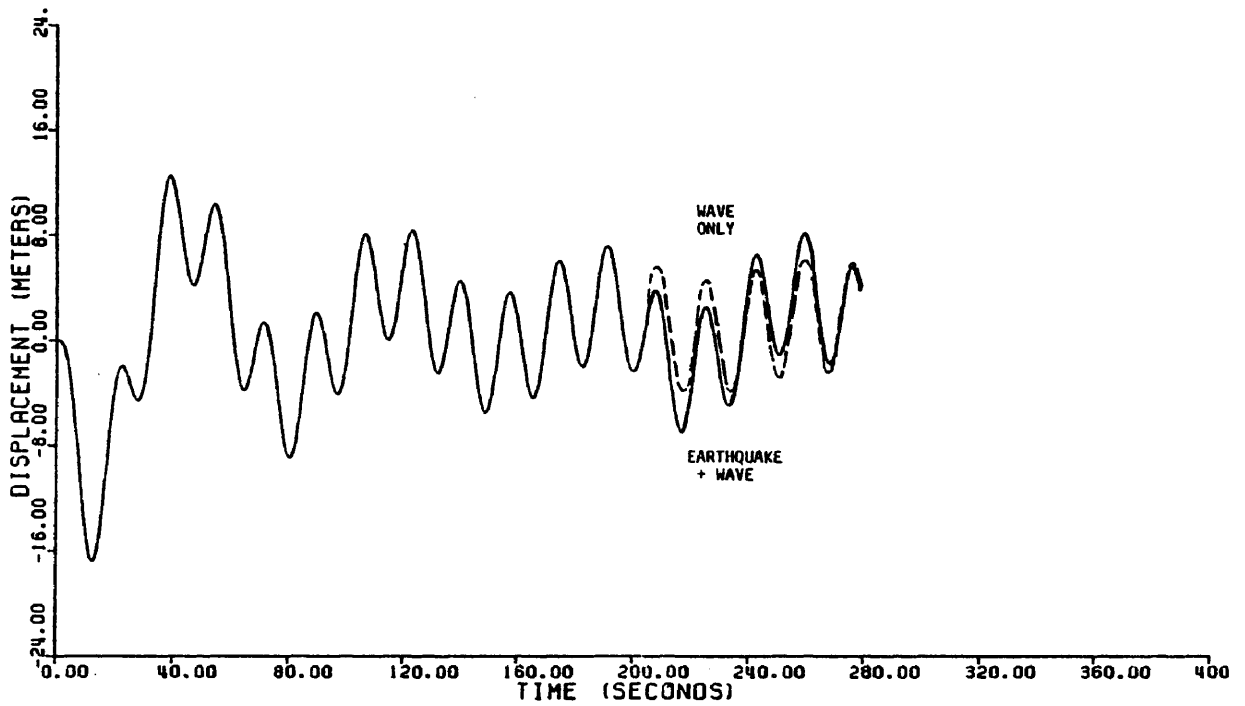


Fig. 86 - Time History of Surge Response to 17 Second Wave and Combined Loadings with El Centro Earthquake Introduced at $t = 200$ Seconds

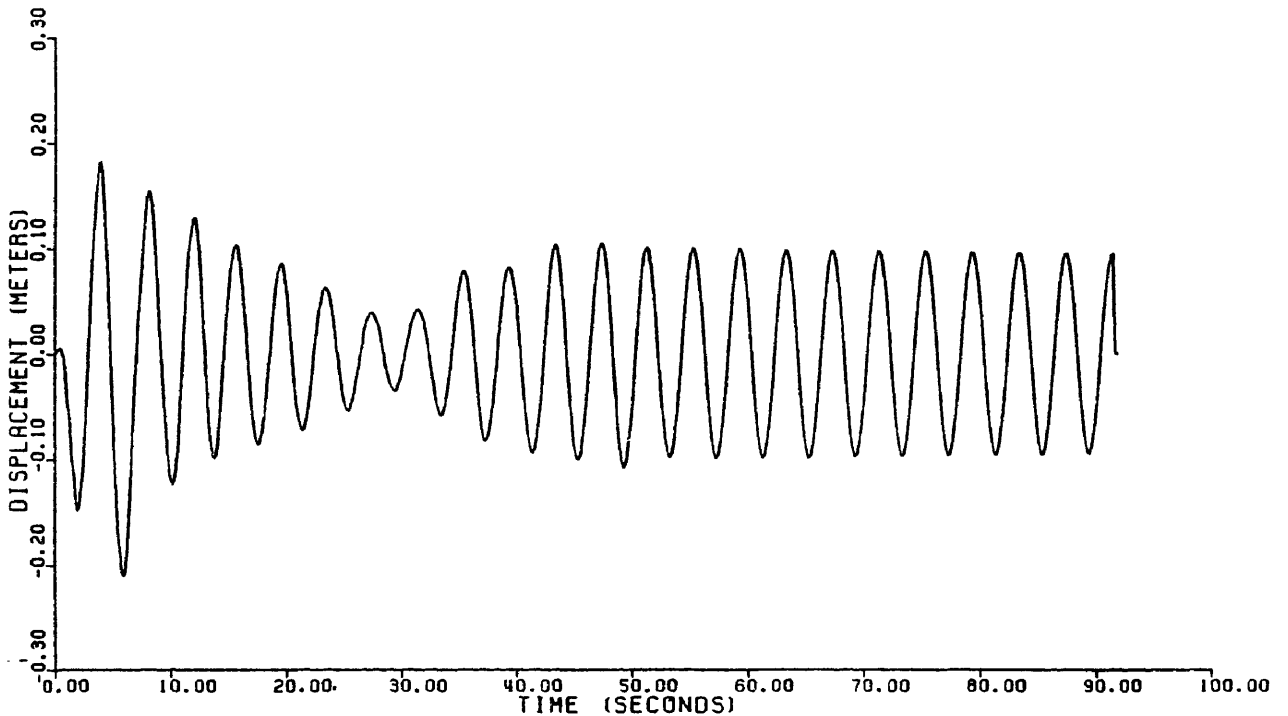


Fig. 87 - Time History of Heave Response to El Centro (Vertical) Earthquake

reason that superposition does not apply in this case is that the peak responses from earthquake forces are out of phase with those caused by wave forces. Similarly, the maximum heave response cannot be obtained from a superposition of the separate loadings; however, in some cases the sum of maximum heave response to individual loadings is less than the value obtained for the combined loading (see 800-meter water depth). This result is another illustration of the importance of coupling between heave and surge responses.

Vertical Component

Vertical components of three different earthquakes (El Centro, 1949; Pacoima Dam, 1971; and Taft Lincoln School, 1952) were used to study the effect of vertical ground motion on tension-leg platforms. Figures 87, 88, and 89 show the time histories of heave, heave velocity, and heave acceleration, respectively, for El Centro earthquake. Response time histories for Pacoima Dam earthquake are shown in Figures 90, 91, and 92 and those for Taft Lincoln School earthquake are shown in Figures 93, 94, and 95. The above response time histories showing maximum values of heave displacement, velocity and acceleration for each of the three earthquakes are summarized in Table 7.

It is observed from Table 7 that heave displacement amplitudes are significant compared to those resulting from waves. Platform vertical accelerations also are significant and can be as high as 5.0 meter/sec^2 which is more than $g/2$, where g is the acceleration of gravity. Therefore the cables which make up the legs of the platform should be designed to withstand such high platform vertical displacements and accelerations.

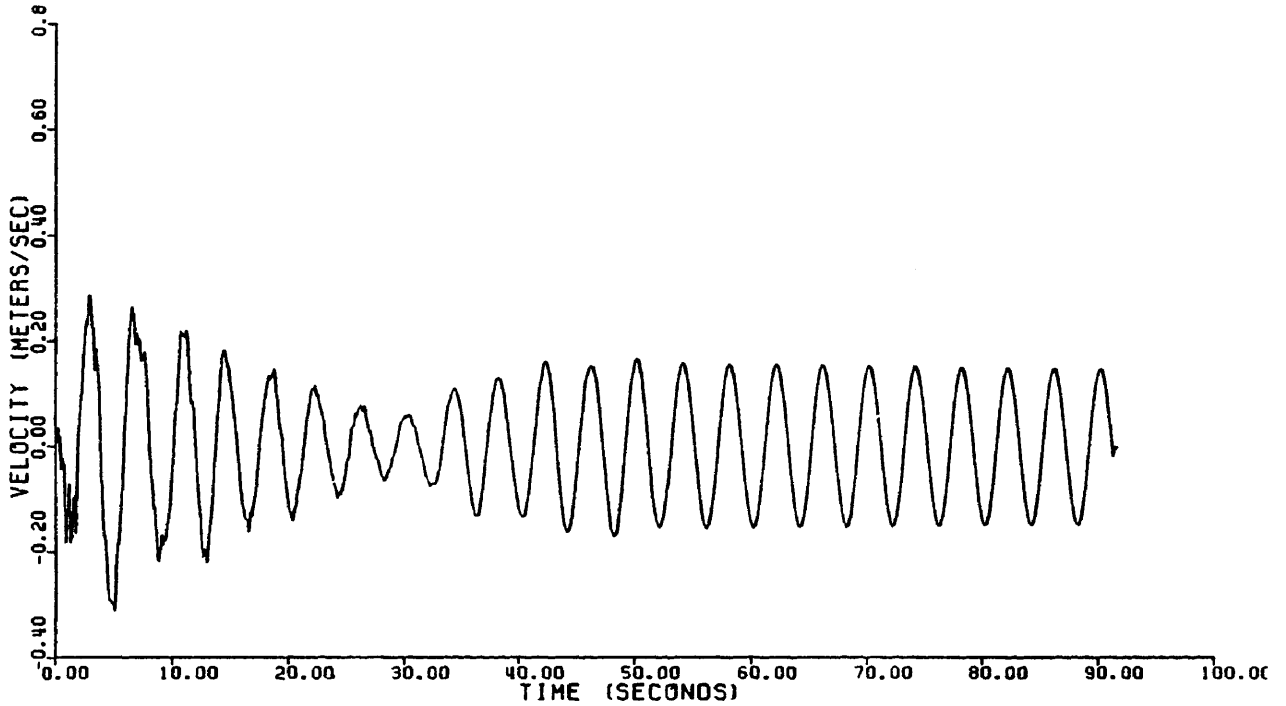


Fig. 88 - Time History of Heave Velocity Response to El Centro (Vertical) Earthquake

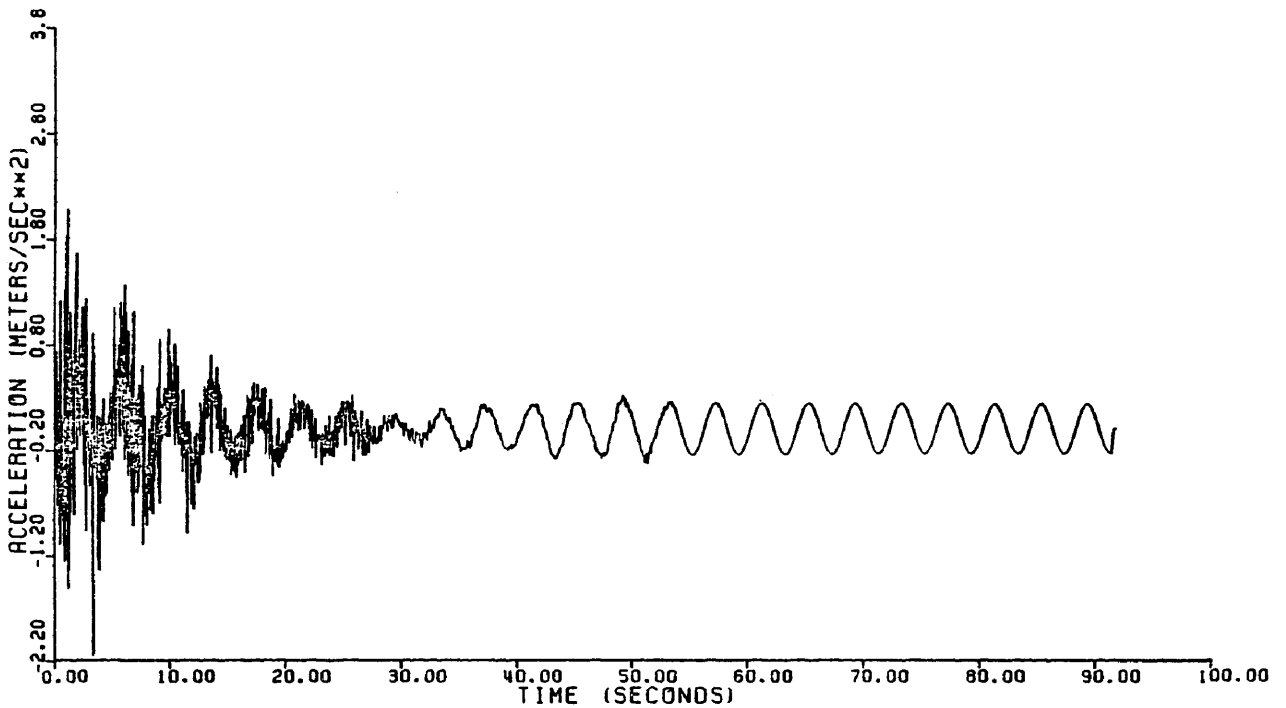


Fig. 89 - Time History of Heave Acceleration Response to El Centro (Vertical) Earthquake

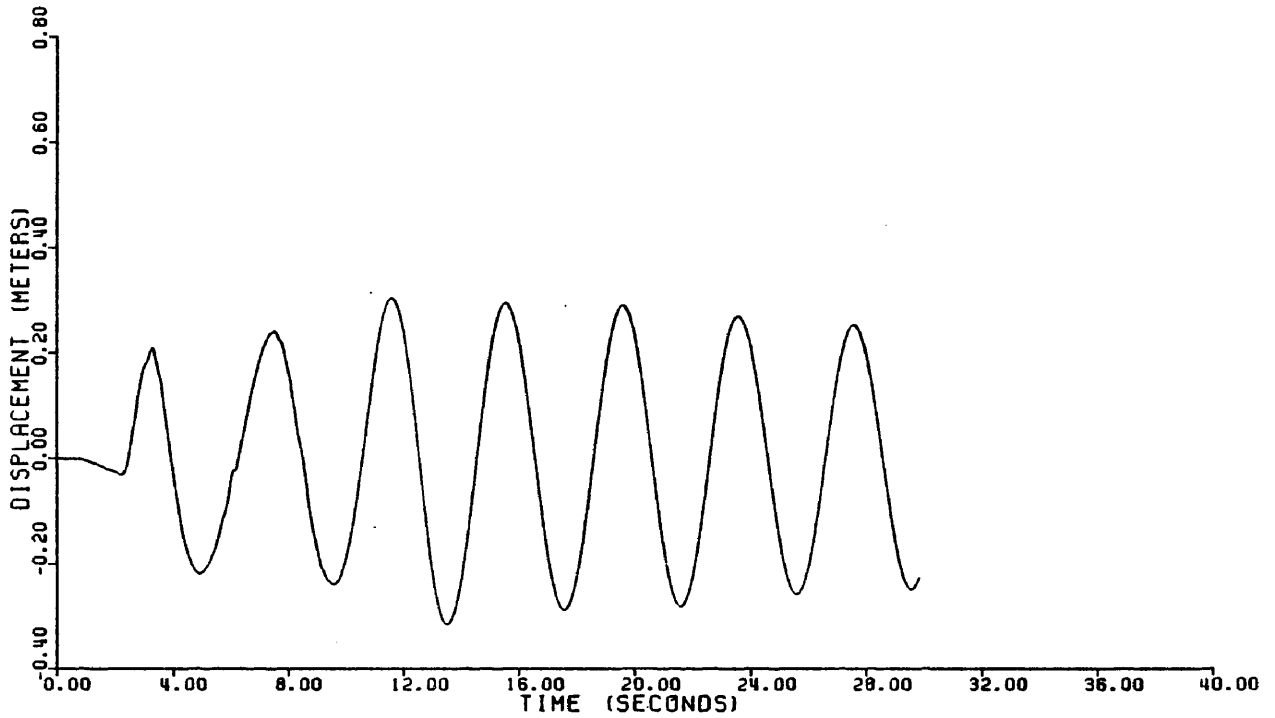


Fig. 90 - Time History of Heave Response to Pacoima Dam (Vertical) Earthquake

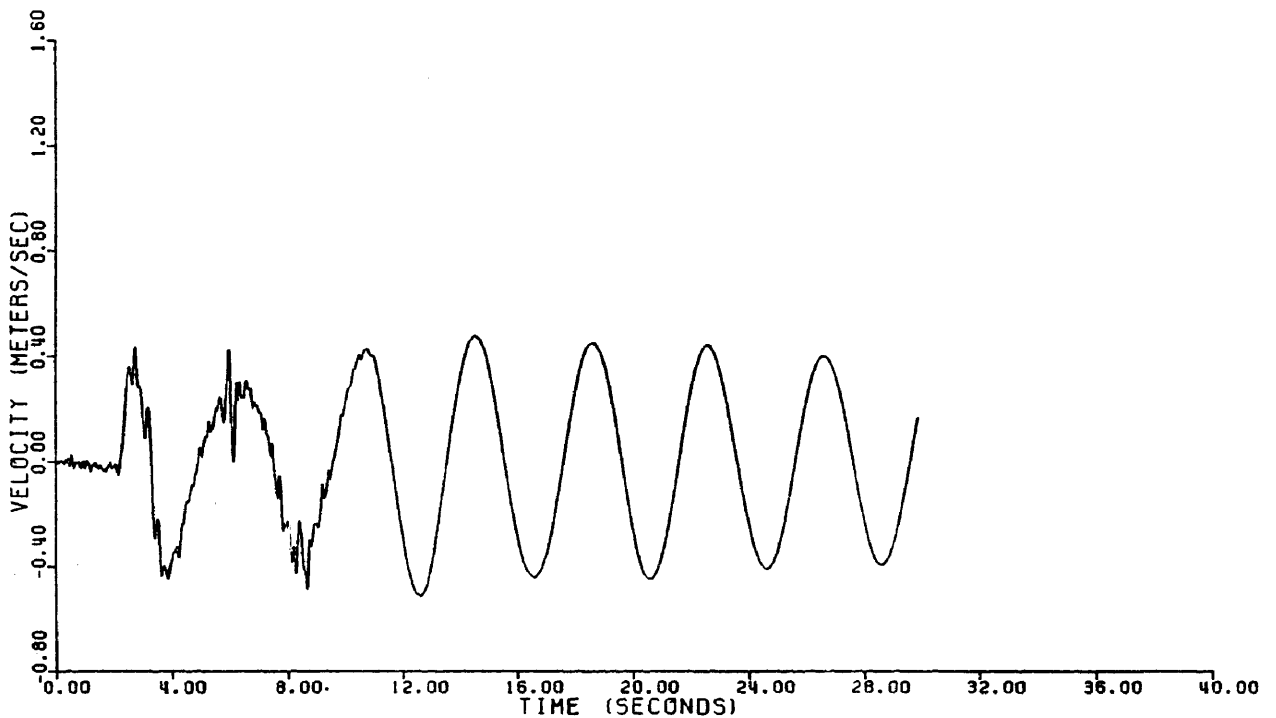


Fig. 91 - Time History of Heave Velocity Response to Pacoima Dam (Vertical) Earthquake

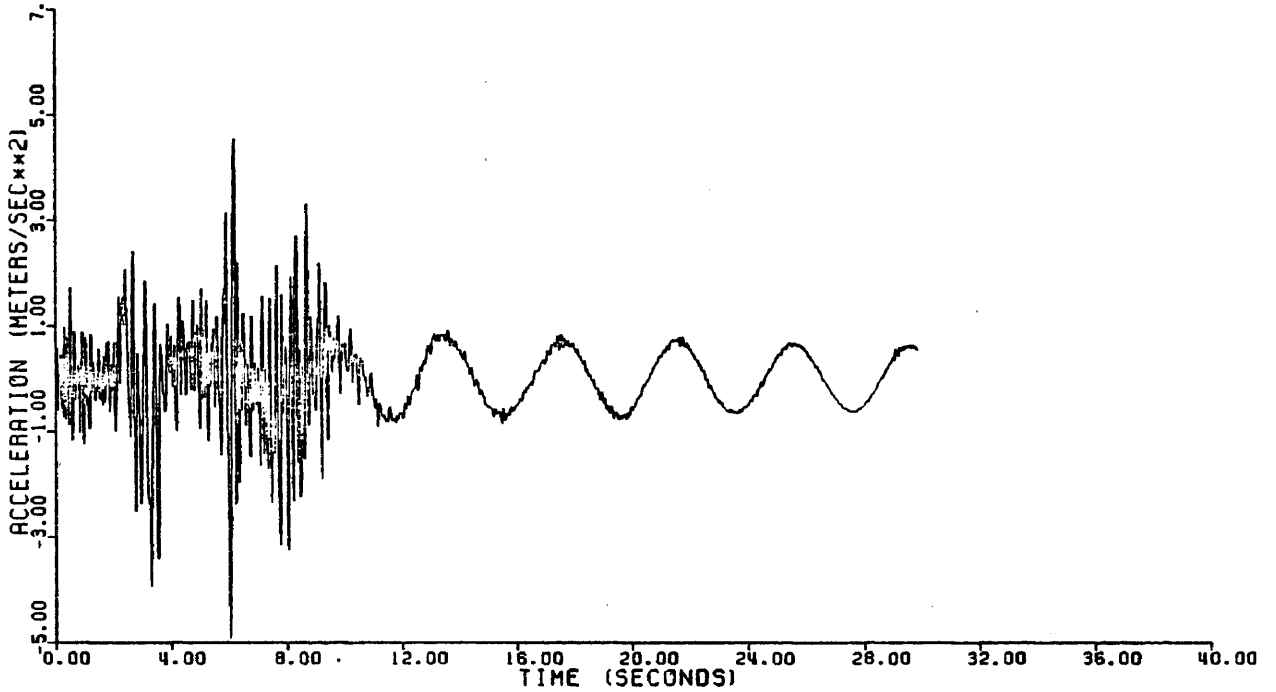


Fig. 92 - Time History of Heave Acceleration Response to Pacoima Dam (Vertical) Earthquake

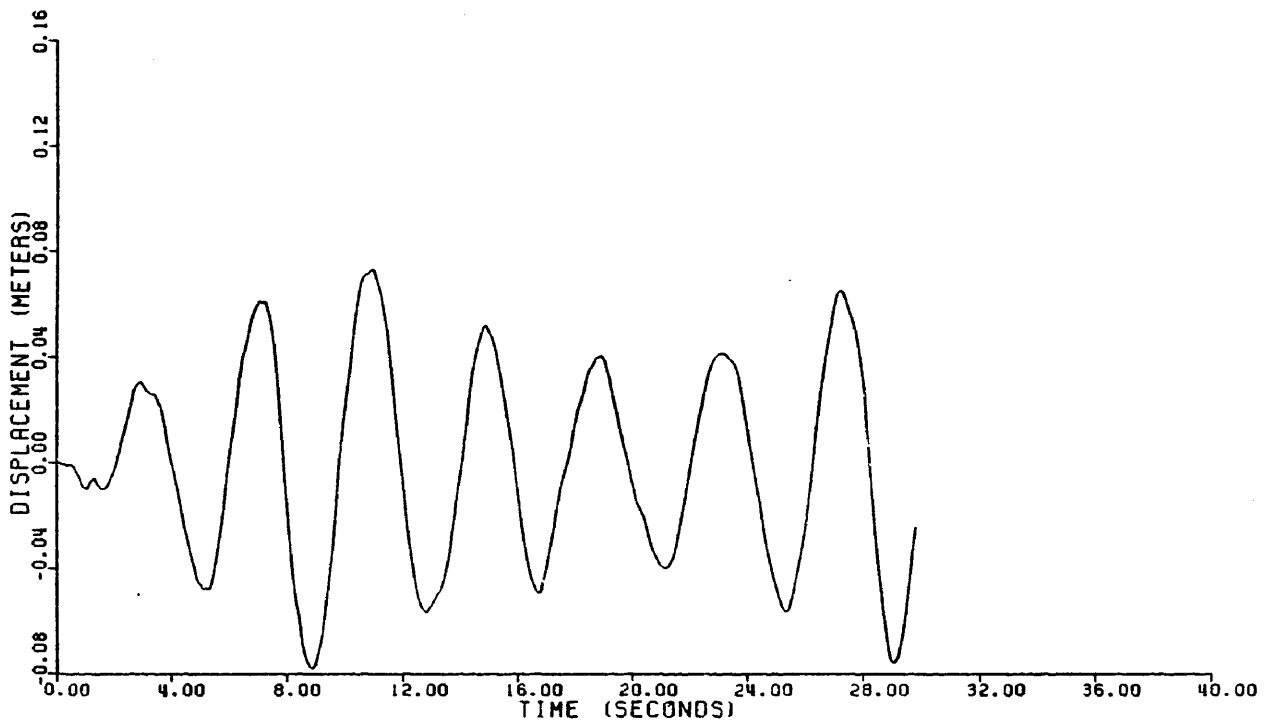


Fig. 93 - Time History of Heave Response to Taft Lincoln School (Vertical) Earthquake

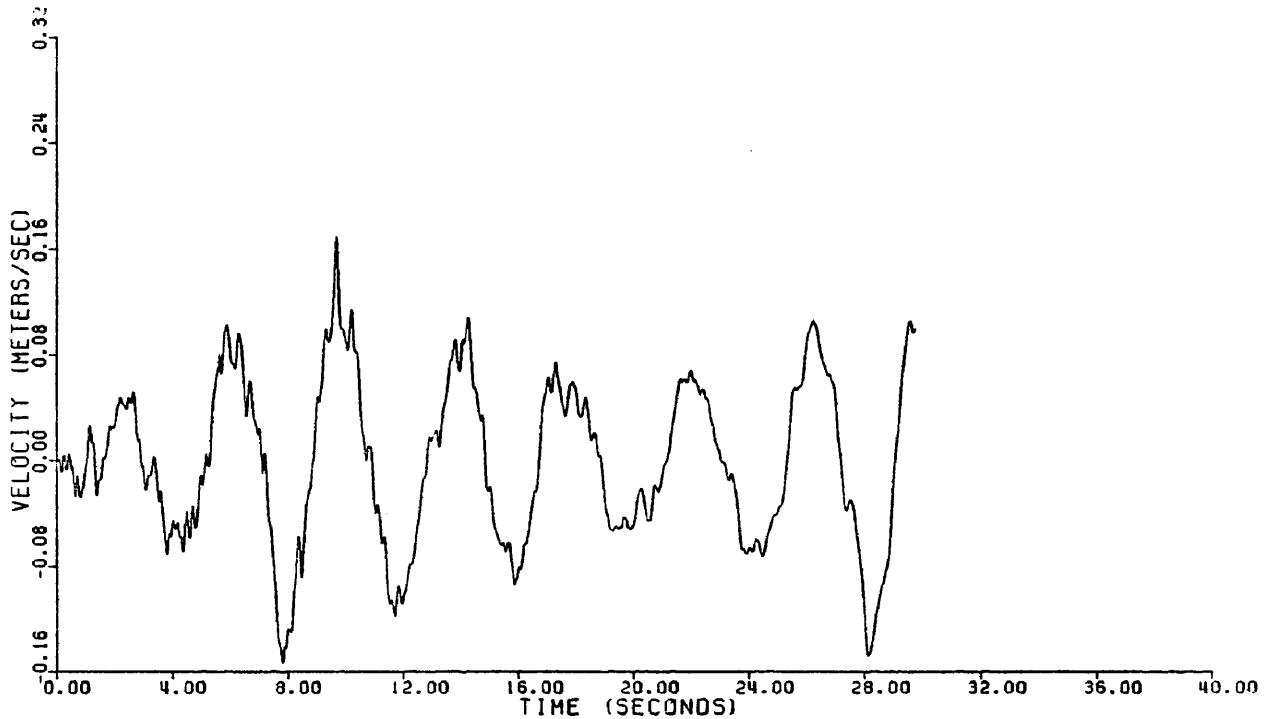


Fig. 94 - Time History of Heave Velocity Response to Taft Lincoln School (Vertical) Earthquake

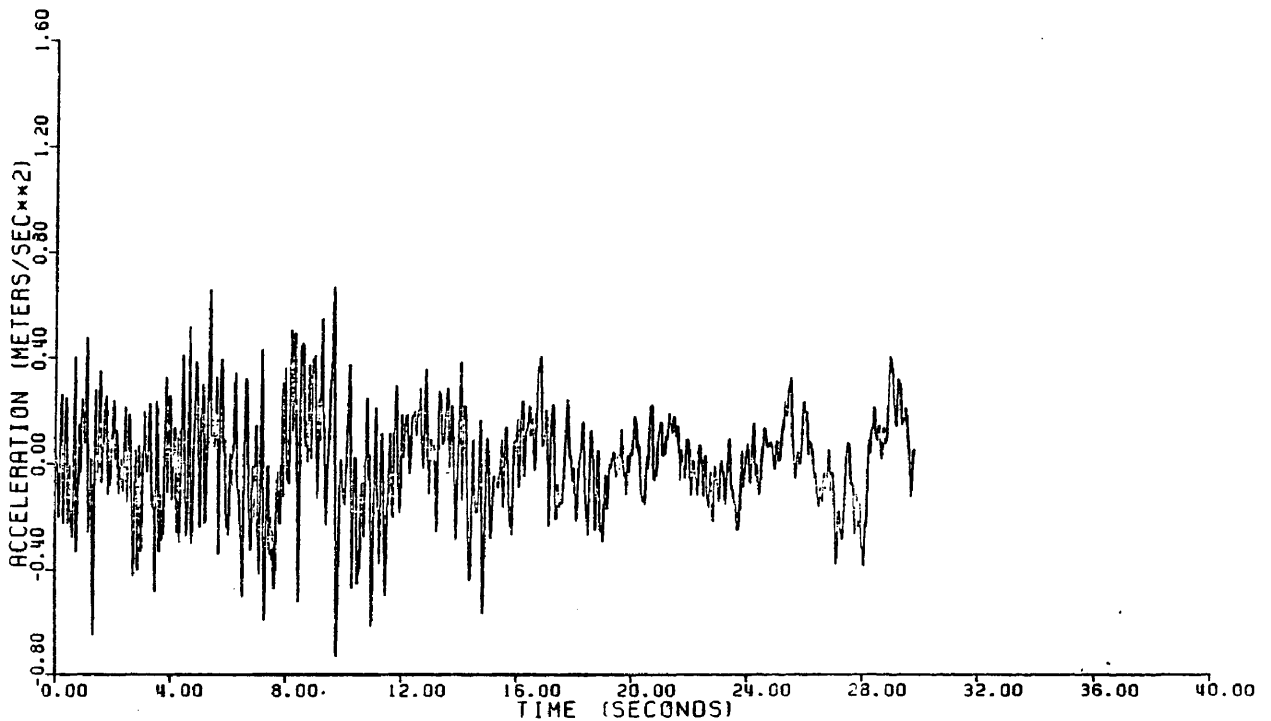


Fig. 95 - Time History of Heave Acceleration Response to Taft Lincoln School (Vertical) Earthquake

TABLE 7
Response to Vertical Ground Motion

Earthquake	Max. Heave Displacement (m)	Max. Heave Velocity (m/s)	Max. Heave Accel. (m/s ²)
El Centro	0.22	0.31	2.20
Pacoima Dam	0.32	0.52	5.00
Taft	0.08	0.16	0.70

Summary of Response to Earthquakes

Time histories of response to earthquake loading and to combined wave and earthquake forces were obtained. For the horizontal earthquake, the displacement response from combined loading was found to be dominated by the wave. However, the accelerations were significantly affected by the earthquake. The maximum acceleration was found to be up to three times that caused by waves alone. The earthquake was introduced at different time spacings measured from the starting time of the wave in order to cover as many different initial conditions as possible. Water depth was varied and its effect on the response amplitudes was studied. An increase of about 10% in displacement response amplitudes due to earthquake forces was noticed throughout the range of water depths used in the analysis.

Large platform accelerations and vertical displacements also were observed for the case of vertical ground motion. The maximum heave from the vertical ground motions studied was about 50% of that caused

by the waves. The effects of compression waves in the water column could increase further, these heave displacements and accelerations. The inclusion of compression wave effects would make the vertical component of the earthquake more important but is dependent on water compressibility which is beyond the scope of this investigation.

CHAPTER VI
SUMMARY, CONCLUSIONS AND RECOMMENDATIONS

Summary

In this study, a complete nonlinear deterministic dynamic analysis model for tension-leg platforms has been developed and response of the platforms to wave and earthquake loadings have been studied. The accomplishments in the development of the dynamic analysis model include:

- 1) The formulation of closed form nonlinear stiffness coefficients and the formation of a stiffness force vector.
- 2) Derivation of closed form nonlinear forcing functions for waves and earthquakes using Morison's equation (modified to include relative motion between structure and fluid particles). Both inertial and drag components of the forcing functions were included, and wave kinematics were obtained from the linear wave theory. Integration of the force equations along the length of each submerged member of the platform was carried out manually, thereby reducing the total cost of dynamic analysis significantly.
- 3) Development of a mathematical model based on a set of coupled nonlinear differential equations whose solution yields the dynamic response of the platform.
- 4) Development of a compact and inexpensive computer code to perform the numerical calculations of the motion of tension-leg platforms. The computer program employs Newmark's Beta method

to integrate the equations of motion sequentially in time and obtain time histories of the response.

Conclusions

Response time histories for each of the six degrees of freedom of the platform were obtained. A parametric analysis was carried out in order to identify the important parameters involved in the behavior of tension-leg platforms. The following conclusions can be made with regard to the platform behavior and response to dynamic loading:

- 1) Coupling can significantly affect the behavior of the structure. The strongest coupling exists between heave and sway and between heave and surge. The coupled heave response amplitude is several times larger than the uncoupled amplitude. Coupling between pitch and surge or roll and sway also has been shown to have a significant effect on computed responses. The extent of this coupling is dependent on the location of the center of rotation, which can be expected to migrate with the level of response. Further research is needed to establish an appropriate location for the center of rotation or to determine the expected variations of its location.
- 2) Two types of nonlinearities are inherent in the analysis:
 - a) Nonlinearity of the stiffness force vector arising from large displacements is found to be significant if surge and sway are more than approximately 5 meters in a water depth of 200 meters.

- b) Nonlinearity of the forcing function arises from the square of the velocity terms in the drag force calculations. Nonlinear drag forces are found to be significant in that they represent the fluid damping arising from the relative motion between the structure and fluid particles and therefore lead to response reduction with time.
- 3) From the parametric study performed on the platform for regular waves the following conclusions are made:
- a) Variation of wave period shows that surge, sway, and heave are most significant for high wave periods (i.e., periods greater than 15 seconds) and pitch, roll and yaw are most significant for periods around 5 seconds.
 - b) Variation of wave height shows linear relationships for wave heights less than about 15 meters and becomes non-linear for larger wave heights.
 - c) Increasing the leg stiffness tends to decrease response; however, for leg stiffness larger than 20,000 kN/m, little additional effect on response was noticed.
 - d) Increasing water depth results in an increase in surge, sway, pitch, and roll response and a decrease in heave response.
 - e) Higher initial tensions tend to make the structure stiffer, hence it reduces the response. However, as the stiffness increases, the period of vibration decreases; and as it approaches that of the wave, higher response amplitudes are observed.

- 4) The general behavior of the platform subjected to random waves is similar to that for regular waves. It also is found that resonance of platform motions does not occur for random waves. It is suggested that regular wave trains be used to provide the necessary information about the behavior of tension-leg platforms.

The behavior of the platform was not significantly affected by the forces resulting from the simplified wave drift formulation utilized in this study. A more complex formulation of wave drift forces may provide additional insight into wave drift effects.

- 5) The displacement response to combined wave and earthquake loading was dominated by the wave. A uniform increase in response of approximately 10% arising from the inclusion of horizontal ground motions was observed. The platform horizontal accelerations, however, were significantly affected by the earthquake. The maximum horizontal acceleration was found to be three times that caused by waves alone.

Vertical ground motion also was found to have significant effects on the platform vertical displacements and accelerations. The maximum heave resulting from vertical ground motion was found to be about 50% of that caused by waves alone, and the maximum heave acceleration was as high as 5.0 meters/sec.² High platform heave displacements and accelerations can affect the cables as well as personnel, equipment, and operations.

Recommendations

The model developed herein is adapted to the response of tension-leg platforms; however, the wave force section could be easily applied to various types of offshore structures. Several enhancements would allow the model to be adapted to a wider range of problems (i.e., shallower water, larger members, larger wave heights, etc.). These enhancements include:

- 1) Application of higher order wave theories,
- 2) Employing the diffraction theory for computing wave forces on large members at low wave periods,
- 3) Varying coefficients of added mass and damping with respect to time,
- 4) Variations in location of the center of rotation,
- 5) Application of other wave drift formulations, and
- 6) Investigation of the heave of the platform caused by compression waves in the water column which result from vertical ground motion.

REFERENCES

1. Airy, G. B., "On Tides and Waves," Encyclopedia Metropolitana, London, 1845.
2. Albrecht, H. G., D. Koenig, "Non-Linear Dynamic Analysis of Tension-Leg Platforms, for Medium and Greater Depths," Proceedings of 10th Annual Offshore Technology Conference, 1978, paper OTC 3044.
3. Borgman, L. E., "Ocean Wave Simulation for Engineering Design," J. Waterways, Harbors & Coastal Eng. Div. ASCE, 95, WW4, November 1969.
4. Bretschneider, C. L., "Wave Variability and Wave Spectra for Wind-Generated Gravity Waves," U.S. Army Corps of Engineers, Beach Erosion Board, Tech. Memo. No. 118, 1959.
5. Burke, B. G., "The Analysis of Motions of Semi-Submersible Drilling Vessels in Waves," Proceedings of 1st Annual Offshore Technology Conference, 1969, paper OTC 1024.
6. Burke, B. G. and J. T. Tighe, "A Time Series Model for Dynamic Behavior of Offshore Structures," Proceedings of the 3rd Annual Offshore Technology Conference, 1971, paper OTC 1403.
7. Chakrabarti, S. K., "Steady and Oscillating Drift Forces on Floating Objects," Journal of the Waterway, Coastal and Ocean Division, ASCE, Vol. 106, No. WW2, May 1980.
8. Chakrabarti, S. K., "Experiments on Wave Drift Force on a Moored Floating Vessel," Proceedings of the Offshore Technology Conference (OTC Paper 4436), 1982.
9. Chappellear, J. E., "Direct Numerical Calculations of Wave Properties," Journal of Geophysical Research, Vol. 66, No. 2, Feb. 1961, pp. 501-508.
10. Cokelet, E. D., "Steep Gravity Waves in Water of Arbitrary Uniform Depth," Institute of Oceanographical Sciences, pp. 183-230, 1977.
11. Dean, R. G., "Stream Function Representation of Nonlinear Ocean Waves," Journal of Geophysical Research, Vol. 70, No. 18, Sept. 1965, pp. 4561-4572.
12. Denise, J. P. F. and N. J. Heaf, "A Comparison Between Linear and Non-Linear Response of a Proposed Tension-Leg Production Platform," Proceedings of 11th Annual Offshore Technology Conference, 1979, paper OTC 3555.

13. Faltinsen, O. M., and Loken, A. E., "Drift Forces and Slowly-Varying Horizontal Forces on Ships and Offshore Structures in Waves," Norwegian Maritime Research, Vol. 6, No. 1, 1978, pp. 2-15.
14. Garrison, C. J., "Dynamic Response of Floating Bodies," Proceedings of 6th Annual Offshore Technology Conference, 1974, paper OTC 2067.
15. Garrison, C. J., "Drag and Inertia Coefficients in Oscillatory Flow about Cylinders," ASCE National Water Resources and Ocean Engineering Convention, Houston, 1976.
16. Garrison, C. J. and Stacy, R., "Wave Loads on North Sea Gravity Platforms: A Comparison of Theory and Experiment," OTC Paper No. 2794, 1977.
17. Hassleman, K. et al., "Measurement of Wind-Wave Growth and Swell Decay During the Joint North Sea Wave Project (JONSWAP)," Deutsches Hydrographisches Institut, Hamburg, 1973.
18. Havelock, T. H., "The Pressure of Water Waves Upon a Fixed Obstacle," Proc. Roy. Soc. Vol. 175A (July 1940), pp. 409-421.
19. Hogben, N. and Stading, R. G., "Experience in Computing Wave Loads on Large Bodies," OTC Paper No. 2189, 1975.
20. Isaacson, M. de St. Q., "Wave Induced Forces in the Diffraction Regime," Mechanics of Wave-Induced Forces on Cylinders, ed. T. L. Shaw, Pitman, London, pp. 68-89, 1979.
21. Jeffrys, E. R. and Patel, M. H., "Dynamic Analysis Models of Tension Leg Platforms," Proceedings of 13th Annual OTC, 1981, paper OTC 4075.
22. Kareem, A., "Dynamic Effects of Wind on Offshore Structures," OTC 3764, 1980.
23. Kirk, C. L. and R. K. Jain, "Wave Induced Oscillations of Tension-Leg Single Buoy Mooring Systems," Proceedings of 8th Annual Offshore Technology Conference, 1976, paper OTC 2494.
24. Kirk, C. L. and E. U. Etok, "Dynamic Response of Tethered Production Platforms in a Random Sea State," Second International Conference on Behavior of Offshore Structures, London, August 1979.
25. Korteweg, D. J. and DeVries, G., "On the Change of Form of Long Waves Advancing in a Rectangular Canal, and on a New Type of Long Stationary Waves," Philosophical Magazine, 5th Series, 1895, pp. 422-443.

26. LeMehaute, B., An Introduction to Hydrodynamics of Water Waves, Water Wave Theories, Vol. II, TR EREL118-POL-3-2, U.S. Dept. Comm., ESSA, Washington, D.C., 1969.
27. Leonard, J. W., Garrison, C. J. and Hudspeth, R. T., "Deterministic Fluid Forces on Structures: A Review," Journal of Structural Division, ASCE, Vol. 107, No. ST6, June 1981.
28. Lowery, L. L. and Hirsch, T. J., "Use of Wave Equation to Predict Soil Resistance on a Pile During Driving," Research Report 33-10, Project 2-5-62-33, TTI, Texas A&M University, December 1967.
29. MacCamy, R. C. and Fuchs, R. A., "Wave Forces on Piles: A Diffraction Theory," U.S. Army, Beach Erosion Board, Tech. Memo No. 69, 1954.
30. Maruo, H., "The Drift of a Body Floating on Waves," Journal of Ship Research, Vol. 4, pp. 1-10, 1960.
31. McDonald, R. D., "Design and Field Testing of the Triton Tension Leg Fixed Platforms," OTC 2104, 1974.
32. Mei, C. C., "Numerical Methods in Water Waves Diffraction and Radiation," Annual Reviews Fluid Mechanics, Vol. 0, pp. 393-416, 1978.
33. Morison, J. R., O'Brien, M. P., Johnson, J. W. and Shaaf, S. A., "The Forces Exerted by Surface Waves on Piles," Petroleum Transaction, 1950, AIME, Vol. 189.
34. Munk, W. H., "The Solitary Wave Theory and its Application to Surf Problems," Annuals of the New York Academy of Sciences, Vol. 51, 1949, pp. 376-462.
35. Natvig, G. J. and J. W. Pendered, "Nonlinear Motion Response of Floating Structures to Wave Excitation," Proceedings of 9th Annual Offshore Technology Conference, 1977, paper OTC 2796.
36. Newman, J. N., "The Drift Force and Moment on Ships in Waves," Journal of Ship Research, Vol. 11, pp. 51-60, 1967.
37. Newmark, N. M., "A Method of Computation for Structural Dynamics," Transactions, ASCE, Vol. 127, pp. 1406-1435, 1962.
38. Pauling, J. R. and E. E. Horton, "Analysis of the Tension-Leg Stable Platform," Proceedings of 2nd Annual Offshore Technology Conference, 1970, paper OTC 1263.
39. Pierson, W. J. and Moskowitz, L., "A Proposed Spectrum Form for Fully Developed Wind Seas Based on the Similarity Theory of S. A. Kitaigorodskii," Journal of Geophysical Research, Vol. 69, pp. 5181-5190, 1964.

40. Pijfers, J. G. L., and Brink, A. W., "Calculated Drift Forces of Two Semisubmersible Platform Types in Regular and Irregular Waves," Proceedings of Offshore Technology Conference, Paper OTC 2977, 1977.
41. Pinkster, J. A., "Low Frequency Phenomena Associated with Vessels Moored at Sea," Spring Meeting, Society of Petroleum Engineers, AIME, Amsterdam, SPE Paper No. 4837, 1974.
42. Remery, G. F. M., and Hermans, A. J., "The Slow Drift Oscillations of a Moored Object in Random Seas," Proceedings of the Offshore Technology Conference, OTC paper 1500, 1971.
43. Rye, H., Rynning, S., and Moshage, H., "On the Slow Drift Oscillations of Moored Structures," Proceedings of the Offshore Technology Conference, OTC Paper 2366, 1975.
44. Salvesen, N., Von Kerczek, C. H., Yue, D. K., and Stern, F., "Computations of Nonlinear Surge Motions of Tension Leg Platforms," Proceedings of the Offshore Technology Conference, OTC Paper 4394, 1982.
45. Sarpkaya, T., "In-Line and Transverse Forces on Cylinders in Oscillatory Flow at High Reynolds Numbers," OTC Paper No. 2533, 1976.
46. Sarpkaya, T., "Hydrodynamic Drag-Wave Forces-Response of Structures to Wave Induced Loads," Lecture at University of Houston, Houston, Texas, 1979.
47. Sarpkaya, T. and Isaacson, M., Mechanics of Wave Forces on Offshore Structures, Van Nostrand Reinhold Publication, New York, 1981.
48. Smith, E. A. L., "Pile-Driving Analysis by the Wave Equation," Transactions, ASCE, Vol. 127, 1964, Part I, p. 1154.
49. Stokes, G. G., "On the Theory of Oscillatory Waves," Transactions Camb. Phil. Soc. 8, pp. 441, 455, 1847.
50. Tickell, R. G., and Holmes, P., "Approaches to Fluid Loading, Probabilistic and Deterministic Analysis," Numerical Methods in Offshore Engineering, Edited by O. C. Zienkiewicz, R. W. Lewis, and K. G. Stagg. John Wiley and Sons, New York, 1979.
51. U.S. Army Coastal Engineering Research Center, Offshore Protection Manual, Dept. of the Army Corps of Engineers, Fort Belvoir, Va., 1977.
52. Wichers, J. E. W., "On the Low-Frequency Surge Motion of Vessels Moored in High Seas," Proceedings of the Offshore Technology Conference, OTC Paper 4437, 1982.

APPENDIX A: DERIVATION OF WAVE FORCES

The following is a detailed derivation of the wave forces on the tension-leg platform based on Morison's equation. It is assumed that the total wave force on the structure is equal to the sum of forces on each individual member. Since Morison's equation is applicable only to cylindrical members, the hulls of the TLP (that have rectangular cross-sections) are treated as cylinders with equivalent hydrodynamic characteristics.

Horizontal Forces

Inertia Force on Columns

The integration of the inertia force acting on element dz of column i (Equation 37) yields:

$$F_{I_i} = \frac{\rho\pi D_i^2}{4} \int_0^{h_i} [C_m \dot{u}_i - (C_m - 1) \{ \ddot{x} - (z - \bar{z})\ddot{\alpha} + \frac{x_i \ddot{\alpha}^2}{2} \}] dz . \quad (A-1)$$

Substituting from Equation (17) and rearranging terms gives:

$$F_{I_i} = \frac{\rho\pi D_i^2}{4} \{ [C_m \frac{2\pi^2 H}{T^2} \sin [k(\bar{X} - ct)] \int_0^{h_i} e^{-kz} dz] - [(C_m - 1) \int_0^{h_i} [\ddot{x} - (z - \bar{z})\ddot{\alpha} + \frac{x_i \ddot{\alpha}^2}{2}] dz] \} , \quad \dots (A-2)$$

which can be simplified by integrating and lumping coefficients as follows:

$$F_{I_i} = a_1 D_i^2 (1 - e^{-kh_i}) \sin [k(\bar{x} - ct)] - a_2 D_i^2 (\ddot{x} + \bar{z} \ddot{\alpha} + \frac{x_i \ddot{\alpha}^2}{2} - \frac{h_i \ddot{\alpha}}{2}) h_i ,$$

(A-3)

where

$$a_1 = \frac{\rho \pi^3 C_m H}{2kT^2} , \quad a_2 = \frac{\rho \pi (C_m - 1)}{4} , \quad \text{and } \bar{x} = x + x_i$$

Where x is the instantaneous position of the center of gravity of the structure taken in the direction of the wave, and x_i is the x -coordinate of each of the eight columns in the direction of the wave and calculated as follows:

$$X_5 = b \sin \alpha - a \cos \alpha,$$

$$X_6 = a \cos \alpha + b \sin \alpha,$$

$$X_7 = -X_6,$$

$$X_8 = -X_5,$$

$$X_9 = b \sin \alpha,$$

$$X_{10} = -X_9,$$

$$X_{11} = -a \cos \alpha, \text{ and}$$

$$X_{12} = -X_{11}$$

with a and b equal to one-half the distance between the corner columns in the x and y directions, respectively, and α is the angle of wave direction measured from the x -axis (see Figure A1).

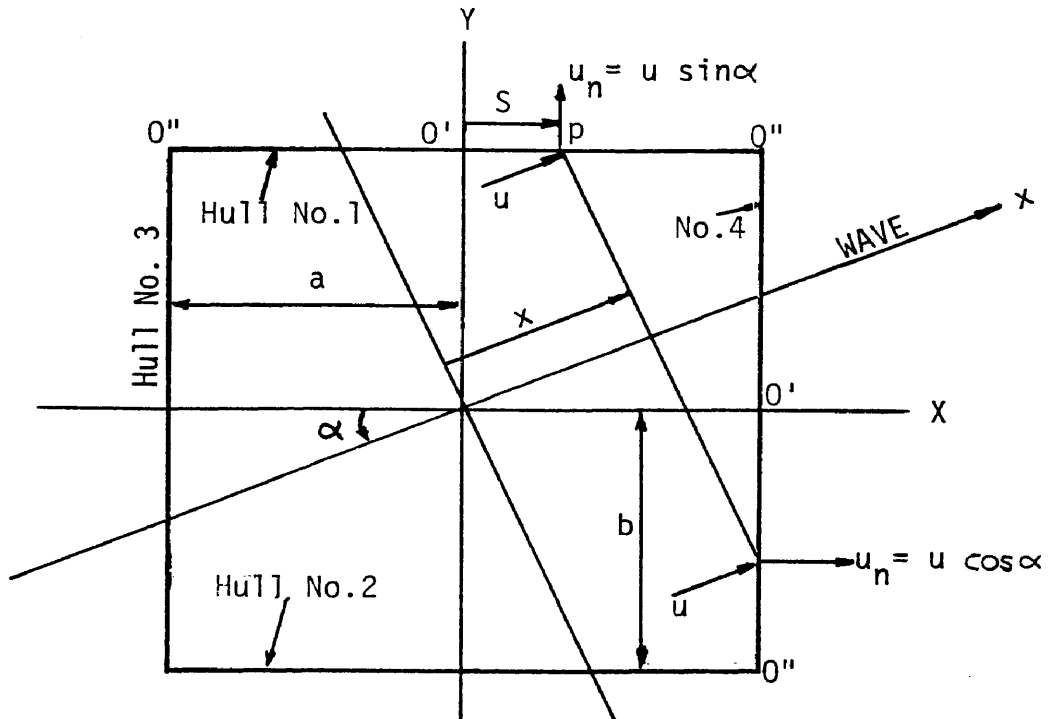


Fig. A1 - Plan View of Hull Locations

Drag Force on Columns

Equation (32) can be rewritten as

$$\delta F_d = (\bar{\tau}) \frac{\rho C_d D}{2} (u_{rel})^2 dz \quad (A-4)$$

where the $(\bar{\tau})$ sign depends on the sign of the relative fluid velocity,

u_{rel} .

Substituting u_{rel} (Equation 34) into Equation (A-4), and integrating over the length of each cylinder gives:

$$F_{d_i} = (\bar{\tau}) \frac{\rho C_d D_i}{2} \int_0^{h_i} \left\{ \frac{\pi H}{T} e^{-kz} \cos [k(\bar{X} - ct)] \right. \\ \left. - [\dot{\bar{x}} - (z - \bar{z}) \dot{\alpha} + \frac{X_i \dot{\alpha}^2}{2}]^2 dz \right.$$

Resolving the square and separating the z-terms gives:

$$F_{d_i} = (\bar{\tau}) \frac{\rho C_d D_i}{2} \left\{ \left[\frac{\pi^2 H^2}{T^2} \cos^2 [k(\bar{X} - ct)] \int_0^{h_i} e^{-2kz} dz \right] - \right. \\ \left. 2 \int_0^{h_i} \frac{\pi H}{T} \cos [k(\bar{X} - ct)] \left[(\dot{x} + \bar{z} \dot{\alpha} + \frac{X_i \dot{\alpha}^2}{2} - z\dot{\alpha}) [e^{-kz}] dz \right] \right. \\ \left. + \int_0^{h_i} \left[(\dot{x} + \bar{z} \dot{\alpha} + \frac{X_i \dot{\alpha}^2}{2})^2 - 2(\dot{x} + \bar{z} \dot{\alpha} + \frac{X_i \dot{\alpha}^2}{2})z\dot{\alpha} + z^2 \dot{\alpha}^2 \right] dz \right\},$$

which gives,

$$F_{d_i} = (\bar{\tau}) \frac{\rho C_d D_i}{2} \left\{ \left[\frac{\pi^2 H^2}{T^2} \cos^2 [k(\bar{X} - ct)] \frac{1}{2k} (1 - e^{-2kh_i}) \right] \right. \\ \left. - 2 \left[\frac{\pi H}{T} \cos [k(\bar{X} - ct)] \left(\dot{x} + z\dot{\alpha} + \frac{X_i \dot{\alpha}^2}{2} \right) (1 - e^{-kh_i}) \left(\frac{1}{k} \right) \right. \right. \\ \left. - \frac{\dot{\alpha} \pi H}{kT} \left(\frac{1}{k} - \frac{e^{-kh_i}}{k} \right) \cos [k(\bar{X} - ct)] \right] + \left[(\dot{x} + \bar{z} \dot{\alpha} + \frac{X_i \dot{\alpha}^2}{2})^2 h_i \right. \\ \left. - (\dot{x} + \bar{z} \dot{\alpha} + \frac{X_i \dot{\alpha}^2}{2}) h_i^2 \dot{\alpha} + \frac{\dot{\alpha}^2 h_i^3}{3} \right] \left. \right\} .$$

By lumping parameters and rearranging terms one obtains:

$$F_{d_i} = (\bar{\tau}) \left\{ b_1 D_i \cos^2 [k(\bar{X} - ct)] (1 - e^{-2kh_i}) - b_2 b_3 D_i (1 - e^{-kh_i}) \right. \\ \left. \cos [k(\bar{X} - ct)] + D_i b_3 \dot{\alpha} \frac{1}{k} (1 - e^{-kh_i}) \cos [k(x - ct)] - b_3 \dot{\alpha} h_i D_i \right. \\ \left. e^{-kh_i} \cos [k(\bar{X} - ct)] + b_2^2 b_0 D_i h_i - b_2 b_0 \dot{\alpha} h_i^2 + \frac{b_0 \dot{\alpha} D_i h_i^3}{3} \right\} ,$$

and a collection of terms that contains: $\cos [k(X - ct) (1 - e^{-kh}) D_i]$

yields:

$$\begin{aligned}
 F_{d_i} = & (\bar{\gamma}) \{ \cos [k(\bar{X} - ct)] (1 - e^{-2kh_i}) D_i [b_1 \cos [k(\bar{X} - ct)] (1 + e^{-kh_i}) \\
 & - b_{2_i} b_3 + \frac{b_3 \dot{\alpha}}{k}] - b_3 \dot{\alpha} h_i D_i e^{-kh_i} \cos [k(\bar{X} - ct)] + b_{2_i}^2 b_0 D_i h_i \\
 & - b_{2_i} b_0 \dot{\alpha} h_i^2 + \frac{1}{3} b_0 \dot{\alpha} D_i h_i^3 \} \quad , \quad (A-5)
 \end{aligned}$$

where

$$b_0 = 1/2 \rho C_d \quad ,$$

$$b_1 = \frac{\pi^2 H^2}{2kT^2} b_0 \quad ,$$

$$b_{2_i} = (\dot{x} + \bar{z} \dot{\alpha} + \frac{X_i \dot{\alpha}^2}{2}) \quad , \text{ and}$$

$$b_3 = \frac{2\pi H}{kT} b_0$$

Inertia Forces on Hulls and Cross Bracings

For hull No. 1 in Figure A1 the normal component of the fluid acceleration at point p, distance S from O_1 , for the section $O_1 O_2$ is:

$$\dot{u}_n = \dot{u} \sin \alpha = \frac{2\pi^2 H}{T^2} e^{-k\bar{h}} \sin [k(\bar{x} - ct)] \sin \alpha$$

and a substitution for \bar{x} in terms of S yields:

$$\bar{x} = \beta' S + \gamma' \quad ,$$

where $\beta' = \cos \alpha$, and $\gamma' = b \sin \alpha$.

Since S is a positive quantity, the value of X for O_1O_3 becomes:

$$\bar{x} = -\beta'S + \gamma' .$$

For hull No. 1, the inertia force in the y -direction is:

$$\begin{aligned} F_{1y} &= \int_{-a}^{a'} \frac{\rho\pi D^2}{4} C_m \left(\frac{2\pi^2 H}{T^2} e^{-kh} \sin [k(\bar{x} - ct)] \right) \sin \alpha d\bar{x} \\ &= a_y \int_0^{a'} \sin [k(-\beta'S + \gamma' - ct)] dS + a_y \int_0^{a'} \\ &\quad \sin [k(\beta'S + \gamma' - ct)] dS , \end{aligned}$$

where $a_y = \frac{\rho\pi^3 D_1^2 H}{2T^2} e^{-k\bar{h}} C_m \sin \alpha$, thus:

$$\begin{aligned} F_{1y} &= \frac{1}{k\beta'} a_y \{ \cos [-k\beta'S + k(\gamma' - ct)] \Big|_0^{a'} - \cos [k\beta'S + k(\gamma' - ct)] \Big|_0^{a'} \\ &= \frac{a_y}{k\beta'} \{ [\cos [-k\beta'a' + k(\gamma' - ct)] - \cos [k(\gamma' - ct)]] \\ &\quad + [-\cos [k\beta'a' + k(\gamma' - ct)] + \cos [k(\gamma' - ct)]] \} . \end{aligned}$$

Using the trigonometric identity: $\cos(a-b) - \cos(a+b) = 2 \sin(a) \cos(b)$, one obtains:

$$F_{1y} = \frac{2a_y}{k\beta'} \sin(k\beta'a') \sin[k(\gamma' - ct)] . \quad (A-6)$$

Similarly, for hull No. 2

$$F_{2y} = \frac{-2a_y}{k\beta} \sin(k\beta'a') \sin[k(\gamma' + ct)] . \quad (A-7)$$

Combining F_{1y} and F_{2y} , the total horizontal inertia force on the hulls becomes:

$$F_y = \frac{-4a_y}{k\beta''} \sin(k\beta'a') \cos(k\gamma') \sin(kct) . \quad (A-8)$$

Similarly, for the cross bracings (hulls No. 3 and No. 4), one can write:

$$\dot{u}_n = \dot{u} \cos \alpha , \quad X = \gamma'' - \beta''s , \quad \gamma'' = a \cos \alpha , \quad \text{and} \quad \beta'' = \sin \alpha .$$

Integrating in the x-direction yields:

$$F_x = \frac{-4a_x}{k\beta''} \sin(k\beta''b') \cos(k\gamma'') \sin(kct) , \quad (A-9)$$

where
$$a_x = \frac{\rho\pi^3 C_m d_3^2 H}{2T^2} e^{-k\bar{h}} \cos \alpha .$$

Drag Forces on Hulls and Cross Bracings

The derivation of the drag forces on hulls and cross bracings is similar to that of inertia forces. For hull No. 1, the drag force in the y-direction gives:

$$\begin{aligned} \bar{F}_{1y} &= (\bar{\tau}) \frac{\rho C_d D_1}{2} \int_{-a'}^{a'} [u_n \sin \alpha]^2 dS \\ &= (\bar{\tau}) \frac{\rho C_d D_1}{2} \int_{-a'}^{a'} \left[\frac{\pi H}{T} e^{-k\bar{h}} \cos [k(\bar{x} - ct)] \sin \alpha \right]^2 dS \\ &= (\bar{\tau}) \frac{\rho C_d D_1}{2} \frac{\pi^2 H^2}{T^2} e^{-2k\bar{h}} \sin^2 \alpha \int_{-a'}^{a'} \cos^2 [k(\bar{x} - ct)] dS . \end{aligned}$$

Using the trigonometric identity: $\cos^2 a = \frac{1}{2} (\cos 2a + 1)$, one obtains:

$$\begin{aligned}
 \bar{F}_{1y} &= c_1 \int_{-a'}^{a'} (\cos [2k(\bar{x} - ct)] + 1) dS \\
 &= c_1 \left\{ \int_0^{a'} (\cos [2k(\beta'S + \gamma' - ct)] + 1) dS \right. \\
 &\quad \left. + \int_{-a'}^0 (\cos [2k(-\beta'S + \gamma' - ct)] + 1) dS \right\} \\
 &= \frac{c_1}{2k\beta'} [\sin [2k\beta'S + 2k(\gamma' - ct)] + S \\
 &\quad - \sin [-2k\beta'S + 2k(\gamma' - ct)] + S] \Big|_0^{a'} \\
 &= \frac{c_1}{2k\beta'} [\{\sin[2k\beta'a' + 2k(\gamma' - ct)] - \sin [2k(\gamma' - ct)]\} \\
 &\quad - \{\sin [-2k\beta'a' + 2k(\gamma' - ct)] - \sin [2k(\gamma' - ct)]\} + 2a'] \\
 &= \frac{c_1}{2k\beta'} [\sin[2k\beta'a' + 2k(\gamma' - ct)] \\
 &\quad - \sin [-2k\beta'a' + 2k(\gamma' - ct)] + 2a'], \text{ therefore} \\
 \bar{F}_{1y} &= \frac{c_1}{k\beta'} \sin (2k\beta'a') \cos [2k(\gamma' - ct)] + 2c_1 a' , \tag{A-10}
 \end{aligned}$$

where $c_1 = (\bar{\tau}) \frac{\rho C_d D_1}{4} \frac{\pi^2 H^2}{T^2} e^{-2k\bar{h}} \sin^2 \alpha$.

Similarly, for hull No. 2, one can write:

$$\bar{F}_{2y} = \frac{c_1}{k\beta} \sin (2k\beta'a') \cos [2k(\gamma' + ct)] + 2c_1 a' . \tag{A-11}$$

Combining \bar{F}_{1y} and \bar{F}_{2y} gives the total horizontal drag force on the hulls in the y-direction as:

$$\bar{F}_y = \frac{2c_1}{k\beta'} \sin(2k\beta'a') \cos(2k\gamma') \cos(2kct) + 4c_1a' . \quad (\text{A-12})$$

Similarly, for the cross bracings (hulls No. 3 and No. 4), one can write:

$$u_n = u \cos \alpha, \quad \bar{x} = \beta'' - \beta''S, \quad \gamma'' = a \cos \alpha, \quad \text{and} \quad \beta'' = \sin \alpha.$$

Through integration in the x-direction one obtains:

$$\bar{F}_x = \frac{2c_2}{k\beta''} \sin(2k\beta''b') \cos(2k\gamma'') \cos(2kct) + 4c_2b' , \quad (\text{A-13})$$

$$\text{where} \quad c_2 = \bar{\tau} \frac{\rho\pi^2 H^2 C_d D_3}{4T^2} e^{-2k\bar{h}} \cos^2 \alpha .$$

In summary, the total horizontal forces on the structure are:

For surge (x-direction):

$$F_{xT} = \sum_{i=5}^{12} (F_{I_i} + F_{D_i}) \cos \alpha + (F_x + \bar{F}_x) . \quad (\text{A-14})$$

For sway (y-direction):

$$F_{yT} = \sum_{i=5}^{12} (F_{I_i} + F_{D_i}) \sin \alpha + (F_y + \bar{F}_y) , \quad (\text{A-15})$$

where the corner columns are numbered 5-8, and the middle columns are numbered 9-12. The instantaneous heights of the water on each column are:

for $i = 5-8$:

$$h_i = h_0 + \frac{H}{2} \cos [k(\bar{X} - ct)] + (\ell - \sqrt{\ell^2 - x^2}) , \quad (\text{A-16})$$

and for $i = 9-12$

$$h_i = h_0 + \frac{H}{2} \cos [k(\bar{X} - ct)] + (\ell - \sqrt{\ell^2 - x^2}) - D_h . \quad (\text{A-17})$$

Heave Forces

Vertical Inertia Force on Hulls

The vertical fluid acceleration at point p of Figure A1 is

$$\dot{v} = \frac{-2\pi^2 H}{T^2} e^{-k\bar{h}} \cos [k(\bar{X} - ct)] \quad (\text{A-18})$$

For hull No. 1: $X = \beta'S + \gamma'$ for $0_1 0_2$, and $X = -\beta'S + \gamma'$ for $0_1 0_3$.

The vertical inertia force on hull No. 1 due to fluid acceleration is

$$\begin{aligned} F_{V_1} &= \int_{-a'}^{a'} \frac{\rho\pi D_1^2}{4} C_m \left\{ \frac{-2\pi^2 H}{T^2} e^{-k\bar{h}} \cos [k(\bar{X} - ct)] \right\} dS \\ &= \frac{-\rho\pi^3 D_1^2 C_m H}{2T^2} e^{-k\bar{h}} \int_{-a'}^{a'} \cos [k(\bar{X} - ct)] dS \\ &= \frac{-a_{V_1}}{2} \left\{ \int_0^{a'} \cos [-k\beta'S + k(\gamma' - ct)] dS \right. \\ &\quad \left. + \int_0^{a'} \cos [k\beta'S + k(\gamma' - ct)] dS \right\} \\ &= \frac{-a_{V_1}}{2k\beta'} \left\{ [-\sin [-k\beta'S + k(\gamma' - ct)]]_0^{a'} + [\sin [k\beta'S + k(\gamma' - ct)]]_0^{a'} \right\} \end{aligned}$$

$$\begin{aligned}
F_{v_1} &= \frac{-a_{v_1}}{2k\beta^1} \{ [-\sin[-k\beta^1 a' + k(\gamma' - ct)] + \sin [k(\gamma' - ct)]] \\
&\quad + [\sin [k\beta^1 a' + k(\gamma' - ct)] - \sin [k(\gamma' - ct)]] \} \\
&= \frac{-a_{v_1}}{2k\beta^1} \{ \sin [k\beta^1 a' + k(\gamma' - ct)] - \sin [-k\beta^1 a' + k(\gamma' - ct)] \} ,
\end{aligned}$$

therefore

$$F_{v_1} = \frac{-a_{v_1}}{k\beta^1} \sin (k\beta^1 a') \cos [k(\gamma' - ct)] . \quad (A-19)$$

Similarly, for hull No. 2,

$$F_{v_2} = \frac{-a_{v_2}}{k\beta^1} \sin (k\beta^1 a') \cos [k(\gamma' + ct)] , \quad (A-20)$$

and for hulls No. 3 and 4:

$$F_{v_3} = \frac{-a_{v_2}}{k\beta^{11}} \sin (k\beta^{11} b') \cos [k(\gamma'' + ct)] , \text{ and} \quad (A-21)$$

$$F_{v_4} = \frac{-a_{v_2}}{k\beta^{11}} \sin (k\beta^{11} b') \cos [k(\gamma'' - ct)] , \quad (A-22)$$

where
$$a_{v_1} = \frac{\rho\pi^3 D_1^2 C_m H}{T^2} e^{-k\bar{h}}$$

and
$$a_{v_2} = \frac{\rho\pi^3 D_3^2 C_m H}{T^2} e^{-k\bar{h}}$$

Adding Equations (A-19) and (A-20) yields:

$$\begin{aligned}
 F_{v_{1,2}} &= \frac{-a_{v1}}{k\beta'} \sin(k\beta'a') [\cos[k\gamma' - kct] + \cos[k\gamma' + kct]] \\
 &= \frac{-2a_{v1}}{k\beta'} \sin(k\beta'a') \cos(k\gamma') \cos(kct) .
 \end{aligned} \tag{A-23}$$

Adding Equations (A-21) and (A-22) gives:

$$F_{v_{3,4}} = \frac{-2a_{v2}}{k\beta''} \sin(k\beta''b') \cos(k\gamma'') \cos(kct) . \tag{A-24}$$

The total vertical inertia forces on the hulls is obtained by adding Equations (A-23) and (A-24):

$$\begin{aligned}
 F_v &= F_{v_{1,2}} + F_{v_{3,4}} \\
 &= \frac{-2 \cos(kct)}{k} \left[\frac{a_{v1}}{\beta'} \sin(k\beta'a') \cos(k\gamma') \right. \\
 &\quad \left. + \frac{a_{v2}}{\beta''} \sin(k\beta''b') \cos(k\gamma'') \right] \dots \tag{A-25}
 \end{aligned}$$

Vertical Drag Force on Hulls

The vertical fluid velocity at point p of Figure A1 is

$$v = \frac{\pi H}{T} e^{-k\bar{h}} \sin[k(x - ct)] . \tag{A-26}$$

The vertical drag force on hull No. 1 due to fluid velocity is

$$\begin{aligned}
 \bar{F}_{v_1} &= (\pm) \int_{-a'}^{a'} \frac{\rho C_d D_1}{2} \left\{ \frac{\pi H}{T} e^{-k\bar{h}} \sin[k(\bar{x} - ct)] \right\}^2 dS \\
 &= (\pm) \frac{\rho C_d D_1 \pi^2 H^2}{4T^2} e^{-2k\bar{h}} \int_{-a'}^{a'} \{1 - \cos[2k(\bar{x} - ct)]\} dS
 \end{aligned}$$

$$\begin{aligned}
\bar{F}_{v_1} &= (\pm) \frac{\rho C_d D_1 \pi^2 H^2}{2T^2} e^{-2k\bar{h}} \int_{-a'}^{a'} \sin^2 [k(\bar{x} - ct)] dS \\
&= c_3 \left\{ \int_0^{a'} \{1 - \cos [2k\beta'S + 2k(\gamma' - ct)]\} dS \right. \\
&\quad \left. + \int_0^{a'} \{1 - \cos [-2k\beta'S + k(\gamma' - ct)]\} dS \right. \\
&= c_3 \left\{ \left[S - \frac{1}{2k\beta'} \sin [2k\beta'S + 2k(\gamma' - ct)] \right]_0^{a'} \right. \\
&\quad \left. + \left[S + \frac{1}{2k\beta'} \sin [-2k\beta'S + 2k(\gamma' - ct)] \right]_0^{a'} \right\} \\
&= 2 c_3 a' + \frac{c_3}{2k\beta'} \{ \sin [-2k\beta'a' + 2k(\gamma' - ct)] \\
&\quad - \sin [2k\beta'S + 2k(\gamma' - ct)] \}
\end{aligned}$$

$$\bar{F}_{v_1} = 2 c_3 a' - \frac{c_3}{k\beta'} \sin (2k\beta'a') \cos [2k(\gamma' - ct)]. \quad (A-27)$$

Similarly, for hull No. 2:

$$\bar{F}_{v_2} = 2 c_3 a' - \frac{c_3}{k\beta'} \sin (2k\beta'a') \cos [2k(\gamma' + ct)], \quad (A-28)$$

and for hulls No. 3 and 4:

$$\bar{F}_{v_3} = 2c_4 b' - \frac{c_4}{k\beta''} \sin (2k\beta''b') \cos [2k(\gamma'' + ct)], \text{ and} \quad (A-29)$$

$$\bar{F}_{v_4} = 2 c_4 b' - \frac{c_4}{k\beta''} \sin (2k\beta''b') \cos [2k(\gamma'' - ct)] \quad (A-30)$$

where $c_3 = (\bar{\tau}) \frac{c_1}{\sin^2 \alpha}$,

and $c_4 = (\bar{\tau}) \frac{c_2}{\cos^2 \alpha}$.

Adding Equations (A-27), (A-28), (A-29), and (A-30) results in the total vertical drag force on the hulls:

$$\begin{aligned} \bar{F}_v &= \bar{F}_{v_1} + \bar{F}_{v_2} + \bar{F}_{v_3} + \bar{F}_{v_4} \\ &= 4 (c_3 a' + c_4 b') - \frac{2}{k} \cos (2kct) \left[\frac{c_3}{\beta'} \sin (2k\beta' a') \cos (2k\gamma') \right. \\ &\quad \left. + \frac{c_4}{\beta''} \sin (2k\beta'' b') \cos (2k\gamma'') \right] . \end{aligned} \quad \dots (A-31)$$

Dynamic Pressure on Corner Column Bases

The dynamic pressure in the fluid is given by:

$$p_i = \frac{\rho g H}{2} e^{-kh_i} \cos [k(\bar{X} - ct)] . \quad (A-32)$$

The total dynamic pressure on all corner columns is

$$F_{cv} = \sum_{i=5}^8 p_i \left(\frac{\pi D_i^2}{4} \right) = \frac{\pi \rho g H}{8} \sum_{i=5}^8 d_i^2 e^{-kh_i} \cos [k(\bar{X} - ct)] . \quad (A-33)$$

The total vertical force on the structure becomes:

$$F_{z_T} = F_v + \bar{F}_v + F_{cv} . \quad (A-34)$$

Forces Producing Pitch and Roll

Moments Due to Inertia Force on Columns

In this analysis, it is assumed that pitch and roll take place about horizontal axes passing through the center of gravity of the structure. The moment about G of the inertia force on column i is (see Fig. 14):

$$\begin{aligned} M_{I_i} &= \frac{-\rho\pi D_i^2}{4} \int_0^{h_i} (z - \bar{z}) [C_m \dot{u}_i - (C_m - 1) [\ddot{x} - (z - \bar{z})\ddot{\alpha} + x_i \ddot{\alpha}^2]] dz \\ &= \bar{z} F_{I_i} - \frac{\rho\pi D_i^2}{4} \left\{ \frac{2c_m \pi^2 H}{T^2} \sin [k(\bar{X} - ct)] \int_0^{h_i} z e^{-kz} dz \right. \\ &\quad \left. - (C_m - 1) \int_0^{h_i} z \left[(\ddot{x} + z\ddot{\alpha} + \frac{x_i \ddot{\alpha}^2}{2}) - z\ddot{\alpha} \right] dz \right\}, \text{ which yields:} \end{aligned}$$

$$\begin{aligned} M_{I_i} &= \bar{z} F_{I_i} - a_1 D_i^2 \left(\frac{1}{k} - e^{-kh_i} - h_i e^{-kh_i} \right) \sin [k(\bar{X} - ct)] \\ &\quad + a_2 D_i \left[(\ddot{x} + z\ddot{\alpha} + \frac{x_i \ddot{\alpha}^2}{2}) \frac{h_i^2}{2} - \frac{h_i^3 \ddot{\alpha}}{3} \right]. \end{aligned} \quad (A-35)$$

Moments Due to Drag Force on Columns

The moment about G of the drag force on column i is (see Fig. 14):

$$\begin{aligned} M_{D_i} &= (\bar{r}) \frac{-\rho c_d D_i}{2} \int_0^{h_i} (z - \bar{z}) \left\{ u_i - \left[\dot{x} - (z - \bar{z})\dot{\alpha} + \frac{x_i \dot{\alpha}^2}{2} \right] \right\}^2 dz \\ &= (\bar{r}) \frac{-\rho c_d D_i}{2} \left\{ \left[\int_0^{h_i} z \left\{ \frac{\pi^2 H^2}{T^2} e^{-2kz} \cos^2 [k(\bar{X} - ct)] \right\} dz \right] \right. \\ &\quad \left. + \left[\int_0^{h_i} -2z \left[(\dot{x} + \bar{z}\dot{\alpha} + \frac{x_i \dot{\alpha}^2}{2}) - z\dot{\alpha} \right] \left(\frac{\pi H}{T} e^{-kz} \cos [k(\bar{X} - ct)] \right) dz \right] \right\} \end{aligned}$$

$$M_{D_i} = + \left[\int_0^{h_i} z \left[(\dot{x} + \bar{z}\dot{\alpha} + \frac{x_i \dot{\alpha}^2}{2}) - z\dot{\alpha} \right]^2 dz \right] + \bar{z} F_{D_i} .$$

Due to its complication, the above equation is divided into three parts as:

$$M_{D_i} = (\bar{z}) - \rho C_d D_i \{ [1] + [2] + [3] \} + \bar{z} F_{D_i} .$$

Evaluating [1], [2], and [3] separately gives:

$$\begin{aligned} [1] &= \int_0^{h_i} \frac{\pi^2 H^2}{T^2} \cos^2 [k(\bar{X} - ct)] z e^{-2kz} dz \\ &= \frac{\pi^2 H^2}{2kT^2} \cos^2 [k(\bar{X} - ct)] \left(\frac{1}{2k} - \frac{e^{-2kh_i}}{2k} - h_i e^{-2kh_i} \right) , \\ [2] &= \int_0^{h_i} -2z \left\{ \left[(\dot{x} + \bar{z}\dot{\alpha} + \frac{x_i \dot{\alpha}^2}{2}) - z\dot{\alpha} \right] \left(\frac{\pi H}{T} e^{-kz} \cos [k(\bar{X} - ct)] \right) \right\} dz \\ &= \frac{-2\pi H}{T} \cos [k(\bar{X} - ct)] \left\{ (\dot{x} + z\dot{\alpha} + \frac{x_i \dot{\alpha}^2}{2}) \int_0^{h_i} z e^{-kz} dz \right. \\ &\quad \left. - \dot{\alpha} \int_0^{h_i} z^2 e^{-kz} dz \right\} \\ &= \frac{-2\pi H}{T} \cos [k(\bar{X} - ct)] \left\{ b_{2_i} \left(\frac{1}{k} \right) \left(\frac{1}{k} - \frac{e^{-kh_i}}{k} - h_i e^{-kh_i} \right) \right. \\ &\quad \left. + h_i^2 e^{-kh_i} - \frac{2}{k} \left(\frac{1}{k} - \frac{e^{-kh_i}}{k} h_i e^{-kh_i} \right) \right\} \\ &= \frac{2\pi H}{kT} \cos [k(\bar{X} - ct)] \left\{ \left(\frac{2\dot{\alpha}}{k} - b_{2_i} \right) \left(\frac{1}{k} - \frac{e^{-kh_i}}{k} h_i e^{-kh_i} \right) - \dot{\alpha} h_i^2 e^{-kh_i} \right\} , \end{aligned}$$

and

$$\begin{aligned}
[3] &= \int_0^{h_i} \left[(\dot{x} + \bar{z}\dot{\alpha} + \frac{x_i \dot{\alpha}^2}{2})^2 z dz - \int_0^{h_i} 2(\dot{x} + \bar{z}\dot{\alpha} + \frac{x_i \dot{\alpha}^2}{2}) \dot{\alpha} z^2 dz \right. \\
&\quad \left. + \int_0^{h_i} \dot{\alpha}^2 z^3 dz \right] \\
&= (b_{2_i})^2 \frac{h_i^2}{2} - 2 b_{2_i} \dot{\alpha} \frac{h_i^3}{3} + \dot{\alpha} \frac{h_i^4}{4} .
\end{aligned}$$

Therefore, the moment of the drag force on column i about G becomes:

$$\begin{aligned}
M_{D_i} &= (\bar{z}) - D_i \{ b_1 \cos^2 [k(\bar{X} - ct)] \left(\frac{1}{2k} - \frac{e^{-2kh_i}}{2k} - h_i e^{-2kh_i} \right) \right. \\
&\quad \left. + b_3 \cos [k(\bar{X} - ct)] \left[\left(\frac{2\dot{\alpha}}{k} - b_{2_i} \right) \left(\frac{1}{k} - \frac{e^{-kh_i}}{k} - h_i e^{-kh_i} \right) - \dot{\alpha} h_i e^{-kh_i} \right] \right. \\
&\quad \left. + (b_{2_i})^2 \frac{h_i^2}{2} - 2 b_{2_i} \dot{\alpha} \frac{h_i^3}{3} + \frac{\dot{\alpha} h_i^4}{3} \right\} + \bar{z} F_{D_i} . \tag{A-36}
\end{aligned}$$

A positive rotational moment about the Y -axis produces a positive y -component (pitch), and a negative x -component (roll), see Figure A2.

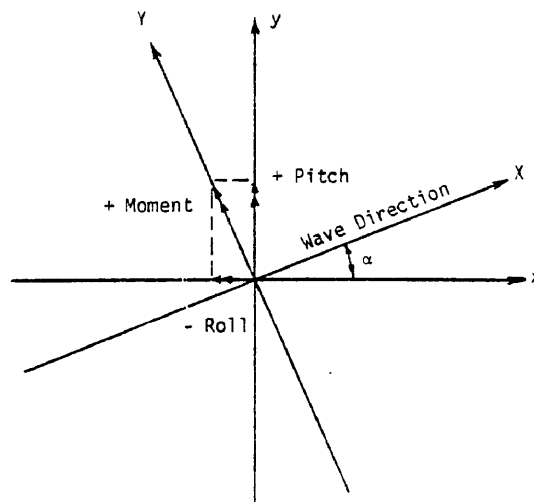


Fig. A2 - Pitch and Roll Components of Rotation

Hence, from Equations (A-35) and (A-36), one can write:

$$M_y = \sum_{i=5}^{12} (M_{D_i} + M_{I_i}) \cos \alpha, \text{ and} \quad (\text{A-37})$$

$$M_x = - \sum_{i=5}^{12} (M_{D_i} + M_{I_i}) \sin \alpha \quad (\text{A-38})$$

Pitch Moment from Horizontal Inertia and Drag Forces on Hulls

As shown in Figure A3, only hulls No. 3 and 4 have pitching effects, thus the pitch moment arising from horizontal inertia and drag forces on these hulls is:

$$M_{3,4}{}_{y_h} = - (F_x + \bar{F}_x) \left(\bar{h} - \frac{D_3}{2} \right), \quad (\text{A-39})$$

where F_x and \bar{F}_x are given in Equations (A-9) and (A-13), respectively.

Roll Moment from Horizontal Inertia and Drag Forces on Hulls

As shown in Figure A3, only hulls No. 1 and 2 have rolling effects:

$$M_{1,2}{}_{x_h} = (F_y + \bar{F}_y) \left(\bar{h} - \frac{D_1}{2} \right), \quad (\text{A-40})$$

where F_y and \bar{F}_y are given in Equations (A-8) and (A-12), respectively.

Pitch Moment from Vertical Inertia Forces on Hulls

The pitching moment caused by forces on hulls No. 3 and 4 has a constant moment arm, a : (See Figure A4)

$$M_{3,4}{}_{y} = [(F_{v_3} + \bar{F}_{v_3}) - (F_{v_4} + \bar{F}_{v_4})]a, \quad (\text{A-41})$$

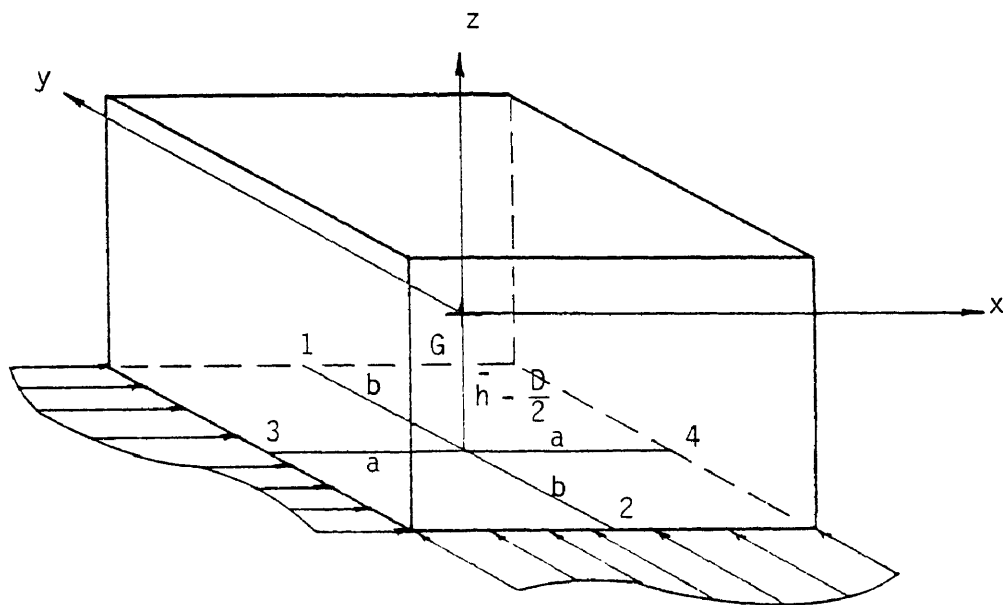


Fig. A3 - Horizontal Forces on Hulls

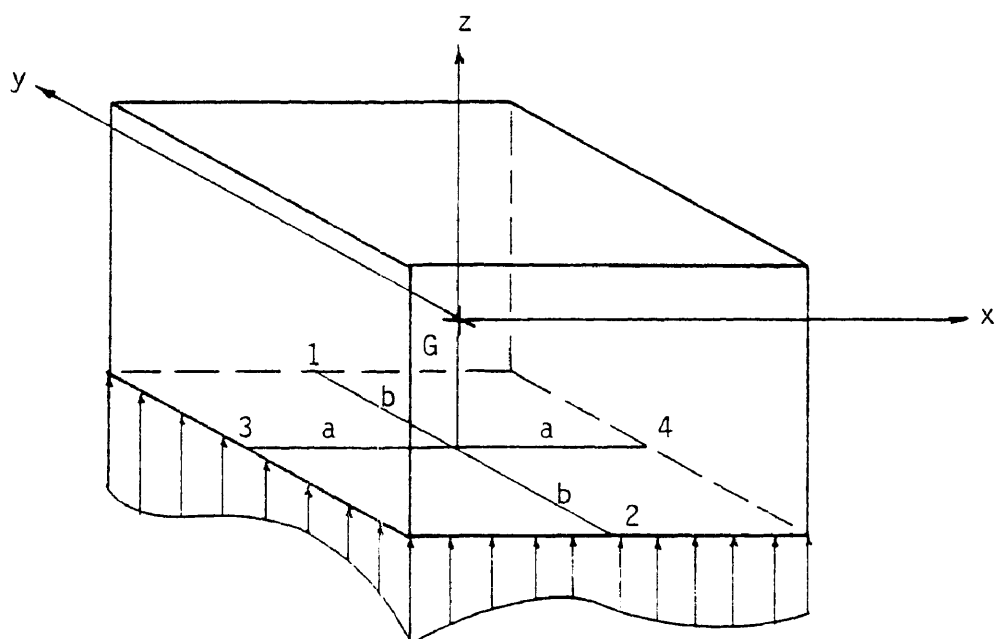


Fig. A4 - Vertical Forces on Hulls

where F_{v_3} , \bar{F}_{v_3} , F_{v_4} , \bar{F}_{v_4} are as given in Equations (A-21), (A-29), (A-22), and (A-30), respectively.

The pitching moments arising from vertical forces on hulls No. 1 and 2 have a variable moment arm S . Therefore, for hull No. 1, the moment about the y -axis of the vertical inertia force is

$$\begin{aligned}
 M_{1y} &= \int_{-a'}^{a'} \frac{\rho \pi D_1^2}{4} c_m \left(\frac{-2\pi^2 H}{T} e^{-k\bar{h}} \cos [k(\bar{x} - ct)] \right) S \, dS \\
 &= \left(\frac{\rho \pi D_1^2}{4} c_m \right) \left(\frac{-2\pi^2 H}{T} e^{-k\bar{h}} \right) \left\{ + \int_0^{a'} S \cos [-k\beta'S + k(\gamma' - ct)] \, dS \right. \\
 &\quad \left. - \int_0^{a'} S \cos [k\beta'S + k(\gamma' - ct)] \, dS \right\} \\
 &= \frac{a_{v1}}{2k\beta'} \left\{ [S \sin [k\beta'S + k(\gamma' - ct)] + \frac{1}{k\beta'} \cos [k\beta'S + k(\gamma' - ct)]]_0^{a'} \right. \\
 &\quad \left. - [-S \sin [-k\beta'S + k(\gamma' - ct)] + \frac{1}{k\beta'} \cos [-k\beta'S + k(\gamma' - ct)]]_0^{a'} \right\} \\
 &= \frac{a_{v1}}{2k\beta'} \left\{ [a' \sin [k\beta'a' + k(\gamma' - ct)] + \frac{1}{k\beta'} \cos [k\beta'a' + k(\gamma' - ct)]] \right. \\
 &\quad \left. - \frac{1}{k\beta'} \cos [k(\gamma' - ct)] \right\} - \left\{ [-a' \sin [-k\beta'a' + k(\gamma' - ct)]] \right. \\
 &\quad \left. + \frac{1}{k\beta'} \cos [-k\beta'a' + k(\gamma' - ct)] - \frac{1}{k\beta'} \cos [k(\gamma' - ct)] \right\} \\
 &= \frac{a_{v1}}{k\beta'} \left\{ [a' \cos (k\beta'a') \sin [k(\gamma' - ct)]] \right. \\
 &\quad \left. - \frac{1}{k\beta'} [\sin (k\beta'a') \sin [k(\gamma' - ct)]] \right\},
 \end{aligned}$$

therefore

$$M_{1y} = \frac{-a_v v_1}{k\beta'} \sin [k(\gamma' - ct)] \left[\frac{\sin (k\beta'a')}{k\beta'} - a' \cos (k\beta'a') \right]. \quad (A-42)$$

Similarly, for hull No. 2:

$$M_{2y} = \frac{a_v v_1}{k\beta'} \sin [k(\gamma' + ct)] \left[\frac{\sin (k\beta'a')}{k\beta'} - a' \cos (k\beta'a') \right]. \quad (A-43)$$

Now, the moment about the y-axis of the vertical drag force for hull No. 1 is

$$\begin{aligned} \bar{M}_{1y} &= (\bar{\tau}) \int_{-a'}^{a'} \frac{\rho C_d D_1}{2} \left[\frac{\pi H}{T} e^{-k\bar{h}} \sin [k(\bar{x} - ct)] \right]^2 S dS \\ &= (\bar{\tau}) \frac{\pi C_d D_1}{2} \frac{\pi^2 H^2}{T^2} e^{-2k\bar{h}} \int_{-a'}^{a'} S \sin^2 [k(x - ct)] dS \\ &= c_3 \left\{ \int_0^{a'} S (1 - \cos [2k\beta'S + 2k(\gamma' - ct)]) dS \right. \\ &\quad \left. + \int_0^{a'} S (1 - \cos [-2k\beta'S + 2k(\gamma' - ct)]) dS \right\} \\ &= c_3 \left\{ \left[\frac{S}{2k\beta'} \sin [2k\beta'S + 2k(\gamma' - ct)] \right. \right. \\ &\quad \left. \left. + \frac{1}{(2k\beta')} \cos [2k\beta'S + 2k(\gamma' - ct)] \right]_0^{a'} \right. \\ &\quad \left. - \left[\frac{-S}{2k\beta'} \sin [-2k\beta'S + 2k(\gamma' - ct)] \right. \right. \\ &\quad \left. \left. + \frac{1}{(2k\beta')} \cos [-2k\beta'S + 2k(\gamma' - ct)] \right]_0^{a'} \right\} \end{aligned}$$

$$\begin{aligned}
\bar{M}_{1y} &= \frac{c_3}{2k\beta'} \{ [a' \sin [2k\beta'a' + 2k(\gamma' - ct)] \\
&+ \frac{1}{2k\beta'} \cos [2k\beta'a' + 2k(\gamma' - ct)] - \frac{1}{2k\beta'} \cos [2k(\gamma' - ct)]] \\
&- [-a' \sin [-2k\beta'a' + 2k(\gamma' - ct)] + \frac{1}{2k\beta'} \cos [-2k\beta'a' + 2k(\gamma' - ct)] \\
&- \frac{1}{2k\beta'} \cos [2k(\gamma' - ct)]] \} \\
&= \frac{c_3}{2k\beta'} \{ 2a' \cos (2k\beta'a') \sin [2k(\gamma' - ct)] \\
&- \frac{1}{k\beta'} \sin (2k\beta'a') \sin [2k(\gamma' - ct)] \} ,
\end{aligned}$$

therefore

$$\bar{M}_{1y} = \frac{c_3}{k\beta'} \sin [2k(\gamma' - ct)] [a' \cos (2k\beta'a') - \frac{1}{2k\beta'} \sin (2k\beta'a')] \quad (A-44)$$

Similarly, for hull No. 2:

$$\bar{M}_{2y} = \frac{-c_3}{k\beta'} \sin [2k(\gamma' + ct)] [a' \cos (2k\beta'a') - \frac{1}{2k\beta'} \sin (2k\beta'a')] \quad (A-45)$$

In summary, the total pitching moment due to vertical drag and inertia forces on all hulls is

$$M_{Vy} = M_{3,4y} + M_{1y} + M_{2y} + \bar{M}_{1y} + \bar{M}_{2y} , \quad (A-46)$$

where $M_{3,4_y}$, M_{1_y} , M_{2_y} , \bar{M}_{1_y} , \bar{M}_{2_y} are as given in Equations (A-41), (A-42), (A-43), (A-44), and (A-45), respectively.

Roll Moment from Vertical Inertia and Drag Forces on Hulls

As seen in Figure A4, the rolling moments due to hulls No. 1 and 2 have a constant moment arm, b , therefore

$$M_{1,2_x} = [(F_{v_1} - F_{v_2}) + (\bar{F}_{v_1} - \bar{F}_{v_2})] b, \quad (A-47)$$

where F_{v_1} , F_{v_2} , \bar{F}_{v_1} , \bar{F}_{v_2} are as given in Equations (A-19), (A-20), (A-27), (A-28), respectively.

The rolling moments due to vertical inertia forces on hulls No. 3 and 4 are derived by integration, in a way similar to the pitching moment, yielding:

$$M_{3_x} = \frac{-a_{v_2}}{k\beta''} \sin [k(\gamma'' + ct)] \left[\frac{\sin (k\beta''b')}{k\beta'} - b' \cos (k\beta''b') \right], \text{ and} \quad (A-48)$$

$$M_{4_x} = \frac{a_{v_2}}{k\beta''} \sin [k(\gamma'' - ct)] \left[\frac{\sin (k\beta''b')}{k\beta''} - b' \cos (k\beta''b') \right]. \quad (A-49)$$

Similarly, for drag:

$$\bar{M}_{3_x} = \frac{c_3}{k\beta''} \sin [2k(\gamma'' + ct)] \left[b' \cos (2k\beta''b') - \frac{1}{2k\beta''} \sin (2k\beta''b') \right], \text{ and} \quad (A-50)$$

$$\bar{M}_{4_x} = \frac{-c_3}{k\beta''} \sin [2k(\gamma'' - ct)] \left[b' \cos (2k\beta''b') - \frac{1}{2k\beta''} \sin (2k\beta''b') \right] \quad (A-51)$$

Finally, the total rolling moment due to vertical drag and inertia forces on all hulls is

$$M_{V_x} = M_{1,2_x} + M_{3_x} + M_{4_x} + \bar{M}_{3_x} + \bar{M}_{4_x} \quad (\text{A-52})$$

where $M_{1,2_x}$, M_{3_x} , M_{4_x} , \bar{M}_{3_x} , and \bar{M}_{4_x} are as given in Equations (A-47), (A-48), (A-49), (A-50), and (A-51), respectively.

Pitching Moment from Dynamic Pressure on Corner Column Bases

The moment about the y-axis due to the dynamic pressure on the base of the corner columns (5,6,7,8) is:

$$M_{P_y} = \frac{-\rho\pi gH}{8} a \sum_{i=5}^8 (-1)^i D_i^2 e^{-kh_i} \cos [k(x - ct)] . \quad (\text{A-53})$$

Rolling Moment from Dynamic Pressure on Corner Column Bases

Similarly, the rolling moment (about x-axis) is:

$$M_{P_x} = \frac{\rho g \pi H}{8} b \left\{ \left[\sum_{i=5}^6 D_i^2 e^{-kh_i} \cos [k(x - ct)] \right] - \sum_{i=7}^8 D_i^2 e^{-kh_i} \cos [k(x - ct)] \right\} . \quad (\text{A-54})$$

Yaw Moments

The forces causing rotation about the vertical axis are those from horizontal drag and inertia acting on the columns. The moment produced by these forces is:

$$M_z = \sum_{i=5}^{12} (F_{I_i} + F_{D_i}) Y_i , \quad (\text{A-55})$$

where:

$$\begin{aligned}
 Y_5 &= a \sin \alpha + b \cos \alpha , \\
 Y_6 &= b \cos \alpha - a \sin \alpha , \\
 Y_7 &= -Y_6 , \\
 Y_8 &= -Y_5 , \\
 Y_9 &= b \cos \alpha , \\
 Y_{10} &= -Y_9 , \\
 Y_{11} &= a \sin \alpha , \text{ and} \\
 Y_{12} &= -Y_{11} .
 \end{aligned}$$

Limits for $\alpha = 0^\circ$ and $\alpha = 90^\circ$

The derived hull forces and moments contain the terms β and β' in the numerators and denominators, and γ and γ' in their numerators.

These terms are related to the wave direction (α) as follows:

$$\begin{aligned}
 \beta' &= \cos \alpha , \\
 \beta'' &= \sin \alpha , \\
 \gamma' &= b \sin \alpha , \text{ and} \\
 \gamma'' &= a \cos \alpha .
 \end{aligned}
 \tag{A-56}$$

As the wave direction (α) approaches 0° or $\frac{\pi}{2}$, a limiting case exists where L'Hospital's rule must be applied to find the forces and moments associated with these extreme values of α .

Limits of Hull Forces for $\alpha = 0^\circ$

As $\alpha \rightarrow 0$, Equation (A-56) becomes: $\beta' = 1$, $\beta'' = 0$, $\gamma' = 0$, and $\gamma'' = a$. Recalling Equations (A-8), (A-9), (A-12), (A-13), (A-25), and (A-31) and rewriting them gives:

$$F_y = \frac{-4a_y}{k\beta'} \sin(k\beta'a') \cos(k\gamma') \sin(kct) \quad (\text{A-8})$$

$$F_x = \frac{-4a_x}{k\beta''} \sin(k\beta''b') \cos(k\gamma'') \sin(kct) \quad (\text{A-9})$$

$$\bar{F}_y = \frac{2c_1}{k\beta'} \sin(2k\beta'a') \cos(2k\gamma') \cos(2kct) + 4c_1a' \quad (\text{A-12})$$

$$\bar{F}_x = \frac{2c_2}{k\beta''} \sin(2k\beta''b') \cos(2k\gamma'') \cos(2kct) + 4c_2b' \quad (\text{A-13})$$

$$F_v = \frac{-2 \cos(kct)}{k} \left[\frac{a_{v1}}{\beta'} \sin(k\beta'a') \cos(k\gamma') \right. \\ \left. + \frac{a_{v2}}{\beta''} \sin(k\beta''b') \cos(k\gamma'') \right] \quad (\text{A-25})$$

$$\bar{F}_v = 4(c_3a' + c_4b') - \frac{2}{k} \cos(2kct) \left[\frac{c_3}{\beta'} \sin(2k\beta'a') \cos(2k\gamma') \right. \\ \left. + \frac{c_4}{\beta''} \sin(2k\beta''b') \cos(2k\gamma'') \right] \quad (\text{A-31})$$

For $\alpha = 0$, the coefficients a_y and c_1 which are functions of $\sin \alpha$ become equal to zero. Also for $\gamma' = 0$, $\cos(k\gamma')$ becomes equal to 1; and for $\beta'' = 0$, $\frac{\sin(k\beta''b')}{k\beta''} = b'$ (by L'Hospital's rule). Thus, the above equations become:

$$F_y = 0 ,$$

$$\bar{F}_y = 0 ,$$

$$F_x = -4a_x b' \cos(ka) \sin(kct) ,$$

$$\bar{F}_x = 4c_2 b' [\cos(2ka) \cos(2kct) + 1] ,$$

$$F_v = -2 \cos(kct) \left[\frac{a_{v1}}{k} \sin(ka') + a_{v2} b' \cos(ka) \right], \text{ and}$$

$$\bar{F}_v = 4(c_3 a' + c_4 b') - 2 \cos(2kct) \left[\frac{c_3}{k} \sin(2ka') + 2c_4 b' \cos(2ka) \right].$$

Recalling Equations (A-41), (A-42), (A-43), (A-44), and (A-45), and performing similar operations with the above equations yields:

$$M_{3,4y} = 2ab' [a_{v2} \sin(ka) \sin(kct) + 2c_4 \sin(2ka) \sin(2kct)],$$

$$M_{1y} = \frac{a_{v1}}{k} \sin(kct) \left[\frac{\sin(ka')}{k} - a' \cos(ka') \right],$$

$$M_{2y} = \frac{a_{v1}}{k} \sin(kct) [\sin(ka') - a' \cos(ka')],$$

$$\bar{M}_{1y} = \frac{-c_3}{k} \sin(2kct) \left[a' \cos(2ka') - \frac{1}{2k} \sin(2ka') \right], \text{ and}$$

$$\bar{M}_{2y} = \bar{M}_{1y}.$$

Limits of Hull Forces for $\alpha = 90^\circ$

As $\alpha \rightarrow 90^\circ$, Equation (A-56) becomes: $\beta' = 0$, $\beta'' = 1$, $\gamma' = b$, and $\gamma'' = 0$. Similar manipulations as those for $\alpha = 0$, convert Equations (A-8), (A-9), (A-12), (A-13), (A-25), and (A-31) to:

$$F_y = -4a_y a' \cos(kb) \sin(kct),$$

$$\bar{F}_y = 4c_1 a' [\cos(2kb) \cos(2kct) + 1],$$

$$F_x = 0 ,$$

$$\bar{F}_x = 0 ,$$

$$F_v = -2 \cos (kct) \left[a' a_{v_1} \cos (kb) + \frac{a_{v_2}}{k} \sin (kb') \right] , \text{ and}$$

$$\bar{F}_v = 4(c_3 a' + c_4 b') - 2 \cos(2kct) \left[\frac{c_4}{k} \sin(2kb') + 2c_3 a' \cos(2kb) \right] .$$

Similarly, the roll moments become:

$$M_{1,2_x} = -2 a'b \left[a_{v_1} \sin(kb) \sin(kct) + 2c_3 \sin(2kb) \sin(2kct) \right] ,$$

$$M_{3_x} = \frac{-a_{v_2}}{k} \sin(kct) \left[\frac{\sin(kb')}{k} - b' \cos(kb') \right] ,$$

$$M_{4_x} = M_{3_x} ,$$

$$\bar{M}_{3_x} = \frac{c_4}{k} \sin (2kct) \left[b' \cos(2kb') - \frac{1}{2k} \sin(2kb') \right] , \text{ and}$$

$$\bar{M}_{4_x} = \bar{M}_{3_x} .$$

APPENDIX B: DERIVATION OF EARTHQUAKE FORCES

Fluid Inertia and Drag Forces Due to InteractionInertia Forces on Columns

Assuming calm water (no waves), the inertia force from structural motion can be calculated with Morison's equation as:

$$\begin{aligned}
 F_{I_i} &= \frac{\rho\pi D_i^2}{4} \int_0^{h_i} \{0 - (C_m - 1) [\ddot{x} - (z - \bar{z})\ddot{\alpha}]\} dz \\
 &= \frac{-\rho\pi D_i^2}{4} (C_m - 1) \left[\ddot{x}h_i + \bar{z} \ddot{\alpha}h_i - \frac{\ddot{\alpha}h_i^2}{2} \right], \quad (B-1)
 \end{aligned}$$

and the moment caused by this force is:

$$\begin{aligned}
 M_{I_i} &= \frac{-\rho\pi D_i^2}{4} \int_0^{h_i} (z - \bar{z}) \{0 - (C_m - 1) [\ddot{x} - (z - \bar{z})\ddot{\alpha}]\} dz \\
 &= \frac{\rho\pi D_i^2}{4} (C_m - 1) \left[\frac{\ddot{x}h_i^2}{2} + \frac{\bar{z}h_i^2\ddot{\alpha}}{2} - \frac{\ddot{\alpha}h_i^3}{3} \right] + \bar{z} F_{I_i}. \quad (B-2)
 \end{aligned}$$

The total fluid inertia force on columns is:

$$F_I = \sum_{i=5}^{12} (F_{I_i}), \quad (B-3)$$

and the total fluid inertia moment on columns is:

$$M_I = \sum_{i=5}^{12} (M_{I_i}) \quad (B-4)$$

Drag Forces on Columns

An application of Morison's equation for drag forces on the columns yields:

$$\begin{aligned}
 F_{D_i} &= (\text{sgn}) \frac{\rho C_d D_i}{2} \int_0^{h_i} \{0 - [\dot{x} - (z - \bar{z})\dot{\alpha}]\}^2 dz \\
 &= (\text{sgn}) \frac{\rho C_d D_i}{2} \int_0^{h_i} [(\dot{x} + \bar{z}\dot{\alpha})^2 - 2(\dot{x} + \bar{z})\dot{\alpha}z + z^2\dot{\alpha}^2] dz \\
 &= (\text{sgn}) \frac{\rho C_d D_i}{2} \left[(\dot{x} + \bar{z}\dot{\alpha})^2 h_i - (\dot{x} + \bar{z}\dot{\alpha})\dot{\alpha}h_i^2 + \frac{\dot{\alpha}^2 h_i^3}{3} \right]. \quad (\text{B-5})
 \end{aligned}$$

The moment caused by the drag force is:

$$\begin{aligned}
 M_{D_i} &= (\text{sgn}) \left(\frac{-\rho C_d D_i}{2} \right) \int_0^{h_i} (z - \bar{z}) [(\dot{x} + \bar{z}\dot{\alpha}) - z\dot{\alpha}]^2 dz \\
 &= (\text{sgn}) \left(\frac{-\rho C_d D_i}{2} \right) \int_0^{h_i} [z(\dot{x} + \bar{z}\dot{\alpha})^2 - 2z^2(\dot{x} + \bar{z}\dot{\alpha}) \\
 &\quad + z^3\dot{\alpha}^2] dz + \bar{z} F_{D_i} \\
 &= (\text{sgn}) \left(\frac{-\rho C_d D_i}{2} \right) \left[(\dot{x} + \bar{z}\dot{\alpha}) \frac{h_i^2}{2} - \frac{2}{3} (\dot{x} + \bar{z}\dot{\alpha}) h_i^3 + \frac{1}{4} \dot{\alpha}^2 h_i^4 \right] + \bar{z} F_{D_i}, \quad (\text{B-6})
 \end{aligned}$$

$$\text{where } (\text{sgn}) = \begin{cases} +1 & \text{if } (\dot{x} + \bar{z}\dot{\alpha}) < 0 \text{ and } (\dot{x} + \bar{z}\dot{\alpha} - h_i\dot{\alpha}) < 0 & (\text{case 1}) \\ -1 & \text{if } (\dot{x} + \bar{z}\dot{\alpha}) > 0 \text{ and } (\dot{x} + \bar{z}\dot{\alpha} - h_i\dot{\alpha}) > 0 & (\text{case 2}) \end{cases}$$

If neither case 1 nor case 2 applies (see Figure B1), then

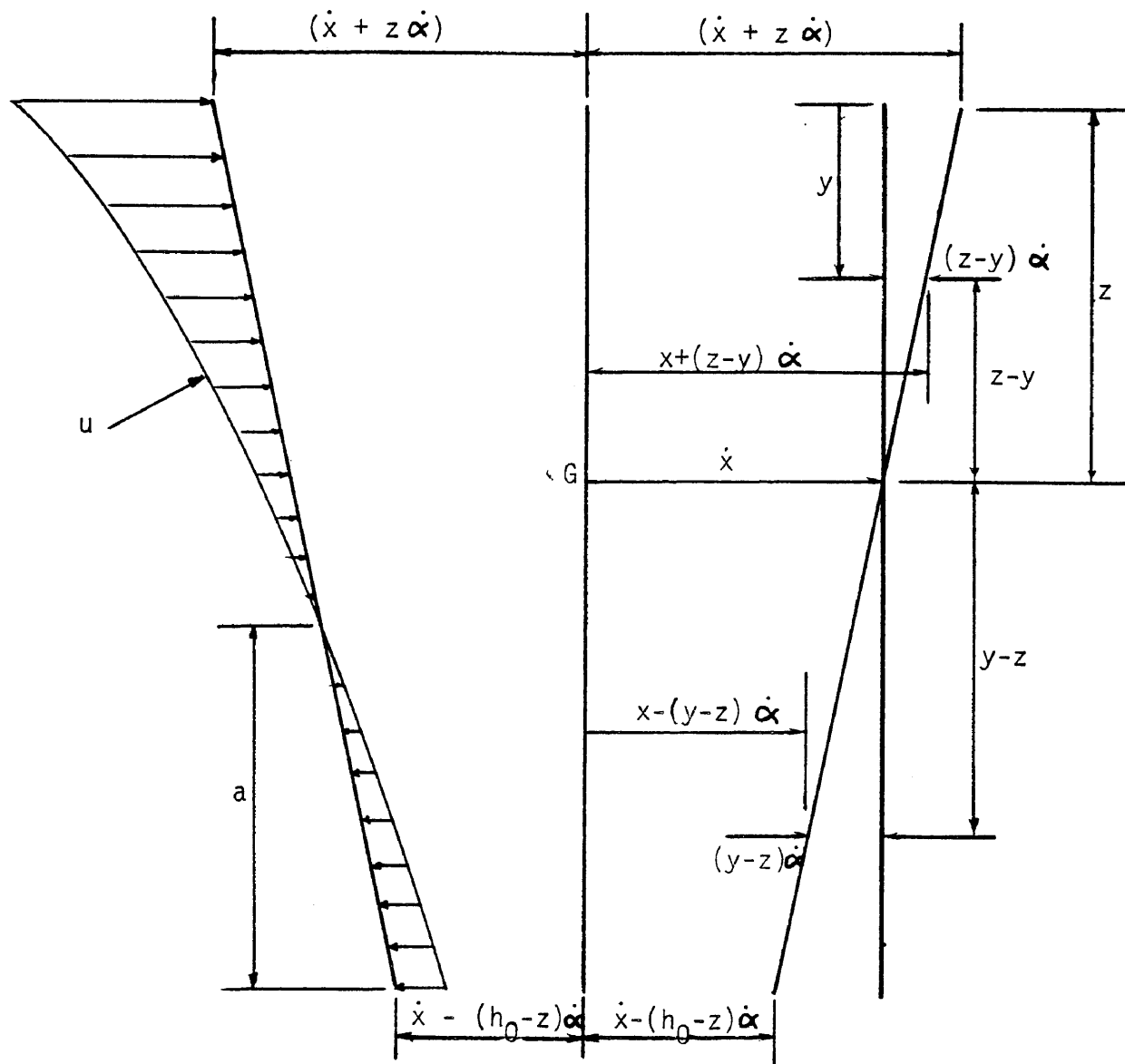


Fig. B1 - Illustration of Relative Motion

$$a_i = \frac{h_i \left| \frac{\dot{x} + \bar{z}\dot{\alpha} - h_i\dot{\alpha}}{x + \bar{z}\dot{\alpha}} \right|}{1 + \left| \frac{x + \bar{z}\dot{\alpha} - h_i\dot{\alpha}}{x + \bar{z}\dot{\alpha}} \right|},$$

and the drag force equation becomes:

$$\begin{aligned} F_{D_i} &= \bar{\tau} \frac{\rho c_d D}{2} \left\{ \int_0^{h_i - a_i} [(\dot{x} + \bar{z}\dot{\alpha}) - z\dot{\alpha}]^2 dz \right. \\ &\quad \left. - \int_{h_i - a_i}^{h_i} [(\dot{x} + \bar{z}\dot{\alpha}) - z\dot{\alpha}]^2 dz \right\} \\ &= \bar{\tau} \frac{\rho c_d D}{2} \left\{ 2[(\dot{x} + \bar{z}\dot{\alpha})^2 (h_i - a_i) - (\dot{x} + \bar{z}\dot{\alpha})(h_i - a_i)^2 \dot{\alpha} \right. \\ &\quad \left. + \frac{\dot{\alpha}^2}{3} (h_i - a_i)^3] \right. \\ &\quad \left. - [(\dot{x} + \bar{z}\dot{\alpha})h_i - (\dot{x} + \bar{z}\dot{\alpha})h_i^2 \dot{\alpha} + \frac{\dot{\alpha}^2}{3} h_i^3] \right\}. \end{aligned} \quad (B-7)$$

If case 1 or case 2 does not apply, M_{D_i} becomes:

$$\begin{aligned} M_{D_i} &= \bar{\tau} \left(\frac{-\rho c_d D}{2} \right) \left[2[(\dot{x} + \bar{z}\dot{\alpha})^2 \left(\frac{h_i - a_i}{2} \right)^2 - \frac{2}{3} (\dot{x} + \bar{z}\dot{\alpha})\dot{\alpha} (h_i - a_i)^3 \right. \\ &\quad \left. + \frac{1}{4} (h_i - a_i)^4 \dot{\alpha}^2] - [(\dot{x} + \bar{z}\dot{\alpha}) \frac{h_i^2}{2} - \frac{2}{3} (\dot{x} + \bar{z}\dot{\alpha})\dot{\alpha} h_i^3 + \frac{1}{4} h_i^4 \dot{\alpha}^2] \right] \\ &\quad + \bar{z} F_{D_i}, \end{aligned} \quad \dots (B-8)$$

$$\text{where } (\bar{f}) = \begin{cases} +1 & \text{if } (x + \bar{z} \dot{\alpha}) < 0 \\ -1 & \text{if } (x + \bar{z} \dot{\alpha}) > 0 \end{cases}$$

Inertia Forces on Hulls

For Hulls No. 1 and 2, the inertia forces are:

$$\begin{aligned} F_{y_1} &= \frac{-\rho\pi D_1^2}{4} (C_m - 1) [2a'\ddot{y}] \\ &= \frac{-\rho\pi D_1^2}{2} (C_m - 1) a' \ddot{x} \sin \alpha, \text{ and} \end{aligned} \quad (\text{B-9})$$

$$F_{y_2} = F_{y_1}$$

Similarly, for Hulls No. 3 and 4, the inertia forces are:

$$F_{x_3} = \frac{-\rho\pi D_3^2}{2} (C_m - 1) a' \ddot{x} \cos \alpha \quad (\text{B-10})$$

$$F_{x_4} = F_{x_3}$$

Moments Due to Inertia Forces on Hulls

The moments of the above inertia forces on hulls about the center of rotation are:

$$M_{1,2_x} = (F_{y_1} + F_{y_2}) \left(\bar{h} - \frac{D_1}{2} \right), \text{ and} \quad (\text{B-11})$$

$$M_{3,4_y} = (F_{x_3} + F_{x_4}) \left(\bar{h} - \frac{D_3}{2} \right) \quad (\text{B-12})$$

Drag Forces on Hulls

For Hulls No. 1 and 2, the drag forces are:

$$\begin{aligned}\bar{F}_{y_1} &= (\text{sgn}) \frac{\rho C_d D_1}{2} [\dot{x} \sin \alpha]^2 (2a') \\ &= (\text{sgn}) \rho C_d D_1 a' \dot{x}^2 \sin^2 \alpha, \text{ and}\end{aligned}\tag{B-13}$$

$$\bar{F}_{y_2} = \bar{F}_{y_1} .\tag{B-14}$$

Similarly, for Hulls No. 3 and 4, the drag forces are:

$$\bar{F}_{x_3} = (\text{sgn}) \rho C_d D_3 b' \dot{x}^2 \cos^2 \alpha, \text{ and}\tag{B-15}$$

$$\bar{F}_{x_4} = \bar{F}_{x_3},\tag{B-16}$$

$$\text{where } (\text{sgn}) = \begin{cases} +1 & \text{if } \dot{x}_{h_0} < 0 \\ -1 & \text{if } \dot{x}_{h_0} > 0 \end{cases}$$

Moments Due to Drag Forces on Hulls:

The moments of the above drag forces on hulls about the center of rotation are:

$$M_{1,2_x} = (\bar{F}_{y_1} + \bar{F}_{y_2}) \left(\bar{h} - \frac{D_1}{2} \right), \text{ and}\tag{B-17}$$

$$M_{3,4_y} = (\bar{F}_{x_3} + \bar{F}_{x_4}) \left(\bar{h} - \frac{D_3}{2} \right) .\tag{B-18}$$

Yaw Moments

The moment of the drag and inertia forces on columns about the z-axis is:

$$M_z = \sum_{i=5}^{12} (F_{I_i} + F_{D_i}) Y_i , \quad (\text{B-19})$$

where Y_i is the distance of column "i" from the z-axis.

APPENDIX C: PLATFORM DATA

Data Used for Evaluation of Platform Motion

The following tension-leg platform data are taken from Kirk & Etok (1979) and used in the analysis:

- Buoyancy = weight of displaced fluid = 436,810kN
- Water depth = 160 meters
- Draft = depth of submerged portion of the structure = 35 m
- Mass of deck equipment = 18,000 tons
- Mass of one main hull + ballast = 2,000 tons
- Total mass of TPP in air = 31,200 tons
- Structural and fluid added mass in heave = 56,000 tons
- Structural and fluid added mass in sway = 82,700 tons
- Structural and fluid added mass moment of inertia in roll = 1.49×10^8 ton-meter square (tm^2)
- Structural and fluid added mass moment of inertia in pitch = 9.68×10^7 tm^2
- Diameter of corner columns = 16 m
- Diameter of middle columns = 3.5 m
- Diameter of cross braces = 6 m
- Depth and width of main hulls = 13 x 9.5 m
- Spacing of corner columns = 70 m
- Height of platform center of gravity = 41.7 m
- Number of cables per leg = 3
- Number of wires per cable = 400
- Diameter of each wire = 7 mm

- Area of wire per leg = $46,180 \text{ mm}^2$
- Cable length = 125 m, 200 m
- Initial tension per leg = 25,000 kN

Some of the above data are modified to meet the objectives of this research. Such modifications include water depth, hull sizes, and masses.